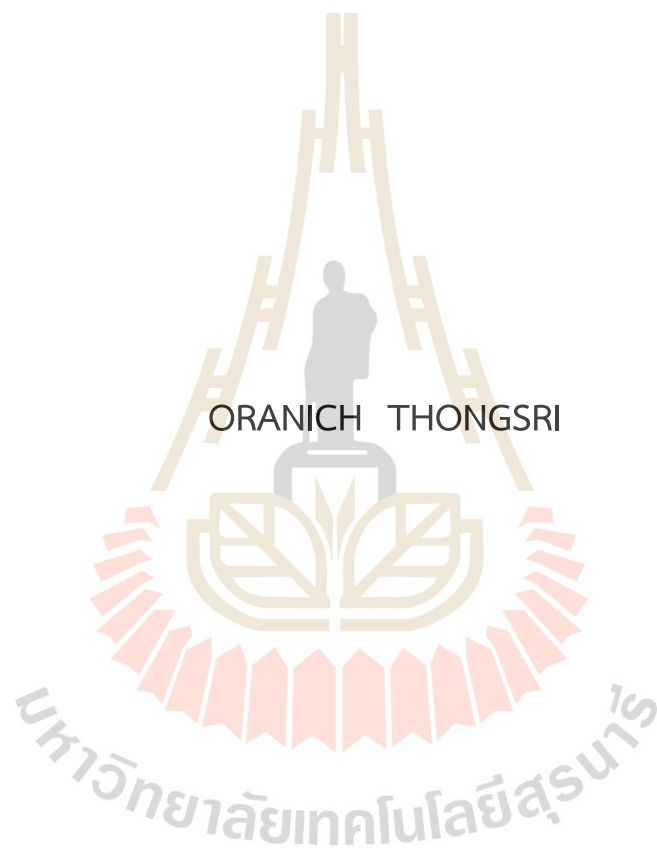


DEVELOPMENT OF ANITIBACTERIAL ACTIVITY AND BIOACTIVITY  
OF GLASS IONOMER CEMENT SYNTHESIZED BY SOL-GEL METHOD  
FOR DENTAL RESTORATIVE MATERIALS



A Thesis Submitted in Partial Fulfillment of the Requirements for the  
Degree of Doctor of Philosophy in Materials Engineering  
Suranaree University of Technology  
Academic Year 2023

การพัฒนาคุณสมบัติด้านทานเชื้อแบคทีเรียและความว่องไวทางชีวภาพ  
ของกลาสไอโอโนเมอร์ซีเมนต์ที่สังเคราะห์ด้วยวิธีโซล-เจล เพื่อใช้สำหรับ  
เป็นวัสดุบูรณะฟัน



นางสาวอรณิชา ทองศรี

วิทยานิพนธ์นี้เป็นส่วนหนึ่งของการศึกษาตามหลักสูตรปริญญาวิศวกรรมศาสตรดุษฎีบัณฑิต  
สาขาวิชาวิศวกรรมวัสดุ  
มหาวิทยาลัยเทคโนโลยีสุรนารี  
ปีการศึกษา 2566

DEVELOPMENT OF ANITIBACTERIAL ACTIVITY AND BIOACTIVITY OF  
GLASS IONOMER CEMENT SYNTHESIZED BY SOL-GEL METHOD FOR  
DENTAL RESTORATIVE MATERIALS

Suranaree University of Technology has approved this thesis submitted in partial fulfillment of the requirements for a Degree of Doctor of Philosophy.

Thesis Examining Committee

*Dujretai Pongkao Kashima*

(Assoc.. Prof. Dr. Dujretai Pongkao Kashima)

Chairperson :

*Siriratt Rattanachan*

(Assoc. Prof. Dr. Sirirat Rattanachan)

Member (Thesis Advisor)

*S. Jiansirisomboon*

(Assoc. Prof. Dr. Sukanda Jiansirisomboon)

Member

*Nitinat Suppakarn*

(Asst. Prof. Dr. Nitinat Suppakarn)

Member

(Dr. Sanong Suksaweang)

Member

*Chatchai Jothiyang*

(Assoc. Prof. Dr. Chatchai Jothiyangkoon)

Vice Rector for Academic Affairs and  
Quality Assurance

*Pornsiri Jongkol*

(Assoc. Prof. Dr. Pornsiri Jongkol)

Dean of Institute of Engineering

อรณิข ทองศรี: การพัฒนาคุณสมบัติด้านทานเชื้อแบคทีเรียและความว่องไวทางชีวภาพของ  
กลาสไอโอโนเมอร์ซีเมนต์ที่สังเคราะห์ด้วยวิธีโซล-เจล เพื่อใช้สำหรับเป็นวัสดุบูรณะฟัน  
(DEVELOPMENT OF ANITIBACTERIAL ACTIVITY AND BIOACTIVITY OF GLASS  
IONOMER CEMENT SYNTHESIZED BY SOL-GEL METHOD FOR DENTAL  
RESTORATIVE MATERIALS)

อาจารย์ที่ปรึกษา: รองศาสตราจารย์ ดร. ศิริรัตน์ ทับสูงเนิน รัตนจันทร์., 156 หน้า.

คำสำคัญ: กลาสไอโอโนเมอร์ซีเมนต์ โซล-เจล การต้านทานเชื้อแบคทีเรีย ความว่องไวทางชีวภาพ  
วัสดุทันตกรรม

โรคฟันผุเป็นโรคในช่องปากที่พบได้บ่อยในทุกประเทศทั่วโลก รวมถึงประเทศไทย โรคฟันผุ  
เกิดจากการสลายตัวของชั้นเคลือบฟันอันเนื่องมาจากการสะสมเชื้อโรคในคราบจุลินทรีย์ที่เกาะติดอยู่  
บริเวณผิวฟันย่อยสลายอาหารพวกน้ำตาลทำให้เกิดความเป็นกรดและกัดกร่อนเนื้อฟัน ซึ่งเป็นที่ทราบ  
กันดีว่าผู้สูงวัยในอายุ 60 ปี มักพบปัญหาฟันผุบริเวณราก ซึ่งอาจส่งผลต่อการติดเชื้อ การสูญเสียฟัน  
และกระทบต่อการใช้ชีวิตประจำวันได้ ในการรักษาอาการดังกล่าวสามารถทำได้โดยการบูรณะฟัน  
ด้วยวัสดุที่สามารถทนความชื้นและปลดปล่อยฟลูออไรด์ได้ดี นั่นคือซีเมนต์บูรณะฟันชนิดกลาสไอโอ  
โนเมอร์ซีเมนต์ (GICs) แต่อย่างไรก็ตามการผลิตวัสดุ GICs ด้วยวิธีการดั้งเดิมต้องอาศัยอุณหภูมิที่สูง  
ถึง 1300 องศาเซลเซียส ซึ่งส่งผลให้ไม่สามารถควบคุมองค์ประกอบในแก้วได้รวมถึงปล่อยก๊าซที่เป็น  
พิษสู่บรรยากาศ ดังนั้น งานวิจัยนี้จึงได้ศึกษาวิธีการสังเคราะห์แก้วไอโอโนเมอร์ด้วยวิธีโซล-เจล ซึ่ง  
เป็นวิธีที่มีการใช้อุณหภูมิในกระบวนการสังเคราะห์ที่ต่ำ ทั้งยังให้ผงแก้วที่มีความบริสุทธิ์สูง ขนาดเล็ก  
ละเอียดและยังสามารถควบคุมองค์ประกอบของแก้วได้ดี นอกจากนี้ การวิจัยนี้ยังมุ่งเน้นการเพิ่ม  
ประสิทธิภาพการต้านเชื้อแบคทีเรียและความว่องไวทางชีวภาพ เพื่อลดโอกาสเกิดอาการฟันผุซ้ำซ้อน  
อีกด้วย

งานวิจัยนี้เริ่มต้นด้วยการสำรวจสภาวะที่เหมาะสมสำหรับการสังเคราะห์แก้วไอโอโนเมอร์  
ด้วยวิธีโซล-เจล ได้แก่ สัดส่วนของน้ำต่อสารตั้งต้น (Rw), ค่า pH, อุณหภูมิการเผาแคลไซน์, ชนิดของ  
สารตั้งต้นฟลูออไรด์ และ วิธีการบ่มเจล จากนั้นจึงมีการปรับปรุงสูตรของแก้วโดยเน้นที่สัดส่วนของ  
 $Al_2O_3$  และ  $P_2O_5$  นอกจากนี้ยังได้ปรับปรุงคุณสมบัติการต้านทานเชื้อแบคทีเรียและความว่องไวทาง  
ชีวภาพของ GICs ที่ได้มาจากการสังเคราะห์โซล-เจล ได้แก่ การเจือองค์ประกอบของแก้วด้วย ZnO  
และการใช้อนุภาคนาโนของ SrFA และ SrBGF เพื่อเป็นสารตัวเติม นอกจากการวิจัยการปรับปรุง  
คุณสมบัติของ SGICs ยังมีการใช้เทคนิคการหาลักษณะทางโครงสร้างในเชิงลึก ได้แก่ X-ray  
diffraction (XRD), Fourier-transform infrared spectroscopy (FTIR), X-ray photoelectron

spectroscopy (XPS), synchrotron-based X-ray absorption spectroscopy (XAS), และ micro computed tomography (microCT) เพื่อวิเคราะห์การเปลี่ยนแปลงโครงสร้างของแก้วที่ส่งผลต่อคุณสมบัติต่างๆ ของวัสดุ SGICs

ผลการศึกษาในงานวิจัยนี้แสดงให้เห็นว่าสภาวะที่เหมาะสมในการสังเคราะห์เป็นปัจจัยสำคัญที่ส่งผลต่อโครงสร้างและคุณสมบัติของ SGICs นอกจากนี้ยังพบว่า การเพิ่มอัตราส่วนของ  $Al_2O_3$  ในสูตรของแก้วช่วยเสริมความแข็งแรงในการกดอัด (compressive strength) ของ SGICs ในขณะที่การเพิ่มอัตราส่วนของ  $P_2O_5$  จะช่วยยืดเวลาการเซตตัว แต่ลดความแข็งแรงในการกดอัดของซีเมนต์ลง ในส่วนของผลการทดลองเจือ ZnO เข้าไปในองค์ประกอบของแก้วไอโอโนเมอร์ สามารถเพิ่มคุณสมบัติต้านเชื้อแบคทีเรียได้ แต่ส่งผลกระทบต่อเวลาในการเซตตัวและความแข็งแรงในการกดอัดซึ่งสามารถปรับให้เหมาะสมโดยการปรับอุณหภูมิการเผาแคลไซน์ เมื่อเติมอนุภาคนาโนของ SrFA หรือ SrBGF เข้าไปยัง SGIC พบว่าสามารถเพิ่มประสิทธิภาพในเรื่องของความแข็งแรง ความว่องไวทางชีวภาพและความเข้ากันได้กับเซลล์ได้ดี แต่อย่างไรก็ตาม การเติมอนุภาคนาโนของ SrFA ส่งผลยับยั้งการดูดซับฟลูออไรด์และการเติมอนุภาคนาโนของ SrBGF สามารถเพิ่มประสิทธิภาพในการปลดปล่อยและดูดซับฟลูออไรด์ แต่ไม่สามารถเพิ่มประสิทธิภาพต้านเชื้อแบคทีเรียแก่ SGIC ซึ่งจำเป็นต้องมีการศึกษาเพิ่มเติมในอนาคต โดยผลที่ได้จากการวิจัยนี้เป็นการนำเสนอแนวทางและความเข้าใจสำหรับการออกแบบและพัฒนา GICs ที่มีคุณสมบัติที่ดีกว่าในการใช้งานทางทันตกรรมและกระดูกต่อไป



สาขาวิชา วิศวกรรมเซรามิก  
ปีการศึกษา 2566

ลายมือชื่อนักศึกษา .....  
ลายมือชื่ออาจารย์ที่ปรึกษา .....

ORANICH THONGSRI: DEVELOPMENT OF ANITIBACTERIAL ACTIVITY AND BIOACTIVITY OF GLASS IONOMER CEMENT SYNTHESIZED BY SOL-GEL METHOD FOR DENTAL RESTORATIVE MATERIALS

THESIS ADVISOR: ASSOC. PROF. SIRIRAT TUBSUNGNOEN RATTANACHAN, Ph.D.,  
156 PP.

Keyword: GLASS IONOMER CEMENT, SOL-GEL SYNTHESIS, ANITIBACTERIAL ACTIVITY, BIOACTIVITY, DENTAL MATERIAL

Dental caries is a chronic disease that persists worldwide, with a significant impact on the elderly population who are particularly vulnerable to disease and infection. This disease is caused by acid-producing bacteria that demineralize the subsurface of teeth, resulting in carious lesions, which are a clear indication of the disease. To minimize the occurrence of caries lesions in patients at higher risk, glass ionomer cement (GICs) has been recommended as the first choice for dental restoration due to its potential to release fluoride. However, the conventional GICs have been produced by melt-quenching method with extremely high production temperatures resulting in loss of composition and air pollution. Hence, this study aimed to enhance the bioactivity and antibacterial properties of glass ionomer powder through the low-temperature sol-gel method, with the goal of reducing the incidence of carious lesions in dental caries disease.

The investigation started with an analysis of the sol-gel synthesis conditions to find the optimal condition for the ionomer glass including water to precursor ratio ( $R_w$ ), pH, calcination temperature, type of fluoride source, and ageing process. It was followed by the optimization of the glass composition, focusing on  $Al_2O_3$  and  $P_2O_5$ . Various factors were also explored to improve the properties of SGICs, including the use of ZnO doping, and the addition of SrFA and SrBGF nanoparticles. In addition to investigating improvements, this study utilized advanced characterization techniques including X-ray diffraction (XRD), Fourier-transform infrared spectroscopy (FTIR), X-ray photoelectron spectroscopy (XPS), synchrotron-based X-ray absorption spectroscopy

(XAS), and micro computed tomography (microCT) to thoroughly analyze structural changes and their corresponding properties.

The finding in this study showed that the conditions used for synthesis played a key role in the obtained glass structure and properties of SGICs. An increase in  $\text{Al}_2\text{O}_3$  in the glass formula enhanced the compressive strength of SGIC, while an increase in  $\text{P}_2\text{O}_5$  content led to prolonging the setting reactivity and lowering compressive strength of the cement. ZnO dopants were incorporated to improve antibacterial properties but had an adverse effect on setting time and compressive strength, which could be optimized by calcination temperature. SGIC modified with SrFA and SrBGF nanoparticles effectively improved the compressive strength, bioactivity, and cytocompatibility of SGIC. However, SrFA inhibited fluoride uptake, and SrBGF did not improve the antibacterial properties of SGIC. These findings provide insights into the design and development of GICs with improved properties for dental and orthopedic applications.



School of Ceramic Engineering  
Academic Year 2023

Student's Signature ..... *Caus*  
Advisor's Signature ..... *Sir Rattana*

## ACKNOWLEDGEMENT

The successful completion of this dissertation would not have been possible without the invaluable support of numerous individuals, to whom I am deeply grateful. I would like to take this opportunity to express my heartfelt appreciation.

First and foremost, I wish to express my appreciation to the Thailand Research Fund (TRF) for their financial support during this study through the Royal Golden Jubilee Ph.D. scholarship. Their invaluable funding enabled me to conduct research and gain knowledge.

I am grateful to my supervisor, Associate Professor Dr. Sirirat Rattanachan, for her invaluable guidance, patience, and encouragement throughout my research project. Her expert advice and insightful feedback have been helpful in shaping the direction and focus of this study.

I would also like to acknowledge the assistance of my dissertation committee members, Asst. Prof. Dr. Dujreutai Pongkao Kashima, Assoc. Prof. Dr. Sukanda Jiansirisomboon, Asst. Prof. Dr. Nitinat Suppakarn, and Dr. Sanong Suksaweang, for their time, expertise, and constructive criticism. Their comments and suggestions have greatly enriched the quality of this work.

Next, my gratitude also goes to Professor Dr. Julie Gough for giving me the opportunity to be a visiting student in her group at the University of Manchester (UoM). I am grateful for their warm welcome, kindly help, and invaluable knowledge provided by staff and the members of the group at the University of Manchester.

I would also like to thank staff of ceramic engineering school, Dr. Sawitri Srisuwan, Dr. Paritat Thaitalay, Dr. Sujinda Chaiyachad, and Rawee Dangviriyakul, for their unwavering support, encouragement, and motivation throughout the ups and downs of my academic journey.

Finally, I would like to express my heartfelt gratitude to my family for their love, support, and patience throughout my studies. Their unwavering encouragement and belief in me have been the driving force behind my success.

To all those who have contributed to my academic and personal growth, I extend my deepest thanks and appreciation.

ORANICH THONGSRI

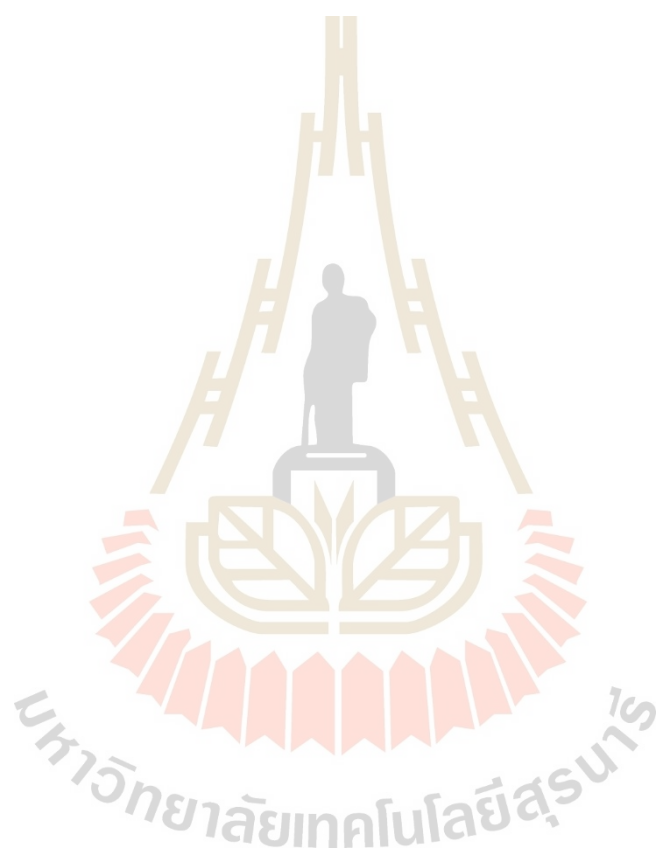


# TABLE OF CONTENTS

	Page
ABSTRACT (Thai).....	I
ABSTRACT (ENGLISH).....	III
ACKNOWLEDGEMENT.....	V
TABLE OF CONTENTS.....	VII
LIST OF TABLES.....	XII
LIST OF FIGURES.....	XIII
LIST OF ABBREVIATIONS.....	XXIII
<b>CHAPTER</b>	
<b>1 INTRODUCTION.....</b>	<b>1</b>
1.1 Rationale and background.....	1
1.2 Research objective.....	4
1.3 Scope and limitation.....	4
1.4 Expected benefits.....	4
1.5 Outline of Thesis.....	4
<b>2 LITERATURE REVIEWS.....</b>	<b>7</b>
2.1 Glass ionomer cement (GICs).....	7
2.1.1 GICs composition and setting reaction.....	7
2.2 Clinical Applications of GICs and problems.....	12
2.2.1 Type of GICs.....	12
2.2.2 Atraumatic restorative treatment (ART).....	12
2.2.3 Secondary caries.....	13
2.3 Properties and limitation of GICs.....	13
2.3.1 Mechanical and physical properties.....	13
2.3.2 Antibacterial activity.....	15
2.3.3 Bioactivity.....	15

## TABLE OF CONTENTS (Continued)

	Page
2.3.4 Biocompatibility .....	16
2.3.5 Fluoride release .....	17
2.4 Production of ionomer glass .....	17
<b>3 SOL-GEL SYNTHESIS CONDITION FOR IONOMER GLASS (<math>4.5\text{SiO}_2\text{-}3\text{Al}_2\text{O}_3\text{-}</math></b>	
<b><math>1.5\text{P}_2\text{O}_5\text{-}3\text{CaO-}2\text{CaF}_2</math>) .....</b>	<b>22</b>
3.1 Introduction.....	22
3.2 Experimental procedure.....	24
3.2.1 The synthesis of $4.5\text{SiO}_2\text{-}3\text{Al}_2\text{O}_3\text{-}1.5\text{P}_2\text{O}_5\text{-}3\text{CaO-}2\text{CaF}_2$ ionomer glass by the sol-gel method .....	24
3.2.2 Cement preparation.....	28
3.2.3 Setting time and compressive strength testing .....	28
3.3 Results and discussions.....	29
3.3.1 Effect of the ratio of TEOS:H <sub>2</sub> O (Rw) .....	29
3.3.2 Effect of the pH of solution .....	33
3.3.3 Effect of calcination temperature.....	36
3.3.4 Effect of fluoride source .....	40
3.3.5 Effect of aging process.....	41
3.4 Conclusions.....	44
<b>4 EFFECT OF IONOMER GLASS COMPOSITON (<math>\text{Al}_2\text{O}_3\text{-P}_2\text{O}_5</math> RATIO) .....</b>	<b>46</b>
4.1 Research background.....	46
4.2 Experimental procedure.....	47
4.2.1 Experimental design.....	47
4.2.2 Sol-gel synthesis of the ionomer glass .....	48
4.2.3 Characterization of the sol-gel ionomer glass.....	49
4.2.4 Preparation of the sol-gel glass ionomer cement (GIC).....	50
4.2.5 Setting time .....	50
4.2.6 Compressive strength testing.....	50

## TABLE OF CONTENTS (Continued)

	Page
4.3 Result and discussion.....	51
4.3.1 Chemical structural analysis and ions releasing from the sol-gel ionomer glasses .....	51
4.3.2 Setting time and compressive strength of SGIC with Al <sub>2</sub> O <sub>3</sub> and P <sub>2</sub> O <sub>5</sub> variation.....	58
4.3.3 DoE analysis .....	61
4.4 Conclusions .....	66
<b>5 EFFECT OF ZnO DOPING AND CALCINATION TEMPERATURE ON SGICs</b>	
<b>(4.5SiO<sub>2</sub>-4Al<sub>2</sub>O<sub>3</sub>-0.3P<sub>2</sub>O<sub>5</sub>-(2-X)CaO-XZnO-2F<sub>2</sub>) .....</b>	<b>67</b>
5.1 Research background.....	67
5.2 Experimental procedure.....	68
5.2.1 Preparation of ionomer glass.....	68
5.2.2 Characterization of the sol-gel glass for glass ionomer cement.....	70
5.2.3 Preparation of the cement and the physical properties testing .....	71
5.2.4 Setting time and compressive strength testing .....	71
5.2.5 Antibacterial testing.....	71
5.2.6 Cell cytotoxicity .....	72
5.2.7 <i>In vitro</i> bioactivity and tooth-GIC interface.....	73
5.3 Results and discussions .....	74
5.3.1 Characterization of the sol-gel derived ionomer glass .....	74
5.3.2 Ion releasing concentrations of the Zn doped sol-gel ionomer glass .....	78
5.3.3 DoE analysis of the compressive strength.....	80
5.3.4 Setting time and compressive strength.....	81
5.3.5 The local structure of ZnO in SGIC by XAS technique .....	84
5.3.6 Antibacterial property .....	88
5.3.7 Cell viability.....	90

## TABLE OF CONTENTS (Continued)

	Page
5.3.8 Bioactivity and tooth-GIC interface.....	91
5.4 Conclusions .....	94
<b>6 EFFECT OF STRONTIUM CONTAINING FLUORAPATITE ADDITIVE ON SGICs</b> <b>(4.5SiO<sub>2</sub>-4Al<sub>2</sub>O<sub>3</sub>-0.45P<sub>2</sub>O<sub>5</sub>-1.4CaO-0.3ZnO-2F<sub>2</sub>) .....</b>	<b>95</b>
6.1 Research background.....	95
6.2 Experimental procedure.....	96
6.2.1 Synthesis of SrFA nanoparticles and characterization .....	96
6.2.2 Preparation of glass ionomer cement.....	97
6.2.3 Setting time and compressive strength testing .....	99
6.2.4 Antibacterial testing.....	99
6.2.5 <i>In vitro</i> bioactivity .....	99
6.2.6 <i>In vitro</i> cytocompatibility.....	100
6.2.7 Fluoride release and uptake ability.....	100
6.3 Results and discussions.....	101
6.3.1 Characterization of SrFA additive.....	101
6.3.2 Setting time and compressive strength.....	102
6.3.3 Antibacterial properties.....	104
6.3.4 <i>In vitro</i> bioactivity .....	106
6.3.5 Cell viability.....	108
6.3.6 Fluoride release and uptake .....	109
6.4 Conclusions .....	111
<b>7 EFFECT OF STRONTIUM CONTAINING FLUORINATED BIOACTIVE GLASS</b> <b>ADDITIVE IN SGIC (4.5SiO<sub>2</sub>-4Al<sub>2</sub>O<sub>3</sub>-0.45P<sub>2</sub>O<sub>5</sub>-1.4CaO-0.3ZnO-2F<sub>2</sub>).....</b>	<b>112</b>
7.1 Research background.....	112
7.2 Experimental procedure.....	114
7.2.1 Synthesis of SrBGF nanoparticles and characterization.....	114
7.2.2 Preparation of glass ionomer cement.....	115

## TABLE OF CONTENTS (Continued)

	Page
7.2.3 Setting time and compressive strength .....	116
7.2.4 Surface roughness.....	116
7.2.5 Antibacterial testing.....	117
7.2.6 Bioactivity testing.....	117
7.2.7 <i>In vitro</i> cytocompatibility on human adipose-derived stem cell (hASCs) .....	119
7.2.8 Preliminary study of human dental pulp stem cells (hDPSCs) cytotoxicity.....	121
7.2.9 Fluoride release and uptake testing.....	121
7.3 RESULTS AND DISCUSSIONS.....	124
7.3.1 Characterization of SrBGF additive .....	124
7.3.2 Setting time and compressive strength.....	124
7.3.3 Surface roughness.....	127
7.3.4 Antibacterial properties.....	128
7.3.5 Bioactivity.....	131
7.3.6 <i>In vitro</i> cytocompatibility.....	135
7.3.7 Fluoride release and uptake ability.....	140
7.4 CONCLUSIONS .....	150
<b>8 CONCLUSIONS.....</b>	<b>152</b>
REFERENCES .....	156
APPENDIX.....	175
APPENDIX A.....	176
APPENDIX B .....	206
BIOGRAPHY .....	210

## LIST OF TABLES

Table	Page
1.1 advantages and disadvantages of the filling dental materials (California, 2005).....	2
2.1 The glass compositions (mol ratio) of the glass ionomer powder and their function.....	9
2.2 Influence of the glass components on the properties of the GICs .....	11
2.3 Mechanical properties of GICs, dentine and enamel.....	14
2.4 The difference between the glass prepared by melting and sol-gel method.....	18
3.1 Amount of the precursors for sol-gel synthesis of ionomer glass .....	26
3.2 pH of the solution, gelation time, and setting time of SGIC prepared with different Rw ratio. ....	32
3.3 The physical properties of SGIC prepared with different pH. ....	35
3.4 The physical properties of SGIC calcination at 400°C 600°C, 700°C and 800°C ...	39
3.5 The physical properties of SGIC prepared from sol-gel glasses prepared using two different fluoride sources, CaF <sub>2</sub> and H <sub>2</sub> SiF <sub>6</sub> .....	41
3.6 The physical properties of SGIC prepared from sol-gel glasses prepared using two different aging method, dry aging and gel aging.....	44
4.1 The variation of the sol-gel ionomer glass compositions for 4.5SiO <sub>2</sub> -xAl <sub>2</sub> O <sub>3</sub> - yP <sub>2</sub> O <sub>5</sub> -2CaO-2F <sub>2</sub> using 2 <sup>k</sup> factorial design.....	48
5.1 Design composition for the sol-gel ionomer glass of 4.5SiO <sub>2</sub> -4Al <sub>2</sub> O <sub>3</sub> - 0.16P <sub>2</sub> O <sub>5</sub> -(2-x)Ca-xZnO-2F <sub>2</sub> , where x= 0, 0.6, 1.0 and 1.4. ....	70
5.2 ANOVA analysis for the compressive strength for SGICs containing different ZnO doping and the calcination temperatures. ....	80
5.3 EXAFT fitting parameters including average coordination number of oxygens around the atom (CN), Debye-Waller factor( $\sigma$ ), interatomic distance (R), and (R-factor) .....	86

## LIST OF FIGURES

Figure	Page
2.1 Setting reaction of glass ionomer cement (Lohbauer, 2010).....	8
2.2 Schematic of calcium-alumino-silicate glass network containing fluorine (Wood and Hill, 1991).....	10
2.3 Sol-gel process for multicomponent glass synthesis (Mukherjee, 1980).....	19
2.4 Gel formation of multicomponent system (Mukherjee, 1980). ....	19
3.1 Schematic of synthesis process of ionomer glass powder by the sol-gel method.....	24
3.2 Flow chart illustrating the sol-gel synthesis of the ionomer glass. ....	25
3.3 schematic of comparison between two different aging process, which were dried aging and gel aging, for synthesis of ionomer glass powder by sol-gel method.....	28
3.4 XRD patterns of sol-gel glass ionomer powders calcined at 700°C.....	30
3.5 FTIR spectra of (a) the sol-gel ionomer glass prepared from the different R <sub>w</sub> ratio calcined at 700°C and (b) the set cements.....	31
3.6 XRD pattern of the ionomer glass belonging the system of 4.5SiO <sub>2</sub> -3Al <sub>2</sub> O <sub>3</sub> - 1.5P <sub>2</sub> O <sub>5</sub> -3CaO-2CaF <sub>2</sub> .....	33
3.7 FTIR spectra of the sol-gel ionomer glass synthesized with different pH.....	34
3.8 The silica gel networks derived form (A) acid- and (B) base-catalyzed TEOS hydrolysis and condensation (Ying et al., 1993).....	36
3.9 XRD pattern of the sol-gel ionomer glass after calcination at 400°C, 600°C, 700°C and 800°C, respectively, as compared with the commercial product. ....	37
3.10 The FTIR spectra of (a) the sol-gel ionomer glass after calcination at 400°C, 600°C, 700°C and 800°C, respectively. ....	38
3.11 XRD pattern compares the sol-gel ionomer glass prepared using CaF <sub>2</sub> and H <sub>2</sub> SiF <sub>6</sub> fluoride precursors, as compared with the commercial GIC.....	40

## LIST OF FIGURES (Continued)

Figure	Page
3.12 XRD pattern compares the sol-gel ionomer glass prepared by different aging process, namely dried aging and gel aging, with the commercial GIC. ....	43
4.1 Schematic of experimental design to determine the optimal $\text{Al}_2\text{O}_3$ and $\text{P}_2\text{O}_5$ ratio by variation of $\text{Al}(\text{NO}_3)_3$ and TEP precursors.....	49
4.2 XRD patterns of the sol-gel ionomer glasses belonging to $4.5\text{SiO}_2\text{-XAl}_2\text{O}_3\text{-0.3P}_2\text{O}_5\text{-2CaO-2F}_2$ glass system, where X= 2, 2.5, 4 and 4.3. ....	51
4.3 High resolution XPS spectra in the (a) Al2p and (b) O1s regions of the sol-gel ionomer glasses belonging to $4.5\text{SiO}_2\text{-XAl}_2\text{O}_3\text{-0.3P}_2\text{O}_5\text{-2CaO-2F}_2$ glass system, where X= 2, 2.5, 4 and 4.3. ....	52
4.4 The concentration of (a) $\text{Si}^{4+}$ , (b) $\text{P}^{5+}$ , (c) $\text{Al}^{3+}$ and (d) $\text{Ca}^{2+}$ ions releasing from the sol-gel ionomer glasses belonging to $4.5\text{SiO}_2\text{-XAl}_2\text{O}_3\text{-0.3P}_2\text{O}_5\text{-2CaO-2F}_2$ system, where X = 2, 2.5, 4 and 4.3, as function of the immersion times. ....	53
4.5 A proposed glass network structure for sol-gel ionomer glass with a variation of $\text{Al}_2\text{O}_3$ contents in the glass composition.....	55
4.6 XRD pattern of the sol-gel ionomer glasses belonging to $4.5\text{SiO}_2\text{-4Al}_2\text{O}_3\text{-YP}_2\text{O}_5\text{-2CaO-2F}_2$ glass compositions, where Y= 0.15, 0.3 0.45 and 1.5. ....	56
4.7 High resolution XPS spectra in the (a) Al2p and (b) O1s regions of the sol-gel ionomer glasses based on $4.5\text{SiO}_2\text{-4Al}_2\text{O}_3\text{-YP}_2\text{O}_5\text{-2CaO-2F}_2$ glass compositions, where Y= 0.15, 0.3, 0.45 and 1.5.....	57
4.8 The concentration of (a) $\text{Si}^{4+}$ , (b) $\text{P}^{5+}$ , (c) $\text{Al}^{3+}$ and (d) $\text{Ca}^{2+}$ ions releasing from the sol-gel ionomer glasses based on $4.5\text{SiO}_2\text{-4Al}_2\text{O}_3\text{-YP}_2\text{O}_5\text{-2CaO-2F}_2$ compositions , where Y=0.15, 0.3, 0.45 and 1.5, as function of the immersion times.....	58
4.9 A proposed glass network structure for sol-gel ionomer glass with a variation of $\text{P}_2\text{O}_5$ contents in the glass composition. ....	58

## LIST OF FIGURES (Continued)

Figure	Page
4.10 The effect of Al <sub>2</sub> O <sub>3</sub> mole in the sol-gel ionomer glass on a) setting time and b) compressive strength of SGIC. The effect of P <sub>2</sub> O <sub>5</sub> mole in the sol-gel ionomer glass on c) setting time and d) compressive strength of SGIC. Note: (*) indicates the sol-gel sample (P/L= 1) and the commercial product (P/L = 3.4) with Al/(Si+P) nearby 1 for comparison. ....	59
4.11 The experimental design analysis of the effects of variation of Al <sub>2</sub> O <sub>3</sub> and P <sub>2</sub> O <sub>5</sub> contents in SGIC compositions on the net setting times .....	63
4.12 The DoE analysis for the compressive strength of SGIC with Al <sub>2</sub> O <sub>3</sub> and P <sub>2</sub> O <sub>5</sub> variation. (a) ANOVA analysis, (b) the main effects plot and (c) the interaction plot of Al <sub>2</sub> O <sub>3</sub> and P <sub>2</sub> O <sub>5</sub> contents in glass compositions for the compressive strength of SGICs.....	65
5.1 Schematic of experimental design to determine the substitution of ZnO for CaO and the optimization of calcination temperature.....	69
5.2 XRD pattern of the sol-gel ionomer glass belonging to the system of 4.5SiO <sub>2</sub> -4.0Al <sub>2</sub> O <sub>3</sub> -0.16P <sub>2</sub> O <sub>5</sub> -(2-x)Ca-xZnO-2F <sub>2</sub> , where x= 0, 0.6, 1.0 and 1.4 calcined at (a) 650°C and (b) 750°C.....	74
5.3 The high-resolution XPS spectra of a) Oxygen (O1s) and b) Aluminium (Al2p) for the sol-gel ionomer glass belonging to the system of 4.5SiO <sub>2</sub> -4.0Al <sub>2</sub> O <sub>3</sub> -0.16P <sub>2</sub> O <sub>5</sub> -(2-x)Ca-xZnO-2F <sub>2</sub> , where x= 0, 0.6, 1.0 and 1.4 calcined at 650°C as compared to the Zn-free ionomer glass calcined at 750°C.....	75
5.4 The high-resolution XPS spectra of a) Calcium (Ca2p) and b) Zinc (Zn2p) for the sol-gel ionomer glass belonging to the system of 4.5SiO <sub>2</sub> -4.0Al <sub>2</sub> O <sub>3</sub> -0.16P <sub>2</sub> O <sub>5</sub> -(2-x)Ca-xZnO-2F <sub>2</sub> , where x= 0, 0.6, 1.0 and 1.4 calcined at 650°C as compared to the Zn-free ionomer glass calcined at 750°C.....	77

## LIST OF FIGURES (Continued)

Figure	Page
5.5 Concentration of a) Al, b) Ca/Sr c) Zn d) Si and e) P ions releasing from the sol-gel ionomer glass belonging to the system of $4.5\text{SiO}_2\text{-}4.0\text{Al}_2\text{O}_3\text{-}0.16\text{P}_2\text{O}_5\text{-(}2\text{-x)Ca-xZnO-}2\text{F}_2$ , where $X= 0, 0.6, 1.0$ and $1.4$ calcined at $650^\circ\text{C}$ in comparison to Zn-free ionomer glass calcined at $750^\circ\text{C}$ as a function of the immersion time.....	79
5.6 Main effect plot and the interaction plot for compressive strength of SGIC containing different ZnO doping and the calcination temperatures.....	81
5.7 Net setting time of SGIC prepared from the sol-gel ionomer glass belonging to the system of $4.5\text{SiO}_2\text{-}4.0\text{Al}_2\text{O}_3\text{-}0.16\text{P}_2\text{O}_5\text{-(}2\text{-x)Ca-xZnO-}2\text{F}_2$ , where $x= 0, 0.2, 0.6, 1.0$ and $1.4$ and calcined at $600^\circ\text{C}$ $650^\circ\text{C}$ , $700^\circ\text{C}$ and $750^\circ\text{C}$ .....	82
5.8 Compressive strength of SGIC belonging to the system of $4.5\text{SiO}_2\text{-}4.0\text{Al}_2\text{O}_3\text{-}0.16\text{P}_2\text{O}_5\text{-(}2\text{-x)Ca-xZnO-}2\text{F}_2$ , where $x= 0.2, 0.6, 1.0,$ and $1.4$ and calcination temperature of $600^\circ\text{C}$ $650^\circ\text{C}$ , $700^\circ\text{C}$ and $750^\circ\text{C}$ .....	83
5.9 XANES spectra of GIC samples prepared with 0, 0.6 and 1.4 Zn doped sol-gel glasses calcined at $650^\circ\text{C}$ at a) Ca K-edge and b) Zn K-edge. ....	85
5.10 Ca and Zn K-edge EXAFS (weighted by $k^2$ ) from the experiment (black line) and fitting (red circle) of GIC samples prepared with 0, 0.6 and 1.4 Zn doped sol-gel glasses calcined at $650^\circ\text{C}$ .....	86
5.11 A proposed glass network structure for ZnO instead of CaO in the sol-gel ionomer glass network and form crosslinking with polyacrylic acid in glass ionomer cement after setting. ....	87
5.12 The diameter of inhibition zone against <i>S. mutans</i> of SGIC samples prepared with 0, 0.6 and 1.4 Zn doped sol-gel glasses calcined at $650^\circ\text{C}$ . ....	89

## LIST OF FIGURES (Continued)

Figure	Page
5.13 Effect of Zn content in SGIC on the NIH/3T3 cell viability (indirect contact). (a) %cell viability treated with different concentrations of the extracted solutions. The cells with fresh culture medium were used as a negative control. Values were expressed as the mean $\pm$ standard error of the mean of three independent experiments and (b) the Zn <sup>2+</sup> ion releasing concentration in the as-received extracted solutions analyzed by the ICP-OES technique. ....	90
5.14 SEM micrographs of the surface for SGIC prepared with the sol-gel glasses doped different ZnO contents and calcined at 650°C after soaking in DI water and artificial saliva for 5 days, respectively (magnification x5000) .....	92
5.15 SEM images of the interfacial area between the tooth and SGIC samples prepared with 0.6 ZnO doped glass and calcined at 650°C as compared to ZnO free SGIC. ....	93
6.1 Hydrothermal synthesis procedure of SrFA .....	97
6.2 Schematic of experimental design to determine the effect of SrBGF additive on the properties of SGIC. ....	98
6.3 Schematic of experiment design to evaluate ability to release and uptake fluoride. ....	101
6.4 a) XRD pattern of the synthesized SrFA additive, and b) TEM micrographs and EDS analysis of SrFA additive .....	102
6.5 Working and net setting time of SGIC containing with 0, 1, 3 and 6 wt.% of SrFA. ....	103
6.6 Compressive strength of SGIC containing with 1, 3, and 6 wt.% of SrFA additives. ....	104

## LIST OF FIGURES (Continued)

Figure	Page
6.7 Agar diffusion method for SGIC containing with 0, 1, 3, and 6 wt.% of SrFA against <i>S.mutans</i> . The inhibition zone was observed and measured by stereo microscope with magnification of 0.67x, using NIS element microscope imaging software. Error bars are standard error of the mean (n=3).....	105
6.8 SEM-EDS of the surface of SGIC containing 0, 1, 3, and 6 wt.% of SrFA after immersion in artificial saliva for 5 days, in comparison with a commercial product.....	107
6.9 AlamarBlue reduction percentage of NIH/3T3 fibroblast cells on SGIC surface with the different SrFA contents at incubation period of 1 day, 7 days and 14days. Control was referred to the cell-cultured on the glass cover slip. Error bars are standard error of the mean (n=3).....	109
6.10 Concentration of fluoride release and uptake of SGIC containing with 0, 1, 3, and 6 wt.% of SrFA in comparison with the commercial product. Error bars are standard error of the mean (n=3).....	110
7.1 Sol-gel synthesis procedure of SrBGF.....	115
7.2 Schematic of experimental design to determine the effect of SrBGF additive on the properties of SGIC.....	116
7.3 Illustration of experiment procedures performed to evaluate remineralization ability.....	119
7.4 The experimental procedure of fluoride release and uptake ability of SrBGF powder and SGIC samples and their characterization. (*F <sup>-</sup> ISE = Fluoride Ion Selective Electrode technique).....	122
7.5 a) XRD pattern of the synthesized SrBGF additive, and b) TEM micrographs and EDS analysis of SrFA additive.....	124
7.6 Working and net setting time of the sol-gel GIC containing with 0, 1, 3 and 6 wt.% of SrBGF.....	125

## LIST OF FIGURES (Continued)

Figure	Page
7.7 Compressive strength of SGIC with the different contents of SrBGF. Error bars are standard error of the mean (n=8). Stars (*) denote $p < 0.05$ .....	126
7.8 Comparison of average surface roughness value of SGIC, SGIC/SrBGF, SGIC/SrFA and commercial GIC. Sa is the arithmetic average of the 3D roughness. Error bars are standard error of the mean (n=8). Stars (*) denote $p < 0.05$ .....	128
7.9 The antibacterial activity of the SGIC, SGIC/SrBGF and SGIC/SrFA against <i>S.mutans</i> . (a) The stereo microscope images of <i>S.mutans</i> inhibition area around the specimens. The average and standard deviation of inhibition zone was calculated from 3 individual samples. (b) The bacterial adhesion to the specimen's surface. Arrows indicated the chain of <i>S. mutans</i> .....	130
7.10 $\mu$ CT visualization of the dentine before and after remineralization. Colors were assigned based on density levels, with darker colors indicating lower density levels and lighter colors reflecting higher density levels.....	131
7.11 a) SEM images and EDS data of mineral deposition on dentin surface during remineralization process. b) the change of atomic percentage of Ca and P deposited on the dentin surface after remineralization. Error bars are standard error of the mean (n=3). Same letters indicate no significance between groups ( $p < 0.05$ ), capital letters representing Ca atomic percentage and non-capital letters representing P atomic percentage.....	133

## LIST OF FIGURES (Continued)

Figure	Page
<p>7.12 (a) ion concentration change after soaking SGIC specimens in cell culture medium at Day 1 and Day 7. All ions of each condition were subtracted by the control cell culture medium (blank), showing that the negative value are the ions absorbed by samples and the positive value are ions released by samples, (b) pH value of cell culture medium after soaking SGIC specimens at Day 1 and Day 7. Error bars are standard error of the mean (n=3). Same letters indicate no significance between groups (<math>p &lt; 0.05</math>).....</p>	136
<p>7.13 hASC proliferation: (a) metabolic activity of cell on tissue plastic plate cultured with sample-conditioned medium (b) DNA concentration of the cell on tissue plastic plate cultured with sample-conditioned medium. (c) metabolic activity of the cell cultured directly on GIC surface (d) DNA concentration of the cell on GIC surface. Error bars are standard error of the mean (n=3). Same letters indicate no significance between groups (<math>p &lt; 0.05</math>). (e) live/dead assay of hASC on each GIC samples, magnification of x10. Red and green stains represent dead and living cells, respectively. ....</p>	138
<p>7.14 Cell viability of hDPSCs treated with the extract solution for 24 hours. Control is referred to the cells-cultured on the tissue culture well with the fresh medium. Values were expressed as the mean <math>\pm</math> standard error (n=3) (<math>P &lt; 0.05</math>). ....</p>	140
<p>7.15 Amount of fluoride released from SGIC, SGIC/1SrBGF, and the commercial GIC in artificial saliva after soaking for 1 week during releasing and after uptake in NaF solution. Note that the P:L ratio of commercial product (com) is 3.4:1. Error bars are standard error of the mean (n=8). Same letters indicate no significance between groups (<math>p &lt; 0.05</math>) Capital letters representing amount of fluoride release and non-capital letters representing amount of fluoride uptake. ....</p>	141

## LIST OF FIGURES (Continued)

Figure	Page
7.16 Surface analysis of SGIC, SGIC/1SrBGF, and the commercial GIC (com), (a) SEM image and EDS analysis of glass and matrix area on the glass ionomer cement surface before fluoride-releasing and (b) Atomic % of fluoride on GIC surfaces during fluoride uptake cycle: before release, after release and after uptake. The values shown in the graph are the mean $\pm$ standard error derived from at least 3 different analysis areas. ....	143
7.17 High-resolution XPS spectra of fluoride (F1s) for (a) SGIC (b) SGIC/1SrBGF and (c) the commercial GIC before fluoride releasing and (d) SGIC (e) SGIC/1SrBGF and (f) the commercial GIC after fluoride uptake. The percentages represent the concentration of each binding state based on the graphed area. ....	145
7.18 High-resolution XPS spectra of fluoride (Sr3d) for (a) SGIC/1SrBGF and (b) the commercial GIC before fluoride releasing and (c) SGIC/1SrBGF and (d) the commercial GIC after fluoride uptake. The percentages represent the concentration of each binding state based on the graphed area. ....	149
7.19 The proposed fluoride release and uptake mechanisms of the SGIC and the SGIC containing SrBGF additive. ....	150

## LIST OF ABBREVIATIONS

$\mu\text{CT}$	=	Micro computed tomography
$\mu\text{g}$	=	Microgram
Al	=	Aluminium
$\text{Al}(\text{NO}_3)_3$	=	Aluminum nitrate
$\text{Ca}(\text{NO}_3)_2$	=	Calcium nitrate
$\text{CaF}_2$	=	Calcium fluoride
CN	=	Average coordination number of oxygens around the atom
Com	=	Commercial
DI	=	Deionized water
EDS	=	Energy dispersive spectroscopy
ETOH	=	Absolute ethanol
EXAFS	=	Extended X-ray absorption fine structure
$\text{F}^-$	=	Fluoride
F	=	Fluorine
FTIR	=	Fourier-transform infrared spectroscopy
g	=	Gram
GICs	=	Glass ionomer cements
$\text{H}_2\text{SiF}_6$	=	Hexafluoro silicic acid
hASCs	=	Human adipose stem cells
hDPSCs	=	Human Dental pulp stem cells
$\text{HNO}_3$	=	Nitric acid
ICP-OES	=	Inductively coupled plasma optical emission spectroscopy
ml	=	Milliliter
mm	=	Millimeter
Na	=	Sodium
$\text{NH}_4\text{OH}$	=	Ammonium hydroxide solution
$\emptyset$	=	Diameter

## LIST OF ABBREVIATIONS (Continued)

O	=	Oxygen
O <sup>2-</sup>	=	Oxide
°C	=	Degree Celsius
OH <sup>-</sup>	=	Hydroxide
P	=	Phosphorus
P:L	=	Powder to liquid
PAA	=	Poly(acrylic acid)
PAA-Co-MA	=	Poly(acrylic acid-co-maleic acid)
R	=	Interatomic distance
Rw	=	water to precursor ratio
SEM	=	Scanning electron microscopy
SGICs	=	Sol-gel derived glass ionomer cements
Si	=	Silicon
Sr	=	Strontium
Sr(NO <sub>3</sub> ) <sub>2</sub>	=	Strontium nitrate
SrBGF	=	Strontium containing fluorinated bioactive glass
SrFA	=	Strontium containing fluorapatite
TEM	=	Transmission electron microscopy
TEOS	=	Tetraethyl orthosilicate
TEP	=	Triethyl phosphate
XANES	=	X-ray absorption near-edge structure
XAS	=	X-ray absorption spectroscopy
XPS	=	X-ray photoelectron spectroscopy
XRD	=	X-ray diffraction
Zn(NO <sub>3</sub> ) <sub>2</sub>	=	Zinc nitrate
$\sigma^2$	=	Debye-Waller factor

# CHAPTER 1

## INTRODUCTION

### 1.1 Rationale and background

Recently, the elder population around the world has increased continuously. The elderly, those who are 60 years old become weaker and more susceptible to disease. Systemic disease may lead to oral infection such as periodontal disease and dental caries. These problems are mainly caused by acid-produced from bacteria resulting in subsurface demineralization of the teeth (Wong, Subar and Young, 2017). The severe demineralization generates a cavity on the tooth surface. This can be treated by surgical removal of tooth structure and dental restoration such as filling, crown, and root canal. General types of the restorative dental materials are listed in Table 1.1. Among them, the conventional glass ionomer cement is attractive because it is able to release the fluoride ions into the oral cavity leading to tooth decay resistivity. Moreover, it is able to bond with moist tooth surface leading to an unnecessary for removal tooth surface (California, 2005)

Glass Ionomer Cement (GIC) has been widely used in clinical practice to treat patients with high-risk dental caries, including the elderly, children, or bedridden patients. GIC is often used in combination with the minimally invasive Atraumatic Restorative Treatment (ART) technique, which involves removing decayed tooth tissue using hand instruments and placing GIC material (Holmgren, Roux and Doméjean, 2013). However, this technique may not completely remove the caries lesion. To prevent further expansion of caries lesion, GIC was expected to have bioactivity and antibacterial properties. Otherwise, it could develop to secondary caries, leading to the filling loosening and eventually fail.

Table 1.1 advantages and disadvantages of the filling dental materials (California, 2005)

Materials	Setting	Advantages	Disadvantages
Amalgam	Self-hardening	<ul style="list-style-type: none"> <li>- Long lasting</li> <li>- Wears well</li> <li>- Inexpensive</li> <li>- No shrinkage and resist leakage</li> <li>- Resistance to further decay</li> </ul>	<ul style="list-style-type: none"> <li>- Grey color</li> <li>- Able to be corroded</li> <li>- Require removal of some healthy tooth</li> <li>- High thermal conductivity</li> <li>- Inducible to electricity</li> </ul>
Composite resin filling	Light-cure hardening	<ul style="list-style-type: none"> <li>- Strong and durable</li> <li>- Tooth color</li> <li>- No corrosion</li> <li>- Maximum amount of tooth preserves</li> </ul>	<ul style="list-style-type: none"> <li>- High cost</li> <li>- Shrinkable and could lead to further decay</li> <li>- Wear faster than dental enamel</li> </ul>
Glass ionomer cement	Self-hardening	<ul style="list-style-type: none"> <li>- Able to release fluoride</li> <li>- Not necessary to removal tooth surface</li> <li>- Low incident of producing tooth sensitivity</li> <li>- Able to mix by hand</li> </ul>	<ul style="list-style-type: none"> <li>- High cost (similar to the composite resin)</li> <li>- Not recommend for biting surface of permanent teeth</li> <li>- Easy to crack overtime and can be dislodge</li> </ul>
Resin-ionomer cement	Light cure hardening	<ul style="list-style-type: none"> <li>- Very good esthetics</li> <li>- Able to release fluoride</li> <li>- Minimal amount of tooth needs to be removed</li> <li>- Hold up better that GIC but lower than composite resin</li> <li>- Good resistance to leakage</li> </ul>	<ul style="list-style-type: none"> <li>- High cost (similar to composite resin)</li> <li>- Not recommend restoring the biting surfaces of adults</li> <li>- Wear faster than composite and amalgam</li> </ul>

Bioactivity refers to the ability of a material to form a chemical bond with the surrounding living tissues and support the formation of hydroxyapatite, a mineral compound that forms tooth enamel and dentin. The conventional GIC was reported to have poor bioactive activities since it was composed with polymeric acid that inhibited apatite formation (Chen, Cai, Engqvist et al., 2016). In addition, conventional GIC has been reported to have low antibacterial efficiency because antibacterial activity is primarily affected by fluoride release. However, F ions are unable to prevent the occurrence of initial bacterial adhesion (Farrugia and Camilleri, 2015).

The enhancement of bioactivities and antibacterial properties of biomaterials has been extensively studied. Incorporating biomaterial additives, such as bioactive glass, hydroxyapatite nanoparticles, and chlorhexidine, into GIC has been shown to improve its bioactivity and antibacterial properties. The use of cation dopants has also been considered for the development of ionomer glass compositions. However, it should be noted that these methods may have an adverse effect on the physical properties of the material.

The conventional GIC was typically produced by a melt quenching method at high temperatures (1,200–1,400°C), which resulted in composition loss and air pollution. Furthermore, data from Thai Customs reports that Thailand has been importing GIC products from abroad at a cost of around 100 million baht per year. Therefore, it is interesting to develop this material using an alternative production method. The sol-gel method is an attractive alternative production technique as it can be performed at lower temperatures (600-800°C) and allows for easier control over glass composition.

This study is interested in producing the glass ionomer powder by the low temperature process of sol-gel method including improvement the bioactivity and antibacterial properties of the material in order to overcome the limitations of conventional GIC. Moreover, maintaining the physical properties of the newly developed sol-gel glass ionomer cement (SGIC) is also considered.

## 1.2 Research objective

- 1.2.1 To synthesis the glass ionomer powder by the sol-gel method, which is a simple process, low temperature and cost-effective.
- 1.2.2 To develop the antibacterial activity and bioactivity of the low cost GICs including with remaining of good mechanical properties as comparison to the commercialized product for commercialization as a dental restorative cement.

## 1.3 Scope and limitation

- 1.3.1 To study the factor for synthesis the glass ionomer powder by the low-cost sol-gel method
- 1.3.2 To determine the effect of dopant such as metal ions type and concentration on the antibacterial activity and bioactivity of the glass ionomer cement and maintain the good mechanical properties for using as a dental restorative cement.

## 1.4 Expected benefits

- 1.4.1 To obtain the GIC with the antibacterial activity and bioactivity including with good mechanical properties for dental restorative cement and able to apply for periodontal and caries treatment in elderly people.
- 1.4.2 To reduce the imported commercial products and get knowledge to develop restorative dental materials.

## 1.5 Outline of Thesis

The remainder of this thesis is built up in the following way:

Chapter 2 provides the theoretical background information of GICs including their properties and the synthesis method. This chapter also provides the literature review of the limitation of the conventional GICs, the sol-gels synthesis of glass and the ionomer glass as well as the enhancement of the GICs properties by using the dopant and additive.

Chapter 3 shows the investigation of synthesis condition for ionomer glass by the sol-gel method. The study focuses on the effect of important factors for the sol-gel synthesis process, including water to precursor ratio ( $R_w$ ), pH, calcination temperature, and ageing method. The synthesized ionomer glass was then characterized using XRD and FTIR techniques. Additionally, the basic physical properties of the cement, including setting time and compressive strength, were also determined.

Chapter 4 provides a more comprehensive understanding of the factors that influence the physical properties of ionomer glass by the sol-gel method. By using the synthesis method obtained from Chapter 3, this chapter extended to study the effect of varying the amounts of  $Al_2O_3$  and  $P_2O_5$  on the glass structure and its physical properties. The Design of Experiments (DoE) technique was utilized to design the experiment and assist in result analysis. The study employed the X-ray photoelectron spectroscopy (XPS) technique to determine the structural changes in the glass, while also evaluating the ion releasing behavior to clarify the setting reaction and its related physical properties.

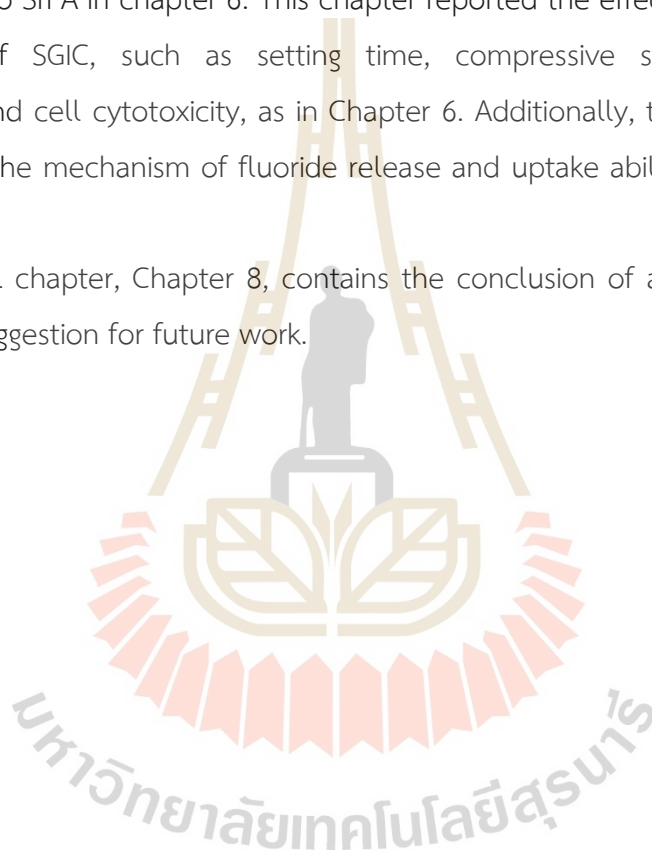
Chapter 5 focuses on improving the biological properties of the ionomer glass obtained from Chapter 4. This was achieved by doping ZnO into the ionomer glass and investigated the effect of calcination temperature to optimize the physical properties of SGIC. As in Chapter 4, the DoE technique is used to design and analyze the effect of the dopant on the physical properties. To gain a deeper understanding of the relationship between the physical properties and the structure of the ionomer glass and cement, XPS techniques and synchrotron-based X-ray absorption spectroscopy (XAS) techniques were utilized. The chapter also investigated the antibacterial properties, ability to form apatite crystal, and cell cytotoxicity of the ionomer glass, further expanding our understanding of its biological properties. The results of this study provided valuable insights into the potential applications of ionomer glass in the field of biomedical materials.

Chapter 6 continues to explore the enhancement of antibacterial properties and bioactivity by incorporating strontium-containing fluorapatite (SrFA) into SGIC which previously obtained from chapter 5. The chapter describes the synthesis of SrFA

nanoparticles through the hydrothermal method and their use as an additive to SGIC. The impact of SrFA on the setting time and compressive strength of SGIC was investigated, as well as its antibacterial properties, cell cytotoxicity, and fluoride release and uptake ability.

Chapter 7 shifts to exploring the benefits of incorporating strontium-containing fluorinated bioactive glass (SrBGF) into SGIC. The purpose was to evaluate its influence on the enhancement of antibacterial properties and bioactivity, in comparison to SrFA in chapter 6. This chapter reported the effect of SrBGF on various properties of SGIC, such as setting time, compressive strength, antibacterial properties, and cell cytotoxicity, as in Chapter 6. Additionally, the study investigated deeper into the mechanism of fluoride release and uptake ability of SGIC containing SrBGF.

The final chapter, Chapter 8, contains the conclusion of all the findings in this thesis and suggestion for future work.



## CHAPTER 2

### LITERATURE REVIEWS

#### 2.1 Glass ionomer cement (GICs)

Glass ionomer cements or glass polyalkenoate cements are based on the reaction between the basic glass powder and the aqueous solution of polymeric acid. They have been widely used in dental application as base, filling and restorative materials because of their interesting properties: self-curing ability, fluoride releasability causing long-term anti-cariogenic potential, ability to place in the cavity without bonding agent, low shrinkage, etc. (Khoroushi and Keshani, 2013).

The GIC was first produced by Wilson and Kent from the Laboratory of the Government Chemist in the late 1960s (Baig and Fleming, 2015). They found that the rapid hardening reaction would be occurred when the alumino-silicate based glass was mixed with aqueous solution of polyacrylic acid (Wilson and Kent, 1971). The glass powder could be produced by melting  $\text{SiO}_2$ ,  $\text{Al}_2\text{O}_3$ ,  $\text{Na}_3\text{AlF}_6$ ,  $\text{CaF}_2$ ,  $\text{AlF}_3$  and  $\text{AlPO}_4$  at 1,050-1,350°C, for 45-120 minutes. Then, the glass was rapidly cooled to form opal glasses and followed by grinding to pass 350-mesh sieved.

##### 2.1.1 GICs composition and setting reaction.

Glass ionomer cement has three ingredients: polymeric acid, ion leachable glass, and water. The GI powders are based on alumino-silicate glass and include calcium, phosphorus, and fluoride. The glass ionomer cement is formed by cross-linking between metal ions ( $\text{M}^+$ ) from the glass powder and the polyacrylate group ( $\text{COO}^-$ ) from the aqueous solution of polymeric acid, resulting in the polysalt formation. The extension of the polysalt crosslinking increases the Young's modulus of the cement, resulting in an improvement of its mechanical properties (Lohbauer, 2010).

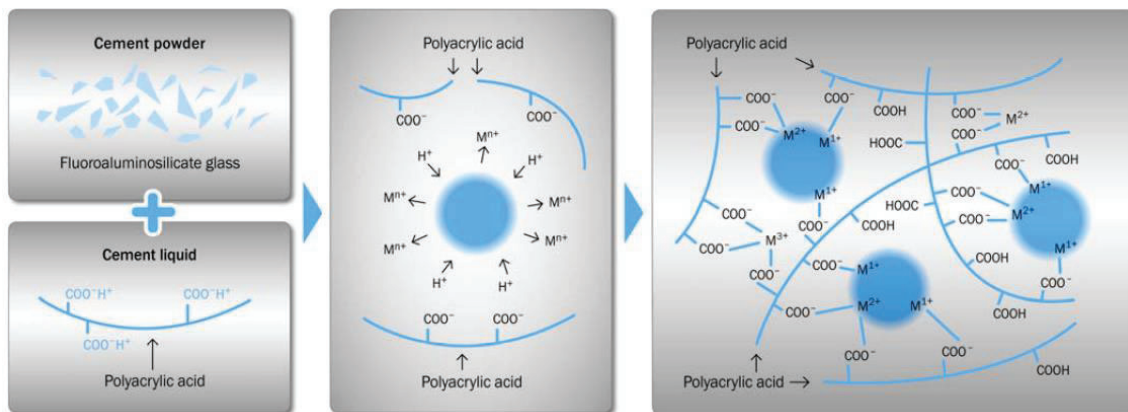


Figure 2.1 Setting reaction of glass ionomer cement (Lohbauer, 2010)

The setting reaction is an acid-base reaction between aluminosilicate powder and polyacrylic acid (Khoroushi and Keshani, 2013, Nicholson and Czarnecka, 2016). The first step of reaction involves with acid attack on the susceptible site of the glass powder. The metallic cations such as  $Ca^{2+}$  ions (or  $Sr^{2+}$  ions) and  $Al^{3+}$  ions are then released. After the cations move into the aqueous phase, the crosslinking between carboxylate group ( $-COOH$ ) of polyacrylic acid and the cations occurs and results in hard polysalt matrix as shown in Figure 2.1. The completed hardening reaction is achieved after 24 hours. The final cement structure consists of unreacted glass, which acts as reinforcing filler, surrounded by the polysalt matrix.

The glass ionomer powder is an amorphous which mainly in system of  $SiO_2-Al_2O_3-P_2O_5-CaO-CaF_2$ , with the network as shown in Figure 2.2. The glass matrix was composed of Si-O-Al network (Nicholson and Czarnecka, 2016). The  $Al^{3+}$  ions are substituted in the tetrahedral site of the  $Si^{4+}$  ions. This substitution results in an excessive negative charge in the glass network. Additional positive charge ions ( $Na^+$ ,  $Ca^{2+}$ ,  $Sr^{2+}$ , or  $Mg^{2+}$ ) can neutralize this charge deficit and act as glass network modifiers. Moreover, incorporation of these cations creates an additional class of oxygen called non-bridging oxygen (NBO). The glass with a high amount of NBO structure tends to react well with the polyacrylic acid because it is degradable by acid attack (Wren, Clarkin, Laffir et al., 2009). The glass powder compositions with their functions are summarized in Table 2.1.

The influence of the glass component on the GIC properties are showed in Figure 2.2. The water is a critical component in the setting reaction of GIC. When the polymeric acid dissolves in water, it releases protons that attack the basic glass and initiate the setting reaction. Once the reaction is complete, the water incorporates into the cement structure, resulting in increased translucency and an enamel-like appearance similar to natural teeth (Czarnecka and Nicholson, 2006, Khoroushi and Keshani, 2013, Nicholson and Czarnecka, 2016)

Table 2.1 The glass compositions (mol ratio) of the glass ionomer powder and their function

Glass components	Melt quenching (G338)	Sol-gel (Cestari, 2016)	Commercial (Fuji IX)	Function
SiO <sub>2</sub>	4.5	4.5	4.5	Glass matrix
Al <sub>2</sub> O <sub>3</sub>	5	6	5	Glass matrix
CaO	2	5	-	Network modifier
P <sub>2</sub> O <sub>5</sub>	2	3	1	Charge balancing agent
F	14	4	5	Fluoride source, The flux for lowering melting temperature
Na <sub>2</sub> O	1	-	0.5	Network modifier, The flux for lowering melting temperature
SrO	-	-	2	Network modifier

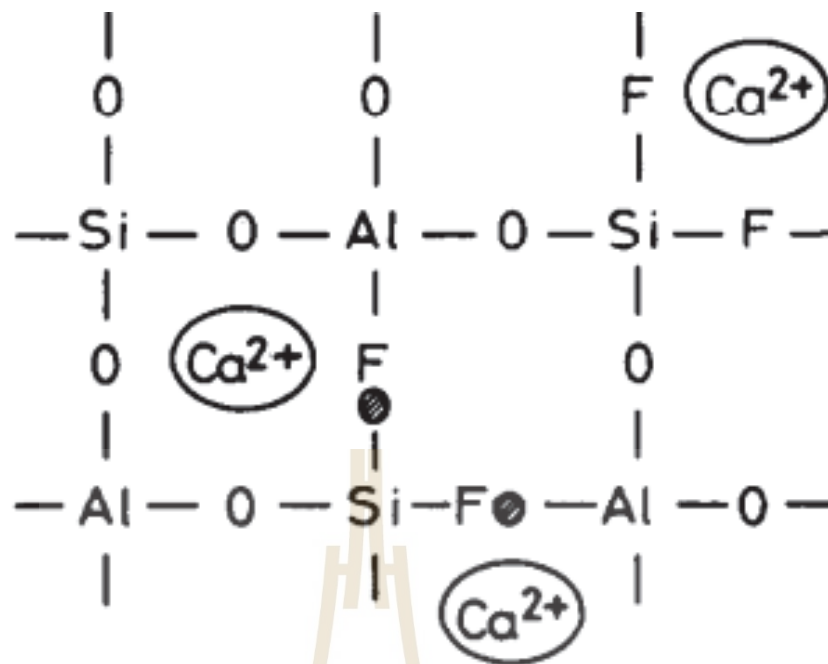


Figure 2.2 Schematic of calcium-alumino-silicate glass network containing fluorine (Wood and Hill, 1991)

The water is a critical component in the setting reaction of GIC. When the polymeric acid dissolves in water, it releases protons that attack the basic glass and initiate the setting reaction. Once the reaction is complete, the water incorporates into the cement structure, resulting in increased translucency and an enamel-like appearance similar to natural teeth (Khoroushi and Keshani, 2013, Nicholson and Czarnecka, 2016).

In addition, tartaric acid also play important role in the setting reaction (Nicholson and Czarnecka, 2016). It is a reaction controlling agent which readily attacks the glass ionomer surfaces. After the attacking, the metallic cations from glass ionomer are released following by bonding to the polyanion of tartaric acid. Hence, in the early state of setting reaction the metal carboxylate formation was retarded resulting in extension of the working time which led to facilitative mixing process (Prosser, Richards and Wilson, 1982, Nicholson, Brookman, Lacy et al., 1988).

Table 2.2 Influence of the glass components on the properties of the GICs

Component	Molar ratio	Working time (minute)	Setting time (minute)	Compressive strength (MPa)	Conclusion	References
Al:Si	5.5:4.5	3	11	148.1±9.3	no significant influence on the properties	(Griffin and Hill, 1999)
	6:4	3.5	11	142.5±5.3		
	7:3	2.7	8.3	146.8±1.2		
P <sub>2</sub> O <sub>5</sub>	0	-	-	-	- extends the setting and working times - high amount of P <sub>2</sub> O <sub>5</sub> disrupts the crosslinking process in the cement matrix	(Griffin and Hill, 2000)
	1.5	3.7	10	191.1±8.1		
	2.3	4.3	88	8.32±0.5		
CaF <sub>2</sub>	0	3.8	44	64	- resulted in shorter working and setting times - increased Young's moduli and compressive strengths	(Griffin and Hill, 2000)
	0.5	3.4	14	150		
	1	2.2	7.8	161		
F <sup>-</sup>	0	43	65	74.3±5.0	improved compressive strength. increased translucency of the set cement inhibited dental carries formation	(Griffin and Hill, 2000)
	1	15	19	165.0±10.9		
	3	6	7.5	190.5±7.9		

\* Setting reaction too fast to form homogenous cement paste

## 2.2 Clinical Applications of GICs and problems

### 2.2.1 Type of GICs

Because conventional GICs are made of brittle materials, materials are always used in the area without bearing load, such as for root caries, rampant caries, temporary filling during root canal treatment, filling classes III and V, and temporary sealant. At present, the GICs have been classified by Wilson and McLean into three type depending on their properties and intended clinical used (Nicholson and Czarnecka, 2016), as followed:

#### Type I: Luting and bonding cement

The first type was used for cementation of crowns, bridges, inlays, on lays and orthodontic application. This typed of GICs are required fast setting with good water resistant at early stage of setting reaction, low powder to liquid ratio and moderate mechanical properties.

#### Type II: Restorative cement

High strength and ratio of powder to liquid are required for this type of cement. Their use has been divided into two sub-appearances. For anterior repair, aesthetic of materials is very important. The color has to be match and translucent. On the other hand, the appearance of the GICs used for the posterior restoration or repair is unimportant but fast set and early resistant to water uptake are required. Thus, a high powder to liquid ratio is needed.

#### Type III: Lining or base cements

This type of GICs is usually used as a base for further treatment such as root canal treatment. The viscosity of the early stage of the cement must be low and a low powder to liquid ratio is required to allow good adaptation to cavity walls.

### 2.2.2 Atraumatic restorative treatment (ART)

Atraumatic Restorative Treatment (ART) is a minimal intervention approach for managing dental caries, which was developed in the 1980s. The ART philosophy focuses on the importance of caries risk diagnosis and evaluation, as well as prevention, stabilization, and remineralization of early lesions, and minimally invasive restorative treatment for cavitated dentine lesions. It was originally designed to provide effective preventive and restorative care in underserved communities. The

ART approach has gained worldwide popularity over the past two decades (Holmgren et al., 2013).

This ART technique involves excavating soft, demineralized tooth tissue using hand instruments rather than rotary instruments, followed by restoring the cavity with a high viscosity GIC using a press finger technique. GICs are considered an ideal material for the ART technique due to their remineralization ability since it is a process of restoring and replacing the missing minerals (hydroxyapatite) of tooth surfaces in order to achieve balancing mechanism. It has been reported that GIC with remineralization ability can replenish the missing mineral and enhance the hardness of demineralized soft tissue.

### **2.2.3 Secondary caries**

Secondary caries is a dental condition that occurs between the restorative material and tooth tissue, and it is a major cause of dental restoration failure (Askar, Krois, Göstemeyer et al., 2020). When using the ART technique for dental restoration, there is a possibility of caries lesions remaining in the tooth tissue, leading to the development of secondary caries from the expansion of the caries lesion. In addition, secondary caries can also form due to cracks or gaps between the tooth and restorative material. These gaps can allow saliva and cariogenic bacteria to penetrate and grow, resulting in the formation of secondary caries. A gap larger than 50  $\mu\text{m}$  is particularly problematic, as it provides enough space for bacterial growth and secondary caries formation (Feng, 2014, Askar et al., 2020). To prevent the formation of secondary caries, it is important for the restorative material to have both antibacterial properties and remineralization ability. These properties help to inhibit bacterial growth and balance the mineral levels of the tooth, reducing the likelihood of secondary caries formation. This can help to improve the overall success and longevity of dental restorations.

## **2.3 Properties and limitation of GICs**

### **2.3.1 Mechanical and physical properties**

The mechanical properties of the commercial GICs and sol-gel synthesized GIC comparison to the natural dentine and enamel are listed in Table 2.3. In general,

the compressive strength of GIC ranges about 70-200 MPa (Lohbauer, 2010). As stated in section 2.1.1, the properties of GICs are influenced by crosslinking between glass particles and polyacrylate group. The glass powder with high susceptible to acid attack structure was more likely to form the polysalt crosslinking resulting in improvement of the cement mechanical properties. Moreover, other factors such as powder to liquid ratio (P:L), size of the GI particles, concentration of polyacrylic acid and age of specimens are also considered (Nicholson and Czarnecka 2016).

In addition, the bonding or adhesive between the GIC and the human tooth is considered because it is essential in preventing of oral fluid leakage (Lin, McIntyre and Davidson, 1992). The adhesion can be the result of two interrelated phenomena. The first one is micromechanical interlocking. The latter is the chemical bonding of  $\text{PO}_4^{3-}$  ions in hydroxyapatite of dental tissue with carboxylate group of polyacrylic acid (Lohbauer, 2010)

Table 2.3 Mechanical properties of GICs, dentine and enamel

Materials	Properties		References
Dentine	Compressive strength	$193.7 \pm 30.6$ MPa	(Chun, Choi and Lee, 2014)
	Hardness	0.5 – 5 GPa	(Zhang, Du, Zhou et al., 2014)
	Elastic modulus	10 – 45 GPa	(Zhang et al., 2014)
Enamel	Compressive strength	$62.2 \pm 23.8$ MPa	(Chun et al., 2014)
	Hardness	3 – 6 GPa	(Zhang et al., 2014)
	Elastic modulus	40 – 105 GPa	(Zhang et al., 2014)
Fuji II	Compressive strength	127-131 MPa	(Lohbauer, 2010)
Fuji IX	Compressive strength	135.4-198 MPa	(Bonifácio, Kleverlaan, Raggio et al., 2009)
Sol-gel GICs (luting cement)	Vickers's Microhardness (HV)	17.5 – 24.9	(Bertolini, Zaghete, Gimenes et al., 2009)
Sol-gel GIC	Compressive strength	103-146.25 MPa	(Tu, Su and Ran, 2016)

### 2.3.2 Antibacterial activity

Bacteria are the main cause of the demineralization of tooth hard tissue and infection of tooth support tissue. Untreated demineralization and infection could lead to the final stage of tooth loss. The dental restorative materials require the properties of preventing bacterial growth and surface colonization. In the case of the conventional GICs, the antibacterial activity is mainly affected by fluoride releasing. However, the  $F^-$  ions are incapable of preventing the occurring process of initial adhesion of bacteria. The old versions of antibacterial activity improvement are focus on the release of incorporated antibacterial agents such as zinc ions, silver ions, antibiotics, iodine, and chlorhexidine (Takahashi, Imazato, Kaneshiro et al., 2006, Farrugia and Camilleri, 2015). On the other hand, high releasing amount of antibactericides lead to decrease in natural characteristic of the restorative materials. Hence, the development of superb antibacterial properties along with acceptable physio-chemical properties are still challenging (Hafshejani, Zamanian, Venugopal et al., 2017).

### 2.3.3 Bioactivity

The bioactivity of dental or orthopedic materials is related to the formation of an apatite interlayer and the integration of the bone with the surface of the restorative material. Dental materials with bioactivity not only exhibit remineralization ability, but also interact with the natural mineral content of the tooth to repair and rebuild it. Therefore, bioactive material is able to reduce a margin gap and prevent recurrent caries at the interface between filling material and tooth surfaces from further acid attacks (Albeshti, 2016, Tiskaya, Al-eesa, Wong et al., 2019).

Conventional GICs were reported to have poor bioactivity since bonding strength between the tooth surface and the material was weak. This is because the polymeric aqueous from the conventional GIC is acidic, which inhibits apatite formation. (Chen et al., 2016). Adding bioactive agents, such as fluorapatite, bioactive glass, etc. has been widely used to improve the bioactivity of GICs. Fluoride-containing bioactive glass, especially when strontium is added, has shown enhanced bioactivity and stability of apatite formation, which can be more beneficial for caries prevention (De Caluwé, Vercruyse, Ladik et al., 2017, Dai, Nudelman, Chu et al.,

2021). The nano-size, spherical shape, and mesoporous structure of the bioactive glass particle can also improve biocompatibility and promote apatite-like formation, resulting in superior bioactivity (Thaitalay, Giannasi, Niada et al., 2022).

Another candidate for improving bioactivity in dental materials is the strontium-containing fluorapatite nanoparticle (SrFA), which has shown promising antibacterial activity and biocompatibility. Incorporating fluorapatite (FA) powder into dental materials can improve their resistance to acid penetration and the ability to form fluorapatite, which is more resistant to acid compared to hydroxyapatite found in human dental structures (Moshaverinia, Ansari, Moshaverinia et al., 2008, Balhuc, Campian, Labunet et al., 2021). FA doped with strontium (SrFA) has also been investigated for its potential to enhance biocompatibility and antibacterial activity, with promising results against *Streptococcus mutans* (Wang, Li, Tang et al., 2019).

#### 2.3.4 Biocompatibility

Biocompatibility is a term used to describe the ability of a dental material to interact with living tissues without causing any negative effects such as inflammation, toxicity, or allergic reactions. A dental material that is considered biocompatible should function effectively within the oral environment without negatively affecting the surrounding tissues, including teeth, gums, bones, and other structures.

In preliminary study, the biocompatibility of GICs can be evaluated based on their toxicity to cells. During the restoration, dental materials can have unexpected effects when they come into contact with periapical tissues. The by-products produced by these materials can penetrate the dentinal tubules and surrounding tissues, potentially causing adverse effects at the apex (Aghazade, Samiei, Imani et al., 2020). Therefore, it is crucial to determine the cytotoxicity of the newly developed dental material.

In a previous study, *in vitro* testing was conducted to determine the cytotoxicity of freshly prepared GIC. The results showed evidence of some toxicity, but after the material had set for 24 hours, it was found to be non-toxic to the cells. It was suggested that the cytotoxicity observed in the freshly prepared GIC was due to the presence of organic residue from incomplete setting reactions (Sasanaluckit,

Albustany, Doherty et al., 1993, Chen, Mestres, Lan et al., 2016). Moreover, *in vivo* testing conducted in monkey and rat presented no sign of irritation or inflammation around the glass ionomer implants. These demonstrated that the GICs have adequate biocompatibility to the animal tissue (Sasanaluckit et al., 1993).

### 2.3.5 Fluoride release

Fluoride ( $F^-$ ) ions have a significant role in tooth structure.  $F^-$  ions can replace the  $OH^-$  ions of hydroxyapatite in tooth structure and form the fluorapatite ( $Ca_5(PO_4)_3F$ ). According to  $F^-$  ions are smaller than  $OH^-$ , it provide readily packing in the apatite crystal lattice than the normal hydroxyapatite (Guida, Hill, Towler et al., 2002). Therefore, this tooth structure can resist the penetration of cariogenic bacteria and acids resulting in the inhibition of demineralization. This might be misunderstanding that  $F^-$  provide antibacterial activity (Francci, Deaton, Arnold et al., 1999). However, it had been found that the  $F^-$  ions effectively reduced formation of bacterial biofilm, which is associate with occurring of secondary caries (Chau, Pandit, Cai et al., 2015)

GICs have ability to sustain the  $F^-$  ions in long period up to 5 years (Nicholson and Czarnecka, 2016). After the materials were applied to the tooth, the released  $F^-$  ions would be greatest after the first week then reduced gradually and become constant at below 10 ppm. However, GICs could take up  $F^-$  ions from the fluoride solution and then probably release them. This phenomenon is called the "burst effect." As a result, when teeth are brushed with fluoride-rich toothpaste, the GIC will absorb the  $F^-$  ions from the tooth paste and slowly release them, resulting in an increase in the  $F^-$  ion level in the mouth cavity. This is very beneficial for preventing further caries, not only for the tooth to which the materials were applied but also the others in the mouth. (Hatibović-Kofman and Koch, 1991).

## 2.4 Production of ionomer glass

The glass ionomer powder is normally prepared by the melt quenching method. In this approach, the glass composition is melted at a high temperature of 1,100–1,400 °C and then immediately cooled to form opal glass. The obtained glass is then pulverized into a fine powder. Since the process is operated at high temperature, the

fluoride content in the glass composition is variable because of its volatile nature, leading to toxic pollution. This problem may be overcome by the soft chemistry synthesis method known as sol-gel because this route is carried out at a lower temperature than the melt quenching method.

Sol-gel is the synthesis method for various ceramics and glass (Chen and Mao, 2007). In general sol-gel process, colloidal suspension or sol is formed by hydrolysis and polymerization reaction of the precursors, which are usually inorganic metal salt or organics metal compound such as metal alkoxides. The liquid sol then transforms to be a wet gel after completely polymerization and loss of solvent. The wet gel is able to convert into dense ceramic by drying and heat treatment.

Table 2.4 The difference between the glass prepared by melting and sol-gel method.

	Melt-derived	Sol-gel derived	References
The thermodynamics and kinetic of glass formation	Base on oxide mixtures in molten and supercooled state	Based on polymerization	(Mukherjee, 1980)
Temperature	1050-1350°C	600-800°C	(Wilson and Kent, 1971, Bertolini, Zaghete and Gimenes, 2005)
Glass composition	Uncontrollable of the F loss	Controllable of glass composition because of low temperature process	(Tu et al., 2016)
Homogeneity	Partial phase separation during cooling process	High homogeneity because the production of the oxide from the central atom to macromolecule	(Cestari, 2016, Nicholson and Czamecka, 2016)
Amount of bridging oxygen	Low	High	(Roy, Jain, Saha et al., 1995, Wren et al., 2009)

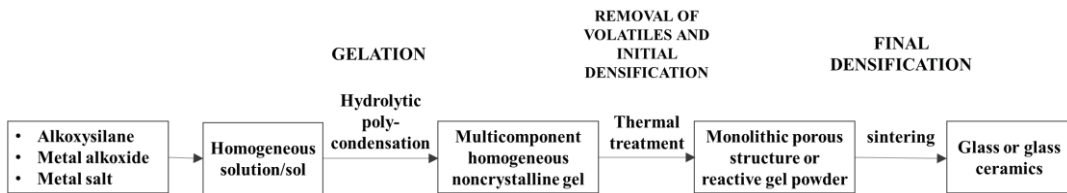


Figure 2.3 Sol-gel process for multicomponent glass synthesis (Mukherjee, 1980)

In the multicomponent glass synthesis, the alkoxysilane and metal salt is widely used as a precursor. The process of sol-gel glass synthesis is shown in Figure 2.3. The completely polymerization reaction is required for producing of “glass-like” gel network of  $-\text{Si-O-M-O-Si}-$  where M is a metal atom (Mukherjee, 1980). The polymerization process of organic compounds starts with condensation of polyfunctional monomer and forming a gel. The gel point is indicated by the point that a viscous liquid suddenly transforms to an elastic gel. At gel point, continuously formation of the infinite network is started, and gel polymerization is raised rapidly. The controlled factors of gelling process are composed of chemical nature of alkoxides and other reactants, ratio of water and alkoxides, pH of the medium, temperature, concentration of the reactant and the nature of solvent. Finally, glass formation can be obtained by heat-treatment of the dried gel at high temperature (Bogomolova, Pavlushkina and Morozova, 2006). The reaction of gel formation in a multicomponent system may occur as presented in Figure 2.4.

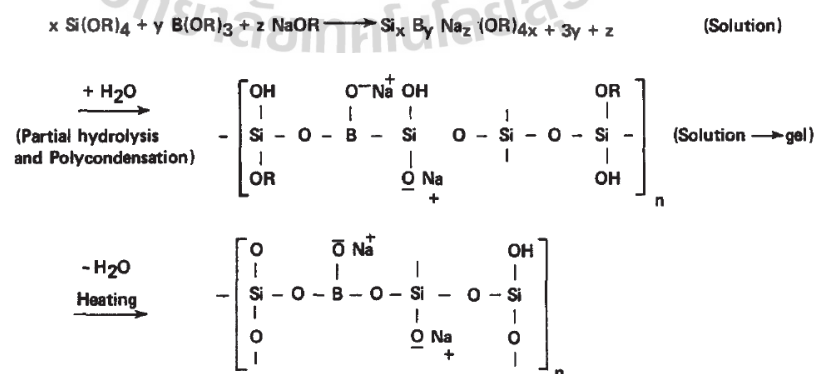


Figure 2.4 Gel formation of multicomponent system (Mukherjee, 1980).

Irwin et al., 1988 studied the structures of alumino-silicates and sodium alumino-silicates prepared by the sol-gel method. The  $^{27}\text{Al}$  and  $^{29}\text{Si}$  MAS-NMR were used for observation of the coordination state. Their result showed that all of the gel obtained the Al-O-Si unit upon gelation. The structure of alumino-silicate was composed of an aluminum network in four and six co-ordinations. The six-fold coordination occurred to balance the charge difference between  $\text{Al}^{3+}$  and  $\text{Si}^{4+}$  ions. While the inclusion of sodium cations could neutralize the charge difference, the sodium alumino-silicate glass network was formed in four-fold coordination of silica linking to alumina.

Taira and Yamaki, 1995 had synthesized the alumino-silicate glass by sol-gel method. The starting solutions amount of tetra orthosilicate (TEOS), ethyl alcohol, deionized water and hydrochloric acid (HCl) were fix to the ratio of 1:10:50:0.02. The obtained powders showed amorphous with the average particle size of  $5\ \mu\text{m}$ . They explained the glass formation mechanism that the substitution of  $\text{Si}^{4+}$  by  $\text{Al}^{3+}$  could occur in coordination of 4 and negative ions were left in the glass structure. This could be balanced by adding of metal cation such as  $\text{Sr}^{2+}$  ions. (Taira and Yamaki, 1995).

Roy et al, 1995 investigated the alumino-silicate glasses, including  $\text{Na}_2\text{O}$  and  $\text{Li}_2\text{O}$ , synthesized by the melt-quench and sol-gel processes. The synthesized glass structure was characterized by x-ray photoelectron spectroscopy (XPS). The result showed that the glass structure prepared by melt quenching had a greater amount of non-bridging oxygen and a lower amount of bridging oxygen than those of the sol-gel glass (Roy et al., 1995).

Bertolini et al., 2005 studied the GI powder belonging to  $4.5\text{SiO}_2\text{-}3\text{Al}_2\text{O}_3\text{-}x\text{Nb}_2\text{O}_5\text{-}2\text{CaO-}3\text{CaF}_2$  system synthesized by the sol-gel method. They found that the glass structure showed tetrahedrally  $[\text{AlO}_4]$  structure which could react with the polyacrylic acid. It could be indicated that the glass ionomer powder was synthesized successfully by the sol-gel method (Bertolini et al., 2005).

Bertolini et al., 2009 had been continuously developing the sol-gel GI powder for use as a luting cement based on the  $4.5\text{SiO}_2\text{-}3\text{Al}_2\text{O}_3\text{-}x\text{Nb}_2\text{O}_5\text{-}2\text{CaO-}3\text{CaF}_2$  system. The result showed that the glass structure was completely amorphous after being calcined at  $600\ \text{C}$ . The mechanical properties of the experimental GICs were similar

to those of the commercial GIC. Moreover, the amount of fluoride was constantly released at a lower level in comparison with the commercial GIC during the period of study (Bertolini et al., 2009).

Wren et al., 2009 investigated the effect of the synthesis route of GI powder in the system of  $48\text{SiO}_2-36\text{ZnO}-12\text{CaO}-4\text{SrO}$ . The GI powders were synthesised by melting and the sol-gel method. The properties of the experimental GICs were determined, including setting time, fluoride release, compressive strength, and biaxial flexural strength. They found that the setting time of the cement based on sol-gel glass was longer than that of the melt-derived cement. The higher strengths of both compressive and biaxial flexure were found in the GICs based on melt derived glass. This difference in the properties of GICs could be attributed to the different structure within the glass. The GI powder produced by the sol-gel method showed the formation of a bridging oxygen structure, resulting in low susceptibility to the acid attack (Wren et al., 2009).

Tu et al, 2016 studied the effect of lanthanum doped in GIC prepared by the sol-gel route. The compressive strength and surface hardness of lanthanum containing GIC were significantly higher than the commercial values of 47.7% and 39.2%, respectively. They also found that fibroblast cells grew well around the GIC samples. However, There was no statistical difference between their studied groups. Thus, lanthanum had no effect on biocompatibility (Tu et al., 2016).

Cestari, 2016 synthesized the dental alumino-silicate glass by the sol-gel method under different conditions: non-hydrolytic, hydrolytic acid, and hydrolytic basic. The results showed that the glass powder presented different structures depending on the conditions. The experimental GIC based on hydrolytic acid presented better characteristics than the commercial GIC because it was homogenous in particle size and shape, elemental distributed without phase separation, amorphous in structure, and able to be produced at a lower temperature (Cestari, 2016).

## CHAPTER 3

### SOL-GEL SYNTHESIS CONDITION FOR IONOMER GLASS (4.5SiO<sub>2</sub>-3Al<sub>2</sub>O<sub>3</sub>-1.5P<sub>2</sub>O<sub>5</sub>-3CaO-2CaF<sub>2</sub>)

This chapter shows the investigation of synthesis condition for ionomer glass by the sol-gel method. The study focused on the effect of important factors for the sol-gel synthesis process, including water to precursor ratio (Rw), pH, calcination temperature, and aging method. The synthesized ionomer glass was then characterized using XRD and FTIR techniques. Additionally, the basic physical properties of the cement, including setting time and compressive strength, were also determined.

#### 3.1 Introduction

The sol-gel method is interesting for the preparation of glass ionomers because it can control the consistency of the glass composition at low temperatures and use low energy (Taira and Yamaki, 1995, Bertolini et al., 2009, Wren et al., 2009, Cestari, 2016, Fujihara, 2018, Ilipronti, Clare, Berndt et al., 2019, Pierre, 2019). However, this process is sensitive to synthetic conditions such as chemical type, gel heat history, and the pH of sol that affect the final product structure (Mukherjee, 1980, Cestari, 2016). These conditions can significantly impact the final structure of the glass material, resulting in variations in chemical composition, particle size, and homogeneity (Cestari, 2016). As such, it is essential to optimize the synthesis conditions to ensure consistent and reliable results. There were three major processes involved in the sol-gel synthesis, as follows:

- 1) Dissolving of precursor:

This process involved the hydrolyzation of the metal organic precursor or an inorganic salt with water. The resulting homogeneous solution is then converted into a homogeneous sol. One crucial factor in this process is the ratio

of alkoxy silane precursor to water ( $R_w$  ratio), which must be carefully controlled to ensure complete dissolution (Jones and Fischbach, 1988, Kessler, 2015). If the  $R_w$  ratio is too high, the precursor may not dissolve completely. At low  $R_w$  ratio, excess water acts to inhibit the condensation reaction (Jones and Fischbach, 1988). Moreover, it was reported that when the catalyst is absent, no significant reaction was observed. Therefore, both the  $R_w$  ratio and the catalyst utilized substantially influence the properties of the resulting silica gels (Jones and Fischbach, 1988). The addition of a catalyst to the sol plays a critical role in determining the pH of the solution, which significantly influences the rate of dissolution and condensation. As a result, the pH of the solution could have an impact on the shape, size, and chemical composition of the resulting particles. (Visser, 2018).

## 2) Aging process:

Once all the species have undertaken hydrolysis at an early stage of the reaction, they can then condense to form small clusters or chains of precursor molecules through an aging process (Kessler, 2015). This involves incubating the gel under a specific temperature to initiate the reaction, which includes gel aging and dried aging. During gel aging, the polycondensation reaction continues while the gel remains in a gel-like state. After gel aging, some literature had employed the gel to dried aging before calcination to remove the residual liquid phase from the gel pores following by gradually transforms from a gel into a solid phase (Bogomolova et al., 2006).

## 3) Calcination

Calcination is the process of heating the gel at a high temperature to remove the organic components and to cause densification and crystallization of the inorganic network (Brinker and Scherer, 1990). Higher calcination temperatures can lead to an increase in the crystallinity and particle size of the resulting materials. Therefore, the choice of calcination temperature must be carefully considered to achieve the desired properties for a given application.

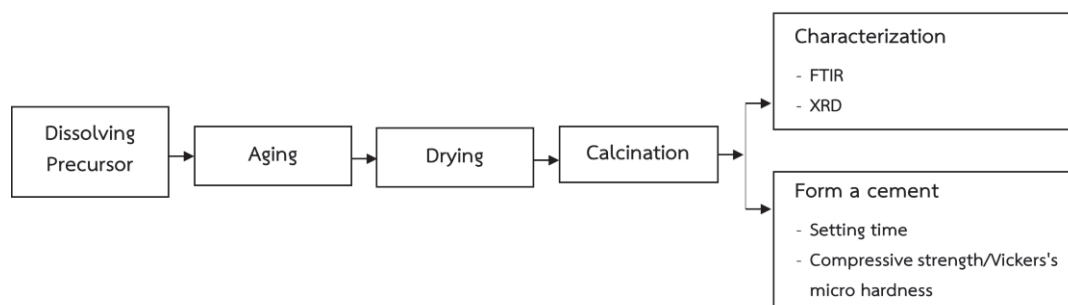


Figure 3.1 Schematic of synthesis process of ionomer glass powder by the sol-gel method

As there have been only a few studies on the synthesis of ionomer glass using the sol-gel method, it is crucial to explore the synthesis conditions in order to identify the optimal conditions for synthesizing ionomer glass. This chapter focuses on the investigation of various synthesis conditions, including Rw ratio, pH of the solution, calcination temperature, type of the fluoride source, and aging method. The synthesized ionomer glass was characterized using FTIR and XRD techniques. Additionally, the cement was fabricated and evaluated for setting time and compressive strength, as summarized in Figure 3.1.

## 3.2 Experimental procedure

### 3.2.1 The synthesis of $4.5\text{SiO}_2\text{-}3\text{Al}_2\text{O}_3\text{-}1.5\text{P}_2\text{O}_5\text{-}3\text{CaO-}2\text{CaF}_2$ ionomer glass by the sol-gel method

In this chapter, the ionomer glass with composition of  $4.5\text{SiO}_2\text{-}3\text{Al}_2\text{O}_3\text{-}1.5\text{P}_2\text{O}_5\text{-}3\text{CaO-}2\text{CaF}_2$  was synthesized by the sol-gel method. The chemicals employed in this thesis are listed in Table I of Appendix B. Firstly, EtOH and DI was mixed by a magnetic stirrer for 15 minutes. Then, TEOS,  $\text{Al}(\text{NO}_3)_3$ , TEP,  $\text{Ca}(\text{NO}_3)_2$  and  $\text{CaF}_2$  were subsequently added into the mixed solution. Each step of adding the materials took 30 minutes to blend. The pH of the solution was adjusted by  $\text{HNO}_3$  and  $\text{NH}_4\text{OH}$ . The final solution was aged  $80^\circ\text{C}$  for 15 hours and dried at  $120^\circ\text{C}$  for 5 hours. The dried gel was then calcined for two hours with the rate of  $2^\circ\text{C}/\text{minutes}$ . Finally, the obtained glass was pulverized by a high-speed planetary ball mill for 2 hours. The synthesis process is summarized in Figure 3.2.

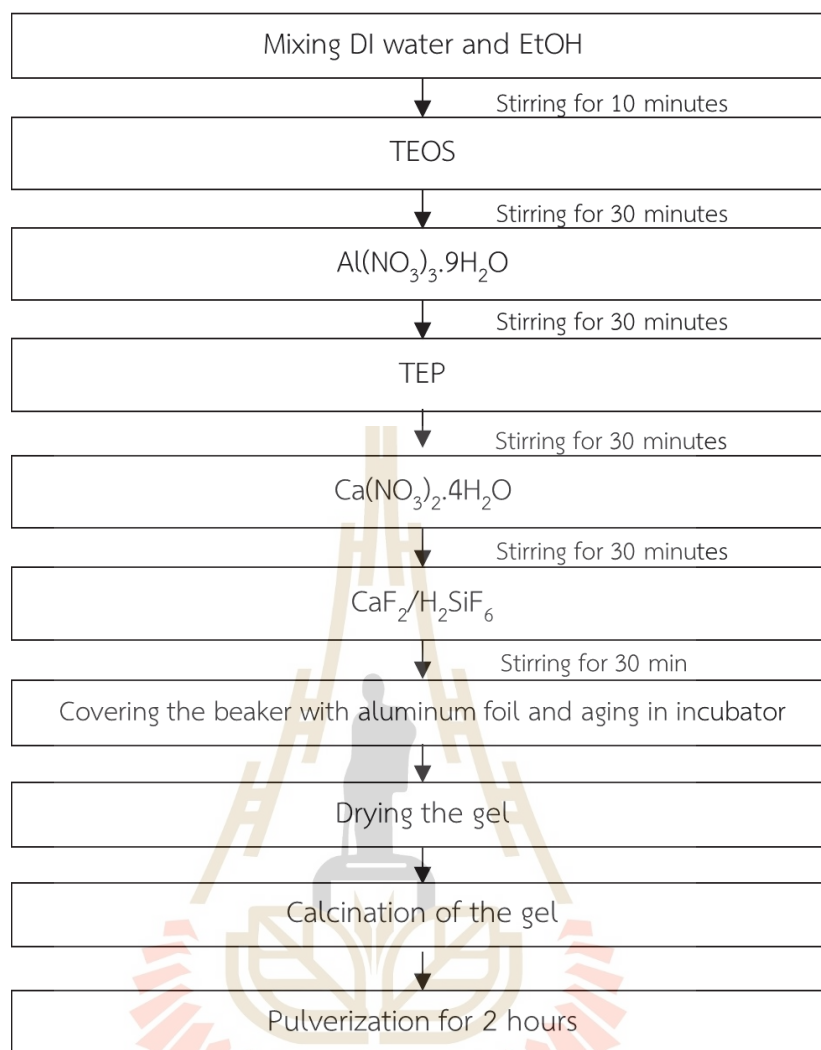


Figure 3.2 Flow chart illustrating the sol-gel synthesis of the ionomer glass.

In this chapter, five experiments were conducted to optimize the synthesis conditions for ionomer glass using the sol-gel method. The experiments focused on determining the optimal precursor to water ratio (Rw), pH of the solution, calcination temperature, the fluoride precursor, and aging method.

### 3.2.1.1 TEOS : H<sub>2</sub>O (Rw)

According to the Mukherjee's report, the ratio of the alkoxide and the water influenced to the densification rate and the composition of the gel (Mukherjee, 1980). In this study, ionomer glass was synthesized using the method

outlined in section 1, with varying ratios of TEOS precursor and water (0.001, 0.01, 0.1, 1, and 2). The precise amount of each precursor used is shown in Table 3.1. Finally, all the resulting gels were subjected to calcination at 700°C to produce glass.

Table 3.1 Amount of the precursors for sol-gel synthesis of ionomer glass

Precursor	Volume				
	Rw = 0.001	Rw = 0.01	Rw = 0.1	Rw = 1	Rw = 2
EtOH (ml)	20.04	20.04	20.04	20.04	20.04
Water (ml)	619.60	61.9	6.19	0.62	0.31
TEOS (ml)	6.50	6.50	6.50	6.50	6.50
Al(NO <sub>3</sub> ) <sub>3</sub> (g)	8.58	8.58	8.58	8.58	8.58
TEP (ml)	0.39	0.39	0.39	0.39	0.39
Ca(NO <sub>3</sub> ) <sub>2</sub> (g)	3.60	3.60	3.60	3.60	3.60
CaF <sub>2</sub> (g)	0.91	0.91	0.91	0.91	0.91

### 3.2.1.2 pH of solution

Ionomer glass in this experiment was synthesized using the method outlined in section 3.2.1, with varying pH values (0.6, 1.5, 7 and 10). The pH was adjusted by using HNO<sub>3</sub> and NH<sub>4</sub>OH. The starting solution utilized Rw ratio of 0.01, and the resulting dried gel was calcined at 700°C. In addition, the commercial GIC (Fuji IX) was characterized for comparison in this study.

### 3.2.1.3 Calcination temperature

Ionomer glass in this experiment was synthesized using the method outlined in section 3.2.1, with Rw ratio of 0.01 and pH value of 1.5. To investigate the effect of crystallization temperature on the properties of SGIC, the resulting gel was calcined at 400°C, 600°C, 700°C and 800°C. The commercial GIC (Fuji IX) was also characterized for comparison in this study.

#### 3.2.1.4 Fluoride sources

As reported in Cestari's study, the presence of  $\text{CaF}_2$  crystals in the sol-gel ionomer glass structure could result from incomplete dissolution of the  $\text{CaF}_2$  precursor (Cestari, Avila, Nassor et al., 2009). In our experiment,  $\text{CaF}_2$  powder was also used as a fluoride precursor as same as the Cestari's work. In order to eliminate the crystal structure of  $\text{CaF}_2$ , an alternative fluoride precursor was investigated.  $\text{H}_2\text{SiF}_6$  has been commonly used as a fluoride precursor in the sol-gel synthesis of ionomer glass in other research works (Bertolini et al., 2009, Tu et al., 2016). Therefore, the different fluoride precursors for the sol-gel process, which were  $\text{CaF}_2$  and  $\text{H}_2\text{SiF}_6$ , were studied in this section for their effect on the crystallinity and compressive strength of SGIC.

This study was to investigate the difference fluoride precursors for ionomer glass which were  $\text{CaF}_2$  and  $\text{H}_2\text{SiF}_6$ . The ionomer glass in this experiment also prepared using the method outlined in section 3.2.1, with Rw ratio of 0.01, pH 1.5 and calcination temperature of  $700^\circ\text{C}$ .

#### 3.2.1.5 Aging process

In this section, it was aimed to reduce the occurrence of crystal precipitation by exploring the possibility of minimizing the dried aging process. The ionomer glass used in this experiment was prepared following the methodology described in section 3.2.1, which used an Rw ratio of 0.01, a pH of 1.5, and a calcination temperature of  $700^\circ\text{C}$ . During the aging process, two experimental conditions were employed, as illustrated in Figure 3.3. Schematic of comparison between two different aging process, which were dried aging and gel aging, for synthesis of ionomer glass powder by sol-gel method. Figure 3.3. The first condition denoted as gel aging, whereby the sol was incubated at  $80^\circ\text{C}$  for 15 hours to form a gel and then immediately calcined. The second condition, denoted as dry aging, involved incubating the sol at  $80^\circ\text{C}$  for 15 hours, followed by drying at  $120^\circ\text{C}$  for 5 hours.

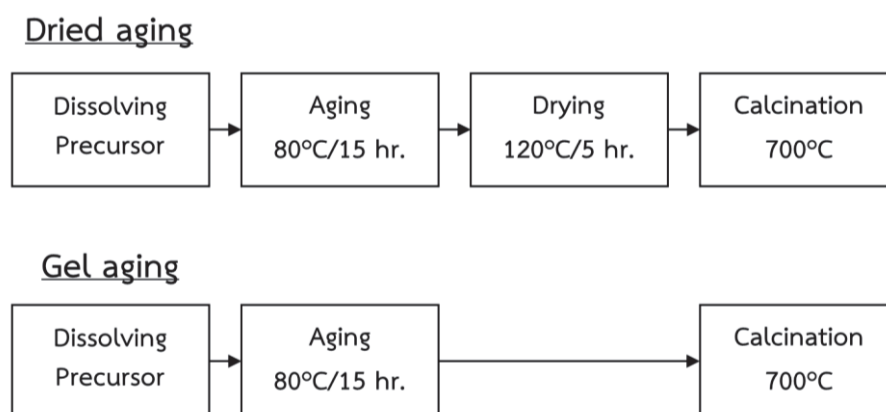


Figure 3.3 Schematic of comparison between two different aging process, which were dried aging and gel aging, for synthesis of ionomer glass powder by sol-gel method.

### 3.2.1.6 Characterization of the ionomer glass

This experiment analyzed phase identification of the ionomer glass by using X-ray diffractometer (German Bruker D2) with wavelength of  $1.5406 \text{ \AA}$ ,  $40 \text{ K}$ ,  $0.020^\circ/\text{min}$  and scan range of  $10\text{--}60^\circ$ . The chemical bonding structure of the ionomer glass was determined by a Fourier transform infrared spectrometer (ATR-FTIR German Bruker, Tensor 27-Hyperion) with a wavenumber range of  $4000\text{--}400 \text{ cm}^{-1}$  and a resolution of  $4 \text{ cm}^{-1}$ .

### 3.2.2 Cement preparation

In this study, the mixture of the polyacrylic acid (35 wt.% in  $\text{H}_2\text{O}$  PAA; M.W.  $\sim 100,000$ ) and tartaric acid (PAA-TA) in the ratio of 9:1 w/w supplied by Sigma-Aldrich were used as the liquid solution. The obtained glass powder was mixed with the PAA-TAA with the powder to liquid (P:L) ratio of 1:1 (w/v). The mixture was blended on the clean bench for 40 s before placed into the mold for testing.

### 3.2.3 Setting time and compressive strength testing

The net setting time of the GICs was determined using a Gillmore Apparatus (Humboldt, H-3150F) following ISO 9917-1 guidelines for dental glass polyalkenoate cement. Once the cement paste was mixed, it was filled into a

cylindrical Teflon mold with a diameter of 10 mm and a height of 2 mm. The net setting time was determined by placing a heavy and thin needle (453.6 g,  $\varnothing$  1.06 mm) on the surface of the paste every 5 seconds until no mark occurred. This process was repeated three times at room temperature.

Hardness testing of the cement was conducted using a Vickers microhardness tester (FUTURE-TECH CORP/ FM-310) with 10 g load and 10 s indentation time. The specimens were molded in cylindrical shape with a size of 12 mm in diameter and 6 mm in height. After molding for 1 hour, the specimens were pulled out from the mold then soaked in DI water at 37°C for 23 hours. Minimal 5 data points were collected to calculate an average microhardness value for each sample.

To measure the compressive strength of the GICs, the specimens were prepared in cylindrical Teflon molds with a diameter of 4 mm and a height of 6 mm, following ISO 9917-1:2007 guidelines. After molding for 1 hour, all specimens were kept in DI water at 37°C for 23 hours before testing. The universal testing machine (UTM, Instron 5565, Instron GmbH, Germany) with 5 kN load cells was used to measure the compressive strength at a crosshead speed of 0.75 mm/min, according to the previous literature [20]. At least eight specimens were prepared for each experimental condition. The compressive strength was calculated using the equation  $CS = 4P/\pi d^2$ , where CS represents the compressive strength (MPa), P represents the maximum load applied (N), and d represents the radius of the specimen (mm).

### 3.3 Results and discussions

#### 3.3.1 Effect of the ratio of TEOS:H<sub>2</sub>O (Rw)

The XRD pattern of the glass powder prepared by different Rw of 0.001, 0.01, 0.1, 1 and 2 after calcined at 700°C were show in Figure 3.4. The crystalline phase according to fluorapatite (Ca<sub>5</sub>(PO<sub>4</sub>)<sub>3</sub>F) (JCPDS no. 76-0558) and fluorite (CaF<sub>2</sub>) (JCPDS no. 35-0816) were presented in all the glass patterns. The result from XRD technique showed that the glass which prepared with Rw of 0.001 presented the lowest crystallinity.

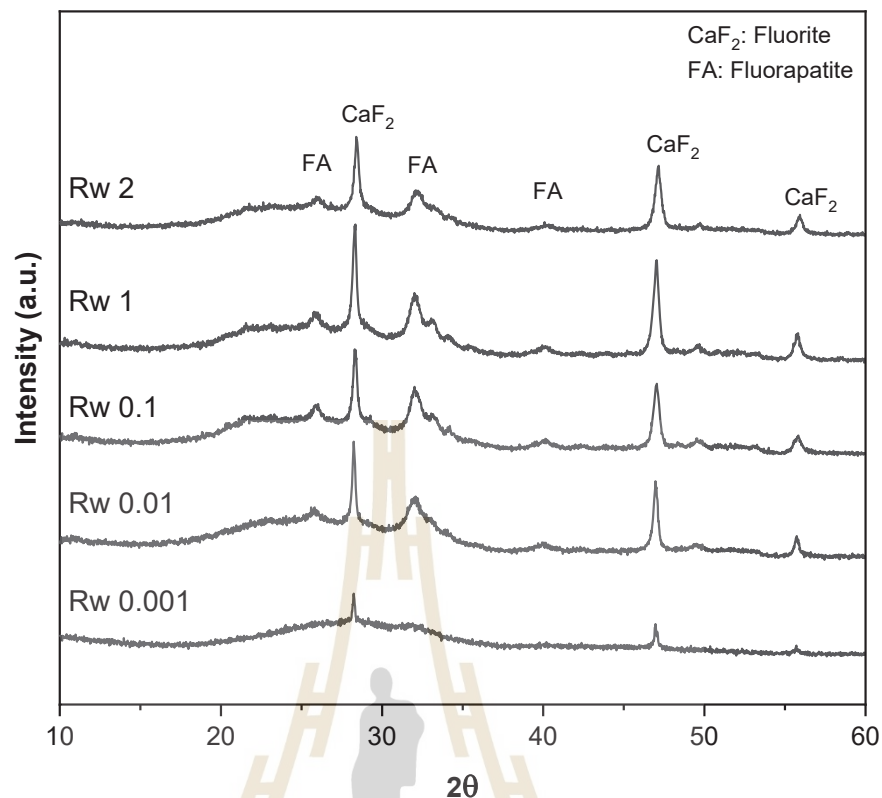


Figure 3.4 XRD patterns of sol-gel glass ionomer powders calcined at 700°C

According to Cestari's study, the sol-gel glass structure exhibited the crystalline phase of  $\text{CaF}_2$  and  $\text{AlPO}_4$  after being calcined at 600°C. This observation suggests that the  $\text{CaF}_2$  and  $\text{AlPO}_4$  precursor might not have been completely dissolved, leading to the remaining crystalline phases of  $\text{CaF}_2$  and  $\text{AlPO}_4$ . It is possible that the  $\text{CaF}_2$  observed in our glass structure may have resulted from a similar incomplete dissolution, as reported in Cestari's study. (Cestari, 2016).

Previous studies have reported that  $\text{CaF}_2$  substance was the formation of fluorapatite involves incorporating fluoride ions into the crystal structure of apatite (Jmal and Bouaziz, 2018). This process occurs during the sol-gel synthesis of the glass, which involves the separation of  $\text{CaO}$  and  $\text{P}_2\text{O}_5$  in the gel. When  $\text{Ca}^{2+}$  ions were introduced into the phosphate-rich phase,  $\text{P}_2\text{O}_5$  reacted with  $\text{CaO}$  to form the apatite crystal lattice. Moreover, the incorporation of  $\text{F}^-$  ions in highly concentrated  $\text{Ca}^{2+}$  and  $\text{P}^{2+}$  ions was found to promote the nucleation and development of the final fluorapatite crystals (Jmal and Bouaziz, 2018). The presence of the fluorapatite

crystal might be benefit to the SGIC since it could enhance biocompatibility to the material as reported in previous study (Moshaverinia, Borzabadi-Farahani, Sameni et al., 2016)

The FTIR spectra of the sol-gel glass powders calcined at 700°C (Figure 3.5 (a)) were corresponded to the XRD pattern that the same characteristic spectra were found in Rw of 0.01 to 2. These indicated that the different Rw ratio in this range had no effect on the glass structure. As can be seen, the characteristic of the calcium aluminosilicate glass (Si-O-Al and Si-O-Ca) appeared at 1036  $\text{cm}^{-1}$ , 950  $\text{cm}^{-1}$ , 750-850  $\text{cm}^{-1}$  and 450  $\text{cm}^{-1}$  (Crisp, Pringuer, Wardleworth et al., 1974, McMillan and Piriou, 1982, Środa and Paluszkiwicz, 2008). These bonding were degradable by acid attack as suggested by several authors. When the acid attacked the glass surface, the bonding of Al-O-Si or Si-O-Ca was broken following the releasing of  $\text{Al}^{3+}$  and  $\text{Ca}^{2+}$  ions. The released ions were migrated into the aqueous phase forming the polyacrylate salt responsible for the forming of GICs (Bertolini et al., 2005, Cestari, 2016).

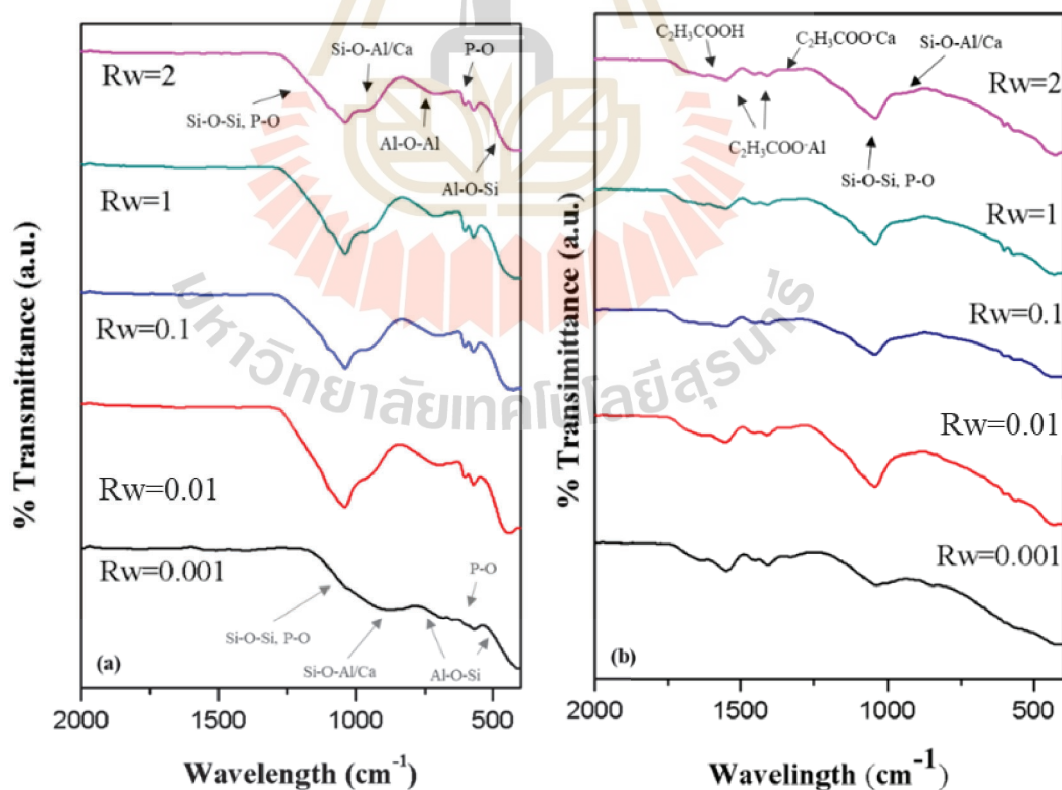


Figure 3.5 FTIR spectra of (a) the sol-gel ionomer glass prepared from the different Rw ratio calcined at 700°C and (b) the set cements.

Figure 3.5 (b) presents the bonding structure of glass ionomer after mixing with the PAA liquid. All of the sol-gel glass exhibited the band at  $1550\text{ cm}^{-1}$ ,  $1410\text{ cm}^{-1}$ ,  $1559\text{ cm}^{-1}$  and  $1460\text{ cm}^{-1}$  which attributed to the formation of the calcium carboxylate ( $\text{COO}^-\text{Ca}$ ) and the aluminium carboxylate ( $\text{COO}^-\text{Al}$ ) (Bertolini, Zaghete, Gimenes et al., 2008, Nicholson and Czarnecka, 2016). The results demonstrated that the crosslinking reaction occurred in the GIC prepared by Rw 0.001 to 2.

Table 3.2 shows that the Rw ratios affected the sol-gel condition and yield. However, the setting time and the surface hardness of the glass prepared with Rw ratios of 0.01 to 2 show no significant difference due to the identical glass structure as presented in Figure 3.4 and Figure 3.5. While the glass prepared with Rw 0.001 could not be molded because it was set very fast after mixing.

Furthermore, the color of the ionomer glass powders varied depending on the Rw ratio, with higher ratios resulting in a darker, grayish hue. It was found that the ionomer glass powder synthesized using an Rw ratio of 0.01 exhibited a clear, white color, and demonstrated an acceptable setting time for SGIC. As a result, this ratio was selected as the optimal choice for synthesizing the glass powder in subsequent experiments.

Table 3.2 pH of the solution, gelation time, and setting time of SGIC prepared with different Rw ratio.

Rw ratio	Sol-gel condition		Cement properties		
	Final pH	Gelation time (hr)	Working time (min)	Setting time (min)	Vicker's hardness
0.001	2.82	No gelation	----- Rapidly set -----		
0.01	1.5	2.40	2:54	9:14	13.18±3.7
0.1	<0.1	1	3:29	12:00	12.37±4.2
1	<0.1	1	3:28	14:56	13.66±3.0
2	<0.1	0.40	4:50	13:43	9.25±2.0

### 3.3.2 Effect of the pH of solution

The XRD pattern of the glass powder prepared by different pH after calcined at 700°C were show in Figure 3.6. All the sol-gel derived ionomer glass revealed their amorphous nature with crystal phase of fluorite ( $\text{CaF}_2$ ) (JCPDS no. 35-0816) and fluorapatite ( $\text{Ca}_5(\text{PO}_4)_3\text{F}$ ) (JCPDS no. 76-0558).

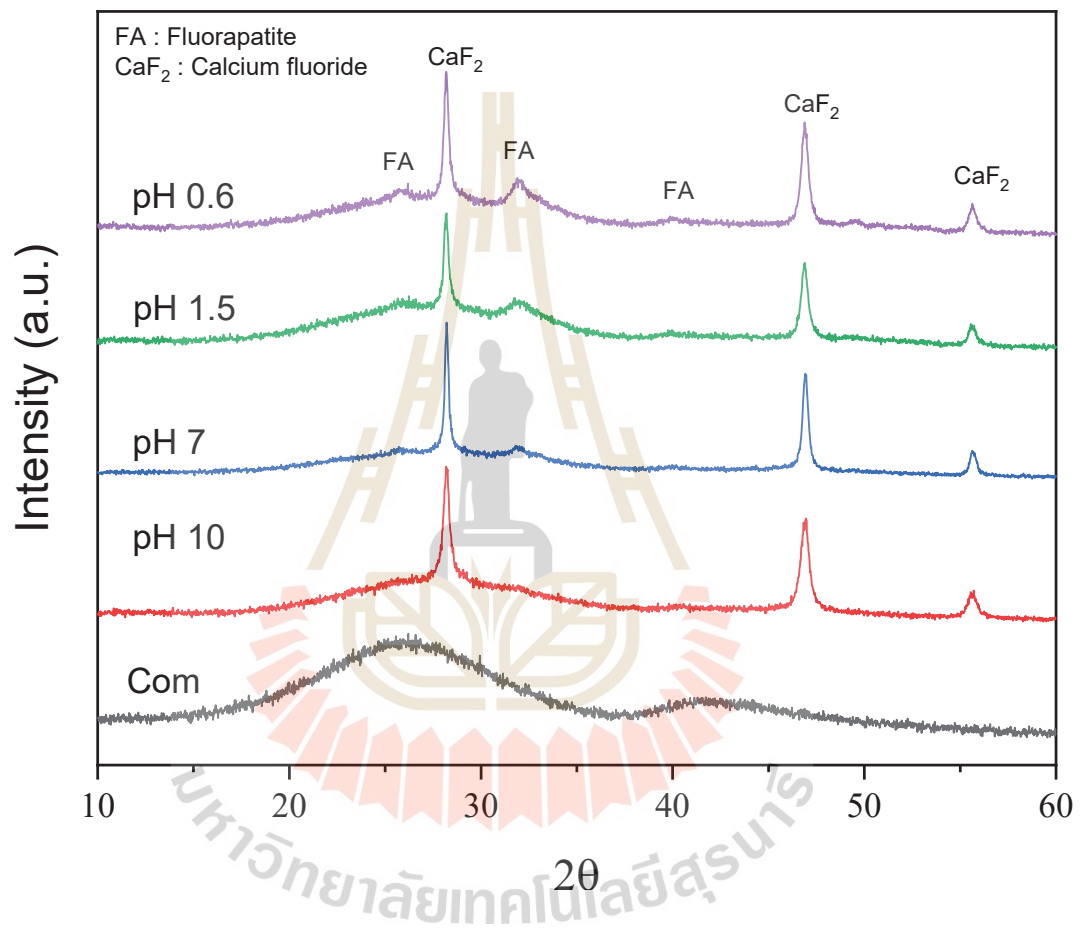


Figure 3.6 XRD pattern of the ionomer glass belonging the system of  $4.5\text{SiO}_2\text{-}3\text{Al}_2\text{O}_3\text{-}1.5\text{P}_2\text{O}_5\text{-}3\text{CaO-}2\text{CaF}_2$

FTIR spectra was used to analyze the structure of the sol-gel derived ionomer glass and the commercial ionomer glass are shown in Figure 3.7. The principal characteristics of calcium alumino-silicate glasses appeared at 400-550, 550-850, and 850-1300  $\text{cm}^{-1}$  (Huang and Behrman, 1991, Środa and Paluszkiwicz, 2008).

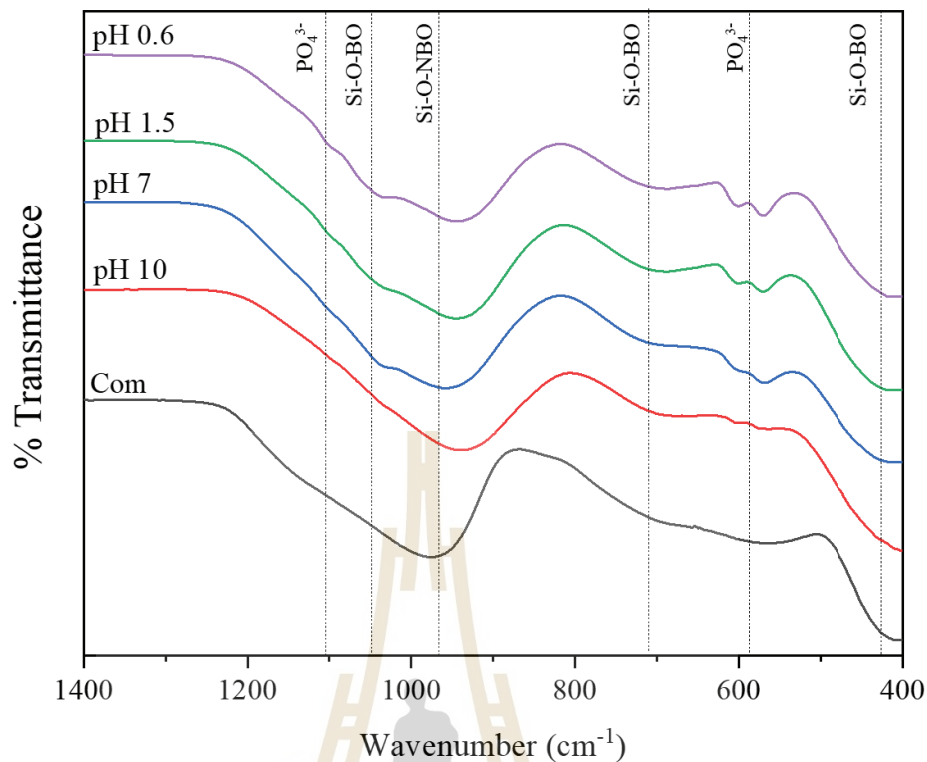


Figure 3.7 FTIR spectra of the sol-gel ionomer glass synthesized with different pH

At pH 0.6-7, the FTIR spectra revealed a strong band around  $450\text{ cm}^{-1}$  which attributed to oxygen vibration in the plane perpendicular to Si-O-Al linkage. The next region appearing around  $750\text{ cm}^{-1}$  was expected to the symmetric stretching of the aluminum-oxygen bonding in  $[\text{AlO}_4]$  tetrahedra and the Si-O bending. At around  $580\text{ cm}^{-1}$ , there were two bands attributed to the crystal  $\text{PO}_4$  from the fluorapatite structure. For the high intensity band appearing around  $1100\text{ cm}^{-1}$ , this band assigned to the antisymmetric stretching vibrations of bridging Si-O-Si bond within  $[\text{SiO}_4]$  tetrahedra (Środa and Paluszkiwicz, 2008). The width of this band referred to existence of the NBO in the glass structure of  $Q^n$  unit, where Q indicated to a silica tetrahedron with 4-n of NBO structure. This  $1100\text{ cm}^{-1}$  band was slightly shifted and broadened toward lower wavenumber when compared with the commercial glass. Hence, the network structure of our sol-gel glass prepared with low pH was composed with high amount of NBO unit. Additionally, the shoulder occurred around  $1050\text{ cm}^{-1}$  and  $1100\text{ cm}^{-1}$  indicated the BO from Si-O-Al bonding and the crystal  $\text{PO}_4$ , respectively.

At pH 10, the band locating around  $1100\text{ cm}^{-1}$  and  $800\text{ cm}^{-1}$  was obviously shifted to  $1000\text{ cm}^{-1}$  and  $760\text{ cm}^{-1}$ , respectively. Moreover, their band width was significantly broadened. This characteristic attributed to formation of Si structural unit with higher NBO unit (Środa and Paluszkiwicz, 2008, Riti, Vulpoi, Ponta et al., 2014). This result is in good agreement with the previous finding of Valliant et al. that increase of pH resulted in increase of NBO unit in glass network (Valliant, Turdean-lonescu, Hanna et al., 2012). Wren et al. demonstrated that the ionomer glass with a high amount of NBO structure tended to react well with the polyacrylic acid because it was susceptible to acid attack (Wren et al., 2009).

Table 3.3 The physical properties of SGIC prepared with different pH.

Sample	P:L ratio	Mixing	Working time (min)	Setting time (min)	Compressive strength (MPa)
Commercial GIC	3.4:1	Easy	3:00	4:55	$109.68 \pm 4.12$
Commercial GIC	1:1	Very easy	4:13	12:17	$36.1 \pm 1.7$
pH 0.6 powder	1:1	Easy	3:30	10:25	$51.62 \pm 4.90$
pH 1.5 powder	1:1	Easy	2:32	4:11	$46.47 \pm 8.47$
pH 7.0 powder	1:1	-----	-----	Rapidly set -----	-----
pH 10 powder	1:1	-----	-----	Rapidly set -----	-----

The working and setting time of the ionomer glass powder prepared in acid catalyst are shown in Table 3.3. The result revealed that SGIC prepared with acid region (pH 0.6-1.5) exhibited favorable compatibility and interaction with the polymeric acid and showed the working and setting time close to the commercial product. Moreover, their compressive strength was higher than the commercial product at the same P:L ratio. On the other hand, the samples prepared with higher pH (7-10) set too fast to be molded and measured the setting time. This fast reaction could be attributed to the high concentration of NBO unit in glass structure. Additionally, a noticeable heat release was observed during the setting reaction. However, precise evaluation of the heat release was difficult due to the rapidity of the reaction. This heat releasing was suggested that ionomer glass synthesized at high pH levels formed a ring structure within its glass network, as presented in Figure

3.8 (B), that required a large amount of energy to break the bonds (Ying, Benziger and Navrotsky, 1993). Furthermore, the heat released during the reaction could have caused harm to surrounding tissue. Therefore, it was more suitable to synthesize ionomer glass using the sol-gel method at lower pH levels in the acidic region.

Based on the findings of this study, the ionomer glass synthesized with a pH value of 1.5 showed a setting time that was comparable to the commercial GIC (with a P:L ratio of 3.4), as shown in Table 3.3. Therefore, a pH value of 1.5 was selected for the synthesis of ionomer glass in the subsequent experiment.

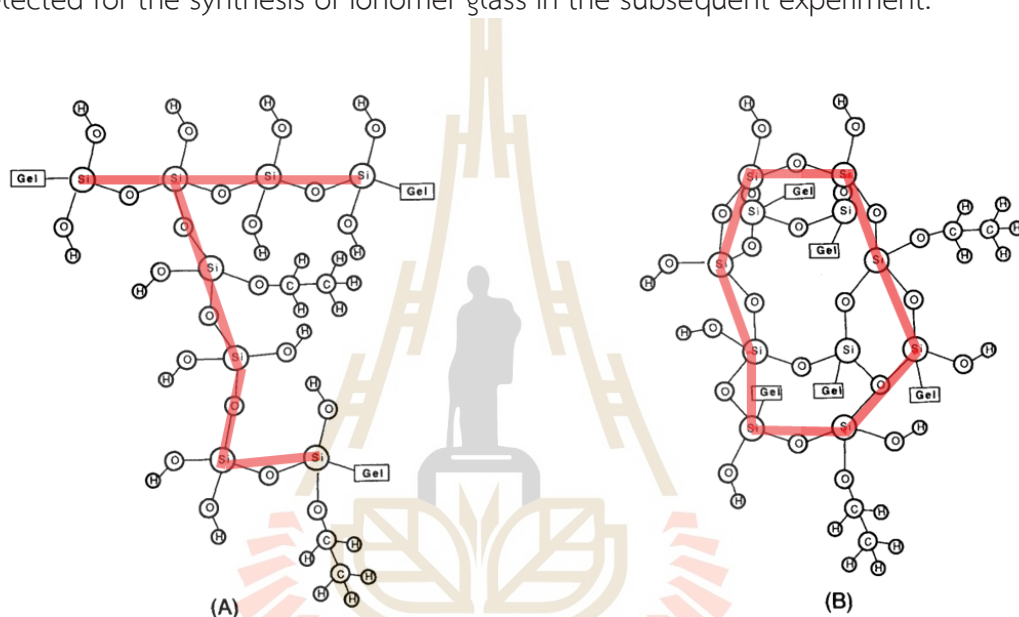


Figure 3.8 The silica gel networks derived from (A) acid- and (B) base-catalyzed TEOS hydrolysis and condensation (Ying et al., 1993)

### 3.3.3 Effect of calcination temperature

Figure 3.9 presents that XRD patterns of the commercial glass structure show amorphous, while the glass powder calcined at 400°C, 600°C, 700°C and 800°C exhibited fluorapatite phase (JCPDS no. 76-0558) and CaF<sub>2</sub> (JCPDS no. 35-0816). After calcining at higher temperature, the crystallinity of fluorapatite was increased. At 800°C, the mullite characteristic peaks were observed.

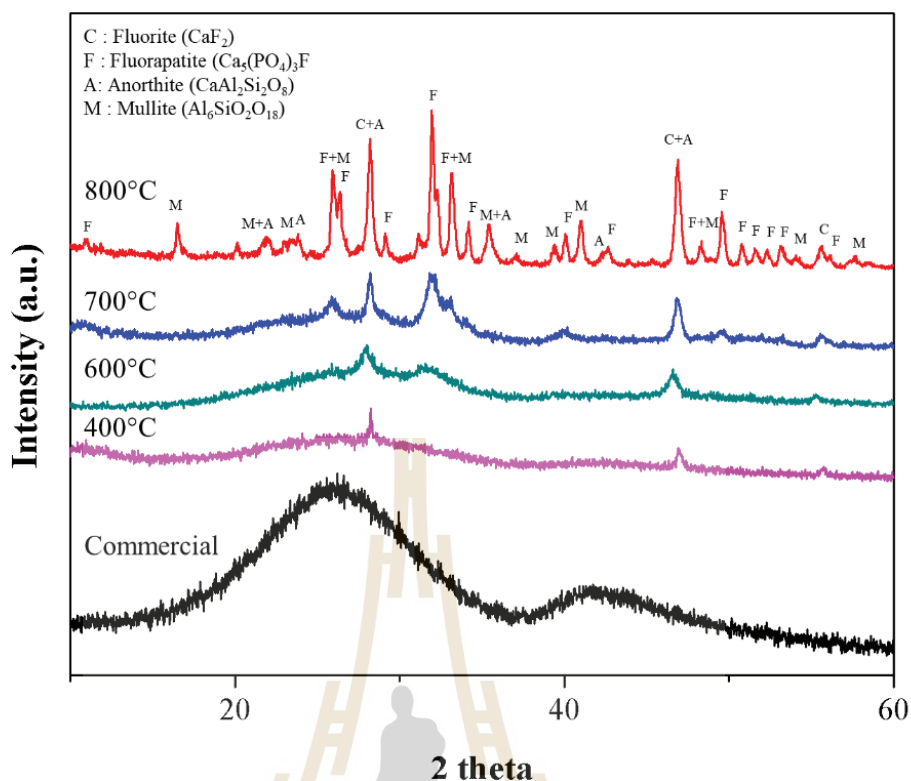


Figure 3.9 XRD pattern of the sol-gel ionomer glass after calcination at 400°C, 600°C, 700°C and 800°C, respectively, as compared with the commercial product.

The FTIR spectra of the sol-gel ionomer glass were corresponded to the XRD pattern that there was the development of the structure upon the calcination temperature (Figure 3.10). For the ionomer glass calcined at 400°C, the water and hydrocarbon species remained in the structure which was found as the bands at 1636 cm<sup>-1</sup> and 1427 cm<sup>-1</sup> and 1350 cm<sup>-1</sup> (Jmal and Bouaziz, 2018). The band observed at 1100 cm<sup>-1</sup> reflected the vibration of Si-O-Si (Riti et al., 2014). At 600 °C, the Si-O-Al/Ca characteristics were found at 1000 cm<sup>-1</sup> and 750 cm<sup>-1</sup>, while the water and the hydrocarbon disappeared. The peak at 550 cm<sup>-1</sup> was assigned to P-O oxygen bridging inside the PO<sub>4</sub><sup>3-</sup> tetrahedron. The crystallization was apparently found in IR spectra of the ionomer glass calcined 700°C. The phosphate peak around 550 cm<sup>-1</sup> was split into two bands at 580 and 550 cm<sup>-1</sup> which attributed to crystalline phosphate of apatite (Jmal and Bouaziz, 2018). After calcining at 800 °C, the glass became a high crystalline material.

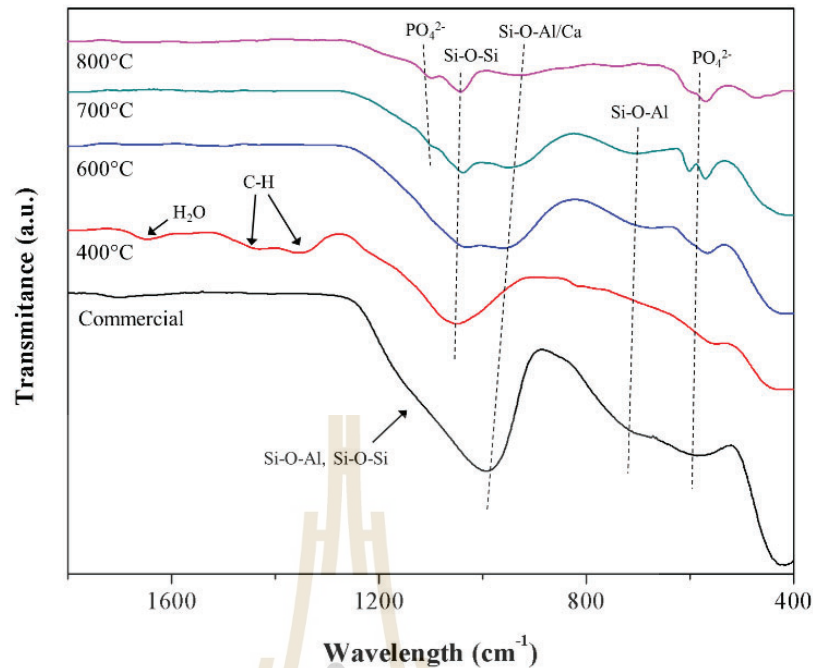


Figure 3.10 The FTIR spectra of (a) the sol-gel ionomer glass after calcination at 400°C, 600°C, 700°C and 800°C, respectively.

Based on the FTIR results, there was a remaining of water and hydrocarbon species in the ionomer glass calcined at 400°C. This finding suggested that the calcination process at a temperature of 400°C was insufficient to completely eliminate the water and hydrocarbon species from the ionomer glass. Furthermore, the sol-gel ionomer glass calcined at 400°C showed an absence of the Si-O-Al/Ca bonding at 1000  $\text{cm}^{-1}$  and 750  $\text{cm}^{-1}$  which played a key role in setting reaction of GICs (Bertolini et al., 2005). The breakdown of this bonding upon acidic attack was responsible for the release of  $\text{Al}^{3+}$  and  $\text{Ca}^{2+}$  ions that react with the PAA liquid to form a poly-salt matrix. Consequently, the lack of this bonding in the sol-gel ionomer glass calcined at 400°C makes it ineffective in reacting with the PAA liquid. On the other hand, it was observed that the calcination process at a higher temperature of 600°C was effective in eliminating the residual water and hydrocarbon species from the ionomer glass. Moreover, Si-O-Al/Ca bonding, which was a key structure for setting reaction of GIC, was observed upon calcination at temperatures of 600°C and higher. After calcining at 700°C, each band had become narrow indicating the

crystallinity characteristic of the glass network. This finding was associated to XRD pattern in Figure 3.9. The high crystallinity of the glass might result in a deficiency of reactive ions for GIC setting reaction, as the crystalline structure is highly stable and less susceptible to acid attack (Huang and Behrman, 1991, Wood and Hill, 1991, Griffin and Hill, 1999, Billington, Williams and Pearson, 2006).

Table 3.4 The physical properties of SGIC calcination at 400°C 600°C, 700°C and 800°C

Sample	P:L ratio	Mixing	Working time (min)	Setting time (min)	Compressive strength
Commercial GIC	3.4:1	Easy	3:00	4:55	109.68 ± 4.12
Commercial GIC	1:1	Very easy	4:13	12:17	36.1±1.7
400 °C	1:1	----- No reaction -----			
600°C	1:1	----- Rapidly set -----			
700°C	1:1	Easy	2:32	4:11	46.47 ± 8.47
800°C	1:1	----- No reaction -----			

Table 3.4 presents the physical properties of SGIC investigated in this study. The results showed that there was no reaction between the PAA liquid and the ionomer glass calcined at 400 °C due to the lack of Si-O-Al/Ca structure. When the sol-gel ionomer glass was calcined at 600°C, it started to form Si-O-Al/Ca structure and reacted satisfactory with the polymeric acid. However, the sol-gel ionomer glass calcined at 600°C provided a short working time that was unable to be mold in desirable shape. On the other hand, the sol-gel ionomer glass calcined at 800°C failed to set as a hard cement even after 60 minutes of mixing with the liquid phase. Interestingly, the setting time of the sol-gel ionomer glass calcined at 700°C was similar to that of the commercial GIC (P:L ratio of 3.4:1). However, the compressive strength of the ionomer glass calcined at 700°C was significantly lower than those of the commercial product.

The current study suggested that the presence of crystal formation within the sol-gel glass structure impeded the desired setting reaction of SGIC. Therefore, the next experiment aimed to reduce the crystallinity of the sol-gel glass.

### 3.3.4 Effect of fluoride source

As reported in Cestari's study, the presence of  $\text{CaF}_2$  crystals in the sol-gel ionomer glass structure could result from incomplete dissolution of the  $\text{CaF}_2$  precursor (Cestari et al., 2009). In order to eliminate crystal structure of  $\text{CaF}_2$ , the alternative fluoride precursor was investigated.  $\text{H}_2\text{SiF}_6$  has been commonly used as a fluoride precursor in the sol-gel synthesis of ionomer glass in other research works (Bertolini et al., 2009, Tu et al., 2016). Therefore, it was interesting to compare the utilization of these two fluoride precursors, which were  $\text{CaF}_2$  and  $\text{H}_2\text{SiF}_6$  in our study to assess their impact on crystallinity and compressive strength of SGIC.

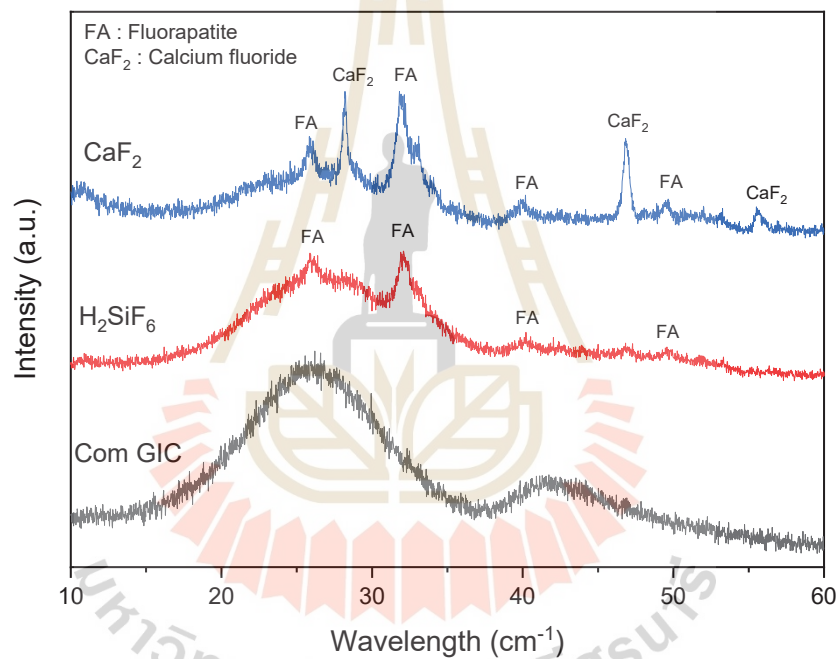


Figure 3.11 XRD pattern compares the sol-gel ionomer glass prepared using  $\text{CaF}_2$  and  $\text{H}_2\text{SiF}_6$  fluoride precursors, as compared with the commercial GIC.

The XRD patterns of the ionomer glass prepared using  $\text{CaF}_2$  as a fluoride precursor revealed crystalline structure comprising of the fluorapatite phase (JCPDS no. 76-0558) and  $\text{CaF}_2$  (JCPDS no. 35-0816). On the other hand, the ionomer glass prepared using  $\text{H}_2\text{SiF}_6$  as a fluoride precursor exhibited only the fluorapatite crystal.

The results of our study demonstrated that when the precursor was changed from  $\text{CaF}_2$  to  $\text{H}_2\text{SiF}_6$ , the crystal structure of  $\text{CaF}_2$  was entirely absent. This

finding suggested that the presence of  $\text{CaF}_2$  crystals in our ionomer glass might be originated from the insoluble  $\text{CaF}_2$  precursor. This highlights the potential of  $\text{H}_2\text{SiF}_6$  as a more effective precursor for reducing crystallinity in sol-gel synthesized ionomer glass.

Table 3.5 The physical properties of SGIC prepared from sol-gel glasses prepared using two different fluoride sources,  $\text{CaF}_2$  and  $\text{H}_2\text{SiF}_6$

Samples	P:L ratio	Mixing	Working time (min)	Setting time (min)	Compressive strength
Commercial GIC	1:3.4	Easy	3:00	4:55	109.68 ± 4.12
Commercial GIC	1:1	Very easy	4:13	12:17	36.1±1.7
$\text{CaF}_2$	1:1	Easy	2:32	4:11	46.47 ± 8.47
$\text{H}_2\text{SiF}_6$	1:1	Easy	2:30	5:40	59.68±9.82

The working and setting time of SGICs are shown in Table 3.5. The findings reveal that SGIC produced using  $\text{H}_2\text{SiF}_6$  as a fluoride precursor had an increased setting time, but it has still in acceptable range of 4-6 minutes. Additionally, the compressive strength of the sol-gel GICs prepared with  $\text{H}_2\text{SiF}_6$  as a fluoride precursor surpassed that of  $\text{CaF}_2$ . This result supports previous result in section 3.3.3 indicating that the crystalline structure in ionomer glass can impede the setting process. Consequently, sol-gel GICs prepared with  $\text{H}_2\text{SiF}_6$ , which have a lower degree of crystallinity, exhibit greater compressive strength.

### 3.3.5 Effect of aging process

The previous experiment in section 3.3.3 suggested that the crystallization in the ionomer glass structure resulted in low compressive strength of SGIC. Moreover, the finding in section 3.3.4 revealed that the absence of  $\text{CaF}_2$  crystal could increase the compressive strength of SGIC. However, there was a remaining FA crystal in the sol-gel ionomer glass. It should be noted that the sol-gel synthesis of glass required a specific duration of heat treatment, either during the aging or calcination process. These thermal treatments induced a gradual rearrangement of the glass network, which could result in phase separation and subsequent crystal precipitation

(Zanotto, 1992, Roy et al., 1995). To reduce the incidence of crystal precipitation, it was necessary to investigate and optimize the heat treatment procedure.

In previous experiments, the calcination temperature was already investigated (Section 3.3.3), and the optimized temperature was found at 700°C. Therefore, the aging process needed to be further investigated. The sol-gel synthesis conducted in previous experiment involved dissolving the precursor to obtain a homogeneous sol, followed by gel aging at a specific temperature of 80°C for 15 hours in a closed container to complete the hydrolysis and initiate condensation. Subsequently, the container was opened and incubated at 120°C for 5 hours to evaporate the remaining water and organic solution, a process referred to as "dried aging". Finally, the obtained dried gel was calcined.

In this section, it was aimed to reduce the occurrence of crystal precipitation by exploring the possibility of minimizing the dried aging process. The previous experiment in section 3.3.3 suggested that the crystallization in the ionomer glass structure resulted in low compressive strength of SGIC. Moreover, the finding in section 3.3.4 revealed that the absence of  $\text{CaF}_2$  crystal could increase the compressive strength of SGIC. However, there was a remaining FA crystal in the sol-gel ionomer glass. It should be noted that the sol-gel synthesis of glass required a specific duration of heat treatment, either during the aging or calcination process. These thermal treatments induced a gradual rearrangement of the glass network, which could result in phase separation and subsequent crystal precipitation (Zanotto, 1992, Roy et al., 1995). To reduce the incidence of crystal precipitation, it was necessary to investigate and optimize the heat treatment procedure.

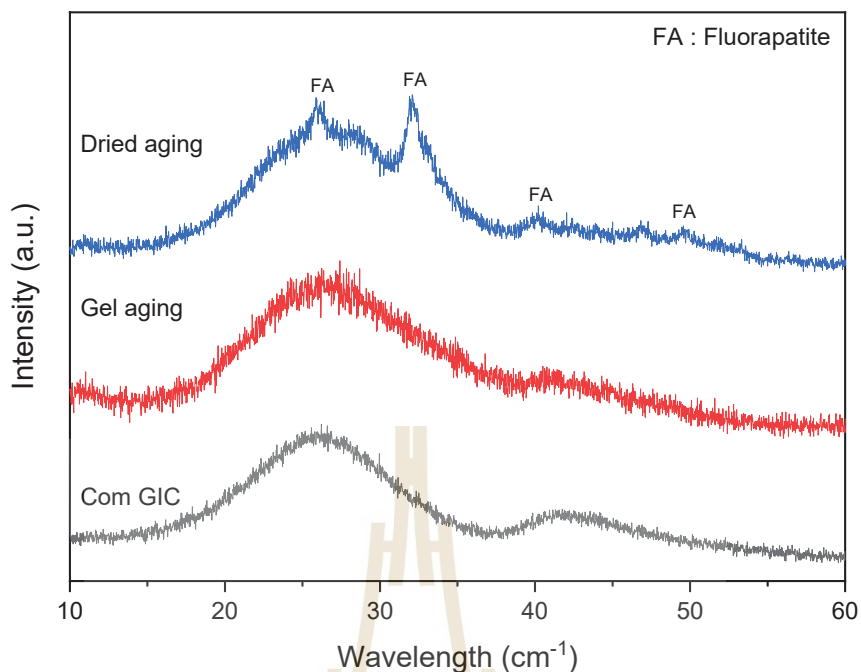


Figure 3.12 XRD pattern compares the sol-gel ionomer glass prepared by different aging process, namely dried aging and gel aging, with the commercial GIC.

In previous experiments, the calcination temperature was already investigated (Section 3.3.3), and the optimized temperature was found at 700°C. Therefore, the aging process needed to be further investigated. The sol-gel synthesis conducted in previous experiment involved dissolving the precursor to obtain a homogeneous sol, followed by gel aging at a specific temperature of 80°C for 15 hours in a closed container to complete the hydrolysis and initiate condensation. Subsequently, the container was opened and incubated at 120°C for 5 hours to evaporate the remaining water and organic solution, a process referred to as "dried aging". Finally, the obtained dried gel was calcined.

Figure 3.12 illustrates the XRD patterns of the ionomer glass obtained from different aging processes in the sol-gel method. The results showed that the ionomer glass obtained from the dry aging process exhibited crystal precipitation of Fluorapatite (JCPDS no. 76-0558). On the other hand, the ionomer glass obtained from the gel aging process presented an amorphous phase without any

crystallization, similar to the commercial GIC. These findings indicated that the dry aging step resulted in crystal formation in the glass structure.

Table 3.6 The physical properties of SGIC prepared from sol-gel glasses prepared using two different aging method, dry aging and gel aging.

Samples	P:L ratio	Mixing	Working time (min)	Setting time (min)	Compressive strength
Commercial GIC	3.4:1	Easy	3:00	4:55	109.68 ± 4.1
Commercial GIC	1:1	Very easy	4:13	12:17	36.1±1.7
Dried aging	1:1	Easy	2:30	5:40	59.68±9.8
Gel aging	1:1	Easy	2:20	5:40	77.84±3.4

The working time, setting time and compressive strength of SGICs are shown in Table 3.6. The setting time results showed no significant difference between the two aging conditions. However, the compressive strength of the ionomer glass obtained from the gel aging process was found to be significantly higher compared to that obtained from the dry aging process. This observation could be attributed to the fact that the ionomer glass obtained from the gel aging process had an amorphous structure, whereas the ionomer glass obtained from the dry aging process had a crystalline structure, as indicated by XRD analysis. It is known that the presence of crystalline phases in the glass structure impeded the setting reaction of GIC, leading to lower mechanical strength.

In summary, the present study suggests that the gel aging process can lead to the formation of an amorphous phase, which enhances the mechanical properties of the ionomer glass, resulting in higher compressive strength.

### 3.4 Conclusions

This study investigated the impact of various synthesis factors on the synthesis of ionomer glass via the sol-gel method, including water-to-precursor ratio, pH, calcination temperature, type of fluoride source, and aging method. The findings

revealed that the sol-gel synthesis conditions significantly influence the resulting glass structure and physical properties of SGICs.

The study demonstrated that an optimal water-to-precursor ratio of 0.01 provides suitable setting time and clear, white-colored ionomer glass for SGICs. An acidic condition at pH 1.5 yielded the most promising results in terms of setting time and compressive strength, while higher pH levels resulted in quick setting time and heat release during the setting reaction.

The optimal calcination temperature was found to be 700°C, providing a net setting time of approximately 4:11 minutes and compressive strength of  $46.47 \pm 8.47$  MPa, with high crystallinity of the glass. The use of  $\text{H}_2\text{SiF}_6$  as a fluoride source resulted in the disappearance of  $\text{CaF}_2$  crystals and increased compressive strength to  $59.68 \pm 9.82$  MPa.

Finally, it was found that the dried aging process could be skipped to reduce glass crystallinity and achieve a significant increase in compressive strength to  $77.84 \pm 3.4$  MPa, while the setting time remains unchanged. These findings provide important insights into the synthesis of ionomer glass for SGICs and have implications for the subsequent experiments that will be conducted in this thesis.

## CHAPTER 4

### EFFECT OF IONOMER GLASS COMPOSITON ( $\text{Al}_2\text{O}_3$ - $\text{P}_2\text{O}_5$ RATIO)

This chapter studied the variation of  $\text{Al}_2\text{O}_3$  and  $\text{P}_2\text{O}_5$  content in the ionomer glass synthesized by the sol-gel method. According to the literature reviews and the results in Chapter 3, it was evident that several factors influence the structure of sol-gel-derived glass. These factors could lead to distinct structural differences between sol-gel-derived and melt-derived glasses, even if their compositions were identical. Therefore, an inclusive evaluation of the composition of ionomer glass in terms of structural changes and associated physical properties was crucial to achieve comparable SGIC to the melt derived GIC. In this study, the change in glass structure was deeply evaluated regarding their compressive strength and setting reactivity. The  $\text{Al}_2\text{O}_3$  and  $\text{P}_2\text{O}_5$  ratio was evaluated by DoE technique using Minitab 16 software.

#### 4.1 Research background

The ionomer glass based on alumino-silicate glass including calcium, phosphorus, and fluoride was extensively investigated by previous literature as a melt-quenching glass (Griffin and Hill, 1999, Griffin and Hill, 2000, Griffin and Hill, 2000, Stamboulis, Hill and Law, 2004). It was reported that the ionomer glass network must be the link of tetrahedral  $[\text{SiO}_4]$  and  $[\text{AlO}_4]$ , which the  $\text{Al}^{3+}$  ions substituted in a site of  $\text{Si}^{4+}$  (Stamboulis et al., 2004, Bertolini et al., 2005, Nicholson and Czarnecka, 2016). This substitution caused the glass network to have an excessively negative charge. To compensate for this charge deficiency, additional positively charged ions (such as  $\text{Ca}^{2+}$ ) were required, resulting in the formation of non-bridging oxygen (NBO) sites that are susceptible to acid attack. (Wren et al., 2009).

To ensure effective reactivity with polymeric acid in the glass ionomer cement reaction, the ionomer glass required a high susceptibility to acid attack. Previous studies have reported that the high formation of  $[\text{AlO}_4]$  tetrahedron in the glass structure was correlated with the susceptibility of the ionomer glass to acid attack

(Stamboulis et al., 2004, Bertolini et al., 2005, Nicholson and Czarnecka, 2016). The  $[\text{AlO}_4]$  tetrahedron formation can be preserved if the ratio of  $\text{Al}/(\text{Si}+\text{P})$  is less than or equal to 1, according to Lowenstein's rule (Loewenstein, 1954, Stamboulis et al., 2004). However, previous research found that the compressive strength of the sol-gel derived glass ionomer cement with an  $\text{Al}/(\text{Si}+\text{P})$  ratio higher than one was better than that of the melt-quenching glass ionomer cement (Tu et al., 2016). The report on the association between glass composition and the properties of GIC synthesized by the sol-gel process was still unclear. Meanwhile, the melt-quenching glass in  $4.5\text{SiO}_2\text{-}3.0\text{Al}_2\text{O}_3\text{-}1.5\text{P}_2\text{O}_5\text{-}3\text{CaO}\text{-}2\text{CaF}_2$  glass system with  $\text{Al}/(\text{Si}+\text{P})$  ratio of 0.8 was commonly prepared and studied in the previous literatures, the sol-gel glass formula of  $4.5\text{SiO}_2\text{-}4.3\text{Al}_2\text{O}_3\text{-}0.15\text{P}_2\text{O}_5\text{-}2\text{Ca}\text{-}\text{F}_2$  with an  $\text{Al}/(\text{Si}+\text{P})$  ratio of 1.79 was successfully synthesized by Tu and his colleague (Tu et al., 2016).

Therefore, the purpose of this study was to investigate the effect of  $\text{Al}_2\text{O}_3$  and  $\text{P}_2\text{O}_5$  content, including the  $\text{Al}/(\text{Si}+\text{P})$  ratio in glass composition, on the glass structure synthesized using the sol-gel method. The glass formula was designed to obtain an  $\text{Al}/(\text{Si}+\text{P})$  ratio in the range of 0.74 to 1.79, which covered the glass composition for both the melt-quenching and the sol-gel processes. The interaction of  $\text{Al}_2\text{O}_3$  and  $\text{P}_2\text{O}_5$  contents on the physical properties of SGIC was analyzed using a  $2^k$  factorial design (Minitab 16 statically software). Additionally, the relationship between the sol-gel glass structure and the physical properties of SGIC were also determined.

## 4.2 Experimental procedure

### 4.2.1 Experimental design

Minitab 16 statistical software was used to construct and evaluate a  $2^k$  full factorial experiment to determine the optimal composition of the sol-gel ionomer glass used in this investigation. The glass composition based on  $4.5\text{SiO}_2\text{-}X\text{Al}_2\text{O}_3\text{-}Y\text{P}_2\text{O}_5\text{-}2\text{CaO}\text{-}2\text{F}_2$  in the molar ratio was selected, where X was varied of 2, 2.5, 4 and 4.3 moles while Y was varied of 0.15, 0.3, 0.45 and 1.5 moles designed by  $2^k$  factorial design as summarized in Table 4.1. In addition, the experimental flow chart was illustrated in Figure 4.1.

Table 4.1 The variation of the sol-gel ionomer glass compositions for  $4.5\text{SiO}_2\text{-XAl}_2\text{O}_3\text{-YP}_2\text{O}_5\text{-2CaO-2F}_2$  using  $2^k$  factorial design.

Sample annotation	Mol ratios		Al/(Si+P) ratio
	$\text{Al}_2\text{O}_3$ (X)	$\text{P}_2\text{O}_5$ (Y)	
2Al-0.15P	2	0.15	$4/(4.5+0.3) = 0.83$
2.5Al-0.15P	2.5		1.04
4Al-0.15P	4		1.67
4.3Al-0.15P	4.3		1.79
2Al-0.3P	2	0.3	0.78
2.5Al-0.3P	2.5		0.98
4Al-0.3P	4		1.57
4.3Al-0.3P	4.3		1.69
2Al-0.45P	2	0.45	0.74
2.5Al-0.45	2.5		0.92
4Al-0.45P	4		1.48
4.3-0.45P	4.3		1.59

#### 4.2.2 Sol-gel synthesis of the ionomer glass

The sol-gel synthesis of the ionomer glass was prepared in accordance with the obtained method from Chapter 3. The process started at mixing of a solution of TEOS:  $\text{H}_2\text{O}$ : EtOH with a molar ratio of 1:50:10 at room temperature using a magnetic stirrer (Taira and Yamaki, 1995). The amount of chemical content was presented in Table II of Appendix B. There was no catalyst added to this experiment. Next,  $\text{Al}(\text{NO}_3)_3$ , TEP, and  $\text{Ca}(\text{NO}_3)_2 \cdot 4\text{H}_2\text{O}$  were added sequentially and mixed for 30 minutes with a magnetic stirrer. The solution was then aged for 15 hours at  $85^\circ\text{C}$ . The gel was semi-dry and white after 15 hours of ageing in the oven. The dried gel was calcined at  $700^\circ\text{C}$  for two hours to remove any organic materials and solvents. The synthesized glass was then ground into a fine powder using a planetary mill with 10 mm alumina balls in alumina vessels at 440 rpm for two hours.

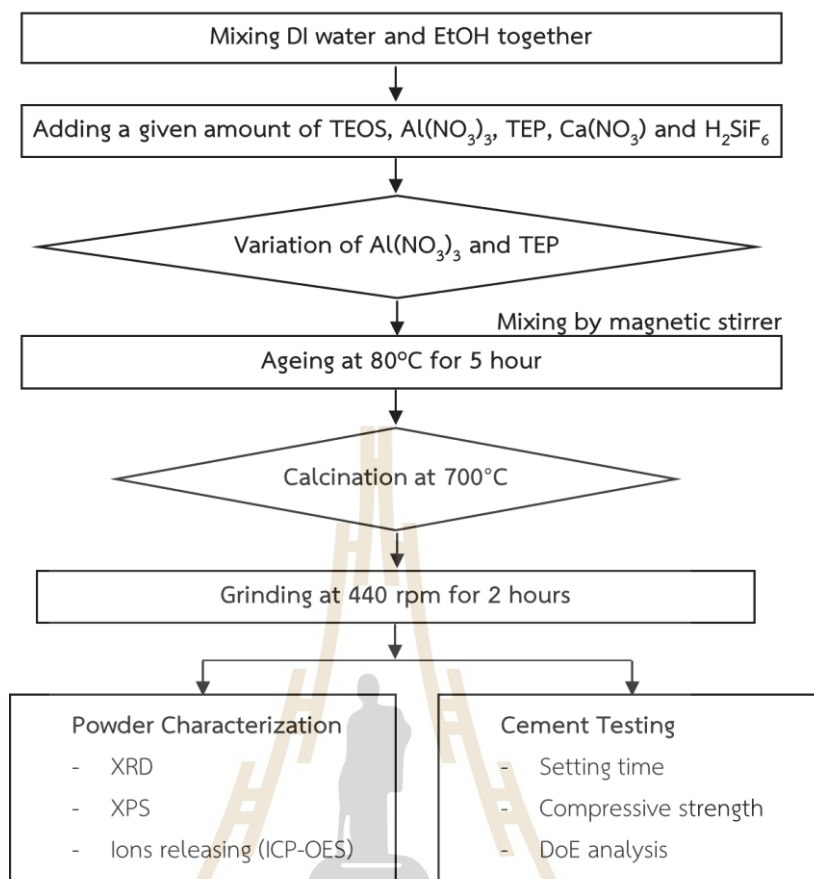


Figure 4.1 Schematic of experimental design to determine the optimal Al<sub>2</sub>O<sub>3</sub> and P<sub>2</sub>O<sub>5</sub> ratio by variation of Al(NO<sub>3</sub>)<sub>3</sub> and TEP precursors.

#### 4.2.3 Characterization of the sol-gel ionomer glass

The phase identification of the ionomer glass was determined using X-ray diffractometer, German Bruker D2 with a step time of 0.02°/min and a scan range of 10-60°. The chemical structure of the ionomer glass was analyzed by X-ray photoelectron spectroscopy (XPS, PHI5000 Versa Probe II, ULVAC-PHI, Japan) at the SUT-NANOTEC-SLRI joint research facility, Synchrotron Light Research Institute (SLRI), Thailand. The excitation source was a monochromatic Al K-alpha radiation (1486.6 eV). All binding energies of the samples were calibrated with the C1s peak at 284.8 eV. PHI MultiPak XPS software was used to process the fitting curves of XPS spectra using a combination of Gaussian-Lorentzian lines with a fixed value of FWHM.

To determine the susceptibility of the glass to the acid, the ions releasing from sol-gel ionomer glasses were measured by immersing 0.05 g of the glass

powders in 10 ml of 5% acetic acid for different lengths of time (2, 6, 10, 60, and 1440 minutes) and then filtering out the glass powder. The ion concentrations ( $\text{Si}^{4+}$ ,  $\text{P}^{5+}$ ,  $\text{Al}^{3+}$ , and  $\text{Ca}^{2+}$ ) of the immersed solution was evaluated using Inductively Coupled Plasma - Optical Emission Spectrometry (ICP-OES optima 8000, Perkin). Elemental stock solutions (1000 ppm) of Silicon (Si), Phosphate (P), Aluminium (Al), and Calcium (Ca) were used to prepare calibration standards. All calibration solutions were made up to volume with 2 wt.% nitric acid ( $\text{HNO}_3$ ).

#### 4.2.4 Preparation of the sol-gel glass ionomer cement (GIC)

A liquid solution composed of polyacrylic acid (35 wt.% in  $\text{H}_2\text{O}$  PAA; M.W. 100,000) and tartaric acid (PAA-TA) at a ratio of 9:1 w/w supplied by Sigma-Aldrich was used for mixing with the sol-gel ionomer glass. For this GIC, the powder-to-liquid mixing ratio was determined at 1:1 (w/w). The components were mixed for 40 seconds on a clean bench, and then poured into the testing mold.

#### 4.2.5 Setting time

According to ISO 9917-1:2007 for dental glass polyalkenoate cement, the working time of the glass ionomer cement (GIC) was recorded from the start of mixing until the cement paste was no longer manipulable. The net setting time of the GIC was measured with Gillmore Apparatus (Humboldt, H-3150F). Once the cement paste was mixed and filled into Teflon cylinders, the net setting time was recorded until a heavy and thin needle (453.6 g, 1.06 mm) could be placed on their surface without leaving a mark. The mean value of at least 3 samples was recorded.

#### 4.2.6 Compressive strength testing

In accordance with ISO 9917-1:2007, compressive strength was determined using a universal testing machine (UTM, Instron 5565, Instron GmbH, Germany) with a 5 kN load cell and a cross speed of 0.75 mm/min. The cylindrical specimens ( $\text{Ø} = 4$  mm,  $h = 6$  mm) were formed. Before testing, all specimens were maintained in DI water at 37°C for 24 hours. For each experimental condition, at least 8 specimens were produced. The compressive strength was calculated by using the equation, CS

=  $4P/\pi d^2$ . Where CS was compressive strength (MPa), P was the maximum load applied (N), and d was specimens radius (mm).

### 4.3 Result and discussion

#### 4.3.1 Chemical structural analysis and ions releasing from the sol-gel ionomer glasses

##### 4.3.1.1 Effect of $\text{Al}_2\text{O}_3$ contents in the sol-gel ionomer glass composition

This experiment evaluated the effect of  $\text{Al}_2\text{O}_3$  contents in ionomer glasses with compositions of  $4.5\text{SiO}_2\text{-XAl}_2\text{O}_3\text{-}0.3\text{P}_2\text{O}_5\text{-}2\text{CaO-}2\text{F}_2$ , where  $X=2, 2.5, 4$  and  $4.3$  moles. The XRD patterns of the ionomer glass with various  $\text{Al}_2\text{O}_3$  content was showed in Figure 4.2. All sol-gel glasses exhibited a broad diffraction peak at  $2\theta$  of  $20^\circ\text{-}40^\circ$ , indicating amorphous for the main phase of the sol-gel glass.

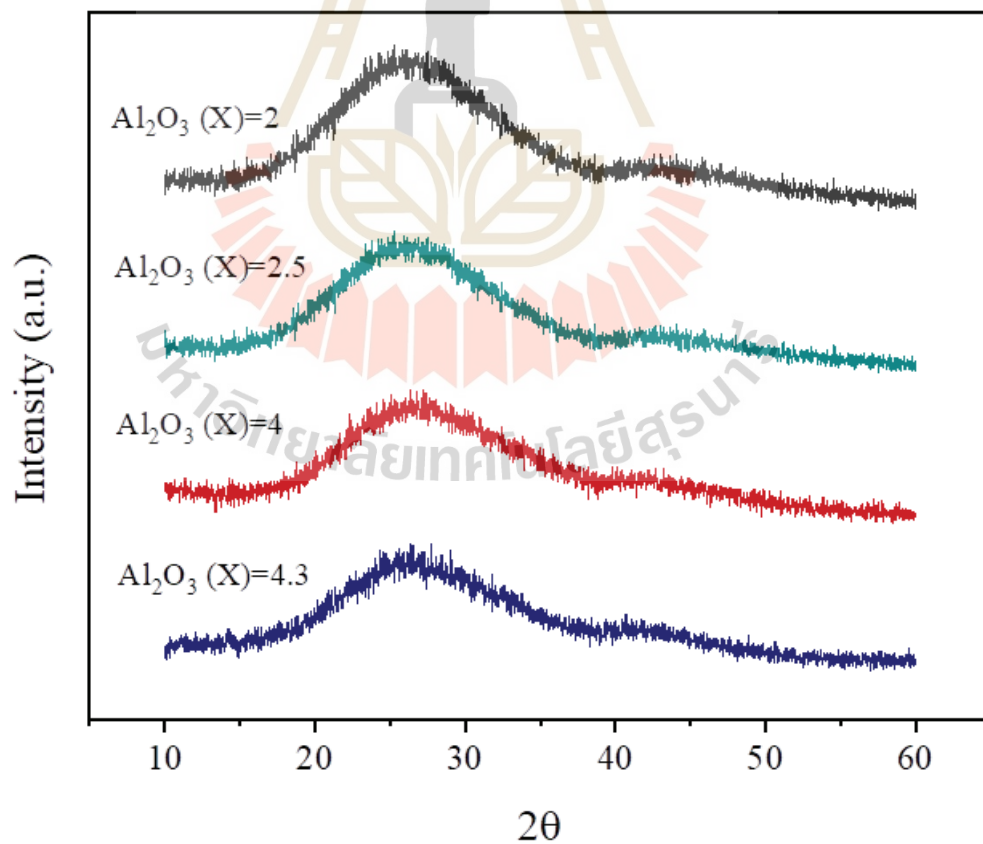


Figure 4.2 XRD patterns of the sol-gel ionomer glasses belonging to  $4.5\text{SiO}_2\text{-XAl}_2\text{O}_3\text{-}0.3\text{P}_2\text{O}_5\text{-}2\text{CaO-}2\text{F}_2$  glass system, where  $X= 2, 2.5, 4$  and  $4.3$ .

Using the XPS technique, an investigation of the chemical structure of the sol-gel glasses was carried out. The high-resolution spectra obtained from the XPS technique was showed in Figure 4.3. The Al2p peak in Figure 4.3 (a) could be deconvoluted into 2 main peak at the binding energies of 74 eV and 75.5 eV which indicated to the  $[AlO_4]$  tetrahedral and  $[AlO_6]$  octahedral structure, respectively (Duan, Wang, Yu et al., 2012). The area of the deconvoluted peaks was used to determine the proportions of  $[AlO_4]$  tetrahedral and  $[AlO_6]$  octahedral sites (Roy et al., 1995). According to the findings, the tetrahedral site percentage was highest in the sol-gel glass containing 2 moles of  $Al_2O_3$ , while the octahedral site fraction was highest in the sol-gel glasses containing 4 and 4.3 moles of  $Al_2O_3$ .

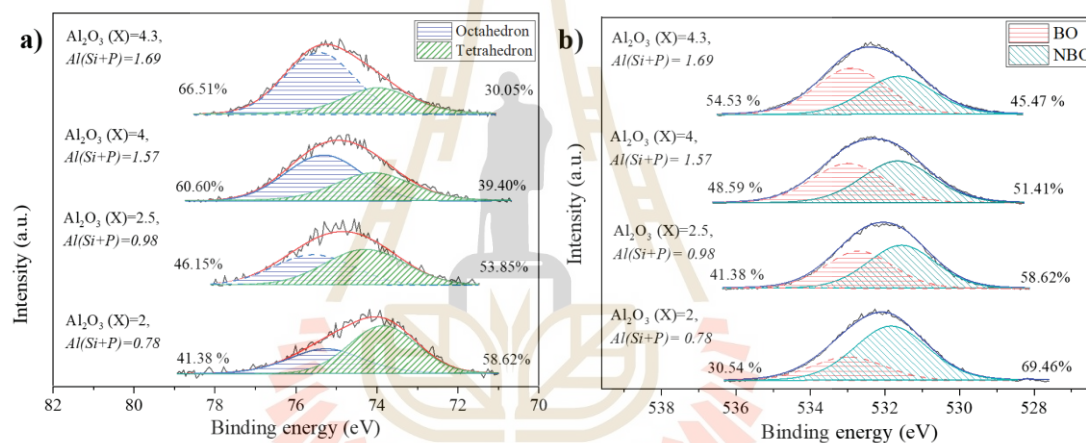


Figure 4.3 High resolution XPS spectra in the (a) Al2p and (b) O1s regions of the sol-gel ionomer glasses belonging to  $4.5SiO_2-XAl_2O_3-0.3P_2O_5-2CaO-2F_2$  glass system, where X= 2, 2.5, 4 and 4.3.

The high-resolution XPS spectra in the O1s region of the sol-gel glasses are shown in Figure 4.3 (b). The spectra showed the characteristics of bridging oxygen (BO) and non-bridging oxygen (NBO) in the ionomer glass structure. The deconvoluted O1s peak at around 532.5 eV was attributed to the BO in the Si-O-Si unit, whereas the peak at around 531.6 eV was ascribed to the NBO (Roy et al., 1995). The results demonstrated that when  $Al_2O_3$  content increased, the proportion of NBO structures decreased.

This study also determined the effect of  $\text{Al}_2\text{O}_3$  variation on the ion releasing behavior over time. The releasing level of  $\text{Si}^{4+}$  ions from all glasses increased with time as seen in Figure 4.4 (a). The glass with 2 moles of  $\text{Al}_2\text{O}_3$  presented the highest concentration of the  $\text{Si}^{4+}$  ions at 2 minutes of soaking time. This finding might be associated with the greatest NBO structure in the glass network, making the glass susceptible to acid attack. After 6 minutes of soaking, however, there was no significant difference in the release of  $\text{Si}^{4+}$  ions.

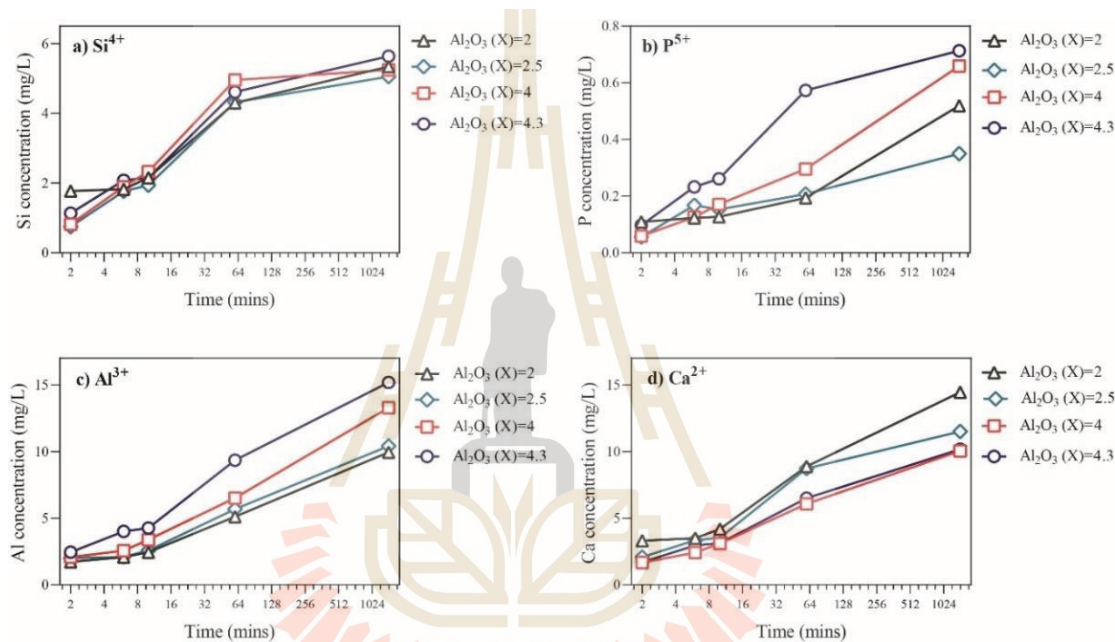


Figure 4.4 The concentration of (a)  $\text{Si}^{4+}$ , (b)  $\text{P}^{5+}$ , (c)  $\text{Al}^{3+}$  and (d)  $\text{Ca}^{2+}$  ions releasing from the sol-gel ionomer glasses belonging to  $4.5\text{SiO}_2\text{-XAl}_2\text{O}_3\text{-}0.3\text{P}_2\text{O}_5\text{-}2\text{CaO-}2\text{F}_2$  system, where  $X = 2, 2.5, 4$  and  $4.3$ , as function of the immersion times.

Figure 4.4 (b) demonstrates an increase in the releasing level of  $\text{P}^{5+}$  ions as the  $\text{Al}_2\text{O}_3$  content and immersion times increase. A similar pattern was seen in Figure 4.4 (c), which reveals the level of  $\text{Al}^{3+}$  ions released from the sol-gel glasses.

Surprisingly, the sol-gel glass with low  $\text{Al}_2\text{O}_3$  ( $X=2$  moles) had the greatest  $\text{Ca}^{2+}$  ion concentration. The sol-gel glass containing 4 or 4.3 moles of  $\text{Al}_2\text{O}_3$  showed dramatically reduced  $\text{Ca}^{2+}$  ion release as shown in Figure 4.4 (d).

The general silicate glass structure is composed of  $\text{SiO}_4$  tetrahedral units that are connected by sharing one corner bridging oxygen (BO). When  $\text{Al}_2\text{O}_3$  is introduced into a pure  $\text{SiO}_2$  glass network, the  $\text{Si}^{4+}$  ions at a tetrahedral site were replaced by the  $\text{Al}^{3+}$  ions. According to Lowenstein's rule, this replacement of  $\text{Al}^{3+}$  ions in the tetrahedral site of the glass network will occur if the  $\text{Al}/(\text{Si}+\text{P})$  ratio is less than or equal to 1 (Stamboulis et al., 2004). The excess  $\text{Al}^{3+}$  ions will occur in the  $[\text{AlO}_6]$  octahedral site when the  $\text{Al}/(\text{Si}+\text{P})$  ratio is greater than 1 (Scholze, 1964). Numerous studies have shown that the  $[\text{AlO}_4]$  tetrahedral unit in the glass structure increases its susceptibility to acid attack (Bertolini et al., 2005). The high acid susceptible glass may release a large concentration of metal ions ( $\text{Al}^{3+}$  and  $\text{Ca}^{2+}$  ions) for cross-linking with the  $-\text{COOH}$  group of the polyacid, followed by the expansion of the polysalt network of GICs (Lohbauer, 2010).

According to the background of the melt-derived glass at  $\text{Al}/(\text{Si}+\text{P})$  less than or equal to 1, the increasing of  $\text{Al}_2\text{O}_3$  content in the glass composition should be accompanied by increasing NBO structure (Stamboulis et al., 2004, Bertolini et al., 2005, Nicholson and Czarnecka, 2016, Zeng, Ye, Li et al., 2017). However, our sol-gel glass with an  $\text{Al}/(\text{Si}+\text{P})$  ratio of 0.74-1.79 demonstrated a different structure, with increasing  $\text{Al}_2\text{O}_3$  content decreasing the proportion of NBO structure, as seen in Figure 4.3. It should be noted that the thermal history of the synthesis process has a significant impact on the glass network structure (Mukherjee, 1980). The sol-gel synthesis involves a low-temperature polymerization reaction followed by calcination to form a network. As a result, the glass network was able to rearrange, allowing the  $\text{Al}^{3+}$  ions that had formed at the  $[\text{AlO}_6]$  octahedral site (high  $\text{Al}/(\text{Si}+\text{P})$  ratio) to join to the glass network as a network former through the BO structure (Brow, Kirkpatrick and Turner, 1993). Therefore, the percentage of BO structures in the glass network structure was increased, while the percentage of NBO structures was decreased, in this study.

Previous research suggested that low levels of NBO structure in the glass network contributed to the low acid susceptibility (as measured by the amount of ions released in acid solution) (Nicholson and Czarnecka, 2009). Our results showed that  $\text{Al}^{3+}$  ions were released in large quantities from glasses with  $\text{Al}/(\text{Si}+\text{P}) > 1$ , despite the fact that tetrahedral species were less abundant than octahedral ones.

It was possible that the  $\text{Al}^{3+}$  ions could be released from the octahedral site in this case and subsequently react with the polymeric liquid, thereby enhancing the setting reaction.

The glass network was added  $\text{Ca}^{2+}$  ions to achieve charge balance on the  $[\text{AlO}_4]$  tetrahedron, which led to the formation of NBO and a tendency for acid susceptibility. The result in this study showed that the existence of NBO in the glass structure contributed to the high amount of  $\text{Ca}^{2+}$  ion release from the glass with  $X=2$  moles. In the glass with higher  $\text{Al}_2\text{O}_3$  ( $X=4$  and  $4.3$ ), the proportion of NBO structure was lower and the amount of  $\text{Ca}^{2+}$  ions released was lower.

Figure 4.5 illustrated the changing in the glass network as an increasing of  $\text{Al}_2\text{O}_3$  content in the glass composition to  $\text{Al}/(\text{Si}+\text{P})$  more than 1. The structural change from the  $[\text{AlO}_4]$  tetrahedron (CN = 4) to the  $[\text{AlO}_6]$  octahedron (CN = 6) and the reduction in the NBO fraction could be attributed to the increase in Al content.

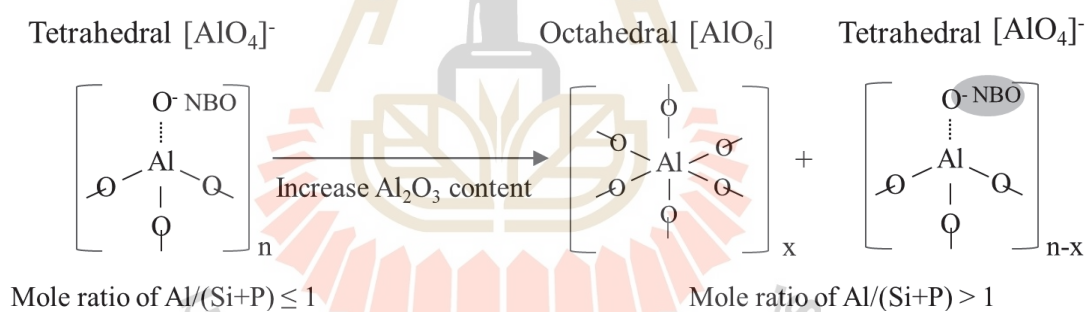


Figure 4.5 A proposed glass network structure for sol-gel ionomer glass with a variation of  $\text{Al}_2\text{O}_3$  contents in the glass composition

#### 4.3.1.2 Effect of $\text{P}_2\text{O}_5$ content in the sol-gel ionomer glass composition

XRD patterns of the sol-gel ionomer glasses based on  $4.5\text{SiO}_2$ - $4\text{Al}_2\text{O}_3$ - $\text{Y}\text{P}_2\text{O}_5$ - $2\text{CaO}$ - $2\text{F}_2$  compositions, where  $\text{Y} = 0.15, 0.3$  and  $0.45$  moles, were showed in Figure 4.6. All sol-gel glasses exhibited a broad diffraction peak at  $2\theta$  of  $20^\circ$ - $40^\circ$ , indicating amorphous for the main phase of the sol-gel glass.

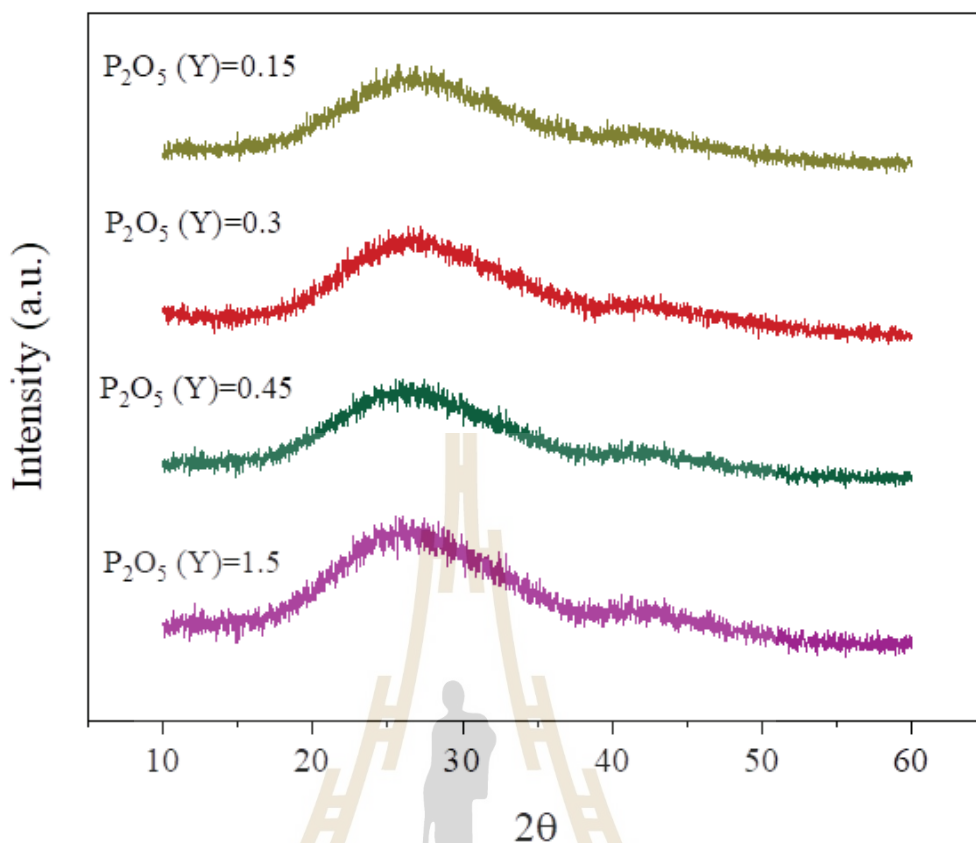


Figure 4.6 XRD pattern of the sol-gel ionomer glasses belonging to  $4.5\text{SiO}_2\text{-}4\text{Al}_2\text{O}_3\text{-}Y\text{P}_2\text{O}_5\text{-}2\text{CaO-}2\text{F}_2$  glass compositions, where  $Y = 0.15, 0.3, 0.45$  and  $1.5$ .

An investigation of the chemical structure of the ionomer glass with variation of P<sub>2</sub>O<sub>5</sub> content by XPS technique was illustrated in Figure 4.7. The high-resolution XPS spectra in the Al2p areas in Figure 4.7 (a) showed that the increasing in P<sub>2</sub>O<sub>5</sub> concentration in the glass composition was resulted in the increasing of tetrahedral [AlO<sub>4</sub>] structure. This showed that the [AlO<sub>6</sub>] octahedron was the dominant structural component of the sol-gel glass containing P<sub>2</sub>O<sub>5</sub> from 0.15 moles.

The percentage of BO and NBO in the ionomer glass structure analyzed by the O1s spectra were showed in Figure 4.7 (b). The results showed that the proportion of NBO decreased as the percentage of P<sub>2</sub>O<sub>5</sub> in the glass composition increased.

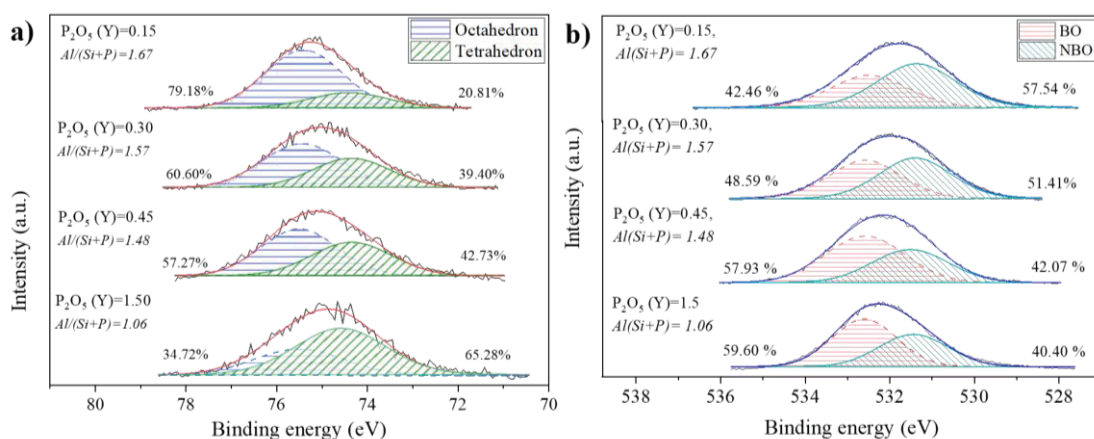


Figure 4.7 High resolution XPS spectra in the (a) Al<sub>2</sub>p and (b) O1s regions of the sol-gel ionomer glasses based on 4.5SiO<sub>2</sub>-4Al<sub>2</sub>O<sub>3</sub>-YP<sub>2</sub>O<sub>5</sub>-2CaO-2F<sub>2</sub> glass compositions, where Y= 0.15, 0.3, 0.45 and 1.5.

The concentrations of ions releasing for Si<sup>4+</sup>, Al<sup>3+</sup>, Ca<sup>2+</sup> and P<sup>5+</sup> ions from the sol-gel glasses were illustrated in Figure 4.8. All ions released in glass decreased significantly as P<sub>2</sub>O<sub>5</sub> concentration increased. This finding could imply that increasing the P<sub>2</sub>O<sub>5</sub> level in the glass composition lowered the acid susceptibility of the glass due to the low quantity of NBO.

Figure 4.8 (b) shows that for sol-gel glasses containing P<sub>2</sub>O<sub>5</sub> in the range of 0.15 to 0.45 moles, there is no significant variation in the P<sup>5+</sup> ions releasing in the acid solution. For the sol-gel glass with P<sub>2</sub>O<sub>5</sub> up to 1.5 moles, the P<sup>5+</sup> ions releasing tended to increase significantly.

In a glass network, P<sup>5+</sup> ions served as a network former to form a [PO<sub>4</sub>] tetrahedron with a single double bond (Scholze, 1964; Brow, 2000). After being introduced to the aluminosilicate based glass, the P<sup>5+</sup> ions preferred to share the valence electron with the Al<sup>3+</sup> ions. As a result, the linkage formation between the [AlO<sub>4</sub>] and [PO<sub>4</sub>] tetrahedra linked by sharing one corner bridging oxygen (BO). The finding in this study showed that the structural change from the [AlO<sub>6</sub>] octahedron to the [AlO<sub>4</sub>] tetrahedron caused by the increase in P<sub>2</sub>O<sub>5</sub> content and led to a decreasing of the NBO fraction in the glass structure, as illustrated in Figure 4.9.

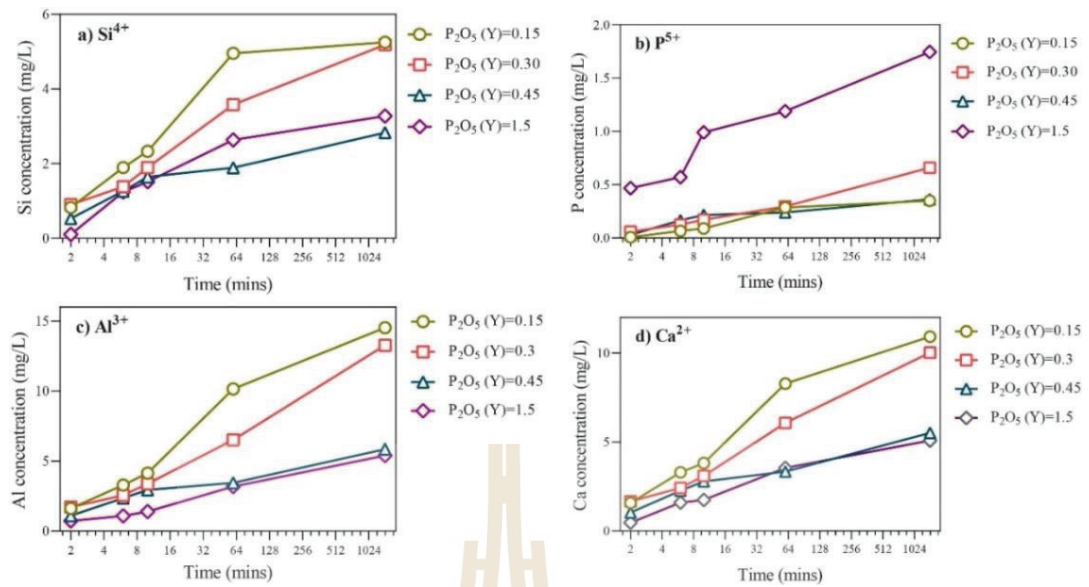


Figure 4.8 The concentration of (a)  $Si^{4+}$ , (b)  $P^{5+}$ , (c)  $Al^{3+}$  and (d)  $Ca^{2+}$  ions releasing from the sol-gel ionomer glasses based on  $4.5SiO_2-4Al_2O_3-YP_2O_5-2CaO-2F_2$  compositions, where  $Y=0.15, 0.3, 0.45$  and  $1.5$ , as function of the immersion times

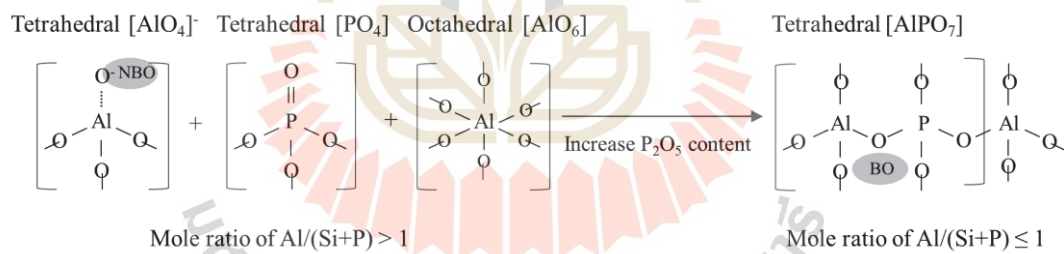


Figure 4.9 A proposed glass network structure for sol-gel ionomer glass with a variation of  $P_2O_5$  contents in the glass composition.

#### 4.3.2 Setting time and compressive strength of SGIC with $Al_2O_3$ and $P_2O_5$ variation

Figure 4.10 a) presents the working and net setting time of SGIC with the glass system of  $4.5SiO_2-XAl_2O_3-0.3P_2O_5-2CaO-2F_2$  system, where  $X = 2, 2.5, 3, 4$  and  $4.3$ , in comparison with the commercial product. The result showed that the working time of the commercial product was 3 min, and the net setting time was 4.55 min. At the same time, there was no significant effect of the variation of  $Al_2O_3$  content on

the working time of the sol-gel group which was presented in the range of 1-1.2 min. Moreover, the net setting time of the cement paste was extended when the  $\text{Al}_2\text{O}_3$  mole was increased from 2 to 3 moles. Up to an increase of  $\text{Al}_2\text{O}_3$  more than 4.3 mole, the net setting time was shortened.

The compressive strength of SGIC with  $\text{Al}_2\text{O}_3$  mole variation were illustrated in Figure 4.10 b). The compressive strength of the commercial product exhibited at  $109.68 \pm 4.12$  MPa. For the sol-gel group, the compressive strength was increased as the  $\text{Al}_2\text{O}_3$  mole in the glass composition and reached maximum at  $79.23 \pm 6.96$  MPa at 4 moles of  $\text{Al}_2\text{O}_3$ .

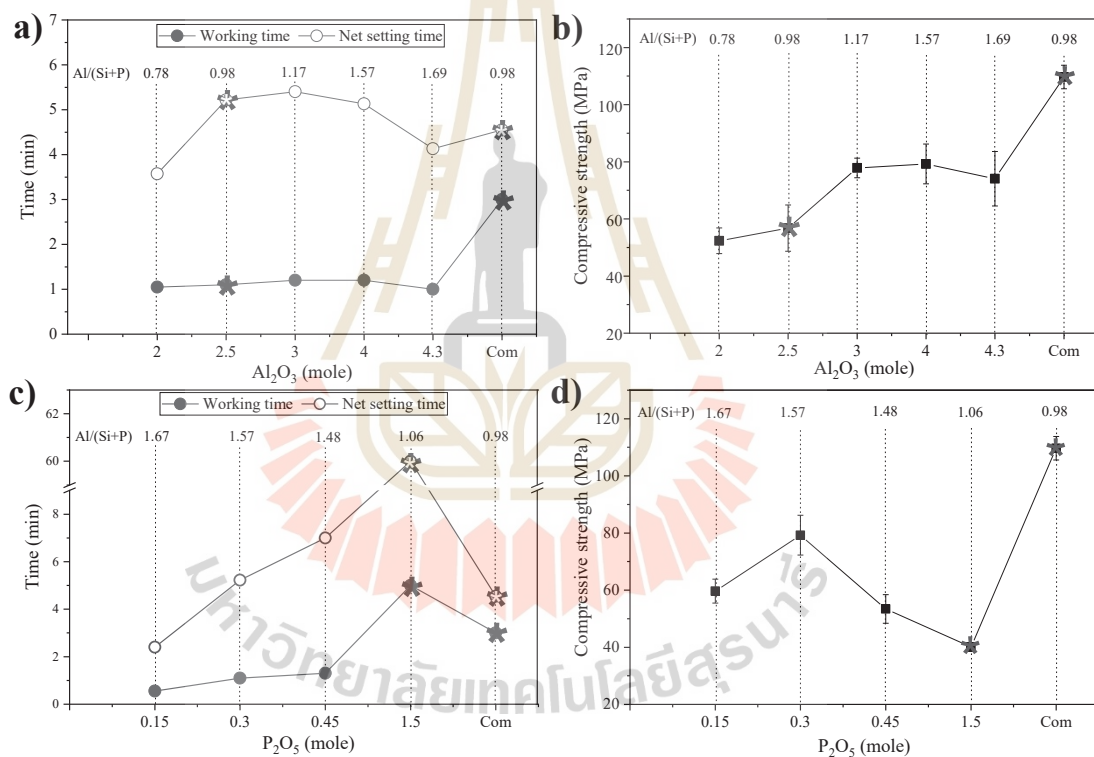


Figure 4.10 The effect of  $\text{Al}_2\text{O}_3$  mole in the sol-gel ionomer glass on a) setting time and b) compressive strength of SGIC. The effect of  $\text{P}_2\text{O}_5$  mole in the sol-gel ionomer glass on c) setting time and d) compressive strength of SGIC. Note: (\*) indicates the sol-gel sample ( $P/L = 1$ ) and the commercial product ( $P/L = 3.4$ ) with  $\text{Al}/(\text{Si}+\text{P})$  nearby 1 for comparison.

According to Billington's report,  $P^{5+}$  ion was probably a controller of working time (Billington et al., 2006). Since the  $P^{5+}$  ions releasing level of the commercial glass was higher than those of the sol-gel glass, the commercial GIC showed longer working time than SGIC in this study. Additionally, our finding on the compressive strength of GIC matched with the previous study that the increase of  $Al_2O_3$  did not affect compressive strength where  $Al/(Si+P) < 1$  (Griffin and Hill, 1999). Interestingly, the compressive strength was improved as increasing of  $Al^{3+}$  ions releasing from glass composition, where  $Al/(Si+P) > 1$ . This was because the  $Al^{3+}$  ion could form three-dimensional crosslinking networks after reacting with the polymeric liquid (Kim, Lee, Jun et al., 2017).

In case of a variation of  $P_2O_5$  moles in SGIC, the working and net setting time of the sol-gel ionomer glasses based on  $4.5SiO_2-4Al_2O_3-YP_2O_5-2CaO-2F_2$  compositions, where  $Y=0.15, 0.3, 0.45$  and  $1.5$  are showed in Figure 4.10 c). The result revealed that the increase of  $P_2O_5$  in glass composition resulted in extension of working and net setting time. At  $P_2O_5$  moles of  $1.5$ , the net setting time was extended to 60 min. It should be note that the setting time of the sol-gel glass with  $Al/(Si+P) \approx 1$  obtained longer than the commercial product.

Figure 4.10 d) presented the changing of compressive strength with the variation of  $P_2O_5$  mole in the sol-gel glass composition. The maximum compressive strength was  $79.23 \pm 6.96$  MPa which was found at  $P_2O_5$  at  $0.3$  moles. Further increase of  $P_2O_5$  moles in glass composition decreased the compressive strength which was vigorously lower than the commercial product.

In case of a variation of  $P_2O_5$  moles in SGIC, all samples prolonged setting time when  $P_2O_5$  mole increased up to  $1.5$  moles. From  $Al2p$  XPS spectra, it found that  $[AlO_4]$  tetrahedral was increased with increasing  $P_2O_5$  moles in SGIC, and  $O1s$  XPS spectra indicated that those bridging oxygens (BO) in the glass network increased as shown in Figure 4.10 (b). The addition of  $P_2O_5$  in the sol-gel glass composition probably form to  $[AlPO_7]$  tetrahedron as  $O^{2-}$  ion bonding between  $[PO_4]$  tetrahedron and  $[AlO_4]$  tetrahedron, so the bridging oxygens (BO) were formed in the glass network as can be explained in Figure 4.9 (scholze, 1964). It was resulting in low acid susceptible of SGIC; thus, the setting time was longer.

The acid resistance of SGIC could be attributed to the increase in BO resulting from the rise in  $P_2O_5$  moles (Kusumoto, 2009). This caused a reduction in the concentrations of ions ( $Al^{3+}$ ,  $Ca^{2+}$ ,  $Si^{4+}$ ) released from the glass, while the level of  $P^{5+}$  ions releasing increased significantly. This finding is consistent with the extended working and net setting time of SGIC.

The setting reactivity of SGIC played a crucial role in the preparation of uniform testing specimens for accurate strength measurements. Rapid working time of GIC might lead to difficulty in preparing uniform test specimens resulting in challenging to measure the exact value of its strength. The compressive strength of  $P_2O_5$  ( $Y$ ) = 0.15 provided significantly low because of shortening working time while the compressive strength of  $P_2O_5$  ( $Y$ ) = 0.30 showed higher due to homogeneous mixing of longer working time. However, the further adding of  $P_2O_5$  moles in glass composition resulted in reducing compressive strength due to the high acid resistance and low released ions ( $Al^{3+}$  and  $Ca^{2+}$ ) of SGIC. This result was similar to Griffin and Hill work that the melt-quenched glass with increasing of  $P_2O_5$  moles in glass composition led to longer setting time while that glass composition without  $P_2O_5$  mole was rapidly setting (Griffin and Hill, 2000). Considering of  $Al/(Si+P)$  ratio nearby 1 of SGIC ( $Al/(Si+P) = 1.06$ ,  $Y = 1.5$ ) in comparison with the melt-quenched glass of commercial GIC ( $Al/(Si+P) = 0.98$ ), the  $Al2p$  spectra result of both samples were similar, but the ion releasing behaviors were rigorous different. Therefore, it indicated that the  $Al/(Si+P)$  ratio near 1 should not be fixed for the sol-gel glass synthesis.

#### 4.3.3 DoE analysis

The Design of Experiments (DoE) technique was used to study how the interaction between  $Al_2O_3$  and  $P_2O_5$  in the sol-gel glass composition affected the setting time and compressive strength. This study was designed and analyzed using 2k full factorial experimental design by the Minitab Release 16 program as presented in Figure 4.11. The ANOVA test for the net setting times of SGIC with various  $Al_2O_3$  and  $P_2O_5$  contents in the glass compositions is shown in Figure 4.11 (a). The effect on the net setting time of SGICs was determined to be significant at 95% confidence level ( $P \leq 0.05$ ). The results showed that the change in  $Al_2O_3$  content had no effect

on the net setting time ( $P= 0.058$ ). The variation of  $P_2O_5$  content and the interaction between  $Al_2O_3$  and  $P_2O_5$  had a significant effect on the net setting time ( $P= 0.000$ ).

Figure 4.11 (b) reveals the main effect plot between the variation of the glass composition and the net setting time. This result supported the ANOVA result and showed that the net setting time of the sol-gel glass was significantly influenced by the  $P_2O_5$  content but was independent of the  $Al_2O_3$  content.

The result in Figure 4.11 (c) confirmed that there was a significant interaction between the variation of  $Al_2O_3$  and  $P_2O_5$  in the glass structure. The non-parallel lines in the interaction plot indicated that there was a strong correlation between the changes in the  $Al_2O_3$  and  $P_2O_5$  contents. The interaction of 0.15, 0.30, and 0.45 moles of  $P_2O_5$  with 3, 4.0, and 4.3 moles of  $Al_2O_3$  led to a significant increase of the net setting time of the sol-gel glasses. It was interesting to note that the interaction between 2 moles of  $Al_2O_3$  and 0.15-0.30 moles of  $P_2O_5$  did not affect the net setting time of the sol-gel glass. However, when the  $Al_2O_3$  content was at 0.2 moles and  $P_2O_5$  was at 0.45 moles, the net setting time was significantly increased. The finding in this study revealed that the addition of a high amount of  $P_2O_5$  in the glass composition could prolong the setting time due to the low susceptibility to acid attack of the glass. These results were consistent with previous research (Griffin and Hill, 2000), which found that the addition of more  $P_2O_5$  content to a melt-quenched glass could extend the setting time, while glass compositions without  $P_2O_5$  were set rapidly.

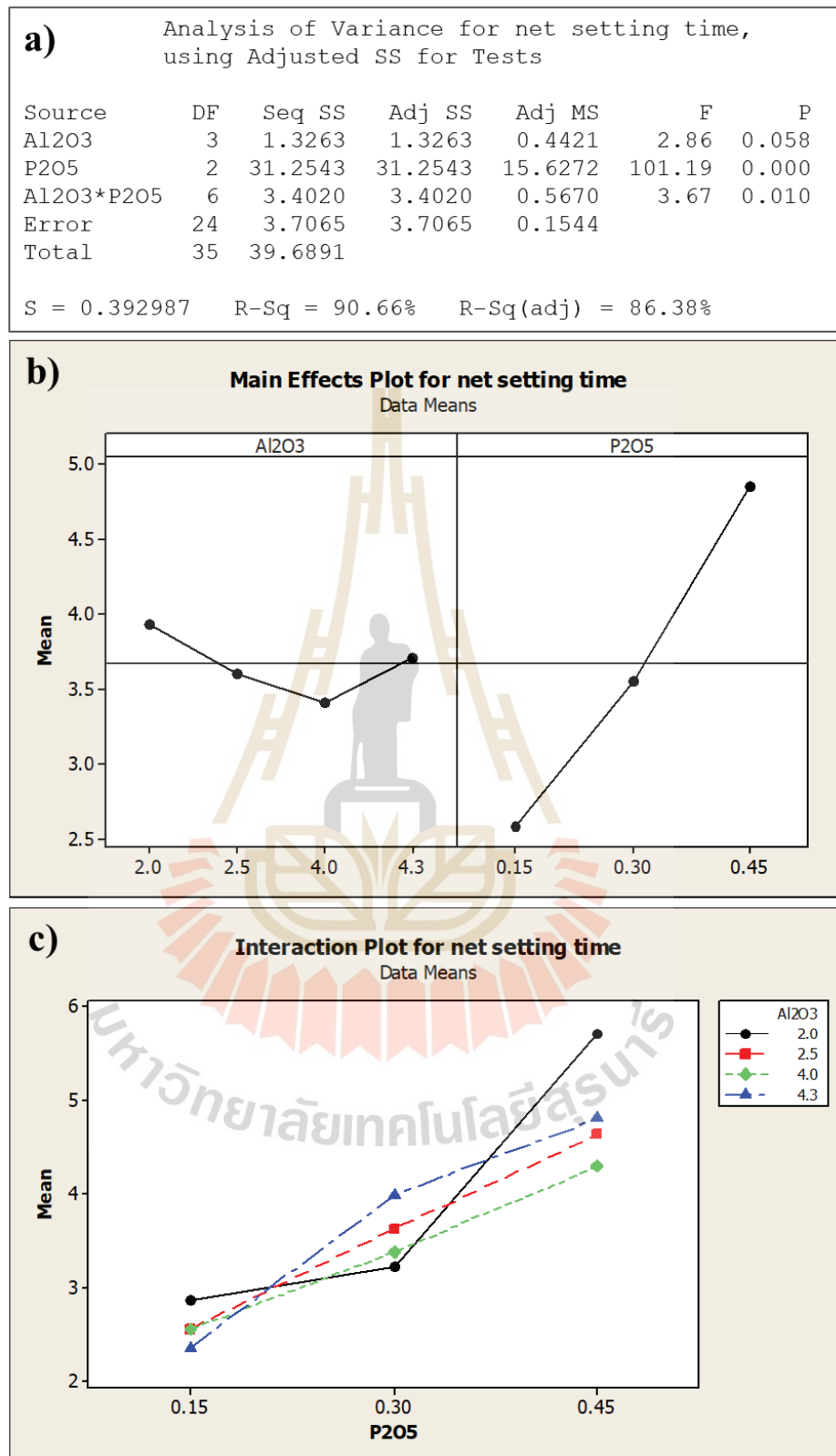


Figure 4.11 The experimental design analysis of the effects of variation of  $\text{Al}_2\text{O}_3$  and  $\text{P}_2\text{O}_5$  contents in SGIC compositions on the net setting times

Compressive strength of sol-gel GIC with varying  $\text{Al}_2\text{O}_3$  and  $\text{P}_2\text{O}_5$  contents was conducted to an ANOVA test, as shown in Figure 4.12 (a). The results showed that the compressive strength of SGIC was significantly impacted by the  $\text{Al}_2\text{O}_3$  content, the  $\text{P}_2\text{O}_5$  content, and their interaction at the 95% confidence level ( $P < 0.05$ ).

The main effect plot for compressive strength on the influence of  $\text{Al}_2\text{O}_3$  and  $\text{P}_2\text{O}_5$  moles variation in the sol-gel glass composition is shown in Figure 4.12 (b). Compressive strength was found to be maximum at 4 moles of  $\text{Al}_2\text{O}_3$  and 0.3 moles of  $\text{P}_2\text{O}_5$ , and any further additions of these two components could lead to a decrease in compressive strength. The reduction of compressive strength for the glass composed with 0.45 moles of  $\text{P}_2\text{O}_5$  was possibly due to the reduction of  $\text{Ca}^{2+}$  and  $\text{Al}^{3+}$  ions as shown in Figure 4.8. For the glass composed with 4.3 moles of  $\text{Al}_2\text{O}_3$ , their low compressive strength was associated with a data error caused by the rapid setting of GIC, resulting in a non-homogeneous sample.

The interaction plot for compressive strength based on the variation in  $\text{Al}_2\text{O}_3$  and  $\text{P}_2\text{O}_5$  contents in the sol-gel glass composition is shown in Figure 4.12 (c). This result showed that 4 moles of  $\text{Al}_2\text{O}_3$  and 0.3 moles of  $\text{P}_2\text{O}_5$  provided the maximum compressive strength of SGIC. Thus, the compressive strength of the GIC was influenced by both  $\text{Al}_2\text{O}_3$  and  $\text{P}_2\text{O}_5$  moles in the composition of the sol-gel glass.

In contrast to the previous findings of the melt derived GIC, this research discovered that the compressive strength of SGIC was significantly affected by the amount of  $\text{Al}_2\text{O}_3$  in the glass composition (Griffin and Hill, 1999). Moreover, compositions of glass with an  $\text{Al}/(\text{Si}+\text{P})$  ratio greater than 1 were found to have greater compressive strength in this investigation. This could be because the glass with an  $\text{Al}/(\text{Si}+\text{P})$  ratio greater than 1 released high amount of  $\text{Al}^{3+}$  ions. When  $\text{Al}^{3+}$  ions interacted with polyacrylic acid during the setting process, they formed a three-dimensional crosslinking network that strengthened the cement (Kim et al., 2017).

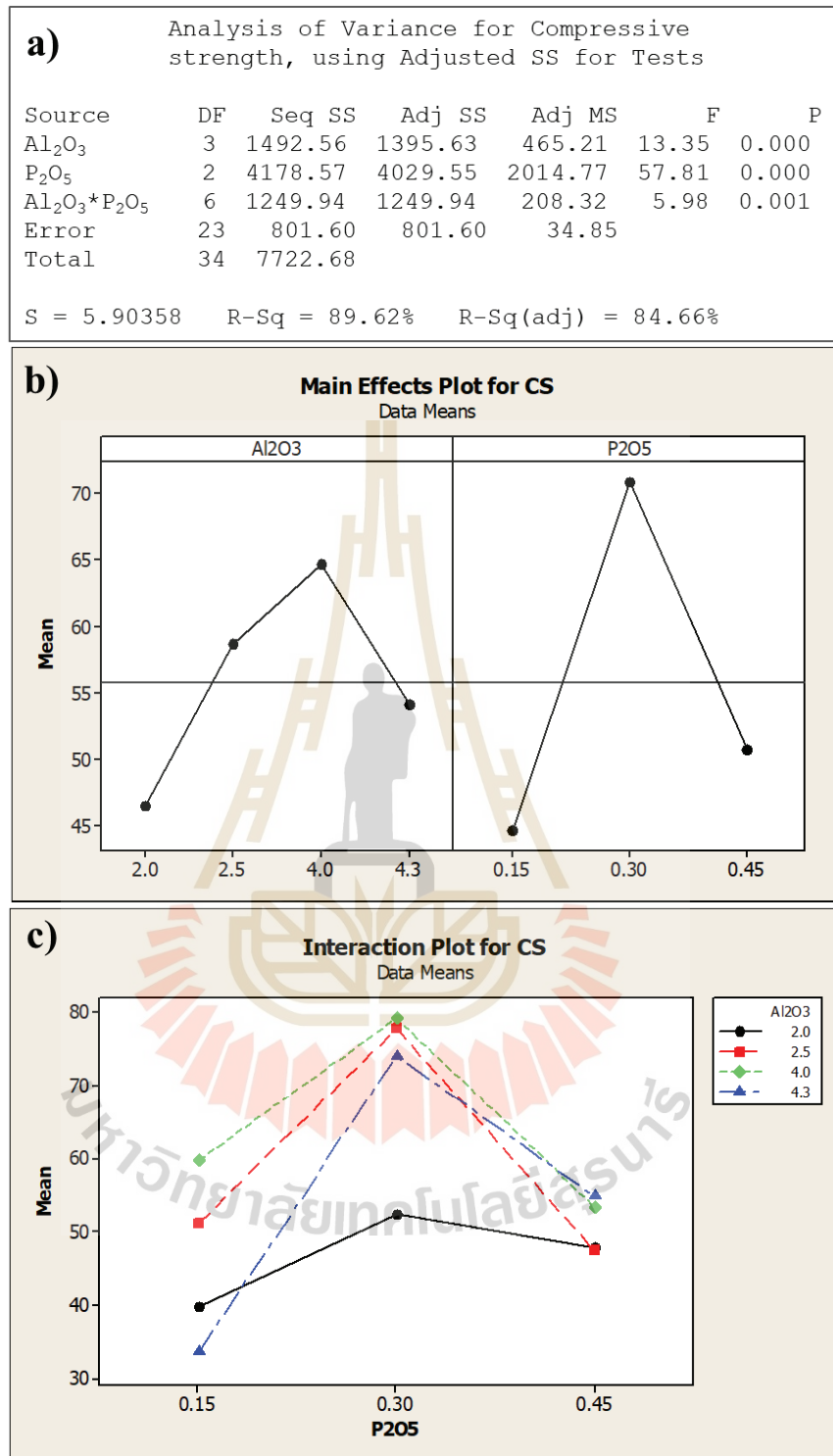


Figure 4.12 The DoE analysis for the compressive strength of SGIC with Al<sub>2</sub>O<sub>3</sub> and P<sub>2</sub>O<sub>5</sub> variation. (a) ANOVA analysis, (b) the main effects plot and (c) the interaction plot of Al<sub>2</sub>O<sub>3</sub> and P<sub>2</sub>O<sub>5</sub> contents in glass compositions for the compressive strength of SGICs.

In the case of SGIC prepared with the low  $P_2O_5$  in glass composition, the cement paste was set rapidly that cause inhomogeneous specimens and low compressive strength. This result related to excessive  $Al^{3+}$  and  $Ca^{2+}$  ions released as shown in Figure 4.8. When the  $P_2O_5$  content was increased,  $Al^{3+}$  and  $Ca^{2+}$  ions releasing level trended to be decreased resulting in prolonging setting time. These findings indicated that the ion releasing level should be optimized for the GIC. The sol-gel glass containing 0.3 moles of  $P_2O_5$  and 0.4 moles of  $Al_2O_3$  ( $Al/(Si+P) = 1.57$ ) was the optimal composition for setting time and compressive strength in this study. Therefore,  $Al/(Si+P)$  ratio might not be equal to 1 for the glass synthesized by the sol-gel method.

#### 4.4 Conclusions

This chapter demonstrated the effect of varying the  $Al_2O_3$  and  $P_2O_5$  contents in the glass composition synthesized by the sol-gel method designed for GIC. The glass composition in this study was designed and analyzed by DoE technique. The results demonstrated that an increase of  $Al_2O_3$  content in the glass formula could enhance the compressive strength of SGIC, although the structure composed of a large proportion of  $[AlO_6]$  octahedra and BO. An increase of  $P_2O_5$  content in the glass composition led to increasing of  $[AlO_4]$  tetrahedron and BO, resulting in prolonging the setting reactivity and lowering compressive strength of the cement. The glass composed of 4.0 mol  $Al_2O_3$  and 0.3 mol  $P_2O_5$  ( $Al/(Si+P) = 1.57$ ) produced the GIC with the highest compressive strength in this study. DoE analysis verified that the setting time and compressive strength were affected by the interaction between  $Al_2O_3$  and  $P_2O_5$  in the glass composition.

## CHAPTER 5

### EFFECT OF ZnO DOPING AND CALCINATION TEMPERATURE ON SGICs ( $4.5\text{SiO}_2\text{-}4\text{Al}_2\text{O}_3\text{-}0.3\text{P}_2\text{O}_5\text{-(}2\text{-X)CaO-XZnO-}2\text{F}_2$ )

This study aimed to improve the biological properties of the sol-gel ionomer glass obtained from Chapter 4 by doping ZnO into the ionomer glass and investigating the effect of calcination temperature to optimize the physical properties of SGIC. The DoE technique was used to design and analyze the effect of the dopant on the physical properties. Additionally, the study utilized X-ray photoelectron spectroscopy (XPS) and synchrotron-based X-ray absorption spectroscopy (XAS) techniques to gain a deeper understanding of the relationship between the physical properties and the structure of the ionomer glass and cement.

Apart from that, this study evaluated the antibacterial properties of the ZnO-doped SGICs, its ability to form apatite crystal, and cell cytotoxicity. The results of these evaluations provided valuable insights into the effectiveness of ZnO-doped SGIC for dental restorative materials and its potential use in various clinical applications. Overall, this study contributed to the understanding of the structural and physical properties of ZnO-doped SGIC and its potential use as a dental restorative material.

#### 5.1 Research background

It was known that dental caries is a prevalent oral health issue that occurs when acid-producing bacteria cause subsurface demineralization of the teeth (Wong et al., 2017). When caries has developed, filling the affected area with dental restorative materials is the primary treatment option. One such material is GICs, which has the advantage of releasing fluoride ions into the oral cavity, thus promoting tooth decay resistance (California, 2005). Based on the literature review in Chapter 2, fluoride release was insufficient to improve the antibacterial properties. Therefore, researchers had attempted to enhance the antibacterial properties of GICs by

incorporating different bactericidal agents (Takahashi et al., 2006, Farrugia and Camilleri, 2015).

Zinc ions are known to be bactericidal agents that inhibit the formation of caries (Li, Zhang, Niu et al., 2012, Tiama, Abd, Tohamy et al., 2017). Incorporating zinc into GIC has several benefits, including enhanced flexural strength, surface roughness, and good abrasive wear (Patil, Patel, Kunte et al., 2020, Kumar, Raj, Singh et al., 2021). Furthermore,  $Zn^{2+}$  ions have the same charge as  $Ca^{2+}$  ions (or  $Sr^{2+}$  ion for the commercial GIC) which play a crucial role in the glass network structure as a charge balancing agent and as a cross-linking ion in GIC structure (Sidhu and Nicholson, 2016, Zhang and Stamboulis, 2016, Thongsri, Srisuwan, Thaitalay et al., 2021).  $Zn^{2+}$  ions are supposed to act as a replacement for  $Ca^{2+}$  ions in the ionomer glass structure. However, a previous literature suggested that incorporating zinc in aluminosilicate glass, which was derived through traditional melt-quenching process, increased glass structural density, and induced some crystallization (Zhang and Stamboulis, 2016). In the case of the sol-gel synthesis, there is currently lack of research available on the effect of ZnO content in ionomer glass composition on the structure of both the glass network and GIC, as well as their properties.

Thus, this study aims to investigate the effects of ZnO doping, instead of CaO, in the ionomer glass composition. This study also investigated the calcination temperature along with variation of ZnO concentration. The relationship of chemical structure of the resulting powder on ion-releasing behavior, setting reactivities and compressive strength was determined. The chemical structure of the ionomer glasses and GICs will be analyzed in-depth using XPS and XAS characterization techniques. In addition, the crucial testing for this experiment included evaluating its antibacterial properties as well as other biological tests i.e., cell cytotoxicity, apatite formation ability, and interface examination between the material and the tooth structure.

## 5.2 Experimental procedure

### 5.2.1 Preparation of ionomer glass

In this study, the ionomer glass system of  $4.5SiO_2-4Al_2O_3-0.16P_2O_5-(2-x)Ca-xZnO-2F_2$ , where  $x= 0, 0.6, 1.0$  and  $1.4$ , synthesized by the sol-gel method at the different calcination temperatures. The synthesis process in this experiment was in

accordance with the previous experiment in Chapter 4. The amount of chemical content was presented in Table II of Appendix B. Briefly, the synthesis process started by adding TEOS into the mixed solution of DI water and EtOH. Next,  $\text{Al}(\text{NO}_3)_3$ , TEP,  $\text{Ca}(\text{NO}_3)_2 \cdot 4\text{H}_2\text{O}$  and  $\text{Zn}(\text{NO}_3)_2 \cdot 6\text{H}_2\text{O}$  were sequentially added and stirred by a magnetic stirrer. Then, the solution was aged under an acid condition at a temperature of  $85^\circ\text{C}$  for 15 hours. The calcination temperature varied in the range of  $600^\circ\text{C}$ - $750^\circ\text{C}$ . The resulting powder was then ground in a planetary mill to obtain the fine glass powder.

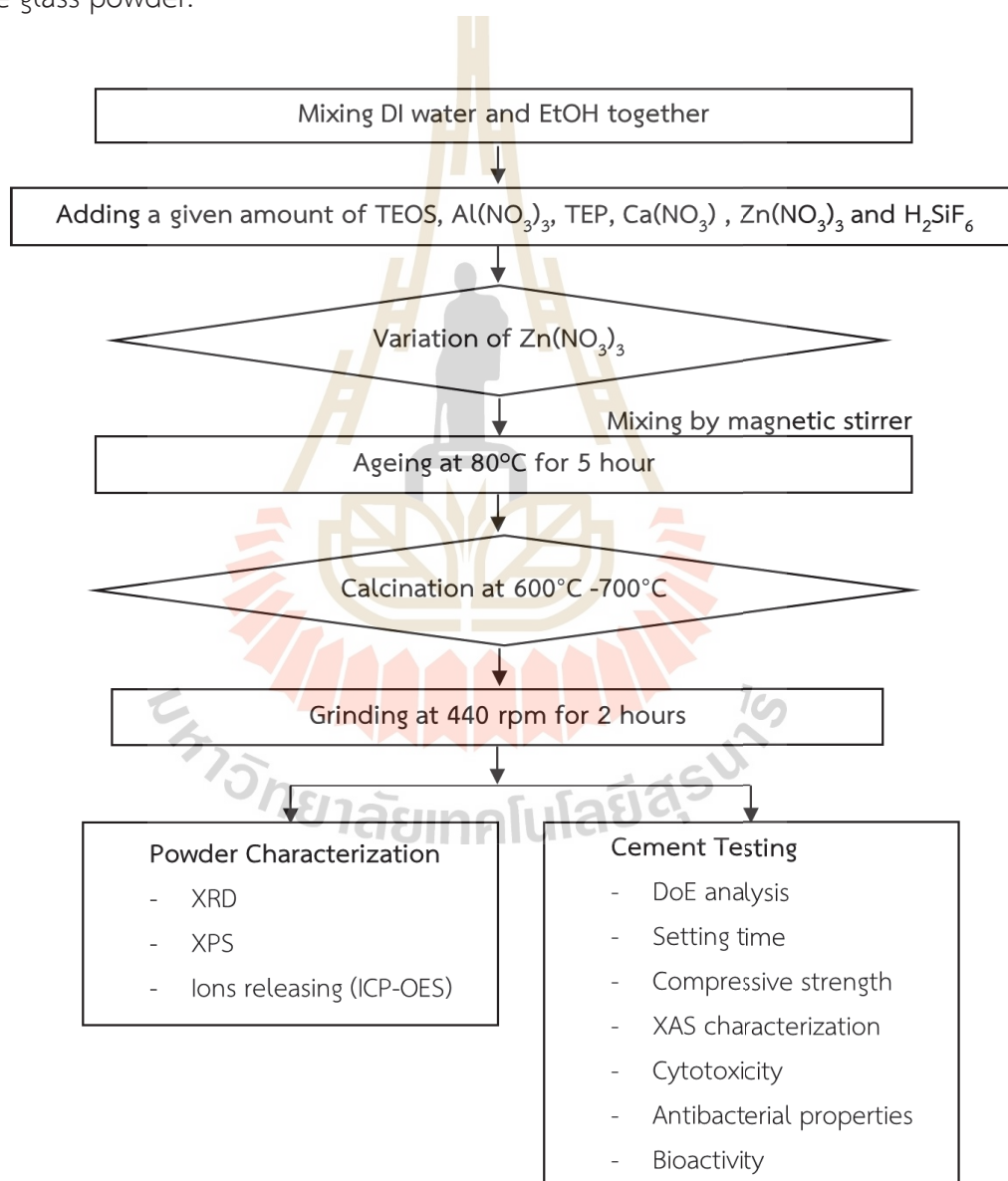


Figure 5.1 Schematic of experimental design to determine the substitution of ZnO for CaO and the optimization of calcination temperature.

The summary of the experiment was illustrated in Figure 5.1. This experimental design was based on the DoE technique. The compressive strength of SGICs was evaluated by designing a 2k full factorial using Minitab 16 statistical software to investigate the effects of ZnO substitution for CaO in the ionomer glass. Moreover, this study also explored the effect of calcination temperatures on the sol-gel ionomer glass. The ionomer glass compositions and calcination temperature studied in this experiment were presented in Table 5.1.

Table 5.1 Design composition for the sol-gel ionomer glass of  $4.5\text{SiO}_2\text{-}4\text{Al}_2\text{O}_3\text{-}0.16\text{P}_2\text{O}_5\text{-(}2\text{-x)Ca-xZnO-}2\text{F}_2$ , where  $x= 0, 0.6, 1.0$  and  $1.4$ .

Sample code	Mol ratio					
	Si	Al	P	F	Ca	Zn
0Zn	4.5	4	0.16	4	2	0
0.6Zn					1.4	0.6
1.0Zn					1	1
1.4Zn					0.6	1.4

### 5.2.2 Characterization of the sol-gel glass for glass ionomer cement

This study utilized various techniques to analyze the chemical and glass network structure of the sol-gel ionomer glass, as well as to investigate the ion-releasing behavior and local structural information around Ca and Zn atoms. The chemical structure of the sol-gel glass was analyzed using a German Bruker D2 X-ray diffractometer (XRD) and X-ray photoelectron spectroscopy (XPS) technique. The XPS measurement was conducted at the Synchrotron Light Research Institute (SLRI) using PHI5000 Versa Probe II with monochromatic Al K-alpha radiation (1486.6 eV) as an excitation source. The ion-releasing concentrations of the ionomer glass powders were evaluated in acetic acid and the concentrations of ions (Si, Al, P, Ca, and Zn) released were measured by immersing 0.05 g of the glass powders in 10 ml of 5% acetic acid for different lengths of time (2, 6, 10, and 60 minutes) and then filtering out the glass powder. Inductively Coupled Plasma (ICP-OES optima 8000, Perkin) was used for evaluation of ions concentrations. Elemental stock solutions (1000 ppm) of

Silicon (Si), Phosphate (P), Aluminium (Al), Zinc (Zn) and Calcium (Ca) were used to prepare calibration standards. All calibration solutions were made up to volume with 2 wt.% nitric acid (HNO<sub>3</sub>).

After the setting reaction, SGIC specimens were evaluated by synchrotron-based X-ray absorption spectroscopy (XAS) techniques, which included in-situ X-ray absorption near edge structure (in-situ XANES) and in-situ extended X-ray absorption fine structure (in-situ EXAFS). The in-situ XAS measurement was conducted at the SUT-NANOTEC-SLRI XAS Beamline (BL5.2) at the Synchrotron Light Research Institute (Public Organization), Thailand (Kidkhunthod, 2017). The data were analyzed and fitted by Athena and Artemis programs as implemented in the IFEFFIT packages (Newville, 2001). The reference standard curves were from the material project (file number; mp-2605\_CaO and mp-1986\_ZnO) (Jain, Ong, Hautier et al., 2013).

### **5.2.3 Preparation of the cement and the physical properties testing**

The preparation of the cement was in accordance with the previous chapter. Briefly, the liquid solution for mixing with the sol-gel glass powder comprised of a mixture of polyacrylic acid (35 wt.% in H<sub>2</sub>O PAA; MW ~ 100,000) and tartaric acid in a 9:1 w/w ratio. To prepare SGIC samples, the sol-gel ionomer glass powders were mixed with the liquid solution at a powder to liquid ratio (P/L) of 1/1 (w/v).

In this experiment, physical properties including setting time and compressive strength were evaluated. The testing methodology for these properties was consistent with that employed in the previous chapter.

### **5.2.4 Setting time and compressive strength testing**

The evaluation of the setting time and compressive strength of SGIC was performed in accordance with the methodology outlined in Chapter 4, sections 4.2.4 and 4.2.5.

### **5.2.5 Antibacterial testing**

In order to evaluate the antibacterial activity of SGICs, the agar disk diffusion method was employed against *Streptococcus mutans* (*S. mutans*, ATCC

27145, MicroBiologics Inc., USA), with a comparison made to a commercially available GIC (Fuji IX extra, GC corporation, Tokyo, Japan). *S. mutans* was cultured at 37°C, 5% CO<sub>2</sub> for 24 hours and then uniformly swabbed on Mueller-Hinton agar (HiMedia Laboratories Pvt.Ltd., India). SGIC samples in disc shape were placed onto the agar and incubated at 37°C for 48 h. The antibacterial testing was performed under both dark and visible light conditions. For the dark condition, plates were immediately placed in a black box prior to incubation, while for the visible light condition, plates were processed and incubated without being placed in the black box. The diameter of the inhibition zone around the SGIC discs was measured to evaluate the bacterial activity. The calculation of the inhibition zone size was performed as follows: size of inhibition zone (mm) = (diameter of inhibition zone – diameter of disc)/2.

### 5.2.6 Cell cytotoxicity

The cytotoxicity of SGICs was assessed by the cell viability of NIH/3T3 fibroblast following treatment with SGIC extracts, as determined by MTS assay. SGICs were molded into disc shape ( $\varnothing = 12$  mm, h = 2 mm), left to set in air for 1 h, sterilized by UV light on each side for 30 min, and rinsed with 1x PBS. SGIC extracts were prepared by immersing the cement discs in 1 ml of cell culture medium and incubated at 37°C for 24 hours. The culture medium was composed of 44% Dulbecco's Modified Eagle Medium (DMEM (1X) from Invitrogen, USA), 44% F-12 Nutrient Mixture (HAM from Invitrogen, USA), 10% Fetal Bovine Serum (FBS from Invitrogen, USA), 1% L-glutamine, and 1% Penicillin-streptomycin (Invitrogen, USA). NIH/3T3 fibroblast cells were seeded at a density of 5,000 cells/well in a 96-well plate. After 24 hours of seeding, the cells were treated with different concentrations of GIC extract (0, 0.6, and 1.4 ZnO) for 24 hours. Culture media with cells were used as a negative control. Cell viability was assessed by adding 20  $\mu$ l of MTS reagent (CellTiter 96® AQueous) to each well plate. After 2 hours of incubation, the optical density was measured at 490 nm (OD<sub>490</sub>) using an automated plate reader. The percentage of viable cells was calculated from OD values using the following equation: %Cell viability = (Sample absorbance value/Control group absorbance value) x100.

In addition, the extracted medium was collected and diluted 20-fold with DI water to evaluate the concentration of released  $Zn^{2+}$  ions using the ICP-OES technique (ICP-OES optima 8000, Perkin). Elemental stock solutions (1000 ppm) of Zinc (Zn) were used to prepare calibration standards. All calibration solutions were made up to volume with 2 wt.% nitric acid ( $HNO_3$ ).

### 5.2.7 *In vitro* bioactivity and tooth-GIC interface

To determine the *in vitro* bioactivity of the material, the ability of apatite-like formation on SGIC surface was investigated. SGIC doping with 0, 0.6 and 1.4 ZnO were prepared in a cylindrical shape, with 2 mm in height and 10 mm in diameter. The specimens were then immersed in artificial saliva for 5 days. The composition of the artificial saliva consisted of 0.4 g Sodium chloride (NaCl, 98%, Carlo Erba), 0.4 g Potassium chloride (KCl, 99.5% , Merck), 0.795 g Calcium chloride ( $CaCl \cdot H_2O$ , Merck), 0.69 g Sodium phosphate monobasic monohydrate ( $NaH_2PO_4 \cdot H_2O$ , 98%, Merck), 0.005 g Sodium sulfide nonahydrate ( $Na_2S \cdot 9H_2O$ , 98%, Carlo Erba), and 1000 mL DI water (El Mallakh and Sarkar, 1990).

In this experiment, the tooth-GIC interface was observed to determine the possibility of the material to attach the tooth structure. To observe the tooth-GIC interface, premolar teeth were prepared and filled with SGIC specimens. After 1 hour of air-drying, all specimens were transferred to the artificial saliva and incubated at 37°C for 7 days. The specimens were then embedded in resin and cross-sectioned to observe the interfacial area between the tooth and GIC. The morphology of surface and interface area of specimens were examined using a scanning electron microscope (SEM, JEOL-6010LV) at an acceleration voltage of 15 kV. Prior to examination, all specimens were coated with gold.

### 5.3 Results and discussions

#### 5.3.1 Characterization of the sol-gel derived ionomer glass

The XRD patterns of  $4.5\text{SiO}_2\text{-}4\text{Al}_2\text{O}_3\text{-}0.16\text{P}_2\text{O}_5\text{-(}2\text{-x)Ca-xZnO-}2\text{F}_2$ , with  $x$  values of 0, 0.6, 1.0, and 1.4, synthesized by the sol-gel method at varying calcination temperatures are presented in Table 5.1. All XRD patterns show an amorphous phase, indicating the absence of a crystalline structure, as shown in Figure 5.2. However, when 1.0 moles of ZnO were doped and the sol-gel glass was calcined at  $750^\circ\text{C}$ , a peak at approximately  $2\theta$  of 38 was observed, indicating the formation of the crystal  $\text{ZnAl}_2\text{O}_4$  (JCPDS:05-0669) and ZnO (JCPDS:01-1150) phase. The crystallinity of the glass increased with the rise in calcination temperature, as illustrated in Figure 5.2 b).

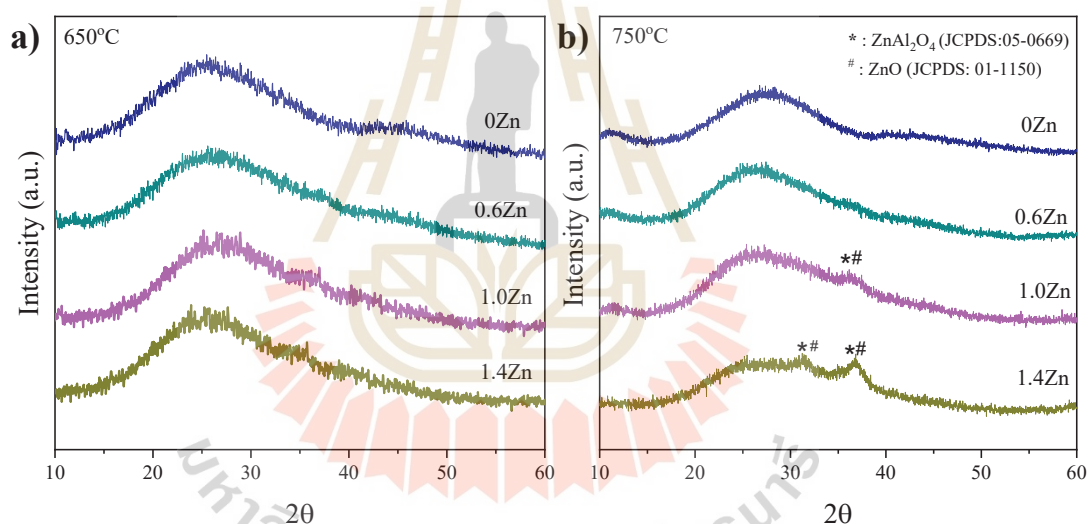


Figure 5.2 XRD pattern of the sol-gel ionomer glass belonging to the system of  $4.5\text{SiO}_2\text{-}4.0\text{Al}_2\text{O}_3\text{-}0.16\text{P}_2\text{O}_5\text{-(}2\text{-x)Ca-xZnO-}2\text{F}_2$ , where  $x=0, 0.6, 1.0$  and  $1.4$  calcined at (a)  $650^\circ\text{C}$  and (b)  $750^\circ\text{C}$ .

The sol-gel process was reported to involve the formation of a colloidal suspension or sol by the hydrolysis of the initial composition. The sol was then transformed into a wet gel during polymerization and finally converted into a dense ceramic by drying and heat treatment (Bogomolova et al., 2006). The heating step and slow cooling rate of the sol-gel process could easily induce phase separation

and crystal growth (Zanotto, 1992, Roy et al., 1995). As shown in Figure 5.2, the crystal structure was observed to form when the calcination temperature was increased.

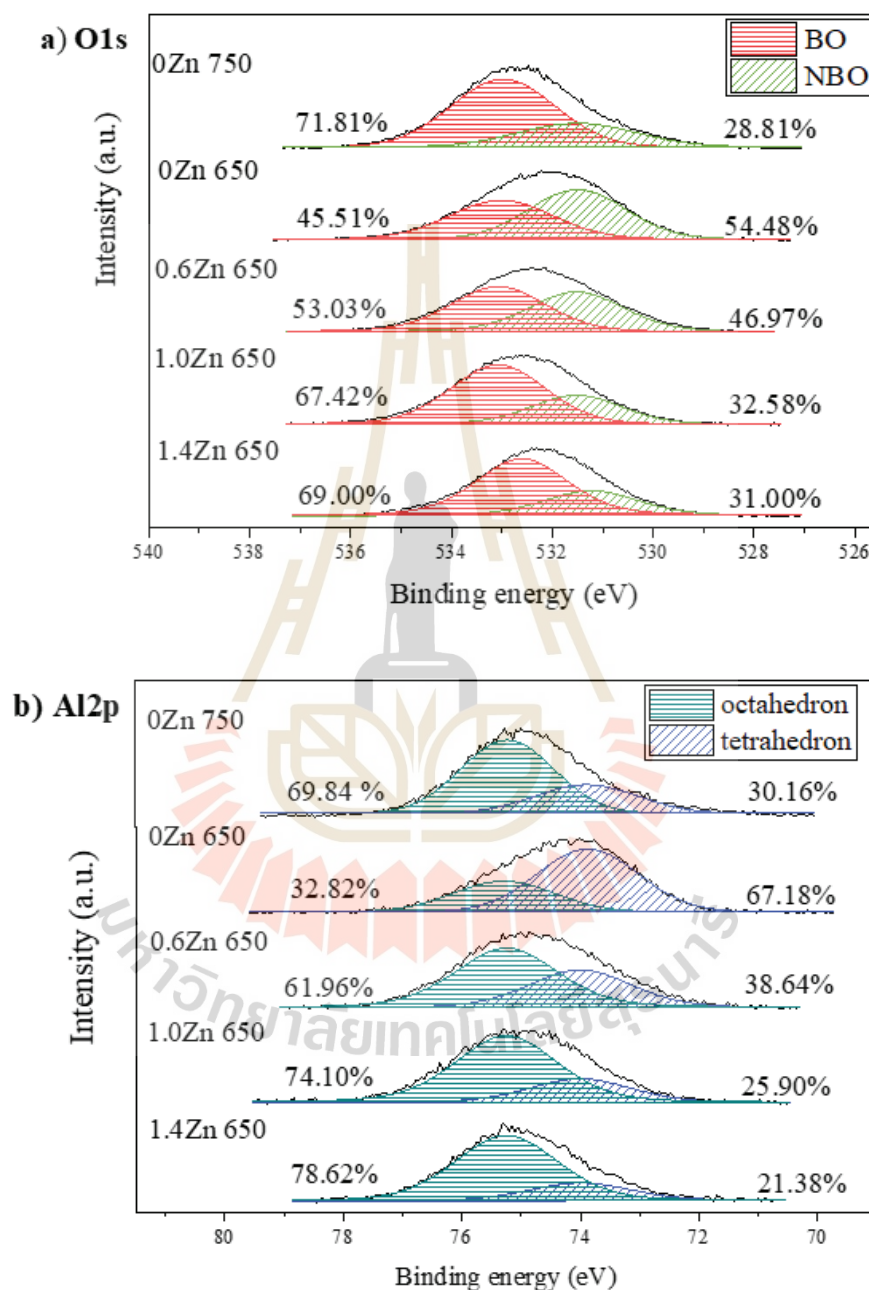


Figure 5.3 The high-resolution XPS spectra of a) Oxygen (O1s) and b) Aluminium (Al2p) for the sol-gel ionomer glass belonging to the system of  $4.5\text{SiO}_2\text{-}4.0\text{Al}_2\text{O}_3\text{-}0.16\text{P}_2\text{O}_5\text{-(}2\text{-x)Ca-xZnO-}2\text{F}_2$ , where  $x=0, 0.6, 1.0$  and  $1.4$  calcined at  $650^\circ\text{C}$  as compared to the Zn-free ionomer glass calcined at  $750^\circ\text{C}$

In this experiment, XPS was used to evaluate the chemical states of oxygen, aluminum, and zinc in sol-gel glasses. This information is important for understanding chemical bonding and interactions, as well as for optimizing the synthesis process and developing new compositions. The result of the chemical states of oxygen, aluminum and zinc for the sol-gel glasses is shown in Figure 5.3.

Figure 5.3 a) shows the XPS spectra of the O1s peak for the sol-gel glasses. Two deconvoluted peaks were observed at around 532.9 eV and 531.0 eV, which corresponded to the bridging oxygen (BO) and non-bridging oxygen (NBO) groups, respectively (Roy et al., 1995). The NBO fraction decreased significantly with increasing calcination temperature in the absence of ZnO doping. Additionally, the NBO fraction decreased with increasing ZnO doping in the glass composition.

In Figure 5.3 b), the high-resolution XPS spectra in the Al2p region of the sol-gel glass is presented. The deconvoluted Al2p peaks at binding energies around 75.3 eV and 74 eV are attributed to [AlO<sub>6</sub>] octahedral and [AlO<sub>4</sub>] tetrahedral structures, respectively (Tshabalala, Cho, Park et al., 2011). For the Zn-free sol-gel glasses, the proportion of [AlO<sub>4</sub>] tetrahedral structure reduced with increasing calcination temperature from 650°C to 750°C. As increasing Zn content in the glass composition, the [AlO<sub>4</sub>] tetrahedron was also decreased.

In Figure 5.4 a), the Ca2p spectra exhibit a spin-orbit doublet with binding energies of around 348.37 and 352.02 eV, characteristic of CaF<sub>2</sub> (Stranick and Root, 1991). In the Zn-free sol-gel glass calcined at 650°C, the peak was slightly broadened and shifted to a higher binding energy due to the presence of Ca-O and Ca-OH bonds (Bezerra and Valerio, 2016).

Figure 5.4 b) shows the Zn2p double spectra of the ZnO-doped glass, with binding energies around 1045 and 1021.5 eV corresponding to tetrahedral Zn<sup>2+</sup> ions, and peaks at 1047.5 and 1024.0 eV assigned to octahedral Zn<sup>2+</sup> ions (Zhang, Qingjie, Ren et al., 2017). Additionally, the fraction of octahedral Zn<sup>2+</sup> ions increased with increasing of the ZnO content in the glass composition.

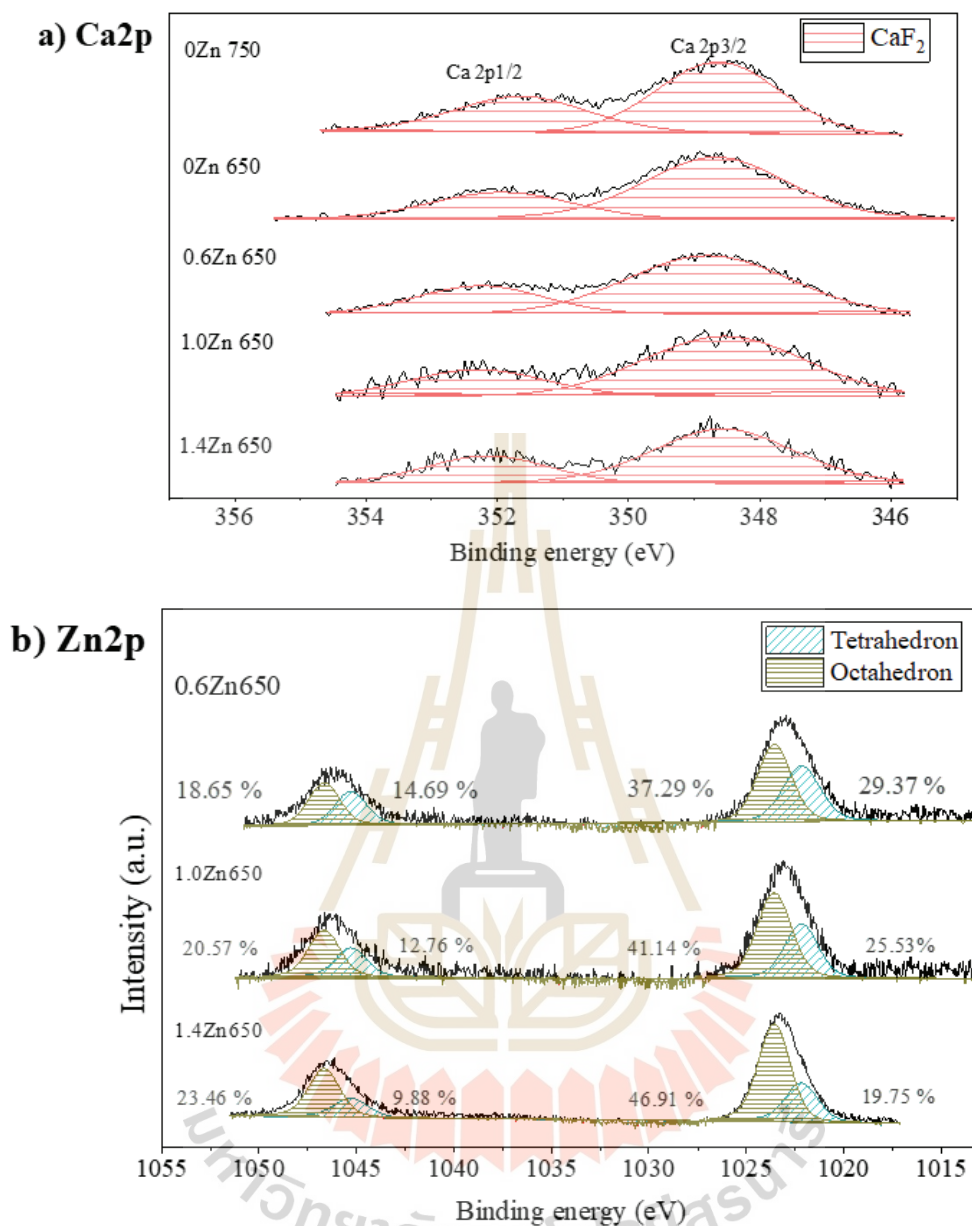


Figure 5.4 The high-resolution XPS spectra of a) Calcium (Ca2p) and b) Zinc (Zn2p) for the sol-gel ionomer glass belonging to the system of  $4.5\text{SiO}_2\text{-}4.0\text{Al}_2\text{O}_3\text{-}0.16\text{P}_2\text{O}_5\text{-(}2\text{-x)Ca-xZnO-}2\text{F}_2$ , where  $x=0, 0.6, 1.0$  and  $1.4$  calcined at  $650^\circ\text{C}$  as compared to the Zn-free ionomer glass calcined at  $750^\circ\text{C}$

The XPS spectra analysis revealed the presence of  $\text{Al}^{3+}$  ions in both tetrahedral and octahedral forms. Addition of ZnO to the glass composition resulted in an increase in the  $[\text{AlO}_6]$  octahedral fraction. Kusumoto suggested that the increase in  $[\text{AlO}_6]$  octahedral species was due to the charge balancing of  $\text{Zn}^{2+}$  ions in Al-O-

$\text{PO}_3^{3-}$  species leading to an insufficient charge balancing ion for maintaining  $[\text{AlO}_4]$  tetrahedron (Kusumoto, 2009). Our finding showed the probability of  $\text{ZnAl}_2\text{O}_4$  existence where  $\text{Al}^{3+}$  ions were in the octahedral site, and  $\text{Zn}^{2+}$  ions were in the tetrahedral site. Additionally,  $\text{Zn}^{2+}$  ions in the octahedral site were increased with ZnO content in the glass composition. It was possible that the excessive  $\text{Zn}^{2+}$  ions formed with  $\text{O}^{2-}$  ions at 6-fold coordination and played a role as a charge compensation for the glass network (Bernasconi, Dapiaggi, Pavese et al., 2016).

### 5.3.2 Ion releasing concentrations of the Zn doped sol-gel ionomer glass

To understand the setting reaction, the ion releasing behavior of ionomer glasses under acidic conditions was evaluated. The ICP-OES technique was used to assess the ion releasing levels of the glass in 5% acetic solutions, and the results are presented in Figure 5.5. The data revealed the concentration of Al, Ca, Zn, Si, and P ions at 2, 6, 10, and 60 minutes of immersing period.

Figure 5.5 (a) shows the level of Al ions released from the sample calcined at 650°C and 750°C. It was observed that the level of Al ions was higher in the sample without Zn doping and calcined at 650°C than in the one calcined at 750°C. In the case of ZnO-doped glass, no significant differences in  $\text{Al}^{3+}$  ion concentration were observed with variations in ZnO content.

Figure 5.5 (b) and (c) present that the addition of ZnO in the glass composition caused a reduction in the releasing level of  $\text{Ca}^{2+}$  ions and an increasing of the releasing level of  $\text{Zn}^{2+}$  ions, respectively, with an increasing of ZnO content. Moreover, the high calcination temperature resulted in a reduction in the level of calcium ions released from the glass.

The addition of ZnO in the glass composition led to a reduction in the amount of Si ions released, as observed in Figure 5.5 (d). However, there was no significant difference in the level of  $\text{Si}^{4+}$  ions release among the ZnO doped series. Interestingly, the glass calcined at 650°C released a higher level of  $\text{Si}^{4+}$  ions than that of the 750°C sample. It was suggested that the ion species of Si released to the acid solution were  $\text{Si}(\text{OH})_4^{2-}$  or  $(\text{SiO}_3)^{2-}$  (Nicholson, Coleman and Sidhu, 2021).

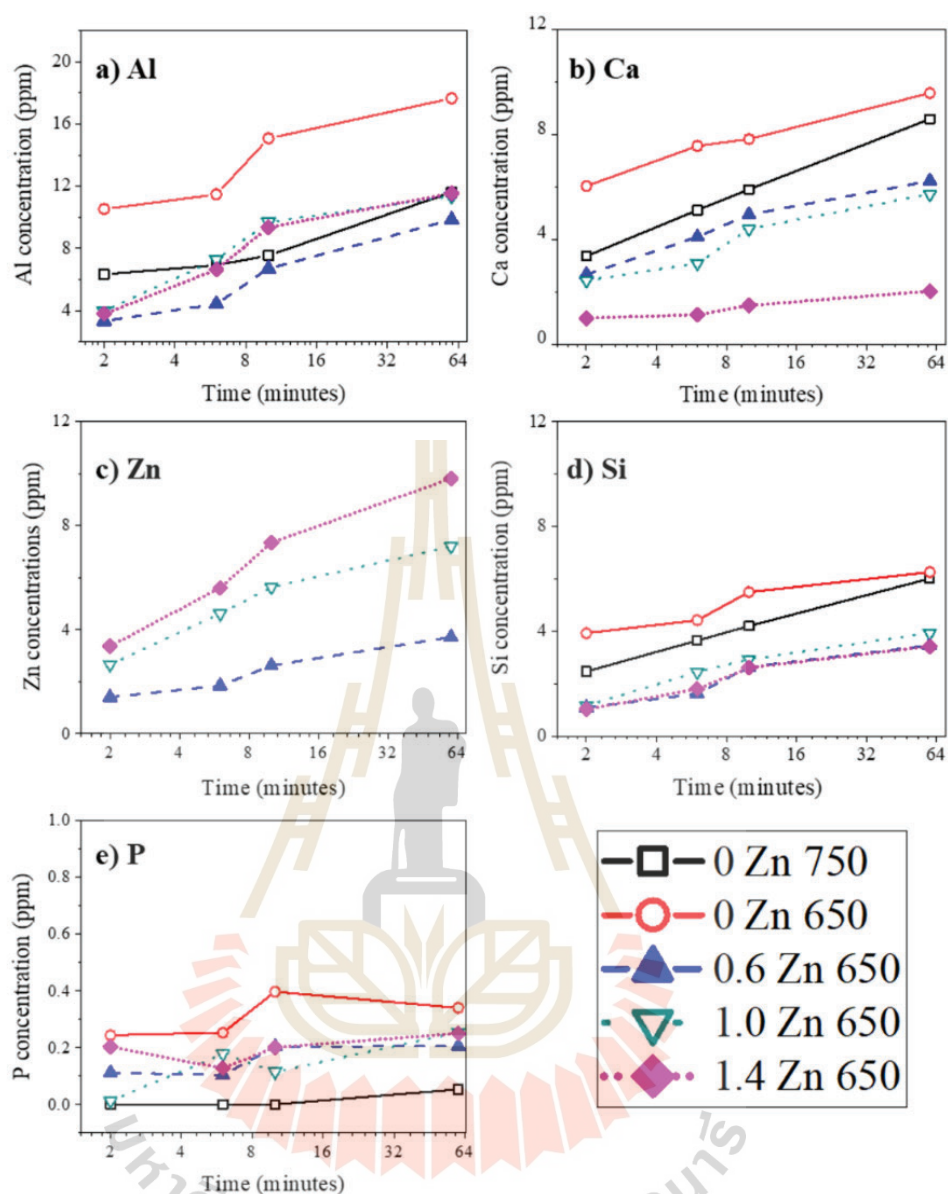


Figure 5.5 Concentration of a) Al, b) Ca/Sr c) Zn d) Si and e) P ions releasing from the sol-gel ionomer glass belonging to the system of  $4.5\text{SiO}_2\text{-}4.0\text{Al}_2\text{O}_3\text{-}0.16\text{P}_2\text{O}_5\text{-(}2\text{-x)Ca-xZnO-}2\text{F}_2$ , where  $X=0, 0.6, 1.0$  and  $1.4$  calcined at  $650^\circ\text{C}$  in comparison to Zn-free ionomer glass calcined at  $750^\circ\text{C}$  as a function of the immersion time.

Furthermore, all the sol-gel glasses released only small amounts of P ions, as shown in Figure 5.5 (e), and there was no significant difference among the

samples. Previous research had reported that the species of  $P^{5+}$  ions released to the acid solution was  $PO_4^{3-}$  (Awosanya Kunle, 2014).

### 5.3.3 DoE analysis of the compressive strength

To determine the significant factor for the compressive strength of SGICs, ZnO content in sol-gel ionomer glass and the calcination temperature were designed by the DOE technique for the primary study. The glass composition used in this study was  $4.5SiO_2-4.3Al_2O_3-0.16P_2O_5-(2-x)Ca-xZnO-2F_2$ , where  $x= 0, 0.6, 1.0$  and  $1.4$ . The sol-gel method was used to synthesize the glass, and it was subsequently calcined at temperatures of  $650^\circ C$  and  $750^\circ C$ .

ANOVA analysis in Table 5.2 presents the influence of ZnO content and calcination temperature on the compressive strength of SGICs. The statistical difference between the groups was judged to be significant when  $p \leq 0.05$ . This result showed that P-values of ZnO content and calcination temperature were lower than 0.05; thus, these two factors were significantly affected by the compressive strength of SGICs. However, there was no interaction between ZnO content and the calcination temperature ( $P>0.05$ ) which affected the compressive strength of the cement.

Table 5.2 ANOVA analysis for the compressive strength for SGICs containing different ZnO doping and the calcination temperatures.

Source	DF	Seq SS	Adj SS	Adj MS	F	P
Zn	2	1686.88	1686.88	843.44	14.95	0.001
Temperature	1	1195.28	1195.28	1195.28	21.19	0.001
Zn*Temperature	2	380.94	380.94	190.47	3.38	0.069
Error	12	676.84	676.84	56.40		
Total	17	3939.94				

Figure 5.6 illustrates the interaction and main effect plot for the compressive strength of GICs with varying ZnO contents and calcination temperatures. The results showed that the compressive strength decreased

significantly when the ZnO content of the glass was between  $x=0.6-1.0$ , but the ZnO content did not have a significant impact when  $x=1.0-1.4$ . Furthermore, it was observed that an increasing calcination temperature had an adverse effect on compressive strength. However, it is worth noting that the compressive strength tended to increase when the ZnO content was below 0.6 and the calcination temperature was set to 650°C. Based on these findings, the subsequent experiment focused on studying the effect of ZnO content ( $x$ ) at 0.2, 0.6, and 1.0, and calcination temperatures at 600°C, 650°C, 700°C, and 750°C on the setting time and compressive strength of SGICs.

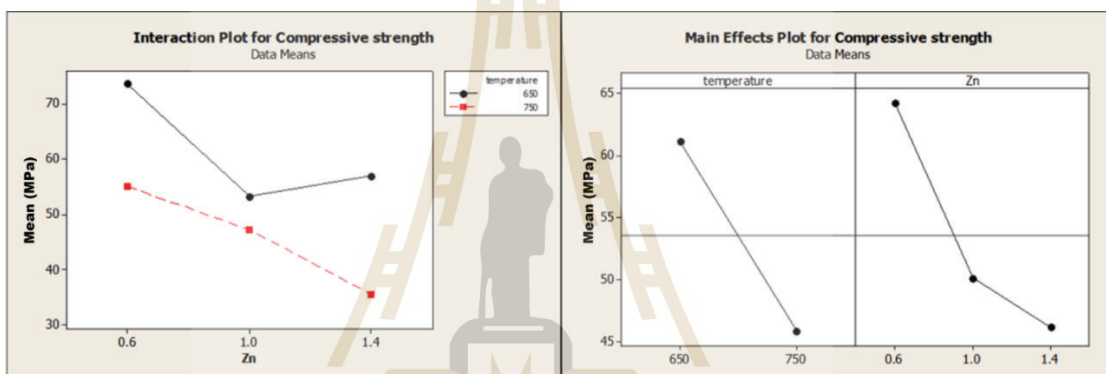


Figure 5.6 Main effect plot and the interaction plot for compressive strength of SGIC containing different ZnO doping and the calcination temperatures.

#### 5.3.4 Setting time and compressive strength

The results presented in Figure 5.7 indicated that increasing the calcination temperature of the sol-gel glass had the effect of extending the setting time of GICs. Additionally, an increase in ZnO content also slightly increased the setting time. It was observed that cements with low ZnO content and those calcined at temperatures below 650°C were unable to form due to their rapid working time. On the other hand, the cement with 1 mole of ZnO calcined at 750°C prolonged setting time due to the presence of a crystal structure.

The extension of the setting time for SGIC can be attributed to the structural changes that occur in the sol-gel glass. Structural analysis revealed that an increase in calcination temperature and ZnO content led to an increase in the BO

structure, which was reported to decrease the acid susceptibility of the glass (Wren et al., 2009). Additionally, increasing ZnO content and calcination temperature reduced the level of  $\text{Ca}^{2+}$  ions released during the setting reaction. Thus, there might have been a lack of ions to crosslink with the polymeric liquid in the setting reaction resulting in the extension of the setting time.

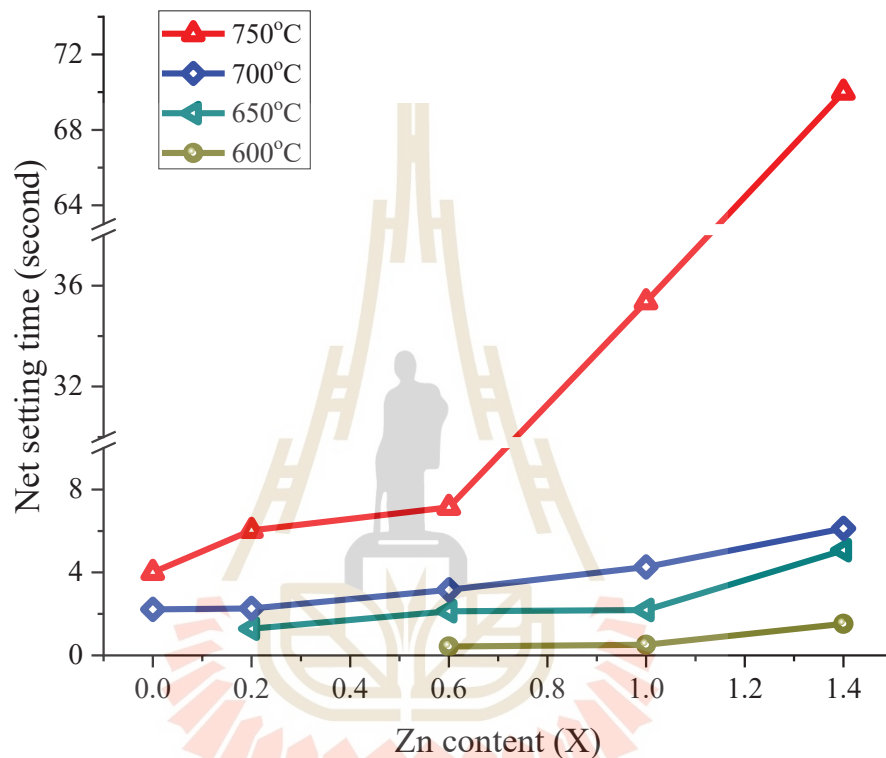


Figure 5.7 Net setting time of SGIC prepared from the sol-gel ionomer glass belonging to the system of  $4.5\text{SiO}_2\text{-}4.0\text{Al}_2\text{O}_3\text{-}0.16\text{P}_2\text{O}_5\text{-(}2\text{-x)Ca-xZnO-}2\text{F}_2$ , where  $x=0, 0.2, 0.6, 1.0$  and  $1.4$  and calcined at  $600^\circ\text{C}$ ,  $650^\circ\text{C}$ ,  $700^\circ\text{C}$  and  $750^\circ\text{C}$

The compressive strength of SGIC doped with various ZnO contents and calcination temperatures was presented in Figure 5.8. The results showed that the compressive strength of the cement calcined at  $750^\circ\text{C}$  decreased as the amount of ZnO content in the glass composition increased. However, at calcination temperatures of  $700^\circ\text{C}$  and  $650^\circ\text{C}$ , the cement with 0.6 moles of ZnO exhibited the highest compressive strength among the ZnO-doped SGIC. It should be noted that

the compressive strength for ZnO doped less than 0.6 moles was poor because it was difficult to handle and could not be molded into homogeneous samples.

Based on our findings, it was crucial to take the calcination temperature into account when aiming to optimize both the setting time and compressive strength of SGIC. Our results indicated that an increase of the ZnO content in the sol-gel glass composition could prolong the setting time while simultaneously reducing the strength. Therefore, it is necessary to optimize the calcination temperature to achieve the suitable setting time and compressive strength.

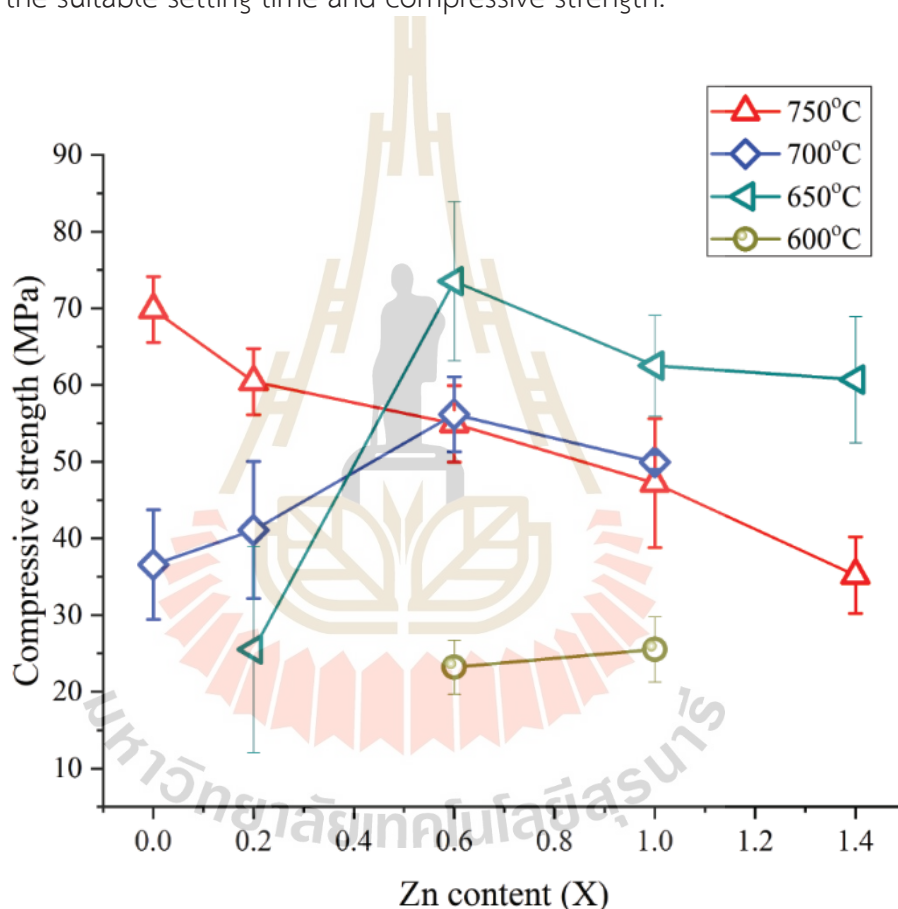


Figure 5.8 Compressive strength of SGIC belonging to the system of  $4.5\text{SiO}_2\text{-}4.0\text{Al}_2\text{O}_3\text{-}0.16\text{P}_2\text{O}_5\text{-(2-x)Ca-xZnO-2F}_2$ , where  $x= 0.2, 0.6, 1.0,$  and  $1.4$  and calcination temperature of  $600^\circ\text{C}$   $650^\circ\text{C}$ ,  $700^\circ\text{C}$  and  $750^\circ\text{C}$ .

The mechanical strength and other properties of glass ionomer cement can be influenced by many factors, such as the composition of the glass, the amount of powder to liquid used, and the type of liquid used (Fleming, Farooq and Barralet,

2003, Baig and Fleming, 2015, Alhalawani, Curran, Boyd et al., 2016). For this study, a sol-gel method was used to synthesize glass powder with a different compositions and ions releasing behavior compared to commercial products. Additionally, the liquid solution and powder to liquid ratio used were also different. While commercial GICs typically use a liquid solution with a P/L ratio greater than 1, the sol-gel ionomer glass was limited to a P/L ratio of 1. By increasing the P/L ratio and modifying the glass structure, the compressive strength of SGIC sample can be improved even further.

Based on the promising compressive strength results obtained from SGIC sample prepared with 0.6 ZnO calcined at 650°C, a comparative study was conducted. This study involved comparing SGIC containing 0.6 moles of ZnO to SGICs containing 0 and 1.4 moles of ZnO, with a focus on investigating the effects of ZnO content on the cement structure using the XAS technique. Additionally, the biological properties including cytocompatibility, antibacterial properties, and bioactivities of SGICs with 0, 0.6, and 1.4 ZnO content were also investigated.

### 5.3.5 The local structure of ZnO in SGIC by XAS technique

In Figure 5.9 (a) and (b), the absorption spectra of SGICs were displayed from Ca-XANES and Zn-XANES results, respectively. The main energetic transition edge position was consistent in all samples, indicating a similar structure among both sample groups, but the intensity of the spectra varied. This intensity was related to the number of O atoms around the core atoms, with high intensity indicating a high amount of O atoms. Figure 5.9 (a) demonstrates that increasing ZnO content in GIC increases O atoms around Ca atoms. In contrast, Figure 5.9 (b) shows that increasing ZnO content in GIC reduces O atoms around Zn atoms. The EXAFS technique further analyzed the number of O atoms around the core atom, as shown in Figure 5.10.

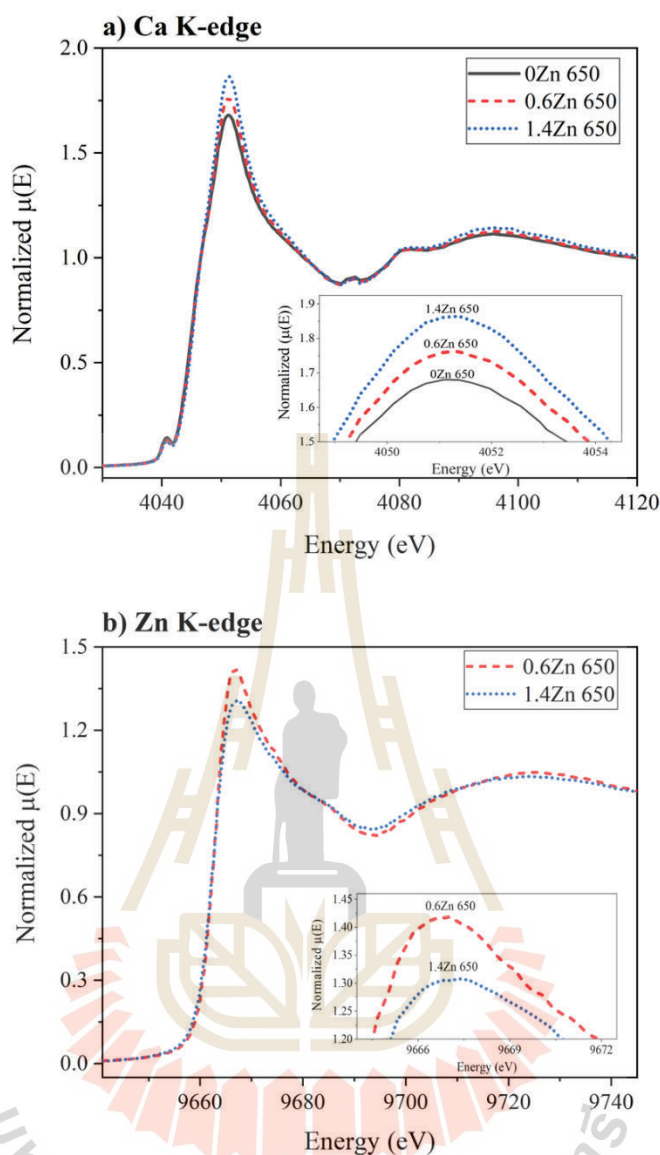


Figure 5.9 XANES spectra of GIC samples prepared with 0, 0.6 and 1.4 Zn doped sol-gel glasses calcined at 650°C at a) Ca K-edge and b) Zn K-edge.

After the setting reaction of SGICs, the local environment of Ca and Zn atoms in the Zn-doped SGIC were determined using EXAFS spectra. The spectra in R-space at Ca and Zn K-edge are presented in Figure 5.10. The coordination number (CN) of O atoms in the first shell of Ca and Zn atoms was observed in this study. The fitting parameter presented in Table 5.3 confirmed the XANES result that increasing ZnO content in GIC increased the average CN of O atoms around Ca atoms but decreased the CN of O atoms around Zn atoms.

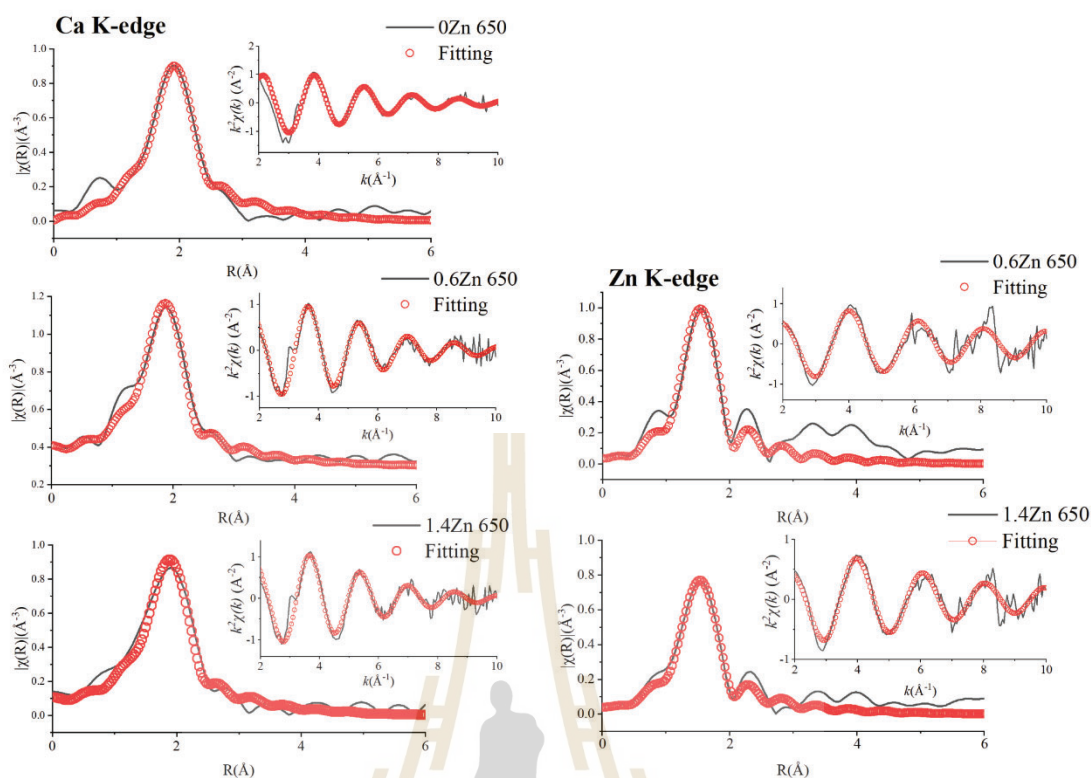


Figure 5.10 Ca and Zn K-edge EXAFS (weighted by  $k^2$ ) from the experiment (black line) and fitting (red circle) of GIC samples prepared with 0, 0.6 and 1.4 Zn doped sol-gel glasses calcined at 650°C

Table 5.3 EXAFS fitting parameters including average coordination number of oxygens around the atom (CN), Debye-Waller factor ( $\sigma$ ), interatomic distance (R), and (R-factor)

Samples	Ca K-edge				Zn K-edge			
	CN	$\sigma^2$	R(Å)	R-factor	CN	$\sigma^2$	R(Å)	R-factor
0Zn	4.326	0.00909	2.380	0.0101	-	-	-	-
0.6Zn	4.746	0.00901	2.382	0.0242	2.092	0.00084	1.993	0.0329
1.4Zn	6.000	0.01068	2.392	0.0257	1.88	0.00265	1.998	0.0198

Based on the fitting parameter analysis in Table 5.3, O atoms showed a higher tendency to bond with Ca atoms than Zn atoms after the setting reaction. This suggests that the O atoms from the carboxyl group of PAA preferred to crosslink with Ca atoms rather than Zn atoms. As a result, the substitution of ZnO for CaO depleted the crosslinking ions necessary for the setting reaction of GIC, ultimately leading to a reduction in compressive strength.

According to XPS and XAS analysis, the structure of  $\text{Ca}^{2+}$  and  $\text{Zn}^{2+}$  ions in the glass network and the cement structure was proposed in Figure 5.11. The XPS result showed that  $\text{Ca}^{2+}$  ions in the Zn-free ionomer glass acted as a network modifier and formed  $\text{CaF}_2$ . When ZnO replaced CaO,  $\text{Ca}^{2+}$  ions were only found in the form of  $\text{CaF}_2$ , while  $\text{Zn}^{2+}$  ions formed in the tetrahedral site and acted as a network former through BO structure. As the amount of ZnO increased, the fraction of octahedral structure also increased, which connected to the glass network through BO structure.

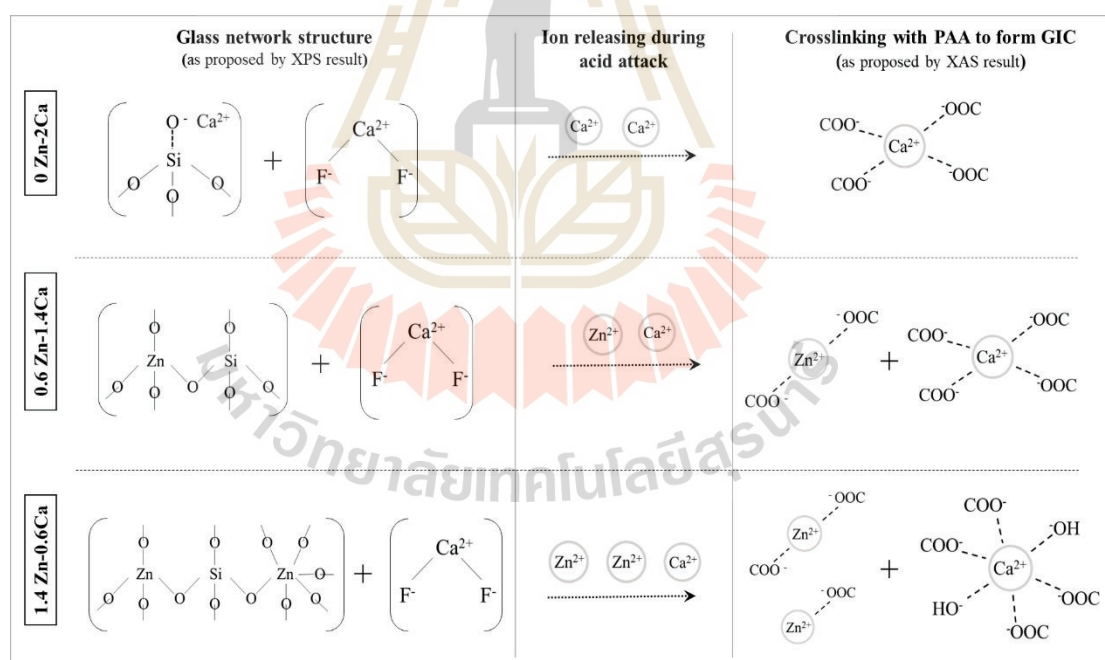


Figure 5.11 A proposed glass network structure for ZnO instead of CaO in the sol-gel ionomer glass network and form crosslinking with polyacrylic acid in glass ionomer cement after setting.

After being exposed to acid liquid, the ionomer glasses released  $\text{Ca}^{2+}$  and  $\text{Zn}^{2+}$  ions in varying amounts based on the glass composition. As a result, XAS analysis indicated that these metal ions could crosslink with the  $-\text{COO}-$  group of PAA with different coordination complexes, influenced by factors such as the metal's size, ligand charge, charge-donating ability, and reaction acidity (Dudev, Wang, Dudev et al., 2006, Pan and Darvell, 2007). Previous studies showed that Ca atoms were likely surrounded by O atoms of the carboxylate group with a CN ranging from 2 to 8, while the CN of O atoms around Zn atoms varied between 2 to 6, with the presence of water and organic molecules (Katz, Glusker, Beebe et al., 1996, Bonapasta, Buda and Colombet, 2001, Vao-soongnern, Merat and Horpibulsuk, 2015, Kręzel and Maret, 2016, Thomas, Mishra and Myneni, 2019, Daley, Opuni, Raj et al., 2021). Our results showed that in the Zn-free GIC, Ca atoms were surrounded by O atoms with a CN of 6. With CN=6, Bonapasta suggested that four of the O atoms of the PAA chains occupied the square bases of the octahedron, while the O atoms of the OH<sup>-</sup> ions occupied the two vertices of the octahedron (Bonapasta et al., 2001). Substituting ZnO for CaO changed the CN around Ca atoms from 6 to 4, and Zn atoms were surrounded by O atoms with a CN of 2. Consequently, increasing ZnO content in the ionomer glass reduced crosslinking for the setting reaction of GIC, resulting in a reduction of compressive strength.

### 5.3.6 Antibacterial property

Figure 5.12 exhibits the antibacterial activity of GIC samples with different concentrations of ZnO (0, 0.6, and 1.4 Zn) doped ionomer glass against *S. mutans* under both light and dark conditions. The samples were incubated in a black box to prevent external light exposure during dark conditions. Our findings revealed that there was no inhibition zone observed in SGIC samples under the dark condition. Interestingly, the ZnO doped GIC showed an inhibition zone around the sample under the light condition, and the zone expanded with an increase in the amount of ZnO in the glass composition.

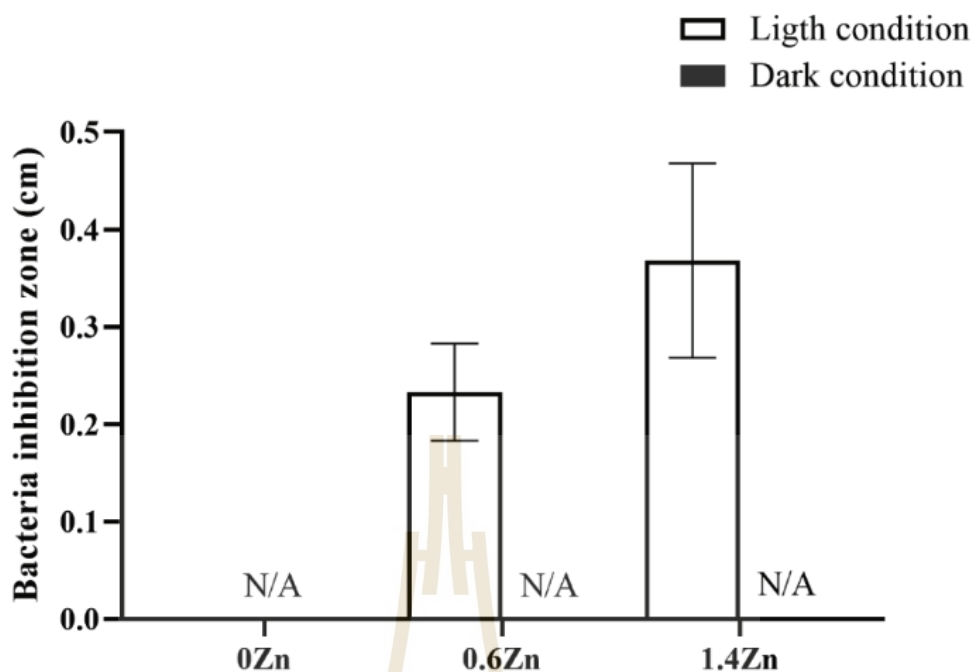


Figure 5.12 The diameter of inhibition zone against *S. mutans* of SGIC samples prepared with 0, 0.6 and 1.4 Zn doped sol-gel glasses calcined at 650°C.

The Zn-doped GIC samples demonstrated an inhibition zone greater than 0.1 cm when incubated under light conditions, which increased with higher ZnO content as compared to the Zn-free GIC. The antibacterial effect was evaluated according to the standard SNV 195920-199 (Schuhladen, Stich, Schmidt et al., 2020). Antibacterial activity of ZnO was reported to be regulated through three mechanisms: photochemical reaction, direct contraction of ZnO particles to the bacteria cell wall, and the release of bactericidal  $Zn^{2+}$  ions (Sirelkhatim, Mahmud, Seeni et al., 2015, Joe, Park, Shim et al., 2017). The data showed that the antibacterial activity of ZnO-doped SGIC was only activated under light conditions, and this effect was attributed to the photochemical reaction. The photochemical reaction involved a photo-induced oxidation process in which ZnO could absorb UV light and generate ROS species such as hydrogen peroxide ( $H_2O_2$ ) and superoxide ions ( $O_2^-$ ). These ROS species could penetrate the cells, inhibit or kill microorganisms (Sirelkhatim et al., 2015).

### 5.3.7 Cell viability

The results of the MTS assay on the cell viability of NIH/3T3 fibroblast cells after treatment with extracts of SGIC with varying ZnO contents in the glass for 24 hours are shown in Figure 5.13 (a). The data indicated that the cell viability of NIH/3T3 fibroblast cells decreased after treatment with ZnO-doped SGICs at 0.6ZnO and 1.4ZnO, while less cytotoxicity was observed for SGIC without ZnO doping. However, upon diluting the extract concentration to 1:2 and 1:4, cell viability for all samples showed an increasing trend.

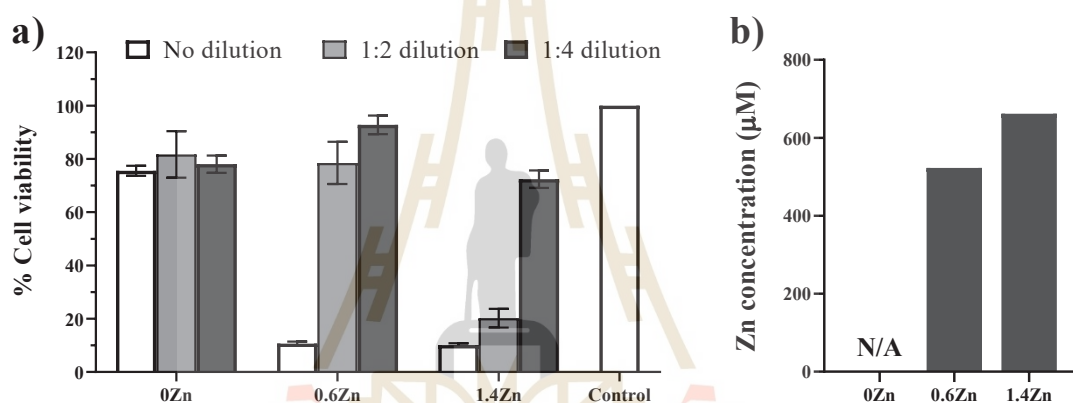


Figure 5.13 Effect of Zn content in SGIC on the NIH/3T3 cell viability (indirect contact). (a) %cell viability treated with different concentrations of the extracted solutions. The cells with fresh culture medium were used as a negative control. Values were expressed as the mean  $\pm$  standard error of the mean of three independent experiments and (b) the  $Zn^{2+}$  ion releasing concentration in the as-received extracted solutions analyzed by the ICP-OES technique.

$Zn^{2+}$  ions have been found to have some drawbacks in terms of biocompatibility. According to Brauer et al., cytotoxicity could be caused by the release of a large amount of  $Zn^{2+}$  ions (Brauer, Gentleman, Farrar et al., 2011). Studies have also shown that the cytotoxicity of  $Zn^{2+}$  ions was associated with the production of ROS species, which was the same mechanism responsible for the antibacterial effect (Patrón-Romero, Luque, Soto-Robles et al., 2020, Saber, Hayaei-

Tehrani, Mokhtari et al., 2021). However, diluting the concentration of  $Zn^{2+}$  ions had been found to reduce toxicity and benefit cell growth (Brauer et al., 2011).

In a previous study, it was reported that the optimal concentration of  $Zn^{2+}$  ions for cell toxicity was 350  $\mu M$  (Brauer et al., 2011). According to our result, SGIC prepared with 0.6ZnO calcined at 650°C released 523  $\mu M$  of  $Zn^{2+}$  ions, as shown in Figure 5.13 (b). This concentration was higher than the optimal concentration and could be the reason for the adverse effect on cell viability. However, after diluting the extracted concentration (1:2), the concentration of  $Zn^{2+}$  ions reduced to approximately 260  $\mu M$ , which significantly increased the cell viability. This improvement in cell viability could be beneficial for clinical use as the concentration of  $Zn^{2+}$  released from SGIC is diluted by fluid circulation in the oral environment.

### 5.3.8 Bioactivity and tooth-GIC interface

Figure 5.14 exhibits SEM images and EDS results of SGIC surfaces following 5-day soaking in DI water and artificial saliva, revealing that an apatite-like layer was formed on all GIC surfaces after immersion in artificial saliva. The thickness of the apatite-like layer increased with the ZnO content; however, there was no such layer formed on any GIC surfaces soaked in DI water. The apatite-like layer could be confirmed by EDS result that the ratio of Ca/P should be in the range of 1.30-1.67 (Drouet, 2013). Our result presented that the Ca/P ratio was around 1.40 where ZnO was substituted for CaO in the ionomer glass composition. This could be indicated that the substitution of ZnO for CaO in the ionomer glass composition was likely to cause the formation of this apatite-like layer on SGIC surfaces during artificial saliva immersion.

The formation of the apatite layer on the cement surface was linked to the deposition of calcium and phosphate, which precipitated into an apatite-like crystal lattice (Lynch, 2011). This apatite layer was reported to enhance a chemical bond between GIC and tooth structure (Chen et al., 2016). Thus, the ability of apatite-like formation on SGIC surface following immersion in saliva solution could indicate the potential for high bioactivity.

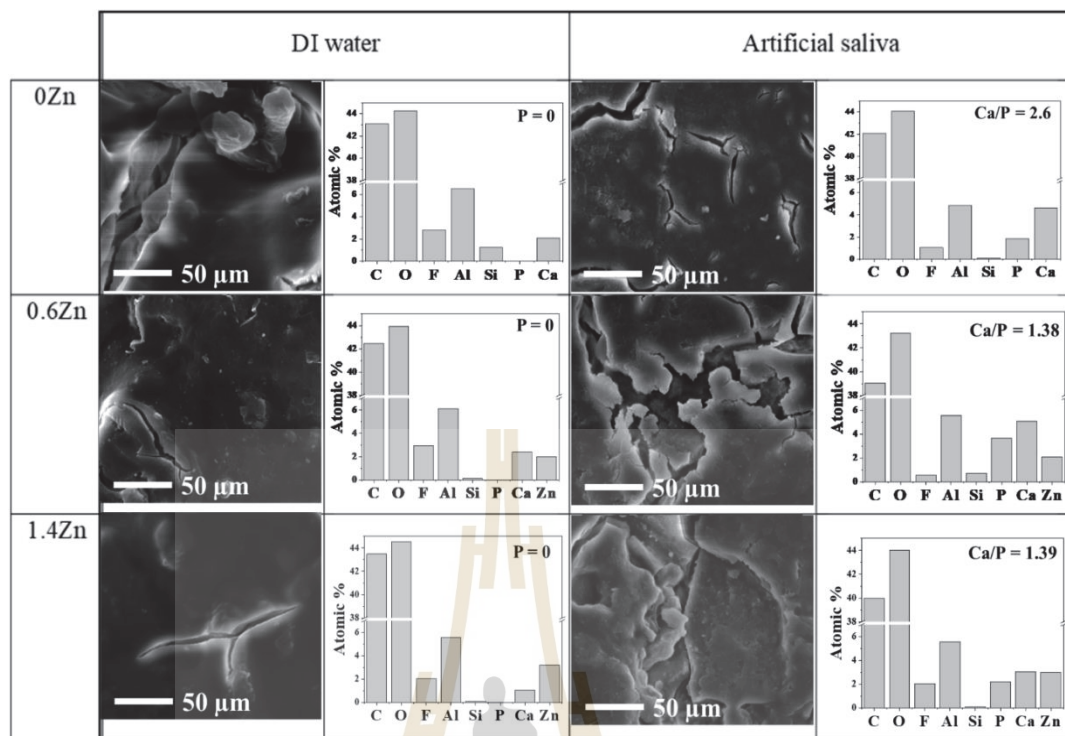


Figure 5.14 SEM micrographs of the surface for SGIC prepared with the sol-gel glasses doped different ZnO contents and calcined at 650°C after soaking in DI water and artificial saliva for 5 days, respectively (magnification x5000)

Figure 5.15 shows the interfacial area between the tooth and SGIC with and without ZnO contents, observed by the SEM technique, to determine the success and failure of the restoration. The SEM images revealed that GIC containing ZnO exhibited better adaptation to the tooth surface than GIC without ZnO, which showed detachment around the interface area. This detachment could be due to the drying of specimens for SEM evaluation. However, the presence of zinc in the SGIC structure was found to promote the sealing of the tooth surface even though it was also employed in the drying process. The previous work reported that zinc potentially stimulates hard-tissue mineralization by interaction with the phosphate in the tooth structure (Lynch, 2011). Therefore, the presence of zinc in SGIC composition could improve the adaptation between tooth structure and the material, thereby improving the durability and longevity of the restoration.

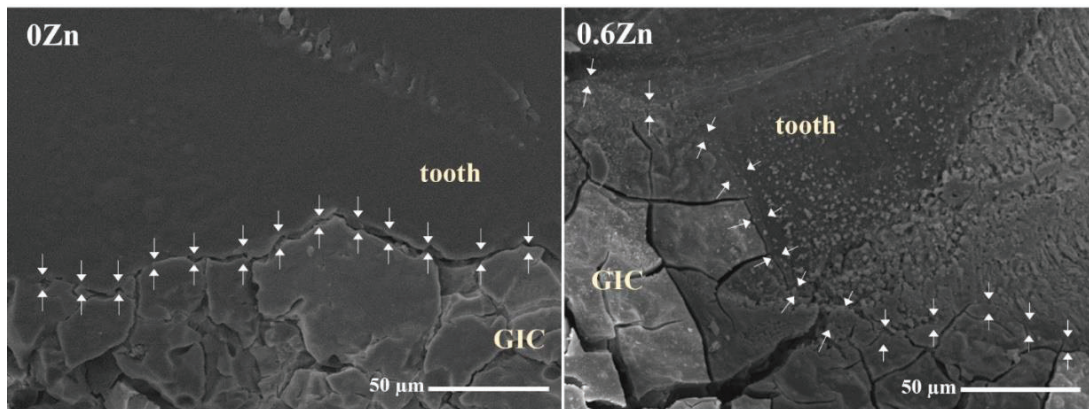


Figure 5.15 SEM images of the interfacial area between the tooth and SGIC samples prepared with 0.6 ZnO doped glass and calcined at 650°C as compared to ZnO free SGIC.

Manufacturers have recently introduced new types of Glass Ionomer Cement (GIC) that contain zinc, such as CAREDYNE RESTORE from GC Japan and ChemFIL™ Rock from Dentsply USA. CAREDYNE RESTORE is a novel GIC product that comprises of "BioUnion Filler," which can release fluoride, calcium, and zinc ions. Studies had reported that the zinc release level from this product was sufficient to inhibit biofilm formation (Kohno, Tsuboi, Kitagawa et al., 2019). Additionally, this product had demonstrated high remineralization performance, making it suitable for the prevention and restoration of root caries (Nagano, Mori and Kumagaia, 2019, Kaga, Nagano-Takebe, Nezu et al., 2020). On the other hand, ChemFIL™ Rock is a new type of GIC that features an enhanced setting reaction due to the presence of zinc in the glass composition. Zinc promoted the durability of the product and enabled its use in stress-bearing situations, making it suitable for posterior tooth restoration (Patil et al., 2020). These commercial products have demonstrated the advantages of incorporating zinc in GIC for dental restorative materials. In this study, a new type of glass ionomer cement was also successfully developed by substituting zinc for calcium in the glass composition, which resulted in improved biological and antibacterial characteristics of the cement, achieved through a sol-gel method at low temperatures.

## 5.4 Conclusions

This study investigated the effects of ZnO doping and calcination temperature on SGICs. Structural analysis using XPS and XAS revealed that ZnO replacement showed different performance to CaO in the glass network structure and the cement structure. The study demonstrated the benefits and limitations of ZnO doping, with higher ZnO content and calcination temperature resulting in the precipitation of  $\text{ZnAl}_2\text{O}_4$  and  $\text{ZnO}_2$  crystal structures. The compressive strength of the ZnO-doped SGIC decreased with increasing ZnO content, but it could be improved by decreasing the calcination temperature. SGIC prepared with 0.6Zn glass calcined at  $650^\circ\text{C}$  showed the most promising results in terms of setting time and compressive strength. Interestingly, the ZnO content in the glass composition exhibited excellent antibacterial activity under light conditions due to its photocatalytic effect. This photocatalytic of SGIC prepared with 0.6ZnO glass also had an adverse effect on the cell viability, but this could be enhanced by reducing the amount of ZnO in the glass composition. Additionally, SGIC with ZnO doping exhibited improved bioactivity and tooth adhesion. These findings suggest that ZnO-doped SGIC has potential applications in dental restorative materials.

## CHAPTER 6

### EFFECT OF STRONTIUM CONTAINING FLUORAPATITE ADDITIVE ON SGICs ( $4.5\text{SiO}_2\text{-}4\text{Al}_2\text{O}_3\text{-}0.45\text{P}_2\text{O}_5\text{-}1.4\text{CaO}\text{-}0.3\text{ZnO}\text{-}2\text{F}_2$ )

According to Chapter 5, the incorporation of ZnO dopants into ionomer glass improved the antibacterial properties of SGIC due to the photocatalytic effect. However, this photocatalytic effect required light to activate the photocatalytic activity and inhibit the bacterial growth. To overcome these limitations, this chapter investigates the modification of SGIC with SrFA nanoparticles for improving antibacterial activity. The chapter focused on incorporating strontium containing fluorapatite (SrFA) into SGIC. The SrFA nanoparticles were synthesized by the hydrothermal method. The study investigated the effect of SrFA on the setting time and compressive strength of SGIC, as well as bioactivity, *in vitro* cytocompatibility, and fluoride release and uptake ability.

#### 6.1 Research background

The development of secondary caries or recurrent infections around dental restorations was a significant issue in restorative treatments, often resulting in treatment failure and tooth loss (Askar et al., 2020). To prevent secondary caries, it was crucial to develop restorative materials with high potential for both antibacterial and remineralization properties. The SGIC synthesized with ZnO doping in Chapter 5 was found to enhance its antibacterial properties. However, the photocatalytic effect of ZnO, which required light for activation, limited its use in the oral environment where light was absent. To overcome this limitation, other approaches have been explored, including the incorporation of antibacterial additives (Takahashi et al., 2006, Chen, 2016, Chen et al., 2016, Chen, Gururaj, Xia et al., 2016, Alatawi, Elsayed and Mohamed, 2018).

One of the most promising antibacterial additives for enhancing dental materials was SrFA, which has demonstrated not only high potential for antibacterial properties but also improved bioactivity. Previous studies found that Sr and F had a synergistic effect that could effectively inhibit bacterial growth, making SrFA a potential candidate for anti-caries applications in dentistry (Dabsie, Gregoire, Sixou et al., 2009). The successful synthesis of highly crystalline SrFA nanoparticles via a hydrothermal method has been reported, which has demonstrated strong antibacterial properties against *S. mutans* (Wang et al., 2019). Furthermore, the existence of Sr dopant in hydroxyapatite showed particularly improving antibacterial effects on *Escherichia coli*, *Staphylococcus aureus*, and *Lactobacillus*. Fluorapatite was also reported to effectively improve biocompatibility and form apatite layer on material surfaces, which enhances resistance to acid penetration in human dental structures and efficiently reduces the risk of secondary caries (Moshaverinia, Ansari, Movasaghi et al., 2008, Balhuc et al., 2021).

In this study, SrFA was synthesized with a composition of  $(Ca_5Sr_5)(PO_4)_6F_2$ , which was modified from a previous literature (Wang, Chang, Chiang et al., 2019) and used it as an additive for ZnO doped SGIC. The SrFA additives were incorporated into the SGIC to enhance its antibacterial properties, including *in vitro* bioactivity and cytocompatibility. Furthermore, the compressive strength and setting time of the material were evaluated.

## 6.2 Experimental procedure

### 6.2.1 Synthesis of SrFA nanoparticles and characterization

SrFA nanoparticles were synthesized by the hydrothermal method, as previously work by Wang et al. (2019). In this method,  $Ca(NO_3)_2 \cdot 4H_2O$  and  $Sr(NO_3)_2$  were dissolved in DI water at room temperature, followed by the preparation of a separate mixed solution of  $(NH_4)_2HPO_4$  and 10% HF in DI water. The two solutions were combined and stirred vigorously to achieve a  $(Ca^{2+}+Sr^{2+}):PO_4^{3-}:(OH^-+F^-)$  molar ratio of 10:6:2. The pH of the solution was immediately adjusted to 11 with ammonia dropwise. The resulting suspension was stirred for an hour before being transferred to a Teflon-lined hydrothermal autoclave and heated to 160°C for 12 hours. The precipitate was then filtered and washed repeatedly with DI water before being

incubated at 50°C until fully dried. The synthesis method for SrFA was summarized as shown in Figure 6.1.

The phase identification of the synthesized SrFA additives was analyzed by XRD technique. The morphology and composition of the SrFA additive was observed by transmission electron microscopy coupled with energy dispersive spectroscopy (TEM-EDS, Tecnai™ G2 20, FEI company, Hillsboro, USA).

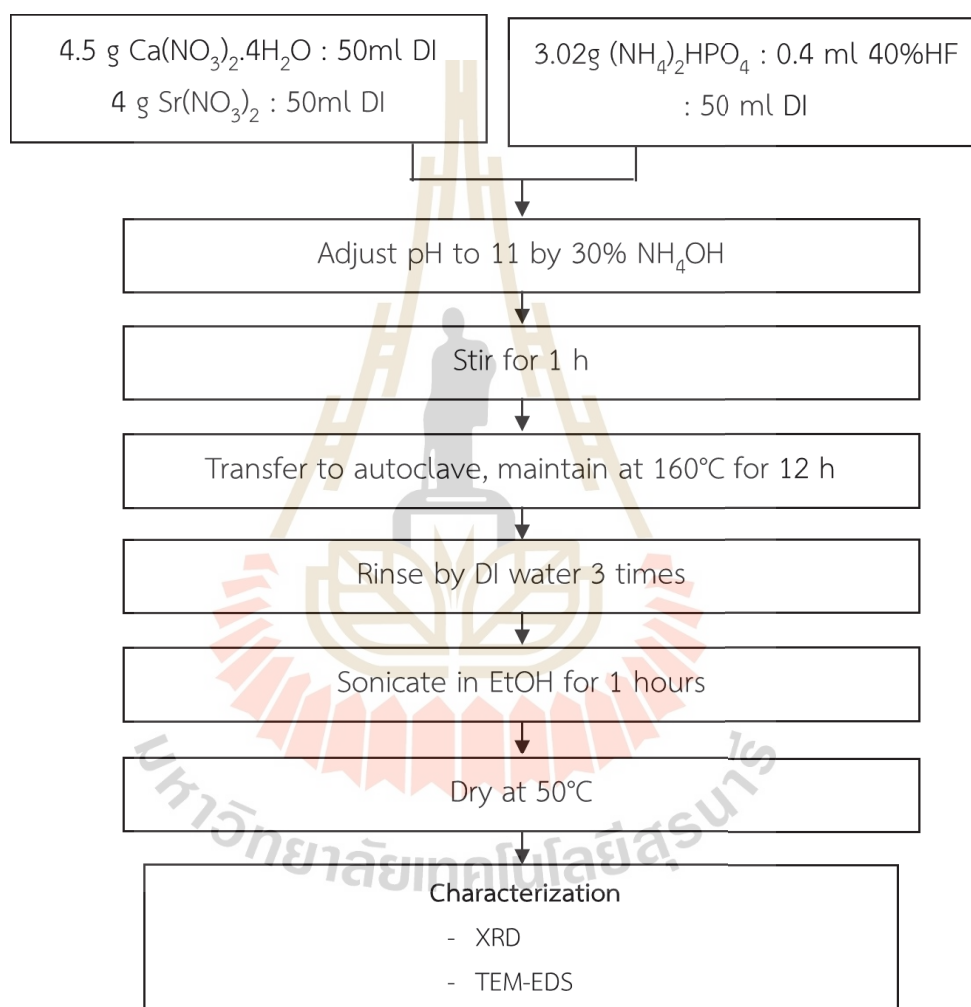


Figure 6.1 Hydrothermal synthesis procedure of SrFA

### 6.2.2 Preparation of glass ionomer cement

In this chapter, SGIC was modified by adding SrFA in the range of 0, 1, 3, and 6 wt.%. The cement was formulated by blending the sol-gel ionomer glass powder with the liquid solution at a ratio of 1.5:1 (w/v). The sol-gel ionomer glass

powder was synthesized in the  $4.5\text{SiO}_2\text{-}4\text{Al}_2\text{O}_3\text{-}0.45\text{P}_2\text{O}_5\text{-}1.7\text{CaO}\text{-}0.3\text{Zn}\text{-}2\text{F}_2$  composition molar ratio system, following the methodology in Chapter 5. The liquid solution contained a mixture of 27 wt.% polyacrylic acid (PAA, M.W.  $\sim 100,000$ , Sigma-Aldrich, Darmstadt, Germany), 64 wt.% poly(acrylic acid-co-maleic acid) (PAA-co-MA, M.W.  $\sim 3,000$ , Sigma-Aldrich, Darmstadt, Germany), and 9 wt.% tartaric acid (Carlo Erba, Val de Reuil, France). The commercial GIC (GC Gold Label 9 HS Posterior EXTRA, GC Corporation, Tokyo, Japan) was employed as a reference material for comparison.

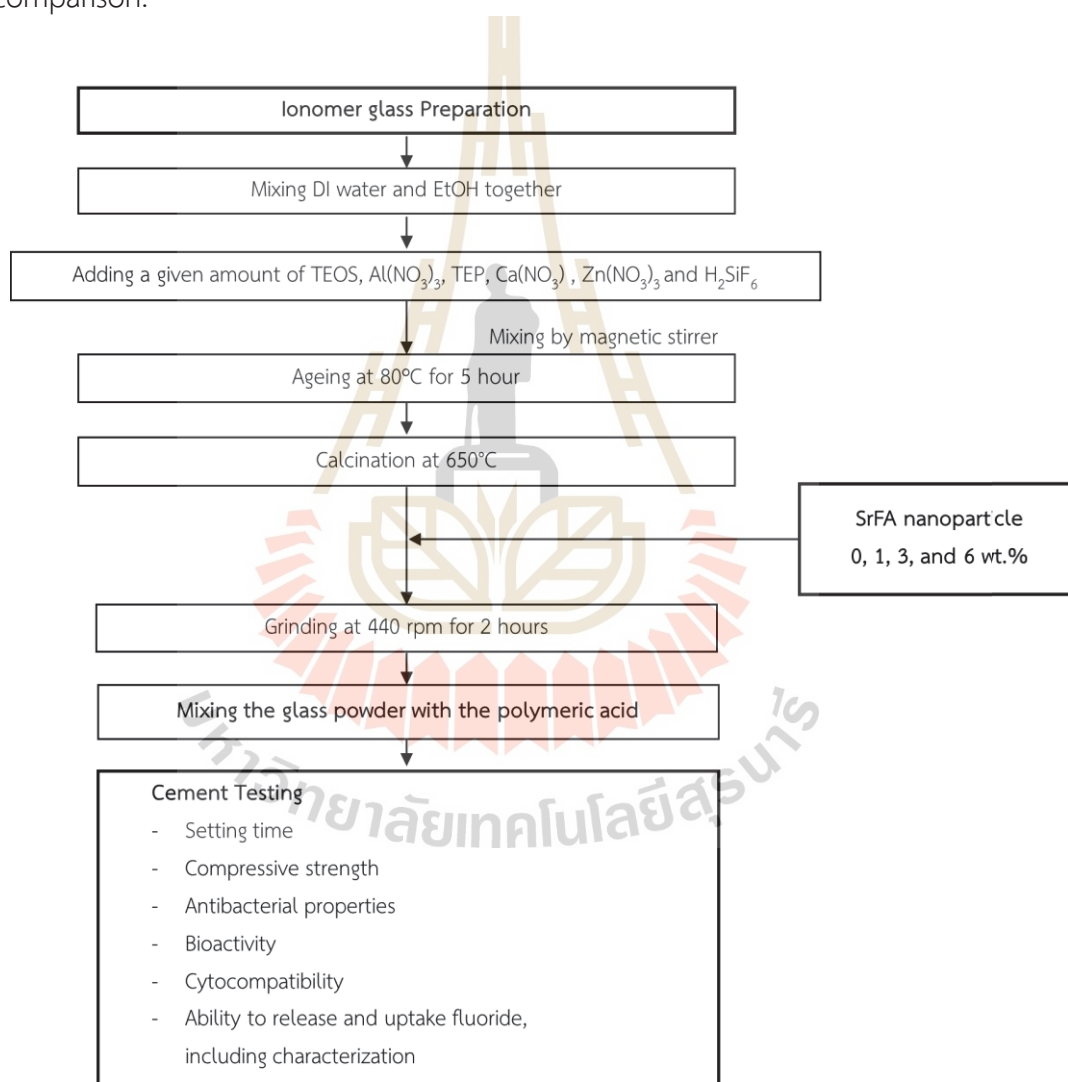


Figure 6.2 Schematic of experimental design to determine the effect of SrBGF additive on the properties of SGIC.

### 6.2.3 Setting time and compressive strength testing

The evaluation of the setting time and compressive strength of SGIC was performed in accordance with the methodology outlined in Chapter 4, sections 4.2.4 and 4.2.5.

### 6.2.4 Antibacterial testing

The antibacterial activity of SGICs, containing SrBGF and SrFA, against *S. mutans* (ATCC 27145), was evaluated using the agar diffusion method on Mueller-Hinton Agar. The adhesion ability of bacteria to the material surface was also determined. To perform the agar diffusion test, the *S. mutans* culture was selected from blood agar plates, cultured at 37°C, 5% CO<sub>2</sub> for 48 hours and then cultured overnight in brain-heart infusion nutrient broth (BHI) at 37°C, 5% CO<sub>2</sub>. The bacteria were then diluted to 1.5x10<sup>8</sup> CFU/ml in a fresh BHI broth and uniformly swabbed on the Mueller-Hinton agar plate. Disc-shaped GIC specimens were placed onto the agar and incubated at 37°C for 72 hours. The diameter of the inhibition zones around the GIC discs was measured to evaluate the inhibition zone of bacterial activities.

### 6.2.5 *In vitro* bioactivity

To determine the *in vitro* bioactivity of the material, the ability of apatite-like formation on the SGIC surface was investigated. The GIC modified with 0, 1, 3, and 6 wt.% SrFA was prepared in a disc shape with 2 mm in height and 10 mm in diameter. The specimens were then immersed in artificial saliva for 5 days. The composition of the artificial saliva consisted of 0.4 g Sodium chloride (NaCl, 98%, Carlo Erba), 0.4 g Potassium chloride (KCl, 99.5% , Merck), 0.795 g Calcium chloride (CaCl<sub>2</sub>·H<sub>2</sub>O, Merck), 0.69 g Sodium phosphate monobasic monohydrate (NaH<sub>2</sub>PO<sub>4</sub>·H<sub>2</sub>O, 98%, Merck), 0.005 g Sodium sulfide nonahydrate (Na<sub>2</sub>S·9H<sub>2</sub>O, 98%, Carlo Erba), and 1000 mL DI water (El Mallakh and Sarkar, 1990). The surface morphology of specimens was examined using a scanning electron microscope (SEM, JEOL-6010LV) at an acceleration voltage of 15 kV. all specimens were coated with gold prior to examination.

### 6.2.6 *In vitro* cytocompatibility

The cytocompatibility of SGICs was evaluated by assessing the metabolic activity of NIH/3T3 fibroblasts cultured on the SGIC surface through AlamarBlue assay. Prior to cell seeding, the cement discs were incubated in 1 mL of PBS for 3 days, followed by a 3-day incubation in complete medium. For cell seeding,  $1 \times 10^4$  cells were suspended in 1 mL of complete medium and added onto the cement discs placed in a 24-well plate. Glass coverslips were used as the control. The complete medium was renewed every 2-3 days. The metabolic activity of cells was monitored on days 1, 7, and 14 using the AlamarBlue assay. A stock solution of the AlamarBlue was prepared by mixing 5 mg Resazurin salt with 40 mL of sterile PBS. To evaluate the metabolic activity, the stock solution was mixed with the complete medium in a ratio of 1:9 v/v and replaced in the well plates. The plates were incubated at 37 °C and 5% CO<sub>2</sub> for 2 hours. Subsequently, the absorbance was measured at a wavelength of 560 nm using a microplate reader (Multiskan GO, Thermo Scientific). Three independent samples were used in the assay.

### 6.2.7 Fluoride release and uptake ability

In order to investigate the fluoride release and uptake ability of SGIC modified with 0, 1, 6, and 8 wt.% SrFA, cylindrical specimens with 2 mm in height and 10 mm in diameter were prepared. The GIC specimens were subsequently immersed in 10 ml of artificial saliva for 1, 7, and 21 days to assess their fluoride release capacity. Following this, the specimens were soaked in APF gel (1,000 ppm fluoride gel) for 6 minutes and then transferred back to artificial saliva for 1, 7, and 21 days to evaluate their fluoride uptake ability. Saliva samples were collected at each point of soaking time, and the fluoride concentration was analyzed using a fluoride ion-selective electrode (FISE, Orion Research, Inc., Cambridge, VSTAR40A).

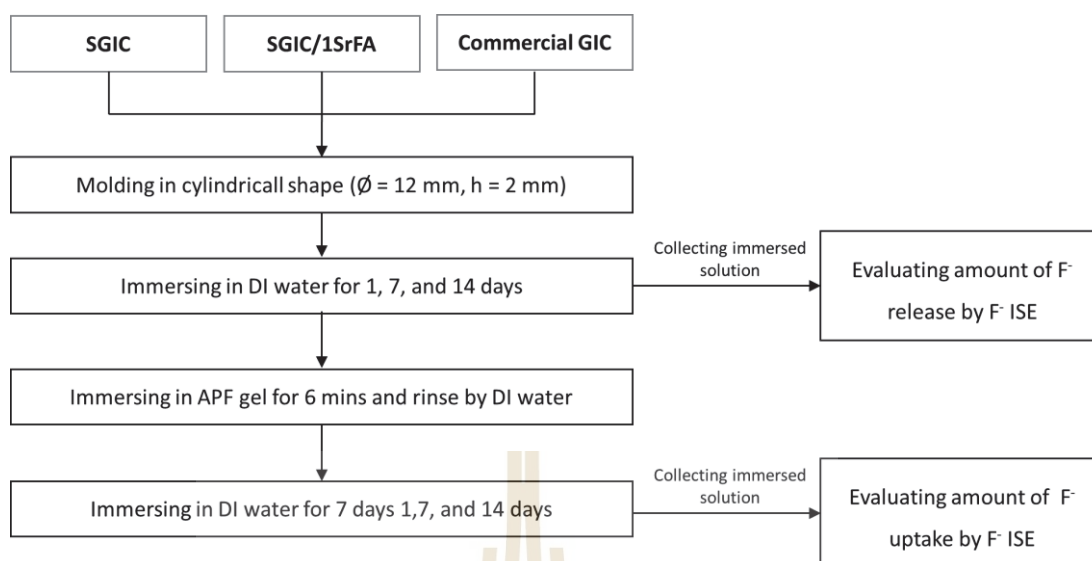


Figure 6.3 Schematic of experiment design to evaluate ability to release and uptake fluoride.

## 6.3 Results and discussions

### 6.3.1 Characterization of SrFA additive

SrFA nanoparticles were successfully synthesized by a hydrothermal method. The obtained particles were characterized by the XRD technique, as illustrated in Figure 6.4 (a). The XRD pattern of SrFA additive showed the characteristic of strontium containing fluorapatite  $((Ca_5Sr_5)(PO_4)_6F_2)$  (JCPDS no. 70-3522). Additionally, the particle shape and chemical composition of the SrFA nanoparticle were observed using a TEM-EDS technique, which is illustrated in Figure 6.4 (b). The results revealed that SrFA particles were needle-shaped, with a length ranging from 10-300 nm and a width of approximately 10 nm.

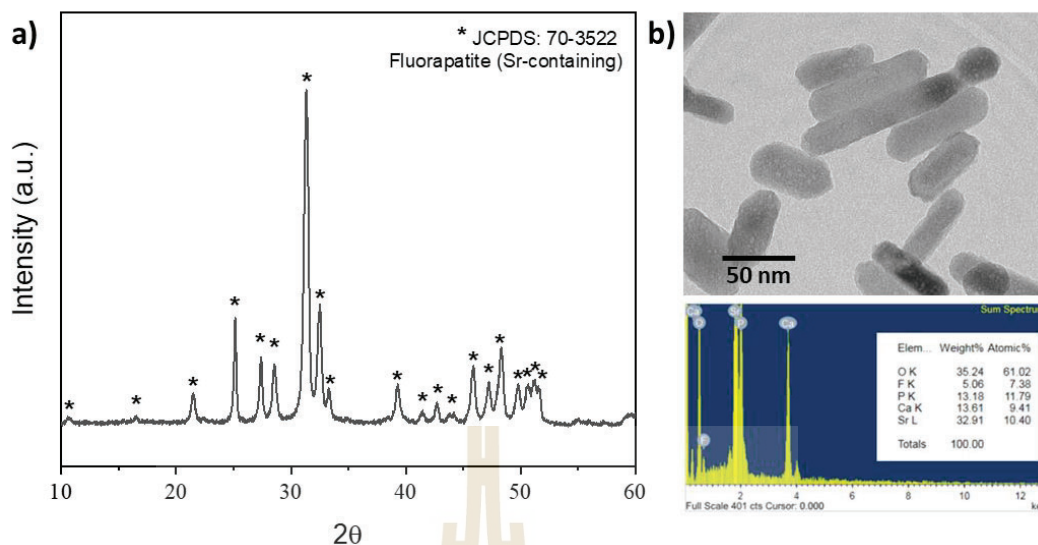


Figure 6.4 a) XRD pattern of the synthesized SrFA additive, and b) TEM micrographs and EDS analysis of SrFA additive

### 6.3.2 Setting time and compressive strength

Figure 6.5 illustrates the working and net setting times obtained for SGIC modified with different concentrations (0, 1, 3, and 6 wt.%) of SrFA. The result revealed that there was no statistically significant difference in working time with increasing SrFA content. The result revealed that there was no statistically significant difference in working time with increasing SrFA content. For the net setting time, there was no significant difference between SGIC modified with 0 and 1 wt.% of SrFA. The further increase of SrFA additives in SGIC to 3 and 6 wt.% significantly increased the net setting time.

These findings indicated that the addition of SrFA to SGIC resulted in a retardation of the setting time. The delay in setting time might be attributed to the high crystallinity of SrFA powder, which acted as a physical barrier during the setting reaction of the cement. As a result, the setting reaction was impeded, leading to an increase in the setting time (Gupta, Mulay, Mahajan et al., 2019).

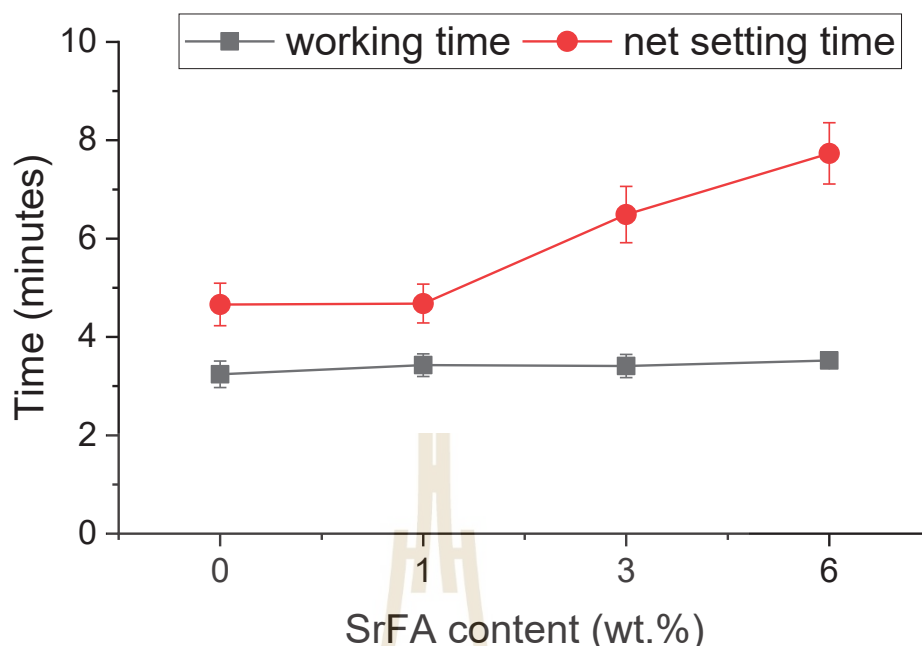


Figure 6.5 Working and net setting time of SGIC containing with 0, 1, 3 and 6 wt.% of SrFA.

The compressive strength of SGIC containing various amounts of SrFA additives is shown in Figure 6.6. The addition of 1 wt.% SrFA resulted in a slight increase in the compressive strength of SGIC. However, the compressive strength of SGIC was significantly reduced with the addition of more than 1 wt.% of SrFA additives to SGIC.

The results indicated that the addition of SrFA at a concentration of 1 wt.% significantly improved the compressive strength of the cement compared to the control group (0 wt.% of SrFA). The increase in compressive strength could be attributed to the reinforcement of the cement matrix through the incorporation of SrFA. However, with further increases in SrFA concentration, the compressive strength of the cement was significantly reduced, which might be due to the excessive amount of additive interfering with the setting reaction. Therefore, 1 wt.% SrFA could be considered optimal for reinforcement in SGIC and improve the compressive strength of SGIC.

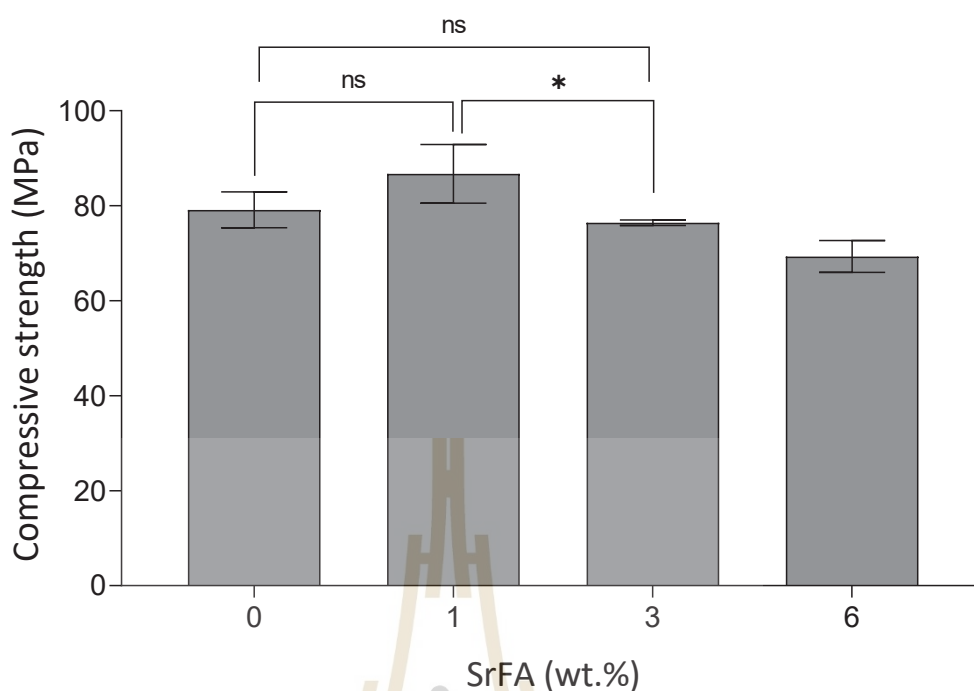


Figure 6.6 Compressive strength of SGIC containing with 1, 3, and 6 wt.% of SrFA additives.

### 6.3.3 Antibacterial properties

The agar diffusion testing of SGIC modified with SrFA at concentrations of 0, 1, 3, and 6 wt.% showed that the addition of 1 wt.% SrFA significantly increased the inhibition zone, with a subsequent increase in the inhibition zone with further SrFA concentration. In addition, the testing was also compared with the commercial GIC, which exhibited an inhibition zone of approximately 1 mm in size.

The size of the inhibition zone observed in the agar diffusion testing reflects the antibacterial activity of the tested materials. In our study, all SGIC specimens modified with different concentrations of SrFA exhibited an inhibition zone size larger than 1 mm, indicating their antibacterial effect according to the standard SNV 195920-199 (Schuhladen et al., 2020). As reported in Chapter 5, the observed antibacterial effect of the unmodified SGIC was attributed to the release of zinc ions from its composition, which are well-known for their antimicrobial properties. Furthermore, the addition of SrFA to SGIC resulted in a significant increase in the inhibition zone size, indicating an improved antibacterial effect. This finding

supports previous literature that suggests strontium-containing fluorapatite has the potential to inhibit bacterial growth for both Gram-negative and Gram-positive bacteria (Alatawi et al., 2018, Anastasiou, Nerantzaki, Gounari et al., 2019, Wang et al., 2019). In contrast, the commercial GIC presented a very small inhibition zone with a size of around 1 mm, indicating weaker antibacterial properties compared to the modified SGIC.

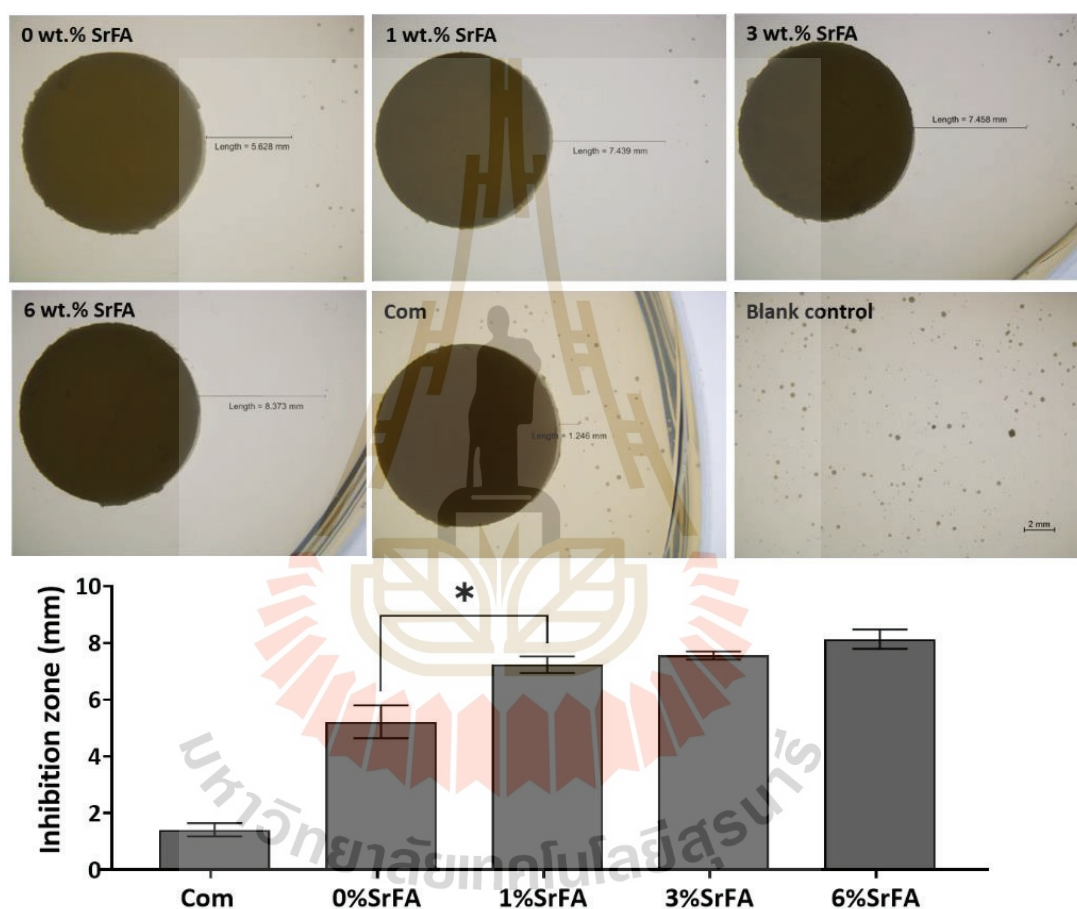


Figure 6.7 Agar diffusion method for SGIC containing with 0, 1, 3, and 6 wt.% of SrFA against *S.mutans*. The inhibition zone was observed and measured by stereo microscope with magnification of 0.67x, using NIS element microscope imaging software. Error bars are standard error of the mean (n=3)

The antibacterial mechanism of SrFA remains unclear. It was believed that the release of strontium ions and fluoride ions from the material played a role in inhibiting bacterial growth. Strontium ions were reported to inhibit the growth of both Gram-positive and Gram-negative bacteria by interfering with bacterial cell membrane function and disrupting intracellular processes. Moreover it was reported that the incorporation of Sr dopants induced a negative surface charge of the material resulting in positive affect the biological properties of material, leading to improved extracellular matrix adsorption, bone cell attachment and enhances antibacterial activity (Ganjali, Mousavi, Nikzamir et al., 2022). Fluoride ions have been known to inhibit bacterial enzymes and disrupt cell membrane function. Additionally, the co-doping of strontium and fluoride in hydroxyapatite created a synergistic effect, leading to enhanced antibacterial activity (Dabsie et al., 2009, Ganjali et al., 2022).

#### **6.3.4 *In vitro* bioactivity**

The surface morphology of SGIC modified with different amounts of SrFA after immersion in DI water and artificial saliva for 5 days was observed by SEM-EDS technique, as shown in Figure 6.8. Upon exposure to artificial saliva, an apatite-like layer was observed on all GIC surfaces. The presence of the apatite-like layer was confirmed by the EDS technique, which showed that the ratio of Ca/P should be in the range of 1.30–1.67, as reported in previous literature (Drouet, 2013). The Ca/P ratio of the unmodified SGIC was found to be 1.87, while the SGIC modified with SrFA showed a Ca/P ratio ranging from 1.50 to 1.77, which was close to the reported range. This reduction in Ca/P ratio could be attributed to an increase in P content resulting from the precipitation of the apatite layer. These results suggested that the precipitate found on the surface of the SGIC was indeed apatite.

The notably apatite-like precipitation on the SGIC modified with SrFA was higher than on the unmodified SGIC. Interestingly, the size of the apatite precipitate on SGIC surface increased proportionally with SrFA content, indicating a positive correlation between SrFA contents and apatite precipitate size. Moreover, the apatite precipitation on the surface of SGICs was distributed more evenly compared to commercial GICs, which tended to be more agglomerated.

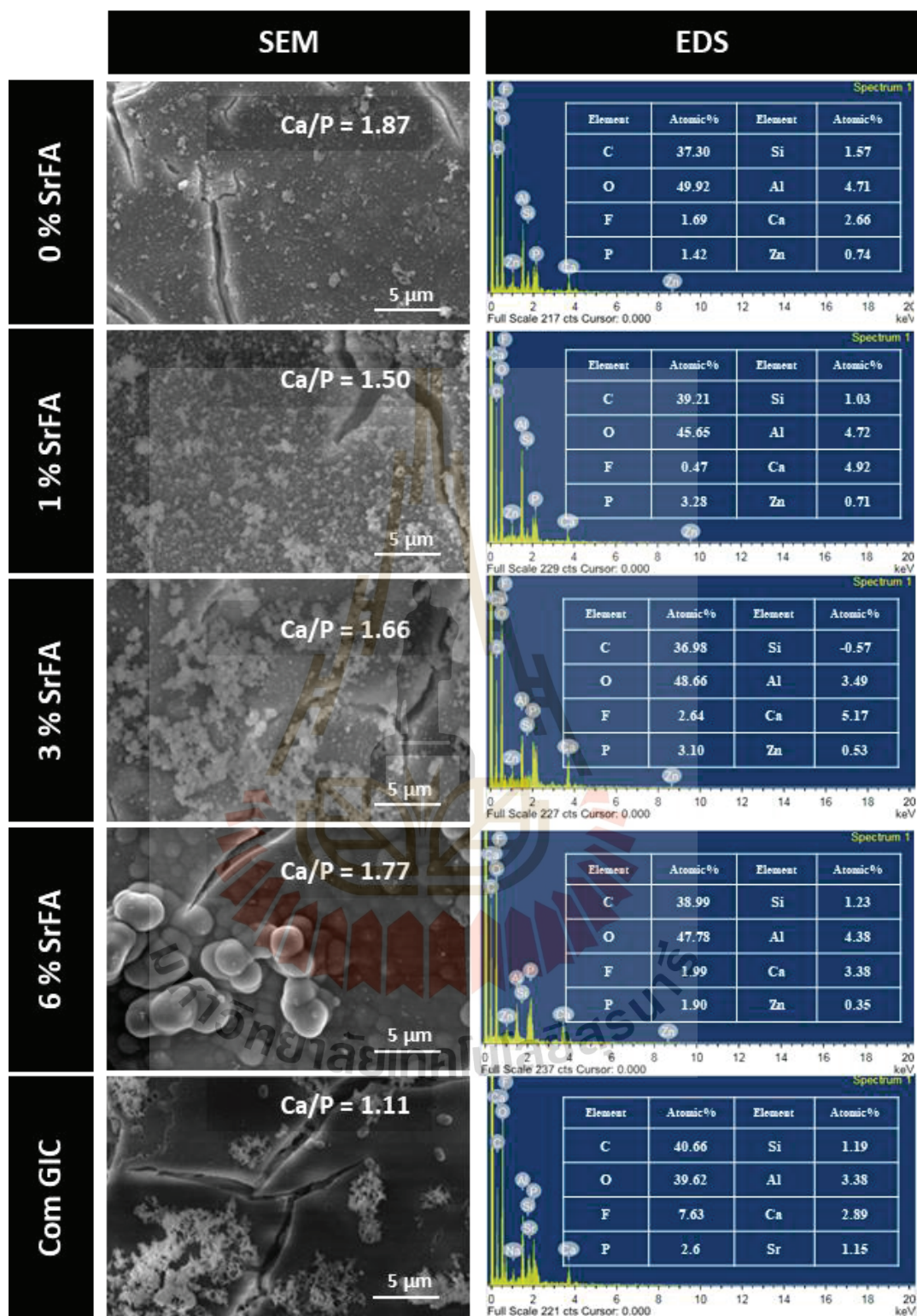


Figure 6.8 SEM-EDS of the surface of SGIC containing 0, 1, 3, and 6 wt.% of SrFA after immersion in artificial saliva for 5 days, in comparison with a commercial product.

The precise mechanism of the effect of SrFA on the crystal growth kinetics of apatite remains unclear. The previous study suggested that HA in the material led to more nucleation sites for apatite crystals to form and larger crystal growth on the material surface (Onuma, Ito, Tateishi et al., 1995, Wu and Nancollas, 1997, Ito and Onuma, 2003). Moreover, the synergistic effect of the Sr and F ions combination was reported to significantly enhanced remineralization (Thuy, Nakagaki, Kato et al., 2008). The larger size of apatite crystal and its ability to mineralize could have benefits for the dental application in that it could induce the penetration of apatite crystal into the surrounding tooth structure (Ito and Onuma, 2003, Osorio, Osorio, Cabello et al., 2014, Albeshti, 2016).

### 6.3.5 Cell viability

The NIH/3T3 cell cytotoxicity of SGICs containing 0, 1, 3, and 6 wt.% of SrFA was evaluated and compared with commercial GIC, with glass coverslips as the negative control. The findings illustrated in Figure 6.9 represent the percentage of AlamarBlue reduction, which served as an indicator the cellular metabolic activity. A high percentage of AlamarBlue reduction suggested high metabolic activity of the cells, which indicated a high level of cell viability. On day 1, there was no significant difference observed among the samples. After incubation for 7 days, all samples exhibited an increase in metabolic activity from day 1 to day 7. Moreover, it could be seen that the addition of 1 wt.% SrFA significantly enhanced metabolic activity on day 7, although there was no significant difference between 1, 3, and 6 wt.% SrFA samples. By day 14, there was a significant increase in metabolic activity observed for all samples, with the highest activity observed in the 6 wt.% SrFA sample.

These findings suggested that the addition of SrFA to SGICs could improve the cell viability of NIH/3T3 cells. Moreover, the study suggests that the optimum weight percentage of SrFA in SGICs is 1 wt.% because higher concentrations of SrFA presented no significant improvement in metabolic activity.

Previous research had demonstrated that incorporating Sr into hydroxyapatite could improve cell viability in human periodontal ligament fibroblast (HPDLF) cells (Ravi, Balu and Sampath Kumar, 2012). The cytotoxic effect of fluorapatite powder on human osteoblast-like cells was found to be non-toxic due

to the release of Ca and P ions in the extract solution. Reports suggest that the released Ca ions could induce osteoblast proliferation and chemotaxis through binding to a G-protein coupled with extracellular calcium sensing receptor (Forghani, Mapar, Kharaziha et al., 2013). Overall, it could be implied that the presence of fluoride in hydroxyapatite could cause cytotoxicity, but the release of Ca, Sr, and P ions from fluorapatite could induce cell proliferation.

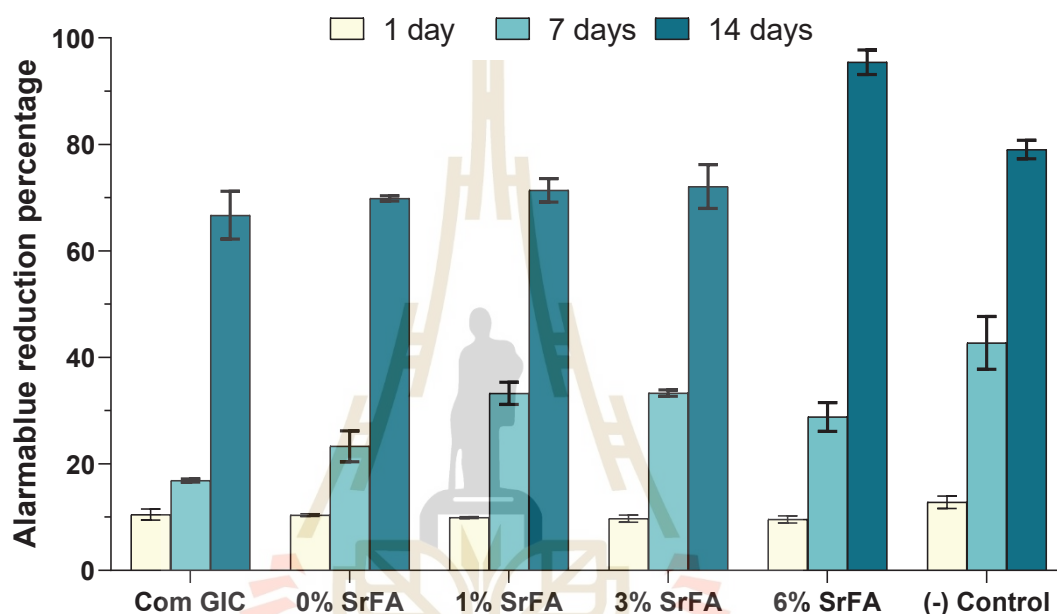


Figure 6.9 AlamarBlue reduction percentage of NIH/3T3 fibroblast cells on SGIC surface with the different SrFA contents at incubation period of 1 day, 7 days and 14 days. Control was referred to the cell-cultured on the glass cover slip. Error bars are standard error of the mean (n=3)

### 6.3.6 Fluoride release and uptake

In this study, the ability of SGICs containing varying concentrations of SrFA (0, 1, 3, and 6 wt.%) to release and uptake fluoride on days 1, 7, and 14 was investigated, and these results were compared with those of a commercial GIC. The results presented in Figure 6.10 showed that the commercial sample initially released the highest amount of fluoride on day 1, but this amount rapidly decreased over time. In contrast, all SGICs release a constant level of fluoride for up to 21 days.

The ability of SGICs to release fluoride constantly for an extended period was consistent with the findings of a previous study on sol-gel derived GICs (Bertolini et al., 2005). This gradual release of low levels of fluoride was an important clinical feature, as it could help reduce the incidence of caries, especially in patients who were at high risk or had a history of dental decay.

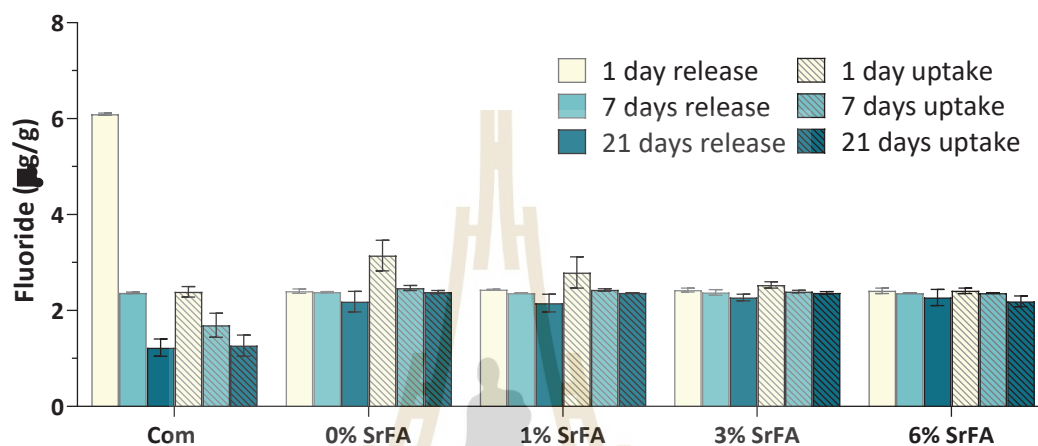


Figure 6.10 Concentration of fluoride release and uptake of SGIC containing with 0, 1, 3, and 6 wt.% of SrFA in comparison with the commercial product. Error bars are standard error of the mean (n=3).

Upon fluoride uptake, there was an increase in fluoride ion concentration on day 1 in the 0 wt.% SrFA, 1 wt.% SrFA, and commercial GIC samples. However, when higher amounts of SrFA were added, the concentration of fluoride uptake was reduced.

Our findings indicate that the addition of SrFA to SGICs resulted in an insignificant improvement in their fluoride release capability. In addition, when higher amounts of SrFA (up to 3 wt%) were added, the concentration of fluoride uptake on day 1 was significantly reduced. This finding suggested that SrFA additive might interfere with the ability to take up fluoride. Therefore, the optimal amount of SrFA that can be added to SGICs should not exceed 1 wt.% to maintain their fluoride uptake capacity.

## 6.4 Conclusions

In this chapter, SrFA nanoparticles were synthesized through the hydrothermal method and used as an additive in SGIC. The obtained particles exhibited a needle-like shape and high crystallinity. The incorporation of SrFA in SGIC was found to retard the setting time; however, the addition of 1 wt.% SrFA significantly improved the compressive strength without significantly affecting the setting time. Furthermore, the results suggest that SrFA had the potential to significantly improve the antibacterial properties, apatite layer formation, and cytocompatibility of SGIC, especially at a concentration of 1 wt.%. In terms of fluoride release and uptake ability, the addition of SrFA to SGIC presented no improvement in fluoride release and inhibited their ability to uptake fluoride.



## CHAPTER 7

### EFFECT OF STRONTIUM CONTAINING FLUORINATED BIOACTIVE GLASS ADDITIVE IN SGIC ( $4.5\text{SiO}_2-4\text{Al}_2\text{O}_3-0.45\text{P}_2\text{O}_5-$ $1.4\text{CaO}-0.3\text{ZnO}-2\text{F}_2$ )

Chapter 6 demonstrated the successful improvement of antibacterial properties, ability to form apatite layer, and cell viability of SGIC modified with SrFA as an additive. However, SrFA did not enhance the fluoride release ability and even reduced the ability to uptake fluoride, which was critical for maintaining fluoride in the oral environment. Therefore, this study aimed to investigate the benefits of another candidate for using as an additive in SGIC which was strontium containing fluorinated bioactive glass (SrBGF) to enhance its antibacterial, bioactivity, and biocompatibility properties. Due to its amorphous structure, SrBGF was expected to have superior properties as compared to SrFA in terms of fluoride release and uptake. This chapter reports the effect of SrBGF on physical properties of SGIC, including setting time, compressive strength, as in Chapter 6. Additionally, the study explored deeper into antibacterial properties, *In vitro* cytocompatibility, and remineralization ability as comparison to SGICs modified with SrFA and the commercial GIC. Finally, the mechanism of fluoride release and uptake ability of SGIC containing SrBGF was thoroughly examined.

#### 7.1 Research background

GICs is known as the first choice for dental restoration in patients at higher risk of caries due to its potential to release fluoride (Krämer, Schmidt, Lücker et al., 2018). The fluoride-releasing behavior of commercial GICs was reported to be released at maximum within the first week and then reduced gradually and became constant (Gao and Smales, 2001). Fluoride ions was reported to be initially released due to trapped fluoride ions in the cement matrix, followed by a constant release from the

glass particle (Suprastiwi, Anggraeni and Npa, 2009). After fluoride release, GICs were able to uptake fluoride from the oral environment. This cycle of fluoride release and uptake by GIC enhanced fluoride release from the cement, thereby preventing caries during long periods of dental restoration, and is known to prevent secondary caries (Yli-Urpo, Lassila, Närhi et al., 2005, Kim, Bae, Lee et al., 2021). However, it was recently found that almost all the fluoride uptake in the commercial GIC was retained in the cement and was unable to be re-released (Madi, Sidhu and Nicholson, 2020).

To improve the fluoride release ability, fluoride-containing bioactive glass has become interesting as an additive, since it could release fluoride ions, support fluoride bioavailability in saliva and improve fluoride uptake ability (Davis, Gwinner, Mitchell et al., 2014, Naumova, Staiger, Kouji et al., 2019). This was even more interesting when strontium was added to the bioactive glass. Some literatures reported that the incorporation of strontium into the bioactive glass enhanced the bioactivity and stability of apatite formation, which could be more beneficial for caries prevention (Dai et al., 2021). The nano-size, spherical shape, and mesoporous structure of the bioactive glass particle could influence biocompatibility, resulting in more viable cells, and improving apatite-like formation, thereby superior bioactivity (Thaitalay et al., 2022). Based on the result of previous literature, it was interesting to incorporate the fluoride containing strontium-based bioactive glass into SGIC to enhance the fluoride release ability and the biological properties. In addition, the ability of SGIC to uptake fluoride and its mechanism should be explored as comparison with the commercial GIC.

The aim of this study was to investigate the ability to release and uptake fluoride of SGIC added with SrBGF additive as compared with the commercial GIC. Additionally, the mechanism of fluoride release and uptake inside GIC sample was also examined. SrBGF additive in this study was based on  $45\text{SiO}_2\text{-}5\text{P}_2\text{O}_5\text{-}35\text{SrO}\text{-}15\text{SrF}_2$  synthesized by sol-gel method. The resulting SrBGF additive was characterized by XRD and FTIR technique. The effect of SrBGF contents on the setting time and compressive strength were evaluated. Additionally, in order to assess the relative performance of SrBGF additives, the antibacterial properties, bioactivity, and cytocompatibility of SGIC containing SrBGF were evaluated in comparison to SGIC

containing SrFA additives. Finally, the mechanism of fluoride release and uptake in SGIC with SrBGF additive were evaluated by fluoride selective electrode, SEM-EDS techniques and XPS technique.

## 7.2 Experimental procedure

### 7.2.1 Synthesis of SrBGF nanoparticles and characterization

In this study, the strontium and fluoride containing nano-bioactive glass powder (SrBGF) belonging to the system of  $45\text{SiO}_2\text{-}5\text{P}_2\text{O}_5\text{-}35\text{SrO}\text{-}15\text{SrF}_2$  was synthesized by the sol-gel method. To prepare SrBGF, a mixture of EtOH, deionized water, and ammonia solution ( $\text{NH}_4\text{OH}$ , 30%, Carlo Erba) was stirred together in a molar ratio of 1:9:0.1, with cetyltrimethyl ammonium bromide (CTAB, 99%, Sigma-Aldrich) added as a particle template. TEOS, TEP,  $\text{Ca}(\text{NO}_3)_2\cdot 4\text{H}_2\text{O}$ , and  $\text{H}_2\text{SiF}_6$  were then added under vigorous stirring. The resulting precipitate was filtered and washed with DI water and EtOH three times. The bioactive glass powder was obtained by drying overnight at  $100^\circ\text{C}$  and then calcining at  $650^\circ\text{C}$  for 2 h ( $2^\circ\text{C}/\text{min}$ ). The synthesis method for SrFA was summarized as shown in Figure 7.1.

Phase identification of the synthesized SrFA additives was analyzed by XRD. Morphology of SrFA additive was determined by a Transmission electron microscopy (TEM, Tecnai™ G<sup>2</sup> 20, FEI company, Hillsboro, USA).

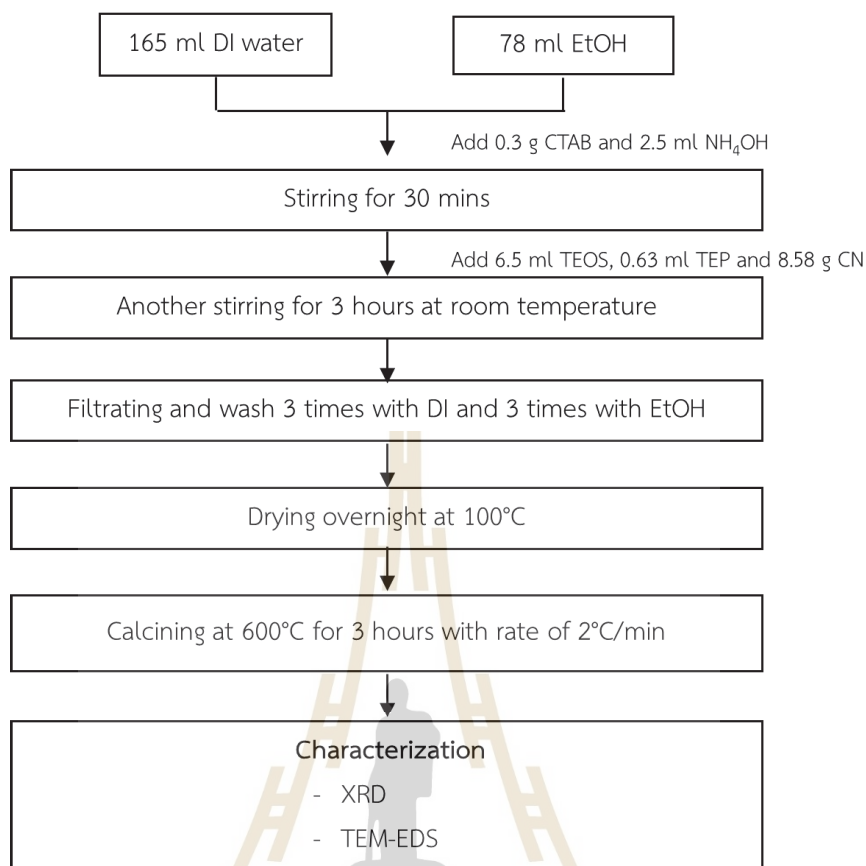


Figure 7.1 sol-gel synthesis procedure of SrBGF

### 7.2.2 Preparation of glass ionomer cement

In this chapter, SGIC was modified by adding SrBGF in the range of 0, 1, 3, and 6 wt.%. The cement was formulated by blending the sol-gel ionomer glass powder with the liquid solution at a ratio of 1.5:1 (w/v). The sol-gel ionomer glass powder was synthesized in the  $4.5\text{SiO}_2\text{-}4\text{Al}_2\text{O}_3\text{-}0.45\text{P}_2\text{O}_5\text{-}1.7\text{CaO}\text{-}0.3\text{Zn}\text{-}2\text{F}_2$  composition molar ratio system, following the methodology in Chapter 5. The liquid solution contained a mixture of 27 wt.% polyacrylic acid (PAA, M.W.  $\sim 100,000$ , Sigma-Aldrich, Darmstadt, Germany), 64 wt.% poly(acrylic acid-co-maleic acid) (PAA-co-MA, M.W.  $\sim 3,000$ , Sigma-Aldrich, Darmstadt, Germany), and 9 wt.% tartaric acid (Carlo Erba, Val de Reuil, France). The commercial GIC (GC Gold Label 9 HS Posterior EXTRA, GC Corporation, Tokyo, Japan) was employed as a reference material for comparison.

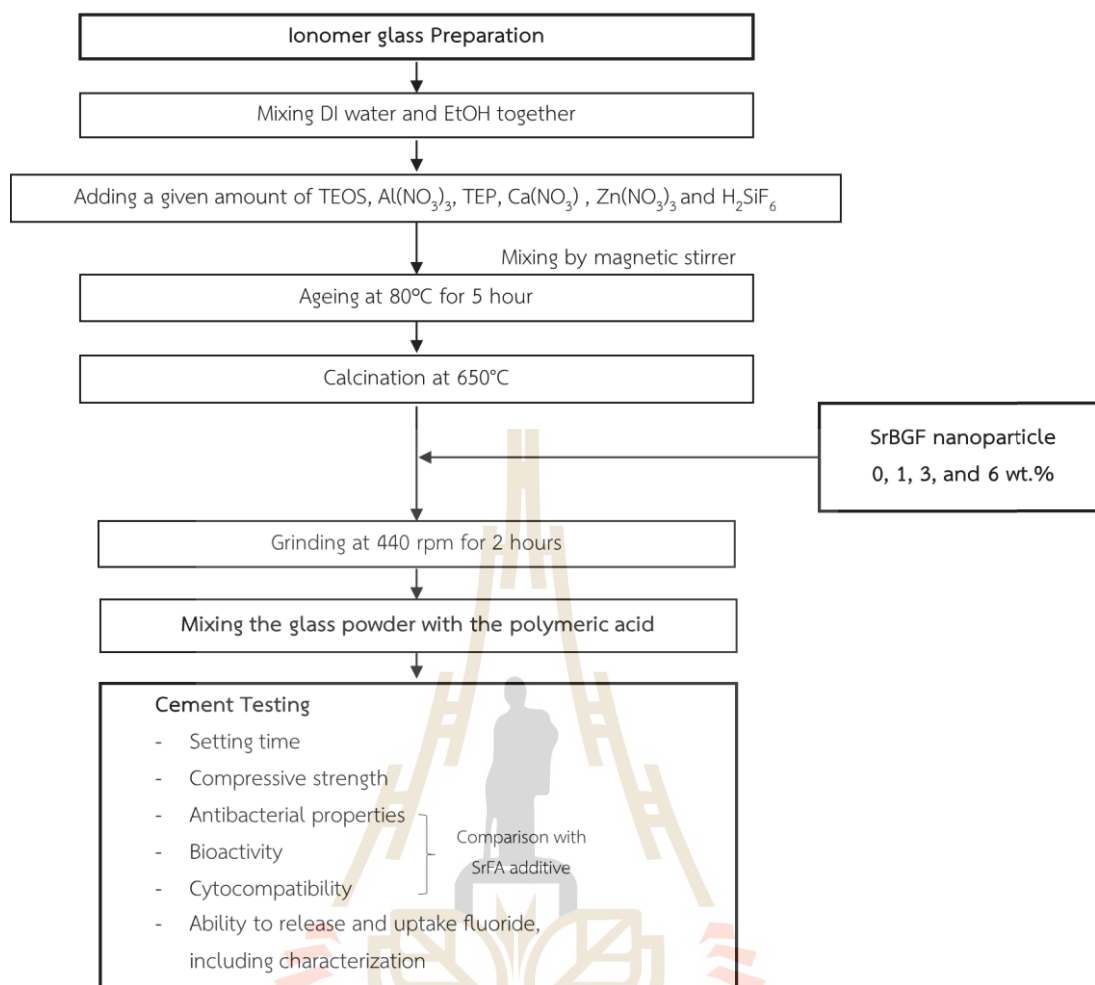


Figure 7.2 Schematic of experimental design to determine the effect of SrBGf additive on the properties of SGIC.

### 7.2.3 Setting time and compressive strength testing

The evaluation of the setting time and compressive strength of SGIC was performed in accordance with the methodology outlined in Chapter 4, sections 4.2.4 and 4.2.5.

### 7.2.4 Surface roughness

After the preparation of the cement, the surface roughness of SGIC modified with 0 and 1 wt.% SrBGf was evaluated in comparison with the SGIC modified with 1 wt.% SrFA and the commercial GIC. The experiment was conducted to determine the possibility of bacteria and cell attachment to the cement surface.

The roughness was detected optically by a three-dimensional (3-D) optical profiler (WYKO NT1100 profiler, WYKO Corp.). The results were compared to those obtained with SGIC modified with SrFA and the commercial GIC. There were three measurements on the top of each specimen.

### 7.2.5 Antibacterial testing

The aim of this experiment was to evaluate the antibacterial activity of SGIC modified with SrBGF against *S. mutans* using the agar diffusion method, as well as to determine the ability of bacteria to adhere to the material surface. The results were compared to those obtained with SGIC modified with SrFA and the commercial GIC.

To perform the agar diffusion method, *S. mutans* were selected from culture on blood agar plates and cultured in BHI broth overnight. The bacterial culture was diluted to  $1.5 \times 10^8$  CFU/ml in a fresh BHI broth, and then uniformly swabbed onto the Mueller-Hinton agar plate. Disc-shaped GIC specimens were then placed onto the agar and incubated at 37°C for 72 hours. The diameter of the inhibition zones around GIC discs was measured to evaluate the bacterial activity.

To determine the adhesion of bacteria to dental surfaces, *S. mutans* was cultured in a BHI broth at 37°C for 18 hours. The bacteria suspension was diluted to  $1.5 \times 10^8$  CFU/ml in a fresh BHI broth, and the disc shaped GIC specimens were transferred into a diluted culture of *S. mutans* with the BHI broth. After incubating the specimens for 12 hours, they were rinsed and soaked in 0.1 M PBS to fix the attached bacteria. The bacterial adhesion was evaluated using a Scanning Electron Microscope (SEM, JEOL-6010LV) after applying a thin gold layer by sputtering method to create a conductive sample.

### 7.2.6 Bioactivity testing

The bioactivity of the material in this study was evaluated in accordance with the ability to induce dentine mineralization. To evaluate the mineralization capacity of GIC materials on dentin, dentine density after employed under simulated oral condition was measured and compared to that of untreated dentin. For this purpose, human third molars were selected from the collection of extracted teeth at the SUT oral health center and the dental clinic of Kham Thale So hospital. The

enamel was polished off to expose the dentin surface, which was then drilled to create a 0.34 mm diameter cavity. The teeth were immersed in a demineralization solution (1.5 mM  $\text{CaCl}_2$ , 0.9 mM  $\text{KH}_2\text{PO}_4$ , 50 mM acetic acid, pH = 4.5) for 8 days to create artificial caries. After rinsing with DI water and drying at room temperature, the cavity was filled with GIC pastes. The specimens were then left in the air at room temperature for 1 hour and soaked in DI water for 24 hours to complete the setting reaction of GICs. The specimens were cross sectioned into two pieces, with the first serving as the control and the second undergoing pH cycling, which simulated the change of pH in oral environment. In the pH cycling process, each specimen was immersed in a remineralization solution (1.5 mM  $\text{CaCl}_2$ , 0.9 mM  $\text{NaH}_2\text{PO}_4$ , 150 mM KCl, pH = 7.0) for 20 hours, rinsed with DI water, and then immersed in demineralization solution for 4 hours. This process was repeated daily using remineralization and demineralization solutions for 14 days. Figure 7.3 provides an overview of the specimen preparation and evaluation process.

In order to evaluate the density of dentin after pH-cycle, the dentin portion of the specimen was trimmed into a rectangular shape measuring 1 mm x 1 mm x 10 mm. The three-dimensional structure of the dentin specimens was then characterized using Synchrotron radiation X-ray micro-computed tomography ( $\mu\text{CT}$ ) at beamline BL1.2W, located at the Synchrotron Light Research Institute (SLRI) in Nakhon Ratchasima, Thailand. X-ray radiation was generated from a 2.2 T multipole wiggler at the 1.2 GeV Siam Photon Source. To support each specimen, a polyimide tube was placed on a rotary stage. For a  $180^\circ$  rotation with a  $0.2^\circ$  step, 900 X-ray projections were recorded. The X-ray beam had a mean energy of 14 keV and was positioned 32 mm from the source. All tomographic scans were acquired at a pixel size of  $1.44 \mu\text{m}$  using a detection system equipped with a  $200 \mu\text{m}$ -thick YAG:Ce scintillator, white-beam microscope (Optique Peter, France) and pco edge 5.5 sCMOS camera ( $2560 \times 2160$  pixels, 16 bits). Data processing and tomographic reconstruction were performed using Octopus Reconstruction software (Tescan Orsay Holding, Brno, Czech Republic). The 3D visualisation of the dentin after pH-cycle was conducted using Drishti software, Version 2.6 (ANU Vizlab, Canberra, Australia).

Furthermore, surface morphology and elemental analysis on the dentin surface after pH cycles were determined using a Scanning Electron Microscope (SEM,

JEOL-6010LV, Peabody, USA) coupled with Energy Dispersive Spectroscopy (EDS, Oxford Instruments X-MaxN 20).

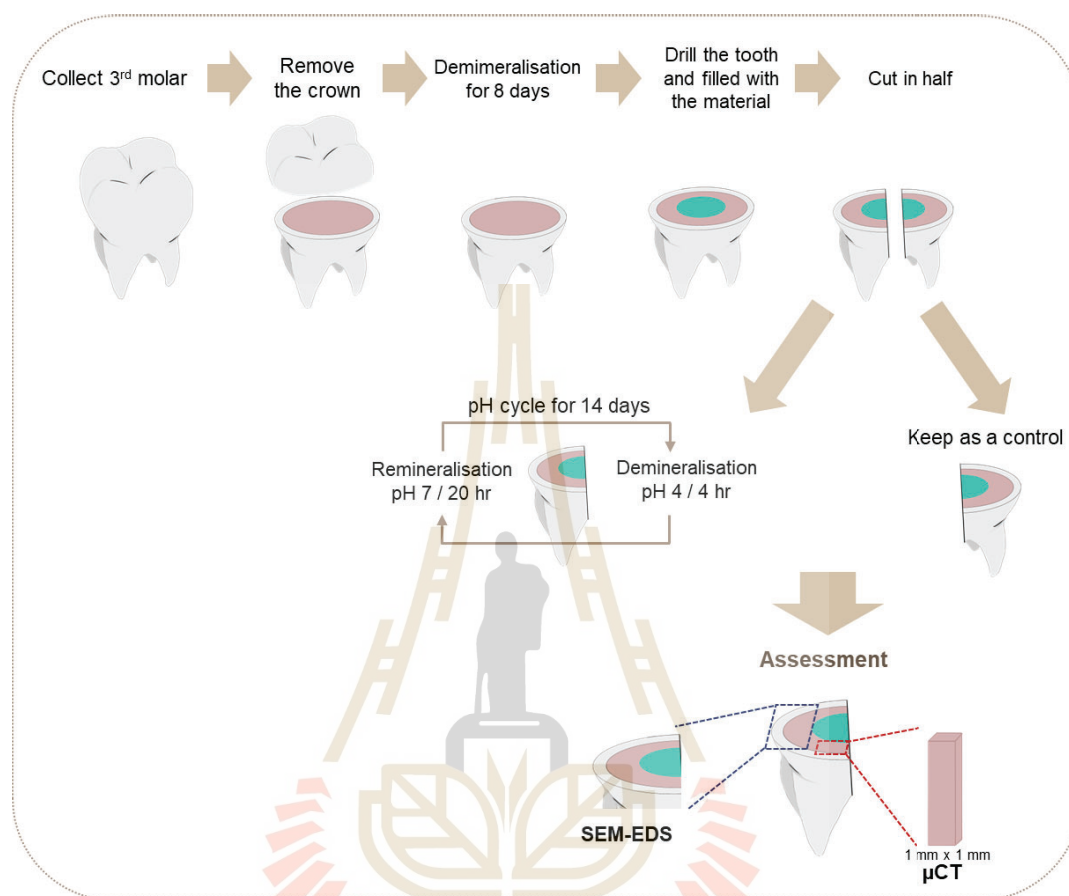


Figure 7.3 Illustration of experiment procedures performed to evaluate remineralization ability.

### 7.2.7 *In vitro* cytocompatibility on human adipose-derived stem cell (hASCs)

hASCs were used as a model to assess several cellular activities including cell cytotoxicity (live/dead assay) and proliferation (AlamarBlue and DNA Picogreen assay).

#### 7.2.7.1 Indirect testing

SGICs were prepared in a disc shape with 2 mm in height and 10 mm in diameter, and subsequently sterilized by UV immersion for 30 minutes on each side. The prepared disc of SGIC samples were rinsed by phosphate-buffered

saline (PBS) solution to remove the organic residual. The extracts were prepared by incubating the discs in 1mL of complete media at 37 °C. The sample-soaked mediums were replaced with 1 mL of fresh complete medium every 2–3 days. The extract was collected on days 1, 7 and day 14 of incubation.

To perform testing, a suspension of  $5 \times 10^3$  cells in 100  $\mu$ l complete medium was seeded into a 96-well tissue culture plate and left to attach overnight. The following day, the medium was replaced with the extract and incubated for 24 hours. Negative controls were run using fresh media, while the wells without cells were utilized as blanks. Once the incubation was completed, the extract medium was replaced with 100 ml of 10 vol.% AlamarBlue solution (5 mg Resazurin salt/ 40 ml sterile PBS, Sigma) in complete medium to measure the metabolic activity of the cells. The plates were then incubated at 37 °C and 5% CO<sub>2</sub> for 2 hours, after which the fluorescence was measured using a microplate reader (Sunrise, Tecan) at 544 nm excitation and 590 nm emission.

To determine the effect of the cement material on the cell environment, the cement extract obtained on day 1 and day 7 was centrifuged, and the resulting supernatant was collected to determine the ions released/adsorbed by the cement discs. The supernatant was then diluted by a factor of 10 and analyzed using Inductive coupled plasma optical emission spectrometry (ICP-OES: 8000, PerkinElmer). Additionally, the pH changes of the cement extract were measured using an electrolyte-type pH meter (Denver pH/mV/Temp. Meter, UB-10).

#### 7.2.7.2 Direct testing

After undergoing sterilization through UV immersion, the cement discs were incubated in 1 mL of PBS for three days, followed by a change to complete medium for an additional three days before cell seeding. A total of  $1 \times 10^4$  cells suspended in 1 mL of complete medium were seeded onto the cement discs in a 24-well plate, and a glass coverslip was used as the control condition. The complete medium was replaced with fresh 1 mL medium every 2-3 days. To assess cell proliferation at days 1 and 7, AlamarBlue assay and DNA quantification, as previously described, were performed. Three independent samples were carried out.

### 7.2.8 Preliminary study of human dental pulp stem cells (hDPSCs) cytotoxicity

In a previous *in vitro* experiment, hASCs were used to evaluate the cytotoxicity of SGIC modified with SrBGF or SrFA additives. In this section, we investigated the suitability of SGIC for dental applications by employing hDPSCs, which are more relevant to dentistry than hASCs.

To investigate the effects of GIC materials on hDPSCs, hDPSCs were cultured in DMEM at 37°C and 5% CO<sub>2</sub> humidified atmosphere. The indirect testing was conducted using material extraction prepared by incubating GIC samples in DMEM at 37°C for 24 h. The hDPSCs were cultured at a density of  $5 \times 10^3$  cells per well in 96-well plates, with 100  $\mu$ l of conditioned media and 100  $\mu$ l of fresh DMEM for 3 days. Negative controls were cultured in 200  $\mu$ l of fresh media.

After 3 days of culture, hDPSCs were incubated with 0.2% 3-(4,5-dimethylthiazol-2-yl)-2,5-diphenyltetrazolium bromide (MTT) solution (Sigma-Aldrich) at 37°C for 4 hours. The reaction was stopped with 200  $\mu$ l of dimethylsulfoxide (Sigma-Aldrich) and 25  $\mu$ l of glycine buffer (Research Organics). The resulting color was measured using a spectrophotometer (Sunrise, Tecan, Switzerland) at 620 nm absorbance. We conducted five independent samples.

### 7.2.9 Fluoride release and uptake testing

In this section, the experiment aimed to evaluate the fluoride release and uptake of SrBGF and GIC materials. The specimens of SrBGF and GIC materials were separately prepared for the evaluation process. The summary of the specimen preparation and characterization is illustrated in Figure 7.4.

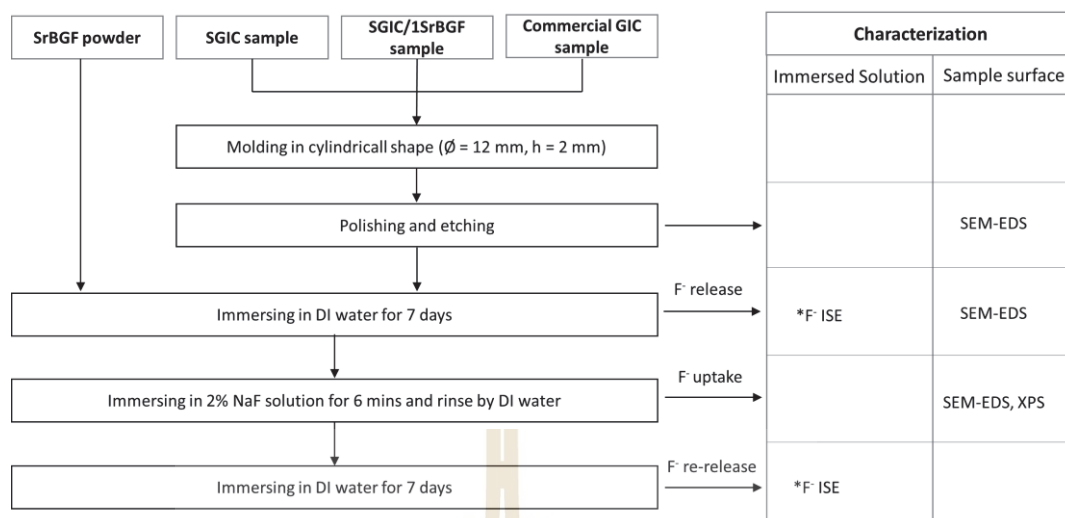


Figure 7.4 The experimental procedure of fluoride release and uptake ability of SrBGF powder and SGIC samples and their characterization. (\*F<sup>-</sup> ISE = Fluoride Ion Selective Electrode technique).

#### 7.2.9.1 Preparation of SrBGF powder samples

In order to assess the fluoride-releasing potential of SrBGF additive, 3 mg of the powder was immersed in DI water at a ratio of 3 mg/ml at 37°C for 7 days. SrBGF powder was then collected by filter paper, and subsequently immersed in a 2% NaF solution for 6 minutes to absorb fluoride. SrBGF powder was rinsed with DI water and dried before being immersed in DI water at the same ratio and temperature for another 7 days to repeat the cycle. At each step of the experiment, SrBGF powder and the immersed solution were collected, particularly after DI water immersion, after fluoride absorption, and after fluoride release, to analyze the fluoride-releasing potential of SrBGF additive.

#### 7.2.9.2 Preparation of GIC specimens

All GIC samples were prepared in a disc shape of 12 mm in diameter and 2 mm in height. The surfaces of all samples were polished with alumina abrasive powder and etched with 2% hydrofluoric acid for 5 seconds. The fluoride release and uptake ability of the glass ionomer cement were evaluated using

the same procedure as that of SrBGF. In addition, the commercial GIC (Fuji IX, GC corporation, Japan) was evaluated as a comparison.

To ensure a clear understanding of the fluoride release and uptake characteristics of SGIC modified with SrBGF additive, the complexity of GIC composition in this study was reduced by utilizing an undoped glass-based material. Therefore, the composition of ionomer glass was chosen to be  $4.5\text{SiO}_2\text{-}4\text{Al}_2\text{O}_3\text{-}0.45\text{P}_2\text{O}_5\text{-}2\text{CaO}\text{-}2\text{F}_2$ .

### 7.2.9.3 Characterization for fluoride release and uptake

The chemical composition of the cement at different stages of immersion was analyzed by SEM-EDS technique using 20 kV with a working distance (WD) of 15. The cement samples were coated with gold using the sputtering technique to ensure better conductivity during the imaging process. In order to determine the fluoride release and uptake mechanism, X-ray photoelectron spectroscopy (XPS) technique was utilized to identify the binding state of Strontium (Sr3d) and fluoride (F1s) with other cations such as  $\text{Al}^{3+}$  ions,  $\text{Ca}^{2+}$  ions,  $\text{Sr}^{2+}$  ions, and  $\text{Si}^{4+}$  ions. For XPS analysis, the cement samples were first pulverized into powder form before the measurement. Origin 2018 software was used to process the fitting curves of XPS spectra using a combination of Gaussian-Lorentzian lines with a fixed value of FWHM. The percentage of each binding state was calculated from the following equation: % binding state = (the area of the deconvoluted peaks/total F1s peak area) x100.

The fluoride ion concentrations in the immersed solution were determined to evaluate the ability of the cement to release fluoride. It was evaluated by a fluoride ion-selective electrode ( $\text{F}^-$  ISE, Orion Research, Inc., Cambridge, VSTAR40A). Fluoride ion concentrations were calculated in the ratio of fluoride ion level to the ionomer glass weight ( $\mu\text{g/g}$ ). The means and standard deviations for three samples of each cement in each group were calculated for accurate statistical analysis.

## 7.3 Results and discussions

### 7.3.1 Characterization of SrBGF additive

SrBGF nanoparticle was successfully synthesized by the sol-gel method. The obtained particle was characterized by the XRD technique, as illustrated in Figure 7.5 (a). The XRD pattern of SrBGF additive showed an amorphous structure with some crystal phases of  $\text{SrF}_2$  (JCPDS no. 06-0262). Additionally, the TEM micrograph of the SrFA nanoparticle, presented in Figure 7.5 (b), demonstrated that the particles were mostly round shape with high porous structure. Their average size was approximately in a range of 20-200 nm analyzed by image analysis.

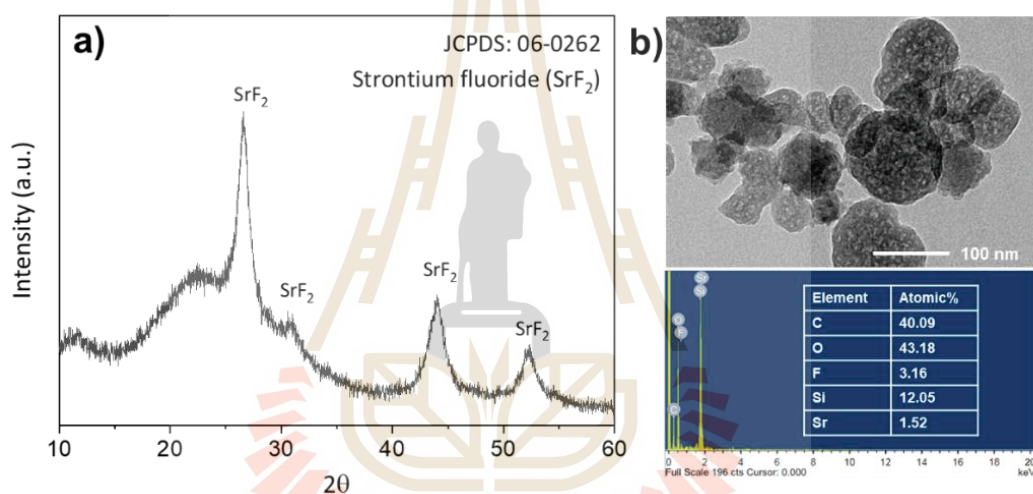


Figure 7.5 a) XRD pattern of the synthesized SrBGF additive, and b) TEM micrographs and EDS analysis of SrFA additive

### 7.3.2 Setting time and compressive strength

The working and net setting time for SGIC modified with different concentrations (0, 1, 3, and 6 wt.%) of SrBGF were illustrated in Figure 7.6. The results indicated that an increase in SrFA concentration did not result in any significant difference in the working time. Additionally, there were no statistically significant differences in the net setting time between SGIC modified with 0 and 1 wt.% of SrBGF. However, when increasing of SrFA addition up to 3 wt.% in SGIC, the net setting time was significantly increased.

This observation was similar to a previous study, which showed that the incorporation of bioactive glass into conventional GIC resulted in the extension of the setting time (Choi, Lee and Kim, 2008). This could be because there was no chemical interaction between SGIC and SrBGF. As the content of SrBGF increased in SGIC, it interfered with the hardening reaction of GIC leading to a delay in the setting time.

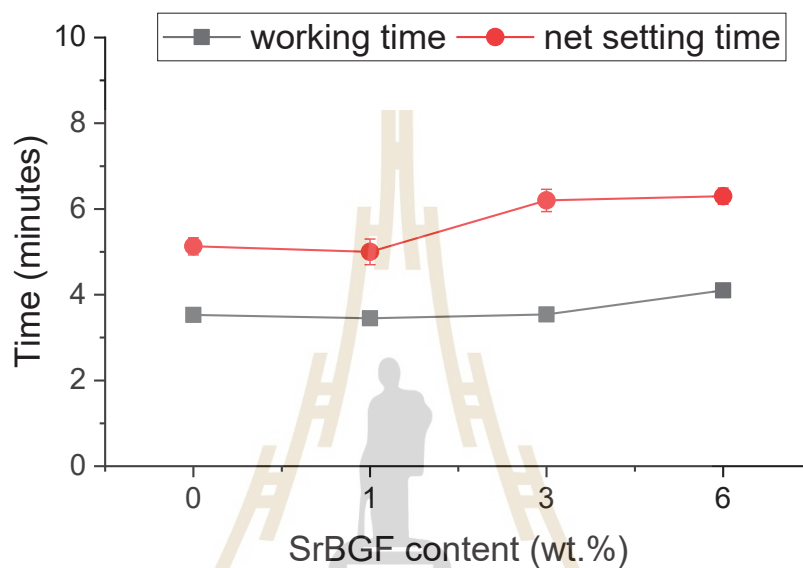


Figure 7.6 Working and net setting time of the sol-gel GIC containing with 0, 1, 3 and 6 wt.% of SrBGF.

Figure 7.7 shows the compressive strength of SGIC containing various concentrations of SrBGF. The results revealed that incorporating 1 wt.% SrBGF significantly enhanced the compressive strength of SGIC. However, the increasing of SrBGF content beyond 1 wt.% appeared to decrease the compressive strength.

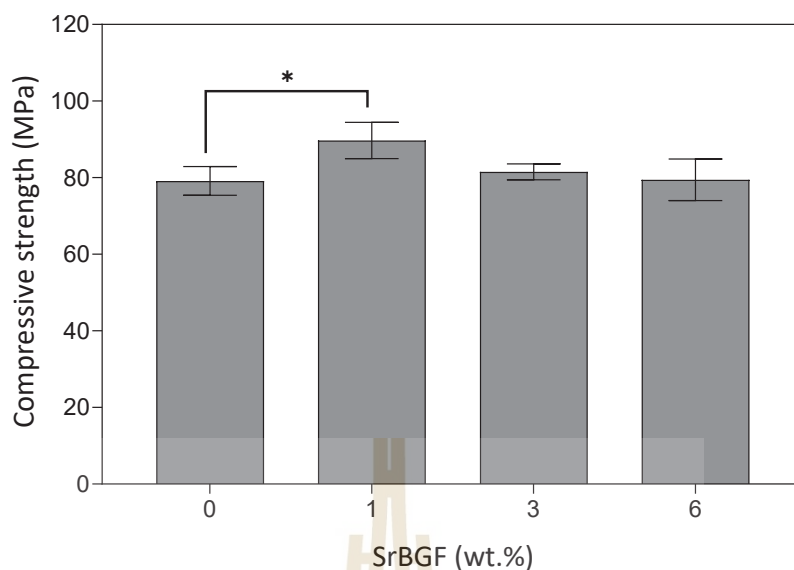


Figure 7.7 Compressive strength of SGIC with the different contents of SrBGF. Error bars are standard error of the mean (n=8). Stars (\*) denote  $p < 0.05$ .

Previous research has reported that the addition of 10 to 30 wt.% of bioactive glass to GIC reduced the compressive strength (Yli-Urpo et al., 2005, Choi et al., 2008). This might be due to excessive incorporation of bioactive glass particles, which acted as fillers that were not chemically attached to GIC matrix (Yli-Urpo et al., 2005). The findings in this study were consistent with previous literature suggesting that SrBGF served as a filler for SGIC without any chemical interaction. Thus, when SrBGF was added to SGIC at concentrations exceeding 1 wt.%, it could interfere with the hardening reaction and result in a reduction of the compressive strength. However, SGIC containing 1 wt.% of SrBGF exhibited a significant improvement in compressive strength, indicating that a 1 wt.% SrBGF concentration is sufficient to serve as an additive for SGIC without any adverse effects on its setting time and compressive strength.

Based on the promising physical property results obtained with the addition of 1 wt.% of SrBGF to SGIC, it was selected for further evaluation. The next experiment will involve evaluation biological properties of the SGIC modified with SrBGF as comparison with SGIC modified with SrFA and commercial GIC. These experiments will focus on several key areas, including the antibacterial properties of the material, its bioactivity, and *in vitro* cytocompatibility. Additionally, the release

and uptake mechanisms of fluoride ions will also be analyzed to better understand the behavior of the material in practical applications.

### 7.3.3 Surface roughness

The optical profilometer was used to measure the surface roughness and perform a 3D scan of the topography in this experiment. Figure 7.8 presents the surface roughness value ( $S_a$ ) of the SGIC samples modified with SrBGF and SrFA additive compared to the commercial GIC. The results indicated that there were no significant differences in surface roughness among the SGIC samples, including SGIC ( $256.46 \pm 10.8$  nm), SGIC/SrBGF ( $247.03 \pm 17.9$  nm), and SGIC/SrFA ( $282.49 \pm 22.3$  nm), respectively. However, the commercial glass ionomer cement exhibited the highest surface roughness value ( $404.70 \pm 14.1$  nm).

Surface roughness had a significant impact on bacterial adhesion and cell activity (Conserva, Consolo and Bellini, 2018). Bacterial adhesion could induce biofilm formation and lead to secondary caries. Surface roughness is one of the main factors for bacterial adhesion extension. It was recommended to consider the surface roughness of materials when developing new dental materials to decrease bacterial adherence (Kozmos, Virant, Rojko et al., 2021). Moderate surface roughness appeared to accelerate the biological processes of cells, promoting better and quicker adhesion and proliferation (Conserva et al., 2018).

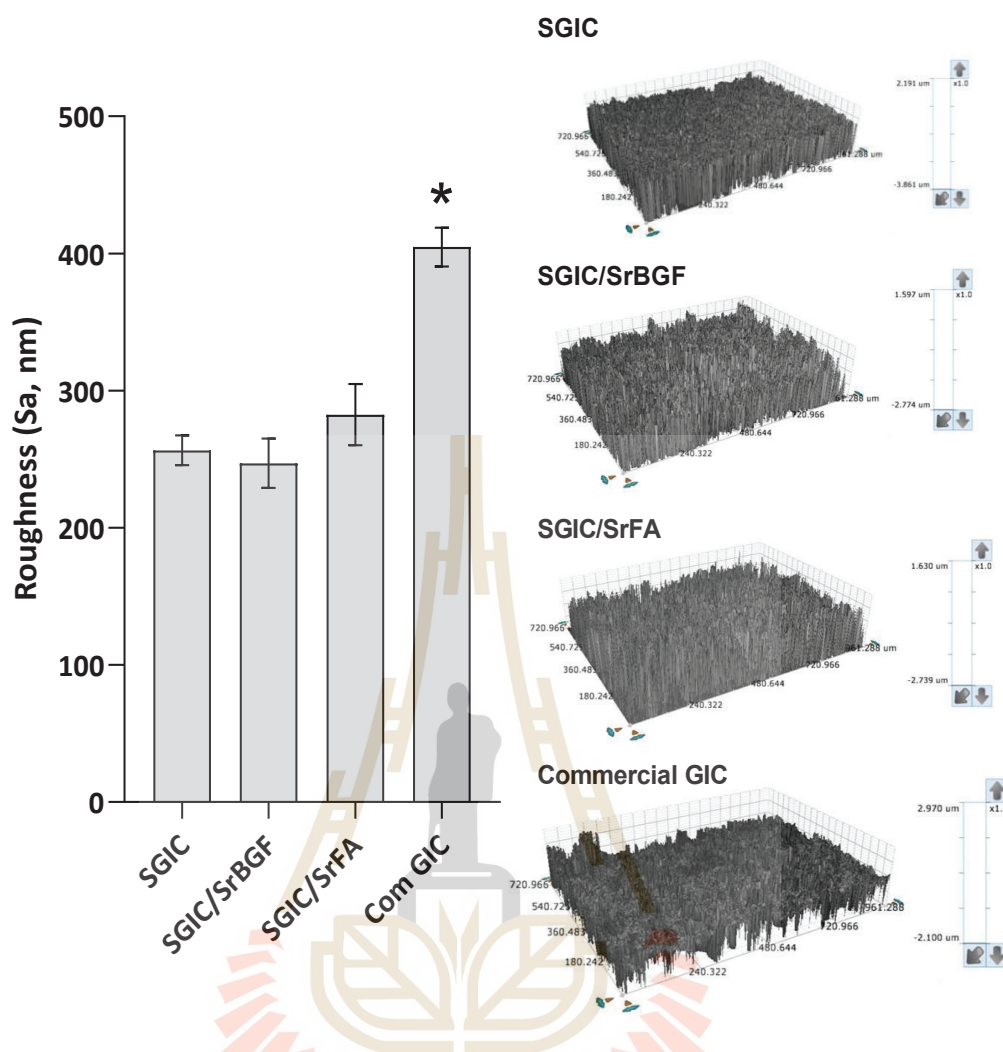


Figure 7.8 Comparison of average surface roughness value of SGIC, SGIC/SrBGF, SGIC/SrFA and commercial GIC. Sa is the arithmetic average of the 3D roughness. Error bars are standard error of the mean (n=8). Stars (\*) denote  $p < 0.05$ .

### 7.3.4 Antibacterial properties

To investigate the antibacterial activity of the SGIC samples, the agar diffusion method and bacterial adherence on the material surface were examined. Figure 7.9 a) illustrates the zone of inhibition produced by the SGIC, SGIC/SrBGF, and SGIC/SrFA against *S. mutans*. The inhibition zones were evaluated by measuring the distance between the specimens and the *S. mutans* colony. The results showed that the inhibition zone of the SGIC and SGIC/SrBGF was similar, while the SGIC/SrFA presented the highest inhibition zone of 7.44 mm. The commercial GIC exhibited the

lowest inhibition radius of less than 1 mm. The findings of the study indicated that the addition of SrBGF to SGIC had no impact on its antibacterial properties. Additionally, the commercial GIC demonstrated no activity against *S. mutans*. The explanation of the inhibition zone of SGIC and the increased inhibition zone following the addition of SrFA to SGIC was previously discussed in Chapter 6, specifically in section 6.3.3.

Figure 7.9 (b) illustrates the SEM micrographs of the specimen surfaces after immersion in the *S. mutans* suspension for 12 hours. The commercial GIC showed heavy bacterial coverage, while the SGIC and SGIC/SrBGF presented less bacterial coverage. For SGIC/SrFA, the bacteria were barely visible on the surface.

The number of bacteria on the specimen surface indicated their ability to adhere to the material. Bacterial adhesion was the first stage in the formation of biofilms and the primary cause of tooth cavities and periodontal disease (Kozmos et al., 2021). The process of bacterial attachment to material surfaces was influenced by several physico-chemical properties. One of the primary focuses on dental biofilm research was surface roughness and topography. This is because bacteria have a tendency to adhere to rough surfaces due to the larger contact area between the material surface and the bacterial cells (Song, Koo and Ren, 2015). In this study, the number of bacterial attachments on the material surface was related to the surface roughness of the material. The results showed that the commercial GIC, which showed the highest surface roughness, had the highest number of bacteria on its surface.

To interfere with bacterial adhesion, the incorporation of antibacterial agents into dental materials is a common strategy (Wang, Shen and Haapasalo, 2014). In this study, SrBGF and SrFA were added to SGIC to improve its antibacterial properties. The results revealed that SrFA was able to effectively inhibit bacterial adhesion on the SGIC surface, indicating an improvement in its antibacterial property. Conversely, the addition of SrBGF to SGIC did not result in any enhancement in its ability to interfere with bacterial adhesion, suggesting that SrBGF had no effect on SGIC's antibacterial property.

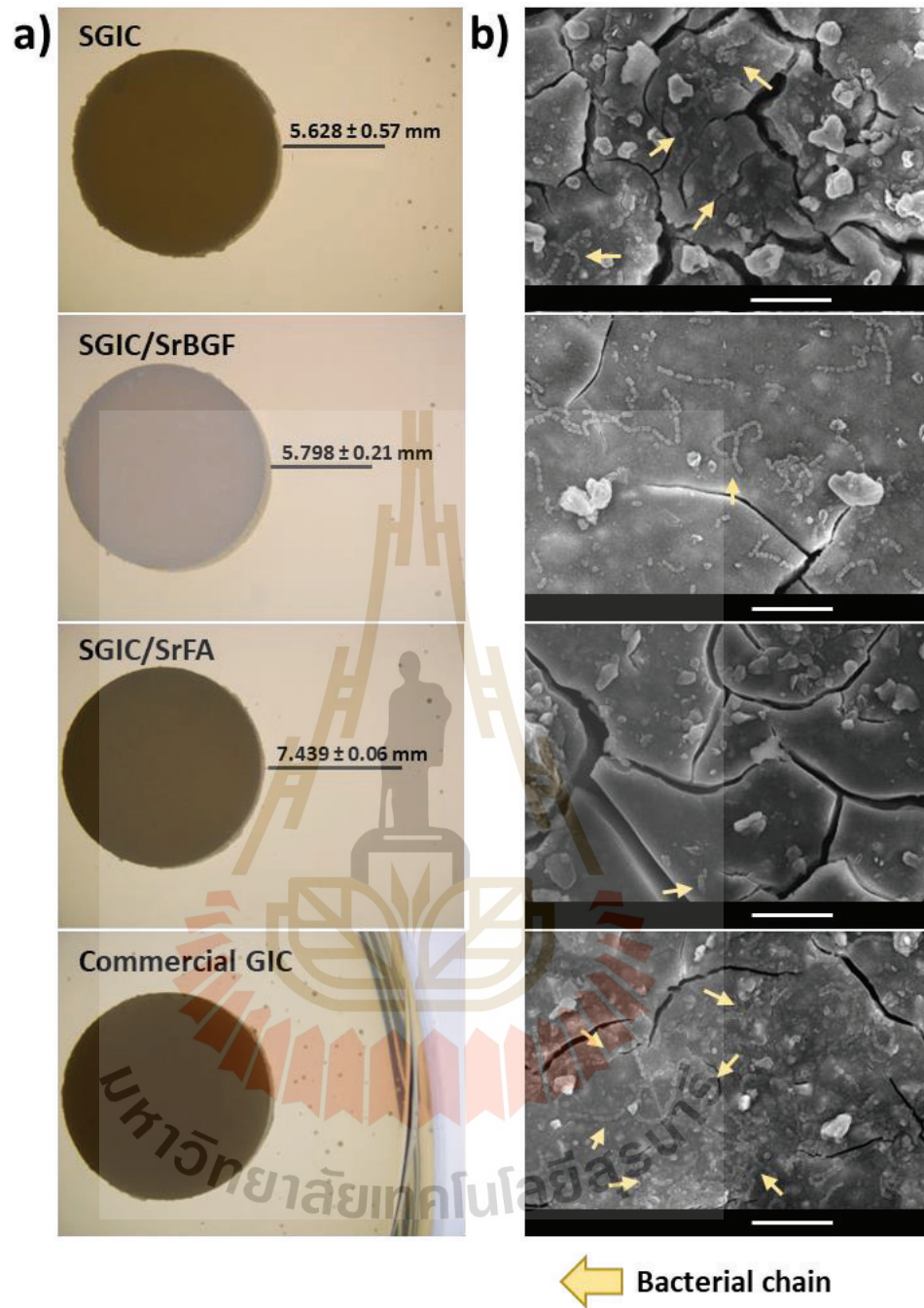


Figure 7.9 The antibacterial activity of the SGIC, SGIC/SrBGF and SGIC/SrFA against *S. mutans*. (a) The stereo microscope images of *S. mutans* inhibition area around the specimens. The average and standard deviation of inhibition zone was calculated from 3 individual samples. (b) The bacterial adhesion to the specimen's surface. Arrows indicated the chain of *S. mutans*.

### 7.3.5 Bioactivity

The bioactivity of the material was evaluated in this study by examining the remineralization process of the dental surface when treated with SGIC specimens in a simulated oral environment. To simulate the natural caries process in the oral cavity, tooth specimens were first demineralized in an acidic solution for 8 days and then subjected to a pH cycle process, imitating the conditions during the natural caries process. The methods used for the pH cycle process were described in a previous publication (Dai, Mei, Chu et al., 2021). The tooth specimens were then analyzed for their density before and after remineralization, using  $\mu$ CT visualization as shown in Figure 7.10. Interestingly, there was no significant difference in density before and after remineralization for the blank and the commercial GIC specimens. In contrast, the SGIC specimens, particularly the SGIC/SrBGF specimen, showed a significant increase in density after the remineralization process.

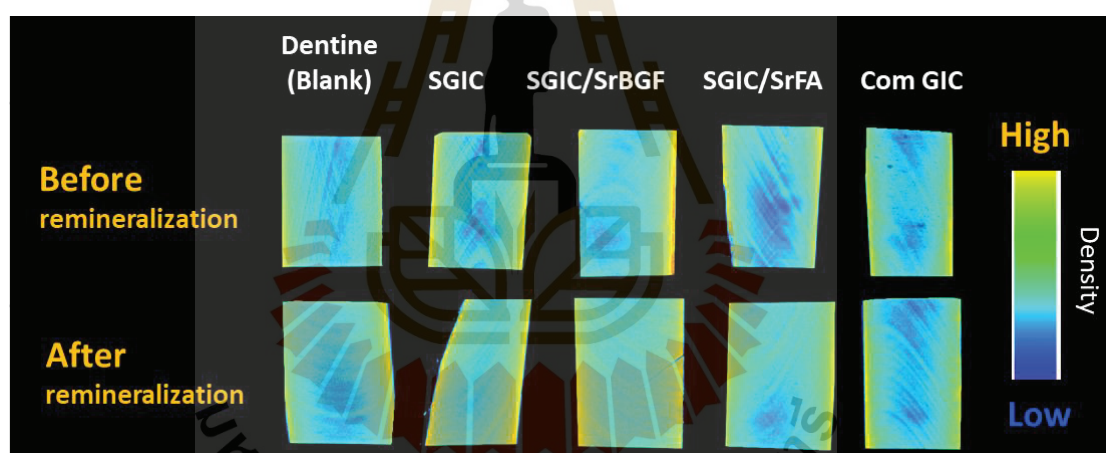


Figure 7.10  $\mu$ CT visualization of the dentine before and after remineralization. Colors were assigned based on density levels, with darker colors indicating lower density levels and lighter colors reflecting higher density levels.

Various indicators, such as protein/mineral composition, mineral density, and microhardness, could be used to measure dental mineralization (Dai et al., 2021). In this study, mineral density was observed using  $\mu$ CT visualization in demineralized dentine treated with SGIC, SGIC/SrBGF, SGIC/SrFA, and commercial GIC after remineralization. The observed increase in mineral density was attributed to the regeneration of hydroxyapatite crystals, which was consistent with previous research

findings (Kantrong, Khongkaphet, Sitornsud et al., 2022). It was noted that dentin cannot undergo natural remineralization in the oral environment (Cao, Mei, Li et al., 2015). The process of remineralization occurs when supersaturated ions in the fluid, such as  $\text{Ca}^{2+}$  and  $\text{PO}_4^{3-}$ , precipitate onto the dentin, forming hydroxyapatite crystals. The remineralization process induced by SGIC in this study was possibly due to the incorporation of soluble  $\text{Ca}^{2+}$ ,  $\text{PO}_4^{3-}$ , and other ions from GIC samples. This finding was further confirmed by SEM-EDS observations on the dentine surface, as shown in Figure 7.11.

The effectiveness of remineralization was assessed by examining the dentine surface before and after treatment using SEM-EDS technique, presented in Figure 7.11 (a). Before remineralization, all specimens exhibited open dentinal tubules on the surface. However, treatment with SGIC, SGIC/SrBGF, SGIC/SrFA, and commercial GIC resulted in the occlusion of dentinal tubules. In contrast, the blank specimen showed persistently open dentinal tubules even after remineralization. Furthermore, the atomic percentages of Ca and P on the dentine surfaces were analyzed before and after remineralization, as depicted in Figure 7.11 (b). The results showed a significant increase in Ca and P contents on the dentine surface after remineralization for SGIC, SGIC/SrBGF, SGIC/SrFA, and commercial GIC. These findings provided evidence for the effective remineralization ability of GIC samples.

The observation of Ca and P deposition on the dentine surface in this study served as evidence of the bioactivity of the material, as bioactivity was defined as the capacity of a material to create a chemical bond with the adjacent tissues. This process was suggested to be involved with the formation of apatite crystals in an environment with an appropriate Ca/P ratio near 1.67. Once formed and enlarged, these crystals can sediment and penetrate the demineralized tooth surface, serving as a template to attract  $\text{Ca}^{2+}$  and  $\text{PO}_4^{3-}$  ions from the remineralizing solution towards the tooth surface. The resulting crystals have the potential to fill up any defects and micropores in the tooth, effectively occluding the dentinal tubules, as illustrated in Figure 7.11 (b).

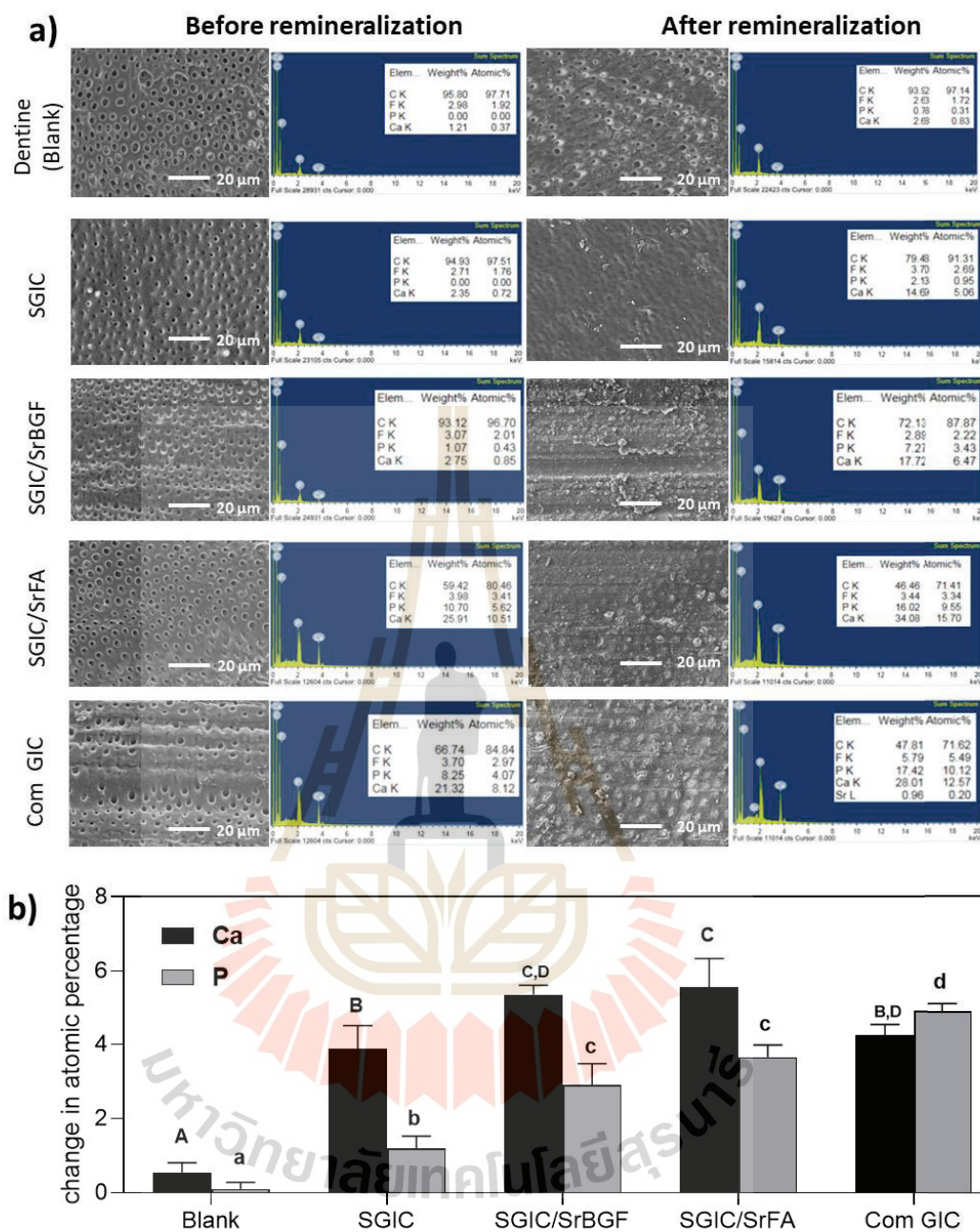


Figure 7.11 a) SEM images and EDS data of mineral deposition on dentin surface during remineralization process. b) the change of atomic percentage of Ca and P deposited on the dentin surface after remineralization. Error bars are standard error of the mean ( $n=3$ ). Same letters indicate no significance between groups ( $p < 0.05$ ), capital letters representing Ca atomic percentage and non-capital letters representing P atomic percentage.

The presence of ZnO in the SGIC composition appears to have potential benefits for promoting the remineralization of demineralized tooth surfaces through the formation of apatite crystals. Previous studies had demonstrated that zinc could enhance calcium deposition and facilitate the occlusion of dentinal tubules through crystal precipitation (Osorio et al., 2014). Furthermore, several studies had found that the incorporation of zinc ions in biomaterials could promote the growth of apatite crystals (LeGeros, Bleiwas, Retino et al., 1999, Du, Chang, Ni et al., 2006, Osorio et al., 2014, Sergi, Bellucci, Salvatori et al., 2019, Thongsri, Srisuwan, Thaitalay et al., 2022). It was important to note that the exact mechanism behind the effect of ZnO on apatite crystal formation had not yet been fully understood and requires further investigation. However, it was thought that the presence of Zn<sup>2+</sup> ions played a role in creating a favorable environment for apatite crystal growth on the tooth surface. Therefore, the presence of Zn ions in the SGIC composition facilitated the growth of apatite crystals on the demineralized tooth surface even further.

In addition to the potential benefits of ZnO in promoting the formation of apatite crystals on demineralized tooth surfaces, the incorporation of SrBGF and SrFA into SGIC has also been found to have a positive effect. Specifically, the addition of these two additives was found to promote the deposition of Ca and P on the sample surface (Figure 7.11 (b)), which could play a critical role in apatite homeostasis and maintenance (Osorio et al., 2014, Albeshti, 2016). According to research conducted by Eden and O'Donnell et al., their findings suggested that an increase in the amount of phosphate presented in the glass led to a proportional increase in the speed and quantity of apatite formation (O'Donnell, Watts, Hill et al., 2009, Edén, 2011). Additionally, despite having different chemical structures and shapes, the incorporation of both SrBGF and SrFA into SGIC provided similar abilities to absorb P ions and promote Ca and P ion deposition.

The ion release and absorption behavior of commercial GIC in Figure 7.12 (a) revealed significant adsorption of Ca and P ions while releasing a high amount of Sr ions. This result was related to the mineral deposition on the demineralized dentin surface, as illustrated in Figure 7.11. The absorption of Ca and P ions in commercial GIC had been reported to induce the formation of the apatite layer on the surface of the material (Yli-Urpo, Vallittu, Närhi et al., 2004). Moreover, the

release of Sr ions also played an important role in inducing apatite crystal precipitation (Albeshti, 2016). However, it could be seen in Figure 7.10 that the dentin applied with the commercial GIC presented no change in dentin density. It was possible that the commercial GIC could induce apatite precipitation only on the dentin surface and be unable to increase dentin density.

### 7.3.6 *In vitro* cytocompatibility

This study was performed to assess the potential of a dental material to induce cytotoxicity in the surrounding tissue, as it is well known that dental materials used in the healing process might have unexpected effects on the local tissue (Aghazade et al., 2020). Due to the fact that the materials or their by-products may come into contact with the tissues through the dentinal tubules and apex, it was critical to evaluate their cytotoxicity and biocompatibility (Chen et al., 2016, Aghazade et al., 2020). hASCs were selected for this investigation as a well-established and widely available source of normal stem cells with the ability to differentiate into various cell types, including dental mesenchymal cells. Furthermore, given the high proliferative and differentiation potential of hASCs, they were deemed an excellent model for *in vitro* assessment of material biocompatibility (Abud, Zych, Reus et al., 2015, Gaur and Agnihotri, 2021). This section provided results and discussions of the effect of the material on the cell culture environment (ions release and pH) and hASCs viability.

#### 7.3.6.1 Ion releasing/adsorption and pH measurement.

To evaluate the influence of ions released from the specimens on cell response, ion concentrations and pH changes of the cell culture media were analyzed. The ion concentrations in the extracts were determined by Figure 7.12 (a). Al, Ca, P, Sr, and Zn ions were detected in the cell culture media after soaking the specimens on Day 1 and 7. The levels of Al ions released from all GIC samples were similar, with the commercial GIC having the highest level (0.024-0.035 mM). The commercial sample absorbed Ca ions from the cell culture media (0.44-0.48 mM), while the SGIC, SGIC/SrBGF, and SGIC/SrFA samples released them (0.01-0.42 mM). P ions concentration in all the cements was in the negative range, indicating that they

absorbed P ions. The commercial GIC, SGIC/SrBGF, and SGIC/SrFA absorbed P ions at the highest concentration on Day 1 (0.164-0.195 mM) and reduced on Day 7 (0.01-0.016 mM). SGIC, SGIC/SrBGF, and SGIC/SrFA released the highest Zn ions on day 1 (0.72-0.96 mM) and decreased after 7 days of soaking (0.36-0.53 mM). The commercial GIC did not release Zn ions due to the absence of ZnO in its composition. The commercial GIC released a large quantity of Sr ions (0.84–1.19 mM) since SrO was its main composition. The Sr ions were also found to be released from SGIC/SrBGF and SGIC/SrFA (0.05-0.11 mM), indicating that SrBGF and SrFA additives could release Sr ions to the surrounding environment.

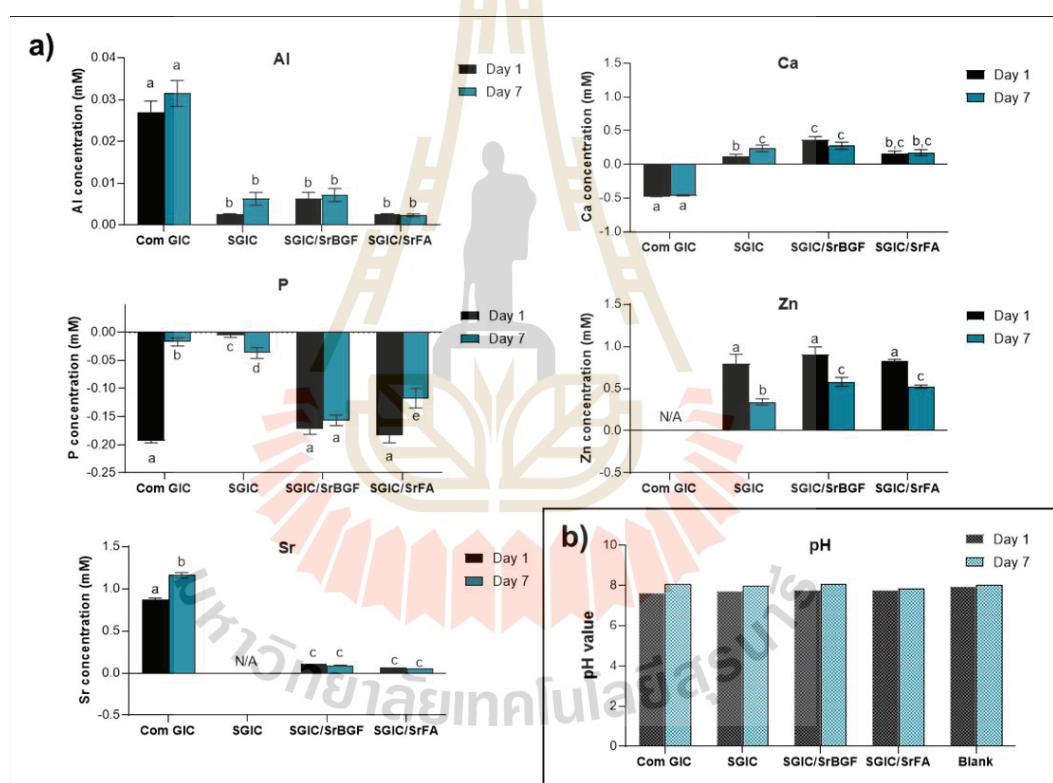


Figure 7.12 (a) ion concentration change after soaking SGIC specimens in cell culture medium at Day 1 and Day 7. All ions of each condition were subtracted by the control cell culture medium (blank), showing that the negative value are the ions absorbed by samples and the positive value are the ions released by samples, (b) pH value of cell culture medium after soaking SGIC specimens at Day 1 and Day 7. Error bars are standard error of the mean (n=3). Same letters indicate no significance between groups ( $p < 0.05$ ).

In Figure 7.12 (b), the pH values of the cell culture media were analyzed. There was no significant difference in pH among the samples at different time points. Additionally, the pH of all the extracted media was in the range of 7-8, which was beneficial for cell viability. This result suggests that the materials had no effect on pH changes and could not be identified as a cause of cytotoxicity.

### 7.3.6.2 hASCs cell culture

To investigate the effect of the environment on the cytocompatibility and cell proliferation of hASCs when cultured on different glass ionomer cement (GIC) samples, an indirect cell culture method was employed. The metabolic activity and DNA concentration of hASCs were assessed, as shown in Figure 7.13 (a) and (b). The metabolic activity at day 1 and day 7 in Figure 7.13 (a) showed that the SGIC, SGIC/SrBGF, and SGIC/SrFA were as high as the glass cover slip control, but the commercial GIC was significantly lower. The result of the DNA concentration in Figure 7.13 (b) supported the metabolic activity result. There was no significant difference in DNA concentration between day 1 and day 7. The commercial GIC was found to have the lowest DNA content, while the DNA contents of SGIC, SGIC/SrBGF, and SGIC/SrFA were as high as the glass cover slip.

To further evaluate the effect of GIC samples on hASCs, the cells were cultured directly on the cement surface, and metabolic activity and DNA concentration were measured using Figure 7.13 (c) and (d). Results showed no significant difference in metabolic activity among samples on day 1 of culture. After being cultured for 7 days, the metabolic activity of hASCs on all GIC surfaces was significantly increased, except for the commercial GIC. For the DNA concentration, all GIC samples presented no significant difference between days 1 and 7. The commercial GIC was found to have the lowest DNA content, while the DNA content was significantly higher for the cover slip control after incubation for 7 days.

The live/dead staining in Figure 7.13 (e) presented viable and dead cells on the cement surfaces. This result supported the trend of the metabolic activity and DNA quantitative data of the direct culture result in Figure 7.13 (c) and (d). The commercial GIC exhibited red fluorescence after being cultured for 7 days,

indicating the presence of mainly dead cells on the surface. Meanwhile, the more viable and well spread cells (green fluorescence) were found on the SGIC, SGIC/SrBGF, and SGIC/SrFA.

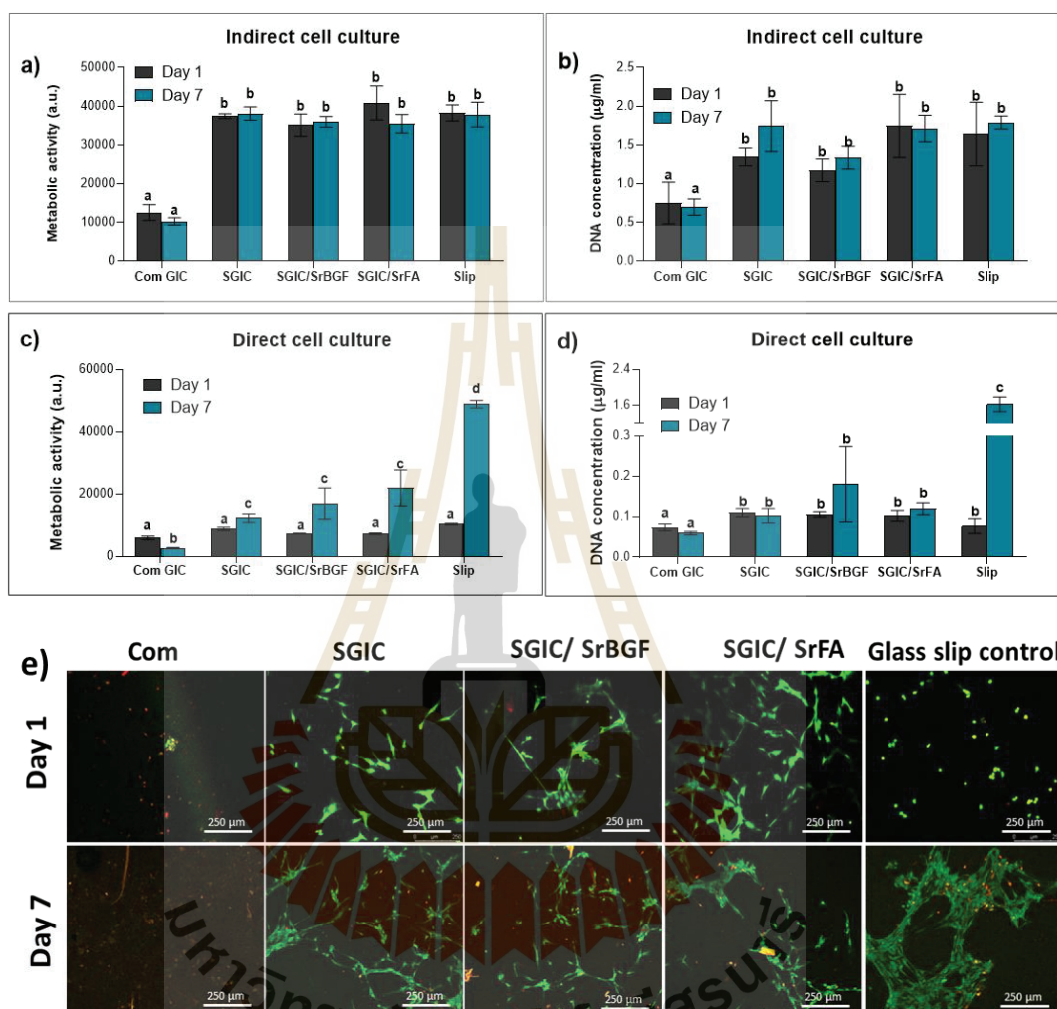


Figure 7.13 hASC proliferation: (a) metabolic activity of cell on tissue plastic plate cultured with sample-conditioned medium (b) DNA concentration of the cell on tissue plastic plate cultured with sample-conditioned medium. (c) metabolic activity of the cell cultured directly on GIC surface (d) DNA concentration of the cell on GIC surface. Error bars are standard error of the mean (n=3). Same letters indicate no significance between groups ( $p < 0.05$ ). (e) live/dead assay of hASC on each GIC samples, magnification of x10. Red and green stains represent dead and living cells, respectively.

Based on the results of both direct and indirect cell cultures shown in Figure 7.13, it can be suggested that hASCs cells preferred the environments of SGIC, SGIC/SrBGF, and SGIC/SrFA over that of the commercial GIC. The cytotoxicity observed in commercial GIC was attributed to its ion-releasing and ion-absorbing properties, as evidenced by Figure 7.12. Commercial GIC released a substantial quantity of Al ions and Sr ions while adsorbing Ca and P ions. Previous research had indicated that at an ion concentration of 1 mM, cell viability decreased by up to 90%, and this reduction might be even more significant when the Al ion concentration was increased (Yu, Wu, Zhai et al., 2019). However, our study showed that the maximum Al ion concentration in the commercial extracts was around 0.035 mM, which was too low to cause a toxic effect on the cells. Regarding the Sr ions concentration, although the commercial GIC released the highest amount of Sr ions (0.8–1.2 mM), Sr ions concentrations below 77 mM had been reported to be non-toxic (Chen et al., 2016), suggesting that the cytotoxicity of the commercial GIC extract was unlikely due to the Sr ions. Prior studies had also linked the massive uptake of  $\text{Ca}^{2+}$  and  $\text{HPO}_4^{2-}$  ions from the extract to cytotoxicity (Klimek, Belcarz, Pazik et al., 2016, Thaitalay et al., 2022). However, the uptake of  $\text{Ca}^{2+}$  and  $\text{HPO}_4^{2-}$  ions by porous ceramic was found to be highly bioactive (i.e., the ability to form apatite) rather than cytotoxic. Therefore, the low cell viability observed with commercial GIC could be due to its ability to uptake ions from the culture medium, which resulted in insufficient ions for cell growth (Klimek et al., 2016). Our results were consistent with these findings, as hASCs exhibited low viability when cultured with commercial GIC due to its high concentration of Ca and P ions.

A considerable amount of Zn ions released from the SGIC sample appears to have a crucial impact on cell viability and proliferation. Previous research suggested that a concentration of Zn ions lower than 0.35 mM benefited cell viability (Brauer et al., 2011, Wang, Li, Xia et al., 2021). However, on both day 1 and day 7 of the soaking period, the Zn ions released from SGIC, SGIC/SrBGF, and SGIC/SrFA exceeded the 0.35 mM threshold. Although no cytotoxicity was observed, this high concentration of Zn ions could inhibit cell proliferation, as demonstrated by the direct culture results in Figure 7.13 (c) and (d). On the other hand, it seemed that dilution of Zn concentration was beneficial to the cell, and in clinical use with body

fluid circulation, the Zn concentration could be reduced (Wang, Li et al. 2021; Thongsri, Srisuwan et al. 2022). Further investigation into this matter is necessary for the *in vivo* study.

### 7.3.6.3 hDPSC cell culture

The preliminary study for the hDPSC cytotoxicity was investigated by MTT assay, as shown in Figure 7.14. The results presented that all GIC samples have no cytotoxicity for the hDPSC. Even though commercial GIC has an adverse effect on the viability of hASC, this study found the opposite effect with hDPSC. This could be because different cell types respond differently to the material (Kanjevac, Milovanovic, Volarevic et al., 2012). However, SGIC samples presented no cytotoxic effect on both hASCs and hDPSCs, indicating that SGIC was a promising material for use in human tissues.

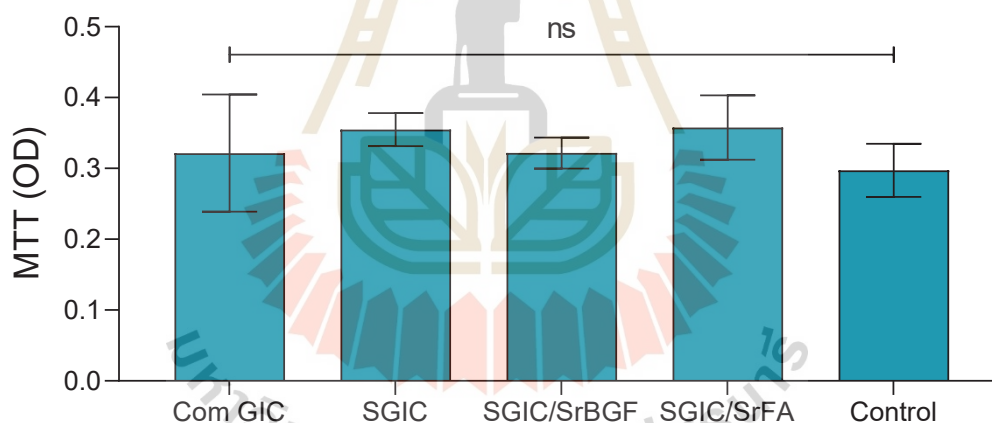


Figure 7.14 Cell viability of hDPSCs treated with the extract solution for 24 hours. Control is referred to the cells-cultured on the tissue culture well with the fresh medium. Values were expressed as the mean  $\pm$  standard error (n=3) ( $P < 0.05$ ).

### 7.3.7 Fluoride release and uptake ability

This section presents an evaluation of the fluoride release and uptake abilities of SGIC and SGIC modified with SrBGF in comparison to commercial GIC. SrFA

was not included in the comparative evaluation due to its lack of fluoride-releasing ability.

### 7.3.7.1 Concentration of fluoride release in immersed solution

Figure 7.15 illustrates the mean concentration of  $F^-$  ions released in artificial saliva from each specimen during their release and uptake in NaF solution. The results indicated that, initially, the commercial GIC (com) released a higher amount of fluoride compared to SGIC/1SrBGF and SGIC. However, following fluoride uptake, the fluoride released from commercial GIC (com) was lower than that of SGIC and SGIC/1SrBGF. This suggests that the fluoride uptake activity of SGIC was superior to that of the commercial GIC. Furthermore, the study revealed that the addition of SrBGF to SGIC significantly improved its ability to release and uptake  $F^-$  ions.

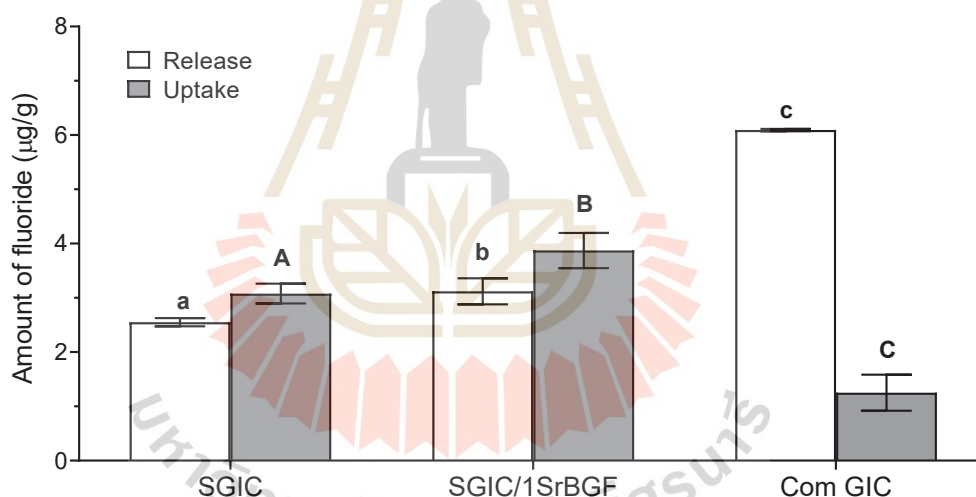


Figure 7.15 Amount of fluoride released from SGIC, SGIC/1SrBGF, and the commercial GIC in artificial saliva after soaking for 1 week during releasing and after uptake in NaF solution. Note that the P:L ratio of commercial product (com) is 3.4:1. Error bars are standard error of the mean (n=8). Same letters indicate no significance between groups ( $p < 0.05$ ) Capital letters representing amount of fluoride release and non-capital letters representing amount of fluoride uptake.

### 7.3.7.2 Concentration of fluoride release on GICs surface

In order to gain insight into the fluoride uptake mechanism, the glass and cement matrix sites in GIC samples were characterized during the release/uptake cycle using SEM-EDS techniques, as illustrated in Figure 7.16. The surfaces of SGIC, SGIC/1SrBGF, and commercial GIC were analyzed using SEM images and EDS after polishing and etching. Overall, our results showed that the ionomer glass remained distributed within the cement matrix on the surfaces of GICs.

The composition of the glass and matrix areas were evaluated using EDS technique. The glass area was predominantly composed of F, Al, and Si, followed by Ca/Sr and P. Notably, the Ca content in the commercial GIC composition was replaced by Sr.

EDS analysis of the glass area in the commercial GIC exhibited a higher content of F than that of the SGIC samples, indicating a higher fluoride content in the commercial product's glass composition. In the matrix area, EDS analysis showed a high level of metal cations (Al, Ca, and Sr) and fluoride anions. These ions were released from the outer layers of the glass particles during the setting reaction and produced metal polyacrylate in the cement matrix.

The fluoride content on the sample surfaces during release/uptake testing was determined using the SEM-EDS technique, as presented in Figure 7.16 (b). Before fluoride release, there was a slight variation in the fluoride content between the glass and matrix areas of SGIC. However, higher fluoride content was found in the matrix area than in the glass area for both SGIC/1SrBGF and the commercial GIC. This higher fluoride content in the matrix area of SGIC/1SrBGF might be attributed to the ability of SrBGF to release fluoride ions, as shown in Figure 7.14 (a). During the setting reaction of SGIC, fluoride ions could have been released from SrBGF and trapped in the polymeric matrix of SGIC, thereby promoting fluoride concentration in the cement matrix. Similarly, in the case of the commercial GIC, the high fluoride content in the matrix area resulted from the high fluoride content of the commercial ionomer glass, which could release fluoride ions into the matrix during the setting reaction, as was the case with SGIC/1SrBGF.

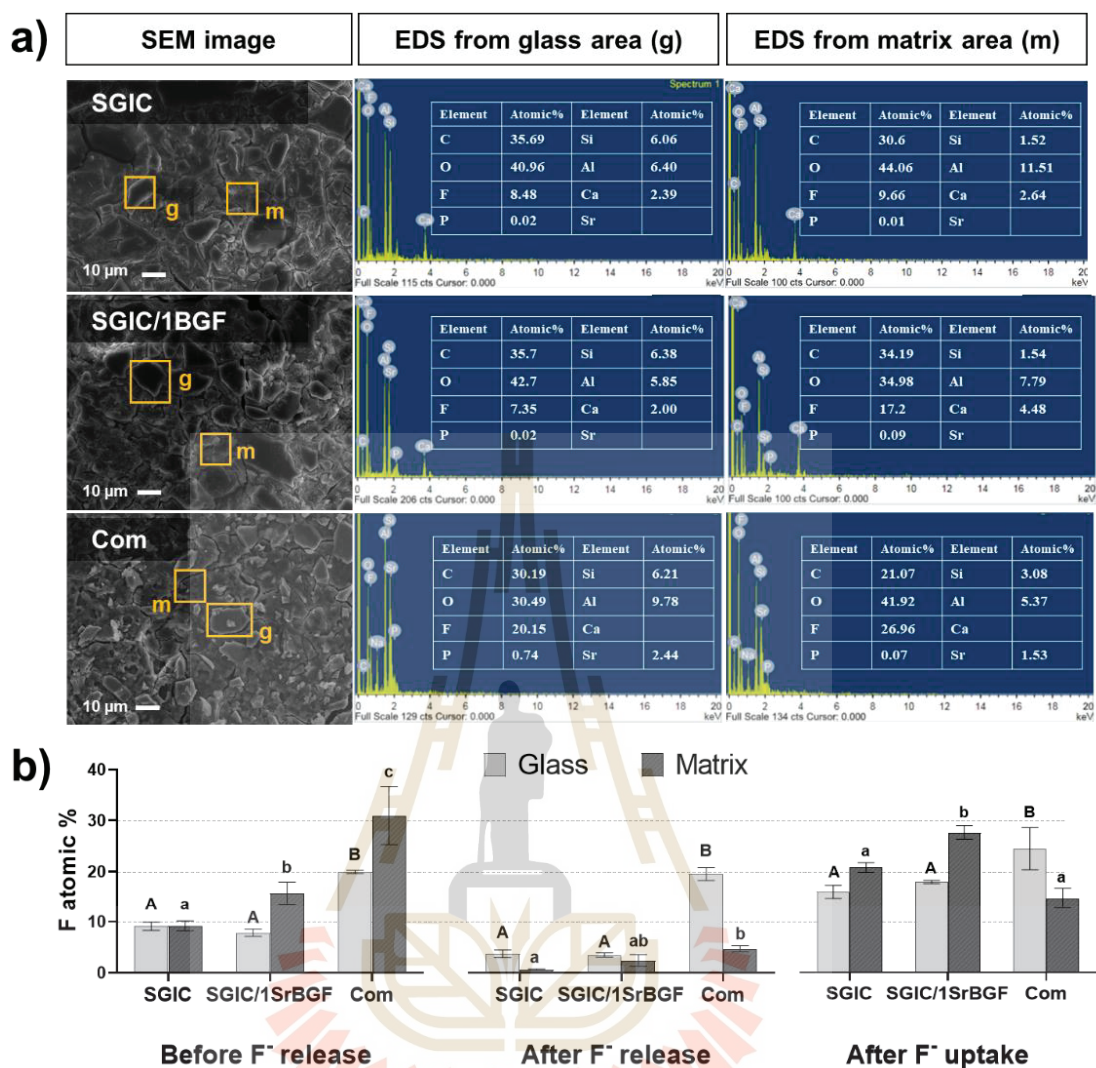


Figure 7.16 Surface analysis of SGIC, SGIC/1SrBGF, and the commercial GIC (com), (a) SEM image and EDS analysis of glass and matrix area on the glass ionomer cement surface before fluoride-releasing and (b) Atomic % of fluoride on GIC surfaces during fluoride uptake cycle: before release, after release and after uptake. The values shown in the graph are the mean  $\pm$  standard error derived from at least 3 different analysis areas.

After fluoride release, all GIC specimens demonstrated a reduction in fluoride content in both the glass and matrix areas, with a greater decrease observed in the matrix area. This indicated a high potential for fluoride release in SGIC and SGIC/1SrBGF specimens. In contrast, the commercial GIC released fluoride

only from the matrix area, and fluoride ions in the glass areas remained at the same level as before the release. However, based on the previous findings presented in Figure 7.15, it was observed that the commercial GIC released fluoride at significantly higher levels compared to the SGIC group. This difference in fluoride release could be attributed to the higher initial fluoride content in the commercial GIC, which was approximately 30%, while the SGIC group had a lower initial fluoride content of approximately 8%.

After fluoride uptake, there was a significant increase in the fluoride content in both the glass and matrix areas of SGIC and SGIC/1SrBGF. Meanwhile, the fluoride content increased significantly only in the matrix area of the commercial GIC. This indicates the ability of these materials to take up fluoride ions. The results suggest that the SGIC group has a greater potential to uptake fluoride ions in comparison to the commercial GIC, thus demonstrating an enhanced fluoride uptake in SGIC.

#### **7.3.7.3 XPS analysis for structural change during fluoride release and uptake**

In this study, XPS technique was used to gain insights into the mechanism of fluoride release and uptake ability of the SGIC, SGIC/1SrBGF, and the commercial GIC. The F1s chemical state was evaluated before fluoride release and after uptake of GICs. However, it was important to note that the XPS technique had lower sensitivity and was unable to detect the amount of fluoride after release, which was not revealed in the result. Additionally, the technique used in this study was unable to differentiate between the glass and matrix areas, and thus the chemical state of fluoride presented in this result was characterized by the entire GIC surfaces.

Figure 7.17 shows that the high-resolution spectra in the F1s region for GICs can be deconvoluted into four main peaks at the binding energies of around 688 eV, 686.7 eV, 684.8 eV, and 684 eV, indicating to Si-F, Al-F, Ca-F or Sr-F and free F<sup>-</sup> ion, respectively (Maeda, Matsuya and Ohta, 1998, Makarowicz, Bailey, Weiher et al., 2009). It was noted that Ca-F and Sr-F had been found to have the same binding energies.

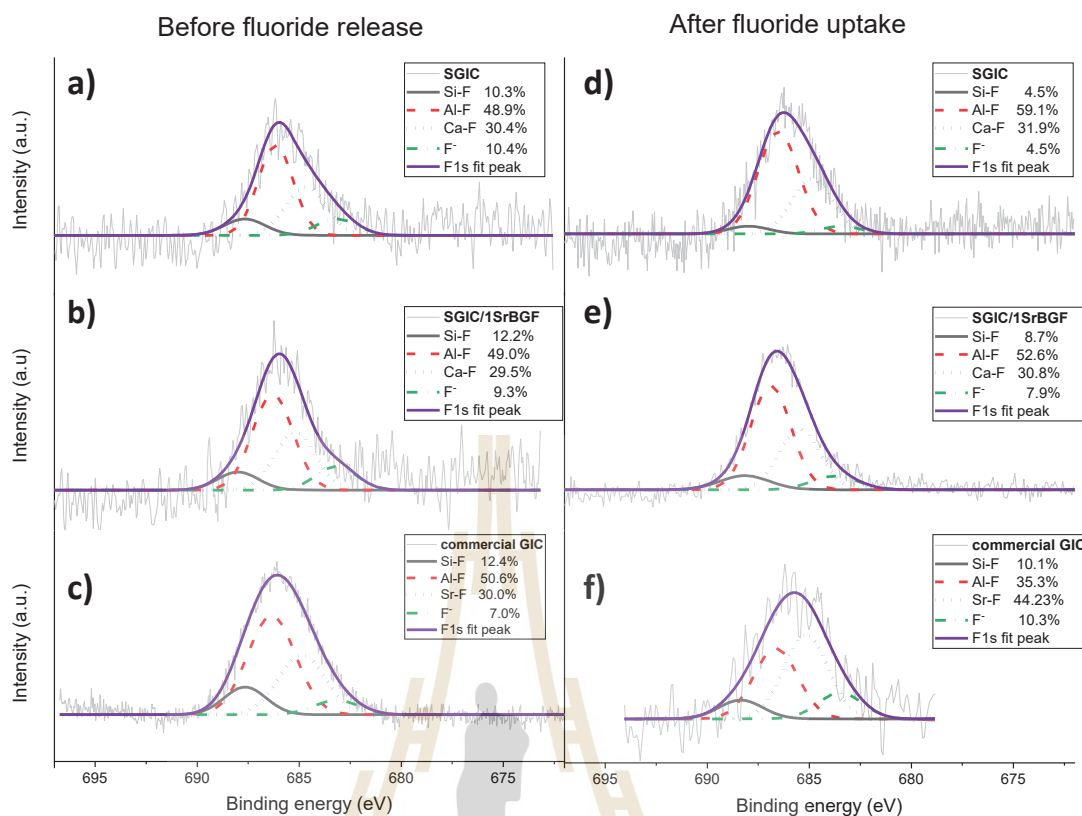


Figure 7.17 High-resolution XPS spectra of fluoride (F1s) for (a) SGIC (b) SGIC/1SrBGF and (c) the commercial GIC before fluoride releasing and (d) SGIC (e) SGIC/1SrBGF and (f) the commercial GIC after fluoride uptake. The percentages represent the concentration of each binding state based on the graphed area.

In Figure 7.17 (a), (b) and (c), the deconvoluted XPS peaks of the SGIC, SGIC/SrBGF, and commercial GIC samples before fluoride release were presented. The spectra revealed the existence of Al-F, Ca-F/Sr-F, Si-F, and the free ion of F. It was remarkable that the percentage of Al-F binding state was the highest among all the detected species, followed by Ca-F/Sr-F, Si-F, and F free ions, respectively.

Figure 7.17 (d) and (e) depict the deconvoluted XPS peak of the SGIC groups (SGIC and SGIC/1SrBGF) after fluoride uptake. The results indicated that the percentage of Al-F was higher than that of GIC samples before fluoride release, followed by Ca-F, Si-F, and free ions of F. Interestingly, the SGIC/1SrBGF group

displayed a higher fraction of free fluoride ions compared to the SGIC group. In contrast, the commercial GIC yielded different findings, where the percentage of Sr-F was the highest, followed by Al-F, Si-F, and free ions of F. The results indicated that the percentage of Al-F was higher than that of GIC samples before fluoride release, followed by Ca-F, Si-F, and free ions of F. Interestingly, the SGIC/1SrBGF group displayed a higher fraction of free fluoride ions compared to the SGIC group. In contrast, the commercial GIC yielded different findings, where the percentage of Sr-F was the highest, followed by Al-F, Si-F, and free ions of F, as illustrated in Figure 7.17 (f).

Each detected fluoride binding state provided valuable information about the potential for forming a fluoride complex with the cations present in GIC samples. This was important because the solubility of each complex could be different, leading to varying potentials for fluoride release from GIC materials (Itota, Carrick, Rusby et al., 2004). The formation of Si-F structure is typically observed in fluoroaluminosilicate glass, but there was a lack of literature regarding the solubility of Si-F complex in GICs (Stamboulis, Hill and Law, 2005).

The initial release of fluoride ions was reported to be from free fluoride ions trapped within the cement matrix, followed by a continuous release from the glass particles (Suprastiwi et al., 2009). However, the deconvolution of the F1s peak in this experiment indicated only a small amount of free fluoride ion in all GIC samples. Therefore, fluoride may mainly be released from other structures.

Calcium or strontium in glass-ionomer cements had similar potential to interact with fluoride ions as aluminum ions (Bueno, Borges, Navarro et al., 2021). However, fluoride might become insoluble in these cements by forming  $\text{CaF}_2$  or  $\text{SrF}_2$ , both of which are insoluble in water (Madi et al., 2020).

Aluminum is known to bond with fluoride in ionomer glasses. Both aluminum and fluoride were reported to be released from GICs in association with each other (Nicholson and Czarnecka, 2009, Bueno et al., 2021).  $\text{AlF}_2^-$  and  $\text{AlF}_2^-$  complex were proposed as the released species (Nicholson and Czarnecka, 2009). Therefore, the presence of Al-F binding state in this study might indicate the release of such species from GIC samples.

This study revealed that the Al-F structure was presented in all GIC samples before fluoride release, indicating their high potential for fluoride release. In SGIC, fluoride release occurred from both the glass and matrix areas, as shown in Figure 7.16 (b). This could be attributed to the presence of the Al-F structure in both the glass and matrix areas of GIC before fluoride release. It was because the glass network was composed of fluoride bonding with  $\text{Al}^{3+}$  ions and other cations, such as  $\text{Na}^+$  or  $\text{Ca}^{2+}$  (Bueno et al., 2021). During the setting reaction, the  $\text{Al}^{3+}$  ions and  $\text{F}^-$  ions were released from the glass and combined with polymeric acid to form the polysalt matrix. The  $\text{Al}^{3+}$  ion in the polysalt matrix could interact with the  $\text{F}^-$  ion to form an Al-F complex (Nicholson and Czarnecka, 2009), resulting in the release of fluoride from both the glass and matrix areas. However, the previous finding depicted in Figure 7.16 (b) suggested that commercial GICs were unable to release fluoride from the glass area, which could be attributed to the fact that the Al-F structure primarily forms in the matrix area.

After fluoride uptake, a slight reduction in the Si-F peak was observed in all GIC samples. This suggests that fluoride could be released from the Si-F structure but was unable to re-incorporate with the Si after uptake. Additionally, the formation of the Sr-F structure was significantly increased in the commercial GIC after fluoride uptake, which was consistent with previous literature (Madi et al., 2020). The production of species such as  $\text{SrF}_2$  may induce fluoride to become insoluble and unable to be re-release. Furthermore, it was observed that the increased Sr-F structure in the commercial GIC was associated with a low re-releasing ability of fluoride after uptake, as depicted in Figure 7.15. For the SGIC and SGIC/1SrBGF, a high fraction of the Al-F complex was found, indicating their potential for high fluoride re-release after uptake.

According to the fact that Sr-F and Ca-F structures appeared at the same binding energy from the F1s result in Figure 7.17, this study analyzed the high-resolution spectra of the Sr3d region using XPS technique to distinguish the Sr-F structure from Ca-F structure for both SGIC/1SrBGF and the commercial product, as illustrated in Figure 7.18. Additionally, the Sr3d chemical state was assessed in order to investigate the interaction between SrBGF and SGIC, as well as to gain further insights into the fluoride release and uptake reactions of the commercial GIC.

The Sr3d region was deconvoluted using doublets with equal FWHM and a 1.7 eV doublet separation (Opitz, Rameshan, Kubicek et al., 2018). The deconvoluted peak for the SGIC/1SrBGF sample demonstrated the formation of the Sr-F structure at 135.7 and 137.2 eV (Yagoub, Swart, Noto et al., 2015). Interestingly, no significant differences were observed in the Sr-F structure before fluoride release and after fluoride uptake, as shown in Figure 7.18 (a) and (c). However, the addition of SrBGF to SGIC led to improved fluoride release and uptake ability, as depicted in Figure 7.15 and Figure 7.16. This enhancement could be attributed to the high porosity of SrBGF, which could adsorb the fluoride free ions within its porous structure. This was further confirmed by the result of the F1s peak shown in Figure 7.17 (e), which demonstrated that the concentration of free fluoride ions within the SGIC/1SrBGF sample (7.9%) was higher than that of the SGIC without SrBGF (4.5%) after fluoride uptake.

The high-resolution spectra of the commercial GIC revealed a notable finding. Before fluoride release, the deconvoluted peak showed the presence of Sr-O at 132.8 and 134.1 eV, in addition to Sr-F at 135.2 and 137.0 eV (Yagoub et al., 2015, Komai, Hirano and Ohtsu, 2020), as illustrated in Fig. 12 (b) and (d). After fluoride uptake, the Sr-O structure disappeared, yielding to the Sr-F structure. This increase in Sr-F structure in the Sr3d spectra corresponded with the increase observed in the F1s result for the commercial product, as demonstrated in Figure 7.17 (f).

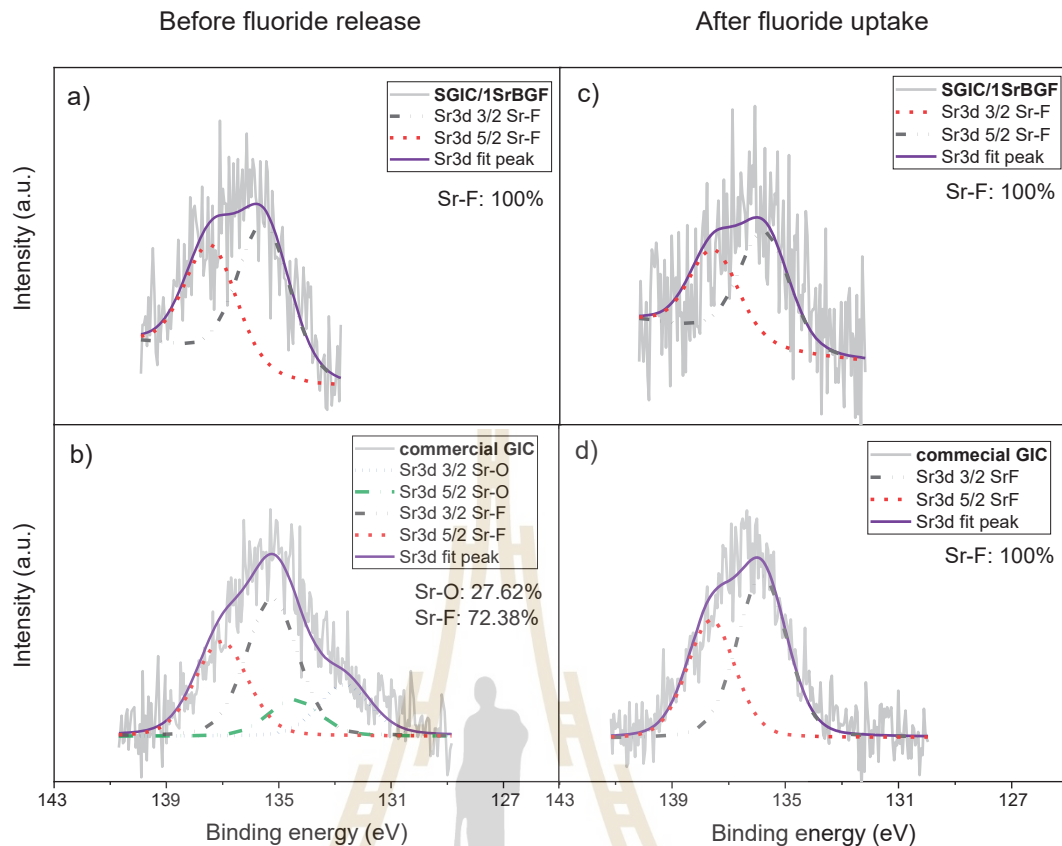


Figure 7.18 High-resolution XPS spectra of fluoride (Sr3d) for (a) SGIC/1SrBGF and (b) the commercial GIC before fluoride releasing and (c) SGIC/1SrBGF and (d) the commercial GIC after fluoride uptake. The percentages represent the concentration of each binding state based on the graphed area.

Here, we propose a model to provide an explanation for the observed results, as illustrated in Figure 7.19. The results indicated that fluoride is mainly released from the Al-F complex, which exists in both the glass and matrix areas of the SGIC. Following fluoride uptake, fluoride can be replaced in the form of Al-F complex in both the glass and matrix areas. By adding SrBGF additive to the SGIC, the fluoride release and uptake abilities were found to be enhanced, likely due to the high porosity of SrBGF additive, which could adsorb fluoride-free ions within its structure. Furthermore, the  $\text{SrF}_2$  crystal in SrBGF was found to be stable and had no effect on the fluoride release and uptake abilities.

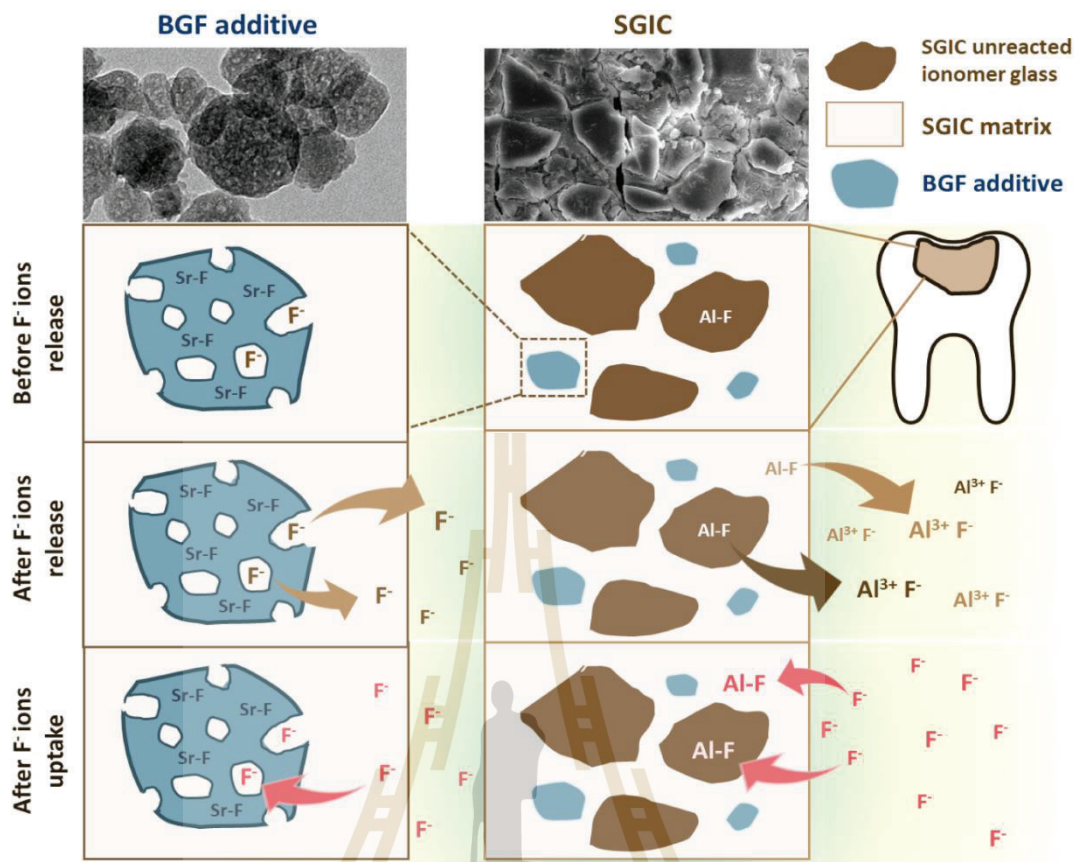


Figure 7.19 The proposed fluoride release and uptake mechanisms of the SGIC and the SGIC containing SrBGF additive.

#### 7.4 Conclusions

The study aimed to evaluate the effects of adding SrBGF additives to SGIC in terms of fluoride release and uptake ability, antibacterial properties, remineralization ability, and cytotoxicity. The study also compared the results with a SIGC added by SrFA and the commercial product. The results showed that the addition of 1 wt.% SrBGF to SGIC did not negatively affect its setting time or compressive strength, making it a promising sample to evaluate further. While both SrFA and SrBGF similarly enhanced the mineralization ability of SGIC, SrFA was found to be more effective in preventing the progression of caries lesions or secondary caries due to its superior antibacterial properties. *In vitro* testing showed that all SGIC samples demonstrated good compatibility with stem cells from human tissue. The difference in glass structure and composition between SGIC and the commercial product resulted in a

difference in fluoride release and uptake ability, with SGIC exhibiting a higher potential for fluoride uptake due to the formation of an Al-F binding state. Additionally, SrBGF enhanced the fluoride release and uptake ability of SGIC by taking up fluoride-free ions in their porous structure. Overall, these findings suggested that the addition of SrFA to dental materials could improve their ability to prevent and treat caries, while the addition of SrBGF could enhance fluoride release and uptake abilities.



## CHAPTER 8

### CONCLUSIONS

This study aimed to produce a glass ionomer powder using the sol-gel method to improve the bioactivity and antibacterial properties of the material, while maintaining its physical properties. The findings in this thesis were concluded as following:

1) The investigation initially started exploring the effect of various synthesis factors on the synthesis of the ionomer glass through the sol-gel method. These factors included the water to precursor ratio, pH, calcination temperature, type of fluoride source, and aging method. This study demonstrated that the different conditions used for sol-gel synthesis played a key role for the obtained glass structure and physical properties of SGICs.

2) The study also examined the variation of  $\text{Al}_2\text{O}_3$  and  $\text{P}_2\text{O}_5$  content in the ionomer glass composition synthesized by the sol-gel method, using a DoE technique. The results demonstrated that an increase in  $\text{Al}_2\text{O}_3$  content in the glass formula could enhance the compressive strength of SGIC, while an increase in  $\text{P}_2\text{O}_5$  content led to prolonging the setting reactivity and reducing the compressive strength of the cement. The glass composed of 4.0 mol  $\text{Al}_2\text{O}_3$  and 0.3 mol  $\text{P}_2\text{O}_5$  ( $\text{Al}/(\text{Si}+\text{P}) = 1.57$ ) produced the GIC with the highest compressive strength in this study. The DoE analysis also verified that the interaction between  $\text{Al}_2\text{O}_3$  and  $\text{P}_2\text{O}_5$  in the glass composition significantly affected the setting time and compressive strength.

3) ZnO dopants were incorporated into the ionomer glass to improve its antibacterial properties. The study found that ZnO had an adverse effect on the setting time and compressive strength of SGIC, but this could be optimized by calcination at a low temperature. SGIC prepared with 0.6ZnO doped ionomer glass calcined at 650 °C showed the most promising results in terms of setting time and compressive strength. Interestingly, the ZnO content in the glass composition exhibited excellent antibacterial activity under light conditions due to its photocatalytic effect,

but it had limited activation under dark conditions. This photocatalytic also had an adverse effect on the cell viability, but this could be enhanced by reducing the amount of ZnO in the glass composition. Additionally, SGIC with ZnO doping exhibited improved bioactivity and tooth adhesion.

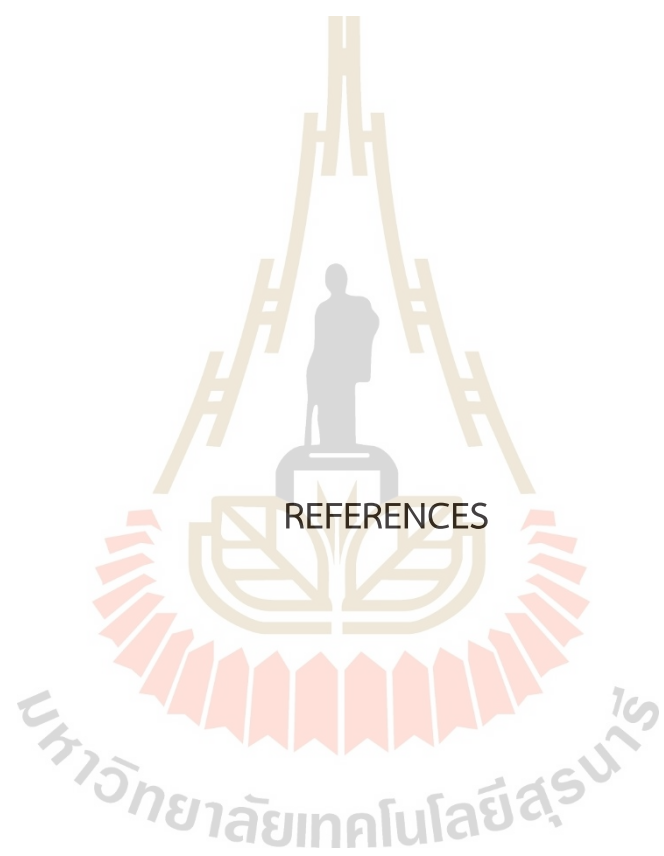
4) To overcome the limitations of ZnO dopants, the study investigated the modification of SGIC with SrFA nanoparticles to improve its antibacterial activity and cytocompatibility. SrFA nanoparticles were successfully synthesized by the hydrothermal method and investigated as an additive in SGIC. The study also investigated the impact of SrFA on the setting time and compressive strength of SGIC, as well as its ability to form an apatite layer, *in vitro* cytocompatibility, and fluoride release and uptake ability. The finding revealed that the addition of SrFA at a concentration of 1 wt.% could increase the compressive strength without significantly affecting the setting time. Additionally, SrFA could effectively improve antibacterial properties, cytocompatibility, and the ability to form an apatite layer.

5) According to SrFA additive had no ability to release fluoride and seemed to inhibit the ability to take up fluoride, the alternative additive as SrBGF was added to SGIC. The effects of SrBGF on antibacterial properties, bioactivity, cytocompatibility, fluoride release, and fluoride uptake ability were investigated and compared with those of SGIC containing SrFA and the commercial GIC. The result of the physical properties showed that 1 wt.% SrBGF added to SGIC significantly increased the compressive strength of the material and had no adverse effect on its setting time. Additionally, SrBGF was found to effectively improve bioactivity, cytocompatibility, fluoride release and uptake ability, but it did not enhance the antibacterial properties.

Overall, this study successfully synthesized a glass ionomer powder through the sol-gel method and investigated various factors that affect its physical properties, bioactivity, and antibacterial properties. The study found that the synthesis condition,  $\text{Al}_2\text{O}_3$  and  $\text{P}_2\text{O}_5$  content, and ZnO doping significantly affected the compressive strength, setting time, antibacterial activity, and cytocompatibility of SGIC. The study also showed that SrFA and SrBGF nanoparticles could effectively improve the compressive strength, bioactivity, and cytocompatibility of SGIC. However, while SrFA demonstrated improved antibacterial properties, it also inhibited fluoride uptake. On

the other hand, SrBGF showed promising results in terms of fluoride release and uptake ability and bioactivity but did not improve the antibacterial properties of SGIC. These findings provided important insights into the design and development of GICs with improved properties, which can potentially be used in various dental and orthopedic applications.





REFERENCES

## REFERENCES

- Abud, A. P. R., J. Zych, T. L. Reus, C. Kuligovski, E. de Moraes, B. Dallagiovanna and A. M. d. Aguiar (2015). The use of human adipose-derived stem cells based cytotoxicity assay for acute toxicity test. **Regul. Toxicol. Pharmacol.** , 73(3), 992-998. doi: 10.1016/j.yrtph.2015.09.015.
- Aghazade, M., M. Samiei, M. Imani, Z. Aghazadeh, E. Alizadeh and F. Rezaie (2020). Evaluation of the adhesion of human dental pulp stem cells to different endodontic biomaterials before and after setting. **J. Dent. Res. Dent. Clin. Dent. Prospects**, 14(2), 97-103. doi: 10.34172/joddd.2020.022.
- Alatawi, R. A. S., N. H. Elsayed and W. S. Mohamed (2018). Influence of hydroxyapatite nanoparticles on the properties of glass ionomer cement. **J. Mater. Res.** doi: 10.1016/j.jmrt.2018.01.010.
- Albeshti, R. (2016). *A Study on Remineralisation of Glass Ionomer Cements by Solid-State Nuclear Magnetic Resonance Spectroscopy*. (PhD) Retrieved from <https://qmro.qmul.ac.uk/xmlui/handle/123456789/80238>.
- Alhalawani, A. M. F., D. J. Curran, D. Boyd and M. R. Towler (2016). The role of poly(acrylic acid) in conventional glass polyalkenoate cements. **Journal of Polymer Engineering**, 36(3), 221-237. doi: 10.1515/polyeng-2015-0079.
- Anastasiou, A. D., M. Nerantzaki, E. Gounari, M. S. Duggal, P. V. Giannoudis, A. Jha and D. Bikiaris (2019). Antibacterial properties and regenerative potential of Sr<sup>2+</sup> and Ce<sup>3+</sup> doped fluorapatites; a potential solution for peri-implantitis. **Sci. Rep.**, 9(1). doi: 10.1038/s41598-019-50916-4.
- Askar, H., J. Krois, G. Göstemeyer, P. Bottenberg, D. Zero, A. Banerjee and F. Schwendicke (2020). Secondary caries: what is it, and how it can be controlled, detected, and managed? **Clin. Oral Investig.**, 24(5), 1869-1876. doi: 10.1007/s00784-020-03268-7.
- Awosanya Kunle, N. J. W. (2014). A study of phosphate ion release from glass-ionomer dental cements. **Ceram. - Silik.**, 58(3), 210 - 214.

- Baig, M. S. and G. J. P. Fleming (2015). Conventional glass-ionomer materials: A review of the developments in glass powder, polyacid liquid and the strategies of reinforcement. **J. Dent.**, 43(8), 897-912. doi: 10.1016/j.jdent.2015.04.004.
- Balhuc, S., R. Campian, A. Labunet, M. Negucioiu, S. Buduru and A. Kui (2021). Dental Applications of Systems Based on Hydroxyapatite Nanoparticles—An Evidence-Based Update. **Crystals**, 11(6), 674.
- Bernasconi, A., M. Dapiaggi, A. Pavese, G. Agostini, M. Bernasconi and D. T. Bowron (2016). Modeling the Structure of Complex Aluminosilicate Glasses: The Effect of Zinc Addition. **J. Phys. Chem. B**, 120(9), 2526-2537. doi: 10.1021/acs.jpcc.5b10886.
- Bertolini, M. J., M. A. Zaghete and R. Gimenes (2005). Development of an experimental glass ionomer cement containing niobium and fluoride. **J. Non-Cryst. Solids**, 351(52), 3884-3887. doi: 10.1016/j.jnoncrysol.2005.10.008.
- Bertolini, M. J., M. A. Zaghete, R. Gimenes and G. C. Padovani (2008). Determination of the properties of an experimental glass polyalkenoate cement prepared from niobium silicate powder containing fluoride. **Dent. Mater.**, 24(1), 124-128. doi: 10.1016/j.dental.2007.03.005.
- Bertolini, M. J., M. A. Zaghete, R. Gimenes, G. C. Padovani and C. A. S. Cruz (2009). Preparation and evaluation of an experimental luting glass ionomer cement to be used in dentistry. **J. Mater. Sci.: Mater. Med.**, 20(9), 1781-1785. doi: 10.1007/s10856-009-3748-7.
- Bezerra, C. d. S. and M. E. G. Valerio (2016). Structural and optical study of CaF<sub>2</sub> nanoparticles produced by a microwave-assisted hydrothermal method. **Physica B Condens. Matter**, 501, 106-112. doi: 10.1016/j.physb.2016.08.025.
- Billington, R. W., J. A. Williams and G. J. Pearson (2006). Ion processes in glass ionomer cements. **J. Dent.**, 34(8), 544-555. doi: 10.1016/j.jdent.2005.09.008.
- Bogomolova, L. D., T. K. Pavlushkina and I. V. Morozova (2006). Formation of glass synthesized by sol-gel technology. **GLASS CERAM+**, 63(7), 254-258. doi: 10.1007/s10717-006-0092-y.

- Bonapasta, A. A., F. Buda and P. Colombet (2001). Interaction between Ca Ions and Poly(acrylic acid) Chains in Macro-Defect-Free Cements: A Theoretical Study. **Chem. Mater.**, 13(1), 64-70. doi: 10.1021/cm000505o.
- Bonifácio, C., C. Kleverlaan, D. Raggio, A. Werner, R. D. Carvalho and W. V. Amerongen (2009). Physical-mechanical properties of glass ionomer cements indicated for atraumatic restorative treatment. **Aust. Dent. J.**, 54(3), 233-237. doi: 10.1111/j.1834-7819.2009.01125.x.
- Brauer, D. S., E. Gentleman, D. F. Farrar, M. M. Stevens and R. G. Hill (2011). Benefits and drawbacks of zinc in glass ionomer bone cements. **Biomedical Materials** 6(4), 045007. doi: 10.1088/1748-6041/6/4/045007.
- Brinker, C. J. and G. W. Scherer (1990). CHAPTER 11 - Sintering. *Sol-Gel Science* (Vol. 1, pp. 674-742). San Diego: Academic Press.
- Brow, R. K. (2000). Review: the structure of simple phosphate glasses. **J. Non. Cryst. Solids**, 263-264, 1-28. doi: 10.1016/S0022-3093(99)00620-1.
- Brow, R. K., R. J. Kirkpatrick and G. L. Turner (1993). Nature of Alumina in Phosphate Glass: II, Structure of Sodium Aluminophosphate Glass. **J. Am. Ceram. Soc.**, 76(4), 919-928. doi: 10.1111/j.1151-2916.1993.tb05316.x.
- Bueno, L. S., A. F. S. Borges, M. F. L. Navarro, J. W. Nicholson, R. G. Hill and S. K. Sidhu (2021). Determination of chemical species of fluoride during uptake mechanism of glass-ionomer cements with NMR spectroscopy. **Dent. Mater.**, 37(7), 1176-1182. doi: 10.1016/j.dental.2021.04.011.
- California, D. B. (2005). The fact about filling. California Department of Consumer Affairs. D. B. o. California.
- Cao, C., M. Mei, Q.-L. Li, E. Lo and C. Chu (2015). Methods for Biomimetic Remineralization of Human Dentine: A Systematic Review. **Int. J. Mol. Sci.**, 16(3), 4615-4627. doi: 10.3390/ijms16034615.
- Cestari, A. (2016). Sol-gel methods for synthesis of aluminosilicates for dental applications. **J. Dent.**, 55, 105-113. doi: 10.1016/j.jdent.2016.10.012.
- Cestari, A., L. R. Avila, E. C. O. Nassor, P. F. d. S. Pereira, P. S. Calefi, K. J. Ciuffi, et al. (2009). Characterization of the calcium-fluoroaluminosilicate glass prepared by a non-hydrolytic sol-gel route for future dental application as glass

- ionomer cement. **Mater. Res.**, 12, 139-143. doi: 10.1590/S1516-14392009000200005.
- Chau, N. P. T., S. Pandit, J.-N. Cai, M.-H. Lee and J.-G. Jeon (2015). Relationship between fluoride release rate and anti-cariogenic biofilm activity of glass ionomer cements. **Dent. Mater.**, 31(4), e100-e108. doi: 10.1016/j.dental.2014.12.016.
- Chen, S. (2016). *Glass Ionomer Cements with Improved Bioactive and Antibacterial Properties*. (PhD) Retrieved from <http://urn.kb.se/resolve?urn=urn:nbn:se:uu:diva-301924>.
- Chen, S., Y. Cai, H. Engqvist and W. Xia (2016). Enhanced bioactivity of glass ionomer cement by incorporating calcium silicates. **Biomatter**, 6(1), e1123842. doi: 10.1080/21592535.2015.1123842.
- Chen, S., S. Gururaj, W. Xia and H. Engqvist (2016). Synthesis of Ag doped calcium phosphate particles and their antibacterial effect as additives in dental glass ionomer cements. **J. Mater. Sci.: Mater. Med.**, 27(11), 172. doi: 10.1007/s10856-016-5785-3.
- Chen, S., G. Mestres, W. Lan, W. Xia and H. Engqvist (2016). Cytotoxicity of modified glass ionomer cement on odontoblast cells. **J. Mater. Sci. Mater. Med.**, 27(7), 116. doi: 10.1007/s10856-016-5729-y.
- Chen, X. and S. S. Mao (2007). Titanium Dioxide Nanomaterials: Synthesis, Properties, Modifications, and Applications. **Chem. Rev.**, 107(7), 2891-2959. doi: 10.1021/cr0500535.
- Choi, J.-Y., H.-H. Lee and H.-W. Kim (2008). Bioactive sol-gel glass added ionomer cement for the regeneration of tooth structure. **J. Mater. Sci. Mater. Med.**, 19(10), 3287. doi: 10.1007/s10856-008-3464-8.
- Chun, K. J., H. H. Choi and J. Y. Lee (2014). Comparison of mechanical property and role between enamel and dentin in the human teeth. **J. Dent. Biomech.**, 5, 1758736014520809. doi: 10.1177/1758736014520809.
- Conserva, E., U. Consolo and P. Bellini (2018). Adhesion and proliferation of human dental pulp stem cells on a laser microtextured implant surface: an *in vitro* study. **Oral Health and Care**, 3(4). doi: 10.15761/ohc.1000154.

- Crisp, S., M. A. Pringuer, D. Wardleworth and A. D. Wilson (1974). Reactions in Glass Ionomer Cements: II. An Infrared Spectroscopic Study. **J. Dent. Res.**, 53(6), 1414-1419. doi: 10.1177/00220345740530062001.
- Czarnecka, B. and J. W. Nicholson (2006). Ion release by resin-modified glass-ionomer cements into water and lactic acid solutions. **J. Dent.**, 34(8), 539-543. doi: 10.1016/j.jdent.2005.08.007.
- Dabsie, F., G. Gregoire, M. Sixou and P. Sharrock (2009). Does strontium play a role in the cariostatic activity of glass ionomer?: Strontium diffusion and antibacterial activity. **J. Dent.**, 37(7), 554-559. doi: 10.1016/j.jdent.2009.03.013.
- Dai, L. L., M. L. Mei, C. H. Chu and E. C. M. Lo (2021). Remineralizing effect of a new strontium-doped bioactive glass and fluoride on demineralized enamel and dentine. **J. Dent.**, 108, 103633. doi: 10.1016/j.jdent.2021.103633.
- Dai, L. L., F. Nudelman, C. H. Chu, E. C. M. Lo and M. L. Mei (2021). The effects of strontium-doped bioactive glass and fluoride on hydroxyapatite crystallization. **J. Dent.**, 105, 103581. doi: 10.1016/j.jdent.2021.103581.
- Daley, T., K. B. Opuni, E. Raj, A. J. Dent, G. Cibin, T. I. Hyde and G. Sankar (2021). Monitoring the process of formation of ZnO from ZnO<sub>2</sub> using in situ combined XRD/XAS technique. **J. Condens. Matter Phys.**, 33(26), 264002. doi: 10.1088/1361-648x/abfb91.
- Davis, H. B., F. Gwinner, J. C. Mitchell and J. L. Ferracane (2014). Ion release from, and fluoride recharge of a composite with a fluoride-containing bioactive glass. **Dent. Mater.**, 30(10), 1187-1194. doi: 10.1016/j.dental.2014.07.012.
- De Caluwé, T., C. W. J. Vercruyse, I. Ladik, R. Convents, H. Declercq, L. C. Martens and R. M. H. Verbeeck (2017). Addition of bioactive glass to glass ionomer cements: Effect on the physico-chemical properties and biocompatibility. **Dent. Mater.**, 33(4), e186-e203. doi: 10.1016/j.dental.2017.01.007.
- Drouet, C. (2013). Apatite Formation: Why It May Not Work as Planned, and How to Conclusively Identify Apatite Compounds. **BioMed Res. Int.**, 2013, 490946. doi: 10.1155/2013/490946.

- Du, R. L., J. Chang, S. Y. Ni, W. Y. Zhai and J. Y. Wang (2006). Characterization and *in vitro* Bioactivity of Zinc-containing Bioactive Glass and Glass-ceramics. **J. Biomater. Appl.**, 20(4), 341-360. doi: 10.1177/0885328206054535.
- Duan, X., X. Wang, F. Yu and D. Yuan (2012). Effects of Annealing Temperature and SiO<sub>2</sub> Matrix on the Structure and Optical Properties of Co-Doped ZnAl<sub>2</sub>O<sub>4</sub>/SiO<sub>2</sub> Nanoglass–Ceramic Composites. **J. Phys. Chem. C**, 116(3), 2313-2321. doi: 10.1021/jp209837q.
- Dudev, M., J. Wang, T. Dudev and C. Lim (2006). Factors Governing the Metal Coordination Number in Metal Complexes from Cambridge Structural Database Analyses. **J. Phys. Chem. B**, 110(4), 1889-1895. doi: 10.1021/jp054975n.
- Edén, M. (2011). The split network analysis for exploring composition–structure correlations in multi-component glasses: I. Rationalizing bioactivity–composition trends of bioglasses. **J. Non. Cryst. Solids**, 357(6), 1595-1602. doi: 10.1016/j.jnoncrysol.2010.11.098.
- El Mallakh, B. F. and N. K. Sarkar (1990). Fluoride release from glass-ionomer cements in de-ionized water and artificial saliva. **Dent. Mater.**, 6(2), 118-122. doi: 10.1016/S0109-5641(05)80041-7.
- Farrugia, C. and J. Camilleri (2015). Antimicrobial properties of conventional restorative filling materials and advances in antimicrobial properties of composite resins and glass ionomer cements—A literature review. **Dent. Mater.**, 31(4), 89-99. doi: 10.1016/j.dental.2014.12.005.
- Feng, X. (2014). [Cause of secondary caries and prevention]. **Hua Xi Kou Qiang Yi Xue Za Zhi**, 32(2), 107-110. doi: 10.7518/hxkq.2014.02.001.
- Fleming, G., A. Farooq and J. Barralet (2003). Influence of powder/liquid mixing ratio on the performance of a restorative glass-ionomer dental cement. **Biomaterials**, 24, 4173-4179. doi: 10.1016/S0142-9612(03)00301-6.
- Forghani, A., M. Mapar, M. Kharaziha, M. H. Fathi and M. Fesharaki (2013). Novel Fluorapatite-Forsterite Nanocomposite Powder for Oral Bone Defects. **Int. J. Appl. Ceram. Technol.**, 10(s1), E282-E289. doi: 10.1111/j.1744-7402.2012.02824.x.

- Francci, C., T. G. Deaton, R. R. Arnold, E. J. Swift, J. Perdigao and J. W. Bawden (1999). Fluoride Release from Restorative Materials and Its Effects on Dentin Demineralization. *J. Dent. Res.*, 78(10), 1647-1654. doi: 10.1177/00220345990780101001.
- Fujihara, S. (2018). Sol-Gel Processing of Fluoride and Oxyfluoride Materials. *Handbook of Sol-Gel Science and Technology: Processing, Characterization and Applications* (Vol., pp. 333-359) Springer Cham.
- Ganjali, M., S. Mousavi, S. Nikzamid, P. B. Milan and M. Mozafari (2022). Effect of laser cladDED co-doped strontium fluorapatite nanopowder coating on the antibacterial and cell attachment of Ti-6Al-4V implants for bone applications. *Mater. Technol.*, 37(8), 829-841. doi: 10.1080/10667857.2021.1898716.
- Gao, W. and R. J. Smales (2001). Fluoride release/uptake of conventional and resin-modified glass ionomers, and compomers. *J. Dent.*, 29(4), 301-306. doi: 10.1016/s0300-5712(00)00053-1.
- Gaur, S. and R. Agnihotri (2021). Application of Adipose Tissue Stem Cells in Regenerative Dentistry: A Systematic Review. *J. Int. Soc. Prev. Community Dent.*, 11(3), 266-271. doi: 10.4103/jispcd.JISPCD\_43\_21.
- Griffin, S. G. and R. G. Hill (1999). Influence of glass composition on the properties of glass polyalkenoate cements. Part I: influence of aluminium to silicon ratio. *Biomaterials*, 20(17), 1579-1586. doi: 10.1016/S0142-9612(99)00058-7.
- Griffin, S. G. and R. G. Hill (2000). Influence of glass composition on the properties of glass polyalkenoate cements. Part II: influence of phosphate content. *Biomaterials*, 21(4), 399-403. doi: 10.1016/S0142-9612(99)00202-1.
- Griffin, S. G. and R. G. Hill (2000). Influence of glass composition on the properties of glass polyalkenoate cements. Part IV: influence of fluorine content. *Biomaterials*, 21(7), 693-698. doi: 10.1016/S0142-9612(99)00216-1.
- Guida, A., R. G. Hill, M. R. Towler and S. Eramo (2002). Fluoride release from model glass ionomer cements. *J. Mater. Sci. Mater. Med.*, 13(7), 645-649. doi: 10.1023/a:1015777406891.
- Gupta, A. A., S. Mulay, P. Mahajan and A. T. Raj (2019). Assessing the effect of ceramic additives on the physical, rheological and mechanical properties of

- conventional glass ionomer luting cement – An in-vitro study. **Heliyon**, 5(7), e02094. doi: 10.1016/j.heliyon.2019.e02094.
- Hafshejani, T. M., A. Zamanian, J. R. Venugopal, Z. Rezvani, F. Sefat, M. R. Saeb, et al. (2017). Antibacterial glass-ionomer cement restorative materials: A critical review on the current status of extended release formulations. **J. Control Release**, 262(Supplement C), 317-328. doi: 10.1016/j.jconrel.2017.07.041.
- Hatibović-Kofman, S. and G. Koch (1991). *Fluoride release from glass ionomer cement in vivo and in vivo*. Vol. 15.
- Holmgren, C. J., D. Roux and S. Doméjean (2013). Minimal intervention dentistry: part 5. Atraumatic restorative treatment (ART) – a minimum intervention and minimally invasive approach for the management of dental caries. **Br. Dent. J.**, 214(1), 11-18. doi: 10.1038/sj.bdj.2012.1175.
- Huang, C. and E. C. Behrman (1991). Structure and properties of calcium aluminosilicate glasses. **J. Non-Cryst. Solids**, 128(3), 310-321. doi: 10.1016/0022-3093(91)90468-L.
- Ilipronti, T., C. K. Clare, G. Berndt, E. A. de Campos, M. H. V. Fernandes and S. D. de Campos (2019). Glass Ionomer Cements Based in TiO<sub>2</sub> by Sol-gel Method. **Orbital: Electron. J. Chem.**, 11(1), 1-9. doi: 10.17807/orbital.v11i1.1176.
- Ito, A. and K. Onuma (2003). 16 - Growth of Hydroxyapatite Crystals. *Crystal Growth Technology* (Vol., pp. 525-559). Norwich, NY: William Andrew Publishing.
- Itota, T., T. E. Carrick, S. Rusby, O. T. Al-Naimi, M. Yoshiyama and J. F. McCabe (2004). Determination of fluoride ions released from resin-based dental materials using ion-selective electrode and ion chromatograph. **J Dent**, 32(2), 117-122. doi: 10.1016/j.jdent.2003.09.002.
- Jain, A., S. P. Ong, G. Hautier, W. Chen, W. D. Richards, S. Dacek, et al. (2013). Commentary: The Materials Project: A materials genome approach to accelerating materials innovation. **APL Mater.**, 1(1), 011002. doi: 10.1063/1.4812323.
- Jmal, N. and J. Bouaziz (2018). Fluorapatite-glass-ceramics obtained by heat treatment of a gel synthesized by the sol-gel processing method. **Mater. Lett.**, 215, 280-283. doi: 10.1016/j.matlet.2017.12.123.

- Joe, A., S.-H. Park, K.-D. Shim, D.-J. Kim, K.-H. Jhee, H.-W. Lee, et al. (2017). Antibacterial mechanism of ZnO nanoparticles under dark conditions. **J. Ind. Eng. Chem.**, 45, 430-439. doi: 10.1016/j.jiec.2016.10.013.
- Jones, W. M. and D. B. Fischbach (1988). Novel processing of silica hydrosols and gels. **J. Non. Cryst. Solids**, 101(1), 123-126. doi: 10.1016/0022-3093(88)90378-X.
- Kaga, N., F. Nagano-Takebe, T. Nezu, T. Matsuura, K. Endo and M. Kaga (2020). Protective Effects of GIC and S-PRG Filler Restoratives on Demineralization of Bovine Enamel in Lactic Acid Solution. **Materials**, 13(9), 2140. doi: 10.3390/ma13092140.
- Kanjevac, T., M. Milovanovic, V. Volarevic, M. L. Lukic, N. Arsenijevic, D. Markovic, et al. (2012). Cytotoxic Effects of Glass Ionomer Cements on Human Dental Pulp Stem Cells Correlate with Fluoride Release. **Curr. Med. Chem.**, 8(1), 40-45. doi: 10.2174/157340612799278351.
- Kantrong, N., K. Khongkaphet, N. Sitornsud, P. Lo-Apirukkul, W. Phanprom, C. Rojviriya, et al. (2022). Synchrotron radiation analysis of root dentin: the roles of fluoride and calcium ions in hydroxyapatite remineralization. **J. Synchrotron. Radiat.**, 29(Pt 2), 496-504. doi: 10.1107/s1600577521013655.
- Katz, A. K., J. P. Glusker, S. A. Beebe and C. W. Bock (1996). Calcium Ion Coordination: A Comparison with That of Beryllium, Magnesium, and Zinc. **J. Am. Chem. Soc.**, 118(24), 5752-5763. doi: 10.1021/ja953943i.
- Kessler, V. G. (2015). Sol-Gel Precursors. *The Sol-Gel Handbook* (Vol., pp. 195-224) Wiley-VCH Verlag GmbH & Co. KGaA.
- Khoroushi, M. and F. Keshani (2013). A review of glass-ionomers: From conventional glass-ionomer to bioactive glass-ionomer. **J. Dent. Res.**, 10(4), 411-420.
- Kidkhunthod, P. (2017). Structural studies of advanced functional materials by synchrotron-based x-ray absorption spectroscopy: BL5.2 at SLRI, Thailand. **Adv. Nat. Sci. Nanosci.**, 8(3), 035007. doi: 10.1088/2043-6254/aa7240.
- Kim, D.-A., J.-H. Lee, S.-K. Jun, H.-W. Kim, M. Eltohamy and H.-H. Lee (2017). Sol-gel-derived bioactive glass nanoparticle-incorporated glass ionomer cement with or without chitosan for enhanced mechanical and biomineralization properties. **Dent. Mater.**, 33(7), 805-817. doi: 10.1016/j.dental.2017.04.017.

- Kim, H.-J., H. E. Bae, J.-E. Lee, I.-S. Park, H.-G. Kim, J. Kwon and D.-S. Kim (2021). Effects of bioactive glass incorporation into glass ionomer cement on demineralized dentin. **Sci. Rep.**, 11(1), 7016. doi: 10.1038/s41598-021-86481-y.
- Klimek, K., A. Belcarz, R. Pazik, P. Sobierajska, T. Han, R. J. Wiglusz and G. Ginalska (2016). “False” cytotoxicity of ions-adsorbing hydroxyapatite — Corrected method of cytotoxicity evaluation for ceramics of high specific surface area. **Mater. Sci. Eng. C**, 65, 70-79. doi: 10.1016/j.msec.2016.03.105.
- Kohno, T., R. Tsuboi, H. Kitagawa and S. Imazato (2019). Zinc-Ion Release and Recharge Ability of GIC Containing BioUnion filler. *2019 IADR/AADR/CADR General Session*, Vancouver, BC, Canada.
- Komai, S., M. Hirano and N. Ohtsu (2020). Spectral analysis of Sr 3d XPS spectrum in Sr-containing hydroxyapatite. **Surf. Interface Anal.**, 52(12), 823-828. doi: 10.1002/sia.6877.
- Kozmos, M., P. Virant, F. Rojko, A. Abram, R. Rudolf, P. Raspor, et al. (2021). Bacterial Adhesion of *Streptococcus mutans* to Dental Material Surfaces. **Molecules**, 26(4), 1152. doi: 10.3390/molecules26041152.
- Krämer, N., M. Schmidt, S. Lücker, E. Domann and R. Frankenberger (2018). Glass ionomer cement inhibits secondary caries in an *in vitro* biofilm model. **Clin. Oral Investig.**, 22(2), 1019-1031. doi: 10.1007/s00784-017-2184-1.
- Krežel, A. and W. Maret (2016). The biological inorganic chemistry of zinc ions. **Arch. Biochem. Biophys.**, 611, 3-19. doi: 10.1016/j.abb.2016.04.010.
- Kumar, A., A. Raj, D. Singh, S. Donthagani, M. Kumar and K. Ramesh (2021). A new zinc reinforced glass ionomer cement: A boon in dentistry. **J. Pharm. Bioallied Sci.**, 13(5), 272-275. doi: 10.4103/jpbs.JPBS\_730\_20.
- Kusumoto, H. (2009). *Characterisation of Mg, Sr, and Zn containing fluoro-aluminosilicate glasses and their glass polyalkenoate cements*. (PhD) Retrieved from <http://hdl.handle.net/10044/1/5509>.
- LeGeros, R., C. Bleiwas, M. Retino, R. Rohanizadeh and J. Legeros (1999). Zinc effect on the *in vitro* formation of calcium phosphates: Relevance to clinical inhibition of calculus formation. **Am. J. Dent.**, 12, 65-71.

- Li, Y., W. Zhang, J. Niu and Y. Chen (2012). Mechanism of Photogenerated Reactive Oxygen Species and Correlation with the Antibacterial Properties of Engineered Metal-Oxide Nanoparticles. **ACS Nano**, 6(6), 5164-5173. doi: 10.1021/nn300934k.
- Lin, A., N. S. McIntyre and R. D. Davidson (1992). Studies on the Adhesion of Glass-ionomer Cements to Dentin. **J. Dent. Res.**, 71(11), 1836-1841. doi: 10.1177/00220345920710111401.
- Loewenstein, W. (1954). The distribution of aluminum in the tetrahedra of silicates and aluminates. **Am. Mineral.**, 39(1-2), 92-96.
- Lohbauer, U. (2010). Dental Glass Ionomer Cements as Permanent Filling Materials? – Properties, Limitations and Future Trends. **Materials**, 3(1), 76-96. doi: 10.3390/ma3010076.
- Lynch, R. (2011). Zinc in the mouth, its interactions with dental enamel and possible effects on caries; A review of the literature. **Int. Dent. J.**, 61 Suppl 3, 46-54. doi: 10.1111/j.1875-595X.2011.00049.x.
- Madi, F., S. K. Sidhu and J. W. Nicholson (2020). The effect of temperature and ionic solutes on the fluoride release and recharge of glass-ionomer cements. **Dent. Mater.**, 36(1), e9-e14. doi: 10.1016/j.dental.2019.11.018.
- Maeda, T., S. Matsuya and M. Ohta (1998). Effects of CaF<sub>2</sub> Addition on the Structure of CaO-Al<sub>2</sub>O<sub>3</sub>-SiO<sub>2</sub> Glasses. **Dent. Mater. J.**, 17(2), 104-114. doi: 10.4012/dmj.17.104.
- Makarowicz, A., C. L. Bailey, N. Weiher, E. Kemnitz, S. L. M. Schroeder, S. Mukhopadhyay, et al. (2009). Electronic structure of Lewis acid sites on high surface area aluminium fluorides: a combined XPS and ab initio investigation. **Phys. Chem. Chem. Phys.**, 11(27), 5664. doi: 10.1039/b821484k.
- McMillan, P. and B. Piriou (1982). The structures and vibrational spectra of crystals and glasses in the silica-alumina system. **J. Non. Cryst. Solids**, 53(3), 279-298. doi: 10.1016/0022-3093(82)90086-2.
- Moshaverinia, A., S. Ansari, M. Moshaverinia, N. Roohpour, J. A. Darr and I. Rehman (2008). Effects of incorporation of hydroxyapatite and fluoroapatite

- nanobioceramics into conventional glass ionomer cements (GIC). **Acta Biomater.**, 4(2), 432-440. doi: 10.1016/j.actbio.2007.07.011.
- Moshaverinia, A., S. Ansari, Z. Movasaghi, R. W. Billington, J. A. Darr and I. U. Rehman (2008). Modification of conventional glass-ionomer cements with N-vinylpyrrolidone containing polyacids, nano-hydroxy and fluoroapatite to improve mechanical properties. **Dent. Mater.**, 24(10), 1381-1390. doi: 10.1016/j.dental.2008.03.008.
- Moshaverinia, M., A. Borzabadi-Farahani, A. Sameni, A. Moshaverinia and S. Ansari (2016). Effects of incorporation of nano-fluorapatite particles on microhardness, fluoride releasing properties, and biocompatibility of a conventional glass ionomer cement (GIC). **Dent. Mater. J.**, 35(5), 817-821. doi: 10.4012/dmj.2015-437.
- Mukherjee, S. P. (1980). Sol-gel processes in glass science and technology. **J. Non. Cryst. Solids**, 42(1), 477-488. doi: 10.1016/0022-3093(80)90046-0.
- Nagano, Y., D. Mori and T. Kumagaia (2019). Evaluation of CareDyne Restore on Shear-bond Strength and Remineralization. *The Third Biennial Meeting of the International Academy of Adhesive Dentistry*, the Palazzo della Cultura e dei Congressi, Bologna, Italy.
- Naumova, E. A., M. Staiger, O. Kouji, J. Modric, T. Pierchalla, M. Rybka, et al. (2019). Randomized investigation of the bioavailability of fluoride in saliva after administration of sodium fluoride, amine fluoride and fluoride containing bioactive glass dentifrices. **BMC Oral Health**, 19(1), 119. doi: 10.1186/s12903-019-0805-6.
- Newville, M. (2001). IFEFFIT : interactive XAFS analysis and FEFF fitting. **J. Synchrotron Radiat.**, 8(2), 322-324. doi: 10.1107/S0909049500016964.
- Nicholson, J. and B. Czarnecka (2016). 6 - Conventional glass-ionomer cements. *Materials for the Direct Restoration of Teeth* (Vol. 1, pp. 107-136) Woodhead Publishing.
- Nicholson, J. W., P. J. Brookman, O. M. Lacy and A. D. Wilson (1988). Fourier Transform Infrared Spectroscopic Study of the Role of Tartaric Acid in Glass-ionomer Dental Cements. **J. Dent. Res.**, 67(12), 1451-1454. doi: 10.1177/00220345880670120201.

- Nicholson, J. W., N. J. Coleman and S. K. Sidhu (2021). Kinetics of ion release from a conventional glass-ionomer cement. **J. Mater. Sci. Mater. Med.**, 32(4). doi: 10.1007/s10856-021-06501-1.
- Nicholson, J. W. and B. Czarnecka (2009). Review Paper: Role of Aluminum in Glass-ionomer Dental Cements and its Biological Effects. **J. Biomater. Appl**, 24(4), 293-308. doi: 10.1177/0885328209344441.
- O'Donnell, M. D., S. J. Watts, R. G. Hill and R. V. Law (2009). The effect of phosphate content on the bioactivity of soda-lime-phosphosilicate glasses. **J. Mater. Sci. Mater. Med.**, 20(8), 1611-1618. doi: 10.1007/s10856-009-3732-2.
- Onuma, K., A. Ito, T. Tateishi and T. Kameyama (1995). Growth kinetics of hydroxyapatite crystal revealed by atomic force microscopy. **J. Cryst. Growth**, 154(1), 118-125. doi: 10.1016/0022-0248(95)00201-4.
- Opitz, A. K., C. Rameshan, M. Kubicek, G. M. Rupp, A. Nanning, T. Götsch, et al. (2018). The Chemical Evolution of the  $\text{La}_{0.6}\text{Sr}_{0.4}\text{CoO}_3-\delta$  Surface Under SOFC Operating Conditions and Its Implications for Electrochemical Oxygen Exchange Activity. **Top. Catal.**, 61(20), 2129-2141. doi: 10.1007/s11244-018-1068-1.
- Osorio, R., E. Osorio, I. Cabello and M. Toledano (2014). Zinc Induces Apatite and Scholzite Formation during Dentin Remineralization. **Caries Res.**, 48(4), 276-290. doi: 10.1159/000356873.
- Pan, H. B. and B. W. Darvell (2007). Solubility of calcium fluoride and fluorapatite by solid titration. **Arch. Oral. Biol.**, 52(9), 861-868. doi: 10.1016/j.archoralbio.2007.03.002.
- Patil, K., A. Patel, S. Kunte, P. Shah, B. Kaur and S. Paranna (2020). Comparative Evaluation of the Mechanical Properties of Zinc-reinforced Glass Ionomer Cement and Glass Ionomer Type IX Cement: An *In Vitro* Study. **Int. J. Clin. Pediatr. Dent.**, 13(4), 381-389. doi: 10.5005/jp-journals-10005-1798.
- Patrón-Romero, L., P. A. Luque, C. A. Soto-Robles, O. Nava, A. R. Vilchis-Nestor, V. W. Barajas-Carrillo, et al. (2020). Synthesis, characterization and cytotoxicity of zinc oxide nanoparticles by green synthesis method. **J. Drug Deliv. Sci. Techno.**, 60, 101925. doi: 10.1016/j.jddst.2020.101925.

- Pierre, A. C. (2019). From random glass networks to random silica gel networks and their use as host for biocatalytic applications. **J. Sol-Gel Sci. Technol.**, 90(1), 172-186. doi: 10.1007/s10971-018-4798-4.
- Prosser, H. J., C. P. Richards and A. D. Wilson (1982). NMR spectroscopy of dental materials. II. The role of tartaric acid in glass-ionomer cements. **J. Biomed. Mater. Res.**, 16(4), 431-445. doi: 10.1002/jbm.820160411.
- Ravi, N. D., R. Balu and T. S. Sampath Kumar (2012). Strontium-Substituted Calcium Deficient Hydroxyapatite Nanoparticles: Synthesis, Characterization, and Antibacterial Properties. **J. Am. Ceram.**, 95(9), 2700-2708. doi: 10.1111/j.1551-2916.2012.05262.x.
- Riti, P. I., A. Vulpoi, O. Ponta and V. Simon (2014). The effect of synthesis route and magnesium addition on structure and bioactivity of sol-gel derived calcium-silicate glasses. **Ceram. Int.**, 40(9, Part B), 14741-14748. doi: 10.1016/j.ceramint.2014.06.063.
- Roy, B., H. Jain, S. K. Saha and D. Chakravorty (1995). Comparison of structure of alkali silicate glasses prepared by sol-gel and melt-quench methods. **J. Non. Cryst. Solids**, 183(3), 268-276. doi: 10.1016/0022-3093(94)00633-4.
- Saber, M., R.-S. Hayaei-Tehrani, S. Mokhtari, P. Hoorzad and F. Esfandiari (2021). *In vitro* cytotoxicity of zinc oxide nanoparticles in mouse ovarian germ cells. **Toxicol. In Vitro**, 70, 105032. doi: 10.1016/j.tiv.2020.105032.
- Sasanaluckit, P., K. R. Albustany, P. J. Doherty and D. F. Williams (1993). Biocompatibility of glass ionomer cements. **Biomaterials**, 14(12), 906-916. doi: 10.1016/0142-9612(93)90132-L.
- scholze, H. (1964). *Glass : Nature, Structure, and Properties*. Vol. New York, Berlin, Heidelberg: englische Übersetzung der 3. deutschen Auflage, 1991 Springer-Verlag.
- Schuhladen, K., L. Stich, J. Schmidt, A. Steinkasserer, A. R. Boccaccini and E. Zinser (2020). Cu, Zn doped borate bioactive glasses: antibacterial efficacy and dose-dependent *in vitro* modulation of murine dendritic cells. **Biomater. Sci.**, 8(8), 2143-2155. doi: 10.1039/C9BM01691K.
- Sergi, R., D. Bellucci, R. Salvatori, G. Maisetta, G. Batoni and V. Cannillo (2019). Zinc containing bioactive glasses with ultra-high crystallization temperature,

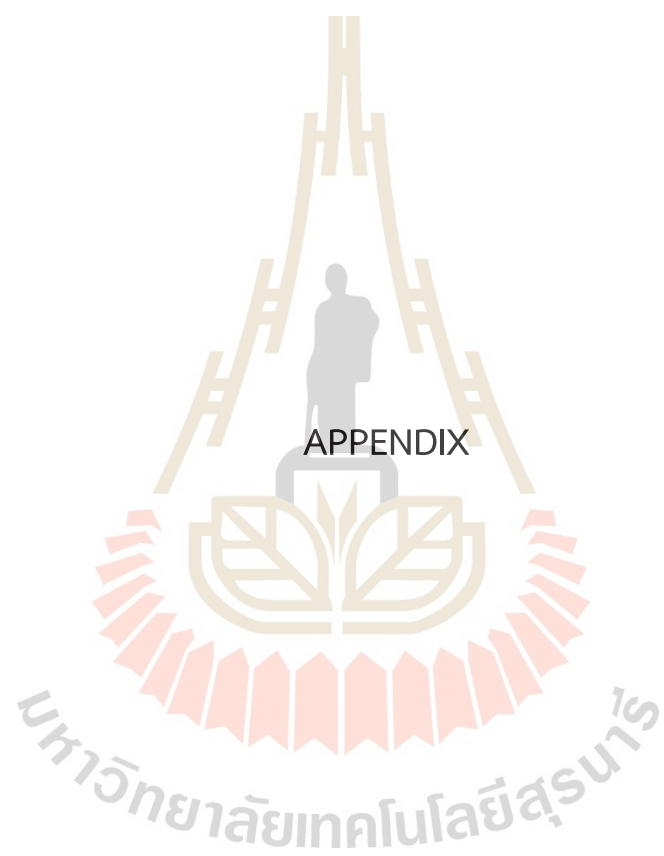
- good biological performance and antibacterial effects. **Mater. Sci. Eng. C**, 104, 109910. doi: 10.1016/j.msec.2019.109910.
- Sidhu, S. K. and J. W. Nicholson (2016). A Review of Glass-Ionomer Cements for Clinical Dentistry. **J. Funct. Biomater.**, 7(3), 16. doi: 10.3390/jfb7030016.
- Sirelkhatim, A., S. Mahmud, A. Seeni, N. H. M. Kaus, L. C. Ann, S. K. M. Bakhori, et al. (2015). Review on Zinc Oxide Nanoparticles: Antibacterial Activity and Toxicity Mechanism. **Nanomicro. Lett.**, 7(3), 219-242. doi: 10.1007/s40820-015-0040-x.
- Song, F., H. Koo and D. Ren (2015). Effects of Material Properties on Bacterial Adhesion and Biofilm Formation. **J. Dent. Res.**, 94(8), 1027-1034. doi: 10.1177/0022034515587690.
- Środa, M. and C. Paluszkiwicz (2008). The structural role of alkaline earth ions in oxyfluoride aluminosilicate glasses—Infrared spectroscopy study. **Vib. Spectrosc.**, 48(2), 246-250. doi: 10.1016/j.vibspec.2008.02.017.
- Stamboulis, A., R. G. Hill and R. V. Law (2004). Characterization of the structure of calcium alumino-silicate and calcium fluoro-alumino-silicate glasses by magic angle spinning nuclear magnetic resonance (MAS-NMR). **J. Non-Cryst. Solids**, 333(1), 101-107. doi: 10.1016/j.jnoncrysol.2003.09.049.
- Stamboulis, A., R. G. Hill and R. V. Law (2005). Structural characterization of fluorine containing glasses by  $^{19}\text{F}$ ,  $^{27}\text{Al}$ ,  $^{29}\text{Si}$  and  $^{31}\text{P}$  MAS-NMR spectroscopy. **J. Non-Cryst. Solids**, 351(40), 3289-3295. doi: 10.1016/j.jnoncrysol.2005.07.029.
- Stranick, M. A. and M. J. Root (1991). Influence of strontium on monofluorophosphate uptake by hydroxyapatite XPS characterization of the hydroxyapatite surface. **Colloids Surf.**, 55, 137-147. doi: 10.1016/0166-6622(91)80088-6.
- Suprastivi, E., Anggraeni and D. A. Npa (2009). Fluoride Released from GIC and RMGIC in Saliva and Dentino-Enamel Substance. **Makara Journal of Health Research**, 13, 53-58. doi: 10.7454/msk.v13i2.356.
- Taira, M. and M. Yamaki (1995). Preparation of  $\text{SiO}_2\text{-Al}_2\text{O}_3$  glass powders by the sol-gel process for dental applications. **J. Mater. Sci.: Mater. Med.**, 6(4), 197-200. doi: 10.1007/bf00146855.

- Takahashi, Y., S. Imazato, A. V. Kaneshiro, S. Ebisu, J. E. Frencken and F. R. Tay (2006). Antibacterial effects and physical properties of glass-ionomer cements containing chlorhexidine for the ART approach. **Dent. Mater.**, 22(7), 647-652. doi: 10.1016/j.dental.2005.08.003.
- Thaitalay, P., C. Giannasi, S. Niada, O. Thongsri, R. Dangviriyakul, S. Srisuwan, et al. (2022). Nano-bioactive glass incorporated polymeric apatite/tricalcium phosphate cement composite supports proliferation and osteogenic differentiation of human adipose-derived stem/stromal cells. **Mater. Today Commun.**, 31, 103590. doi: 10.1016/j.mtcomm.2022.103590.
- Thomas, S. A., B. Mishra and S. C. B. Myneni (2019). High Energy Resolution-X-ray Absorption Near Edge Structure Spectroscopy Reveals Zn Ligation in Whole Cell Bacteria. **J. Phys. Chem. Lett.**, 10(10), 2585-2592. doi: 10.1021/acs.jpcllett.9b01186.
- Thongsri, O., S. Srisuwan, P. Thaitalay, R. Dangviriyakul, P. Aengchuan, N. Chanlek, et al. (2022). Structural evaluation of ZnO substitution for CaO in glass ionomer cement synthesized by sol-gel method and their properties. **J. Mater. Sci.**, 57(1), 633-650. doi: 10.1007/s10853-021-06517-6.
- Thongsri, O., S. Srisuwan, P. Thaitalay, R. Dangviriyakul, P. Aengchuan, N. Chanlek, et al. (2021). Influence of Al<sub>2</sub>O<sub>3</sub> and P<sub>2</sub>O<sub>5</sub> contents in sol-gel ionomer glass system on the structure and their cement properties. **J. Sol-Gel Sci. Technol.**(98), 441-451. doi: 10.1007/s10971-021-05519-9.
- Thuy, T. T., H. Nakagaki, K. Kato, P. A. Hung, J. Inukai, S. Tsuboi, et al. (2008). Effect of strontium in combination with fluoride on enamel remineralisation *in vitro*. **Arch. Oral Biol.**, 53(11), 1017-1022. doi: 10.1016/j.archoralbio.2008.06.005.
- Tiama, T., N. Abd, K. Tohamy and I. Soliman (2017). *In Vitro* Bioactivity and Antibacterial Activity of Zn and Sr Containing Glass Ionomer Cement Prepared by a Quick Alkali-Mediated Sol-Gel Method. **EC Dent. Sci.**, 4, 136-146.
- Tiskaya, M., N. A. Al-eesa, F. S. L. Wong and R. G. Hill (2019). Characterization of the bioactivity of two commercial composites. **Dent. Mater.**, 35(12), 1757-1768. doi: 10.1016/j.dental.2019.10.004.

- Tshabalala, K. G., S. H. Cho, J. K. Park, S. S. Pitale, I. M. Nagpure, R. E. Kroon, et al. (2011). Luminescent properties and X-ray photoelectron spectroscopy study of ZnAl<sub>2</sub>O<sub>4</sub>:Ce<sup>3+</sup>,Tb<sup>3+</sup> phosphor. **J. Alloys. Compd.**, 509(41), 10115-10120. doi: 10.1016/j.jallcom.2011.08.054.
- Tu, X.-m., B.-h. Su and J.-g. Ran (2016). Preparation by sol-gel method and evaluation of lanthanum-containing filling glass ionomer cement powder. **Mater. Lett.**, 183, 236-239. doi: 10.1016/j.matlet.2016.07.108.
- Valliant, E. M., C. A. Turdean-Ionescu, J. V. Hanna, M. E. Smith and J. R. Jones (2012). Role of pH and temperature on silica network formation and calcium incorporation into sol-gel derived bioactive glasses. **Journal of Materials Chemistry**, 22(4), 1613-1619. doi: 10.1039/C1JM13225C.
- Vao-soongnern, V., K. Merat and S. Horpibulsuk (2015). Interaction of the calcium ion with poly(acrylic acid) as investigated by a combination of molecular dynamics simulation and X-ray absorption spectroscopy. **J. Polym. Res.**, 23(1), 7. doi: 10.1007/s10965-015-0895-z.
- Visser, J. H. M. (2018). Fundamentals of alkali-silica gel formation and swelling: Condensation under influence of dissolved salts. **Cem. Concr. Res.**, 105, 18-30. doi: 10.1016/j.cemconres.2017.11.006.
- Wang, Q., P. Li, P. Tang, X. Ge, F. Ren, C. Zhao, et al. (2019). Experimental and simulation studies of strontium/fluoride-codoped hydroxyapatite nanoparticles with osteogenic and antibacterial activities. **Colloids Surf. B**, 182, 110359. doi: 10.1016/j.colsurfb.2019.110359.
- Wang, S., R. Li, D. Xia, X. Zhao, Y. Zhu, R. Gu, et al. (2021). The impact of Zn-doped synthetic polymer materials on bone regeneration: a systematic review. **Stem. Cell. Res. Ther.**, 12(1), 123. doi: 10.1186/s13287-021-02195-y.
- Wang, Y.-L., H.-H. Chang, Y.-C. Chiang, C.-H. Lin and C.-P. Lin (2019). Strontium ion can significantly decrease enamel demineralization and prevent the enamel surface hardness loss in acidic environment. **J. Formos. Med. Assoc.**, 118(1), 39-49. doi: 10.1016/j.jfma.2018.01.001.
- Wang, Z., Y. Shen and M. Haapasalo (2014). Dental materials with antibiofilm properties. **Dent. Mater.**, 30(2), e1-e16. doi: 10.1016/j.dental.2013.12.001.

- Wilson, A. D. and B. E. Kent (1971). The glass-ionomer cement, a new translucent dental filling material. **J. Appl. Chem. Biotechn.**, 21(11), 313-313. doi: 10.1002/jctb.5020211101.
- Wong, A., P. E. Subar and D. A. Young (2017). Dental Caries: An Update on Dental Trends and Therapy. **Adv. Pediatrics**, 64(1), 307-330. doi: 10.1016/j.yapd.2017.03.011.
- Wood, D. and R. Hill (1991). Glass ceramic approach to controlling the properties of a glass-ionomer bone cement. **Biomaterials**, 12(2), 164-170. doi: 10.1016/0142-9612(91)90195-G.
- Wren, A., O. Clarkin, F. Laffir, C. Ohtsuki, I. Y. Kim and M. Towler (2009). The effect of glass synthesis route on mechanical and physical properties of resultant glass ionomer cements. **J. Mater. Sci.: Mater. Med.**, 20, 1991-1999. doi: 10.1007/s10856-009-3781-6.
- Wu, W. and G. H. Nancollas (1997). Kinetics of nucleation and crystal growth of hydroxyapatite and fluorapatite on titanium oxide surfaces. **Colloids Surf. B**, 10(2), 87-94. doi: 10.1016/S0927-7765(97)00054-4.
- Yagoub, M. Y. A., H. C. Swart, L. L. Noto, P. Bergman and E. Coetsee (2015). Surface Characterization and Photoluminescence Properties of Ce(3+),Eu Co-Doped SrF(2) Nanophosphor. **Materials**, 8(5), 2361-2375. doi: 10.3390/ma8052361.
- Ying, J. Y., J. B. Benziger and A. Navrotsky (1993). Structural Evolution of Alkoxide Silica Gels to Glass: Effect of Catalyst pH. **J. Am. Ceram.**, 76(10), 2571-2582. doi: 10.1111/j.1151-2916.1993.tb03983.x.
- Yli-Urpo, H., L. V. J. Lassila, T. Närhi and P. K. Vallittu (2005). Compressive strength and surface characterization of glass ionomer cements modified by particles of bioactive glass. **Dent. Mater.**, 21(3), 201-209. doi: 10.1016/j.dental.2004.03.006.
- Yli-Urpo, H., P. K. Vallittu, T. O. Närhi, A.-P. Forsback and M. Väkiparta (2004). Release of Silica, Calcium, Phosphorus, and Fluoride from Glass Ionomer Cement Containing Bioactive Glass. **J. Biomater. Appl.**, 19(1), 5-20. doi: 10.1177/0085328204044538.

- Yu, L., J. Wu, Q. Zhai, F. Tian, J. Zhao, H. Zhang and W. Chen (2019). Metabolomic analysis reveals the mechanism of aluminum cytotoxicity in HT-29 cells. **PeerJ**, 7, e7524. doi: 10.7717/peerj.7524.
- Zanotto, E. D. (1992). The formation of unusual glasses by sol-gel processing. **J. Non. Cryst. Solids**, 147-148, 820-823. doi: 10.1016/S0022-3093(05)80723-9.
- Zeng, H., F. Ye, X. Li, Q. Jiang, G. Chen, J. Chen and L. Sun (2017). Elucidating the role of AlO<sub>6</sub> -octahedra in aluminum silicophosphate glasses through topological constraint theory. **J. Am. Ceram. Soc.**, 100, 1395-1401. doi: 10.1111/jace.14671.
- Zhang, D., G. Qingjie, Y. Ren, C. Wang, Q. Shi, Q. Wang, et al. (2017). Influence of inversion defects and Cr-Cr pairs on the photoluminescent performance of ZnAl<sub>2</sub>O<sub>4</sub> crystals. **J. Sol-Gel Sci. Technol.**, 1-11. doi: 10.1007/s10971-017-4527-4.
- Zhang, S. and A. Stamboulis (2016). Effect of zinc substitution for calcium on the crystallisation of calcium fluoro-alumino-silicate glasses. **J. Non. Cryst. Solids**, 432, 300-306. doi: 10.1016/j.jnoncrysol.2015.10.025.
- Zhang, Y.-R., W. Du, X.-D. Zhou and H.-Y. Yu (2014). Review of research on the mechanical properties of the human tooth. **Int. J. Oral Sci.**, 6(2), 61-69. doi: 10.1038/ijos.2014.21.



APPENDIX

## APPENDIX A

### List of publications

1. **Thongsri, O.**, Srisuwan, S., Thaitalay, P., Dangwiriyaikul, R., Aengchuan, P., Chanlek, N., Talabnin, C., and Rattanachan, S. T. (2021). Influence of  $Al_2O_3$  and  $P_2O_5$  contents in sol-gel ionomer glass system on the structure and their cement properties. **Journal of Sol-Gel Science and Technology**. 98: 441–451.
2. **Thongsri, O.**, Srisuwan, S., Thaitalay, P., Dangwiriyaikul, R., Aengchuan, P., Chanlek, N., Talabnin, C., and Rattanachan, S. T. (2022). Structural evaluation of ZnO substitution for CaO in glass ionomer cement synthesized by sol-gel method and their properties. **Journal of Materials Science**. 57, 633–650.





## Influence of Al<sub>2</sub>O<sub>3</sub> and P<sub>2</sub>O<sub>5</sub> contents in sol-gel ionomer glass system on the structure and their cement properties

Oranich Thongsri<sup>1</sup> · Sawitri Srisuwan<sup>1</sup> · Paritai Thaitalay<sup>1</sup> · Rawee Dangwiryakul<sup>1</sup> · Prasert Aengchuan<sup>2</sup> · Narong Chanlek<sup>3</sup> · Chutima Talabnin<sup>4</sup> · Sanong Suksaweang<sup>5</sup> · Sirirat Tubsungnoen Rattanachan<sup>1</sup>

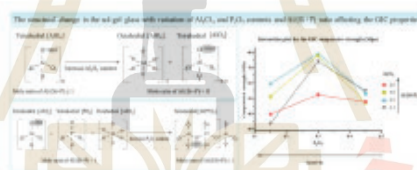
Received: 5 January 2021 / Accepted: 8 March 2021

© The Author(s), under exclusive licence to Springer Science+Business Media, LLC, part of Springer Nature 2021

### Abstract

Glass ionomer dental cement (GIC) is commonly used as a restorative material. The sol-gel synthesis of the ionomer glass is an alternative method, which can produce higher purity and homogeneous at low temperature compared with the traditional melt-quench method. This study synthesized the ionomer glass with the variation of Al<sub>2</sub>O<sub>3</sub> and P<sub>2</sub>O<sub>5</sub> contents in the glass formula by the sol-gel route. The term of Al/(Si+P) ratio was evaluated by XRD and XPS to understand the structural change in the sol-gel glasses. The relationship of the chemical structure of the sol-gel glass, the ions releasing behavior, setting time, and compressive strength of the sol-gel GIC were determined. This study demonstrated that the increase of Al<sub>2</sub>O<sub>3</sub> content in glass formula increased [AlO<sub>4</sub>] octahedron and bridging oxygen (BO) in the glass structure, while the increase of P<sub>2</sub>O<sub>5</sub> content in glass formula led to the increasing of the [AlO<sub>4</sub>] tetrahedron and BO. The sol-gel GIC composition met the maximum compressive strength at Al/(Si+P) = 1.57, whereas the general GIC composition required at Al/(Si+P) nearby 1. Moreover, in vitro cell viability of NIH3T3 fibroblast cells also showed promising result after 2 days culture. This study provided the knowledge for adjusting the sol-gel glass composition for the appropriate properties of GIC.

### Graphical Abstract



**Keyword** Glass ionomer cement · Aluminosilicate glass · Glass composition · Glass network structure · Sol-gel

✉ Sirirat Tubsungnoen Rattanachan  
 sirirat.b@g.sut.ac.th

<sup>1</sup> School of Ceramic Engineering, Institute of Engineering, Suannee University of Technology, Nakhon Ratchasima, Thailand

<sup>2</sup> School of Manufacturing Engineering, Institute of Engineering, Suannee University of Technology, Nakhon Ratchasima, Thailand

<sup>3</sup> Synchrotron Light Research Institute (Public Organization), Nakhon Ratchasima, Thailand

<sup>4</sup> School of Biochemistry, Institute of Science, Suannee University of Technology, Nakhon Ratchasima, Thailand

<sup>5</sup> School of Pathology and Laboratory Medicine, Institute of Medicine, Suannee University of Technology, Nakhon Ratchasima, Thailand

### Highlights

- The variation of  $\text{Al}_2\text{O}_3$  and  $\text{P}_2\text{O}_5$  content in the ionomer glass formula prepared by the sol-gel route was studied.
- XRD and XPS results showed that the glass structural change for the sol-gel glass with the variation of  $\text{Al}_2\text{O}_3$  and  $\text{P}_2\text{O}_5$  contents,  $\text{Al}/(\text{Si}+\text{P})$  ratio affected to the glass ionomer cement (GIC) properties.
- DOE analysis evaluated the interaction effect between  $\text{Al}_2\text{O}_3$  and  $\text{P}_2\text{O}_5$  contents resulting to  $\text{Al}/(\text{Si}+\text{P})$  ratio of 1.57 for the sol-gel glass composition whereas the general GIC composition required at  $\text{Al}/(\text{Si}+\text{P})$  nearby 1.
- This study recommended the adjustment of the sol-gel glass composition for GIC application.

## 1 Background

Glass ionomer cement (GIC) is a well-known material that is useful in the several areas of dentistry such as restorative, basis, or filling. It offers several advantages such as high bioactivity that can form a chemical bond to the dental wet tissue, able to release fluoride causing long-term anti-cariogenic potential, and the low shrinkage of the cement leading to high ability to fill the tooth cavity.

Normally, the commercial ionomer glass is synthesized by the melt-quench method at 1300–1500 °C resulting fluoride loss at 1400 °C and uncontrollable fluoride content in the glass composition [1]. The sol-gel method is based on hydrolysis and condensation reaction, hence, it is possible to prepare homogeneous, high-temperature glasses and glass-ceramics at low temperature, with the controllable doping content in the glass composition [2–4]. For this reason, the sol-gel method becomes more interesting to prepare the ionomer glass because it can control the consistency of the glass composition at low temperature and low energy consumption [5–11]. Even though the sol-gel method has many advantages, this process is sensitive to the synthesis condition, i.e., type of chemical reagent, the thermal history of gel and pH of a sol affecting the structure of final product [3, 6]. Thus, the same glass composition synthesized by the different methods probably provided the different chemical structure, particle size, and homogeneity [6].

The ionomer glass is based on aluminosilicate glass including calcium, phosphorus, and fluoride. Several previous investigations of the melt-derived ionomer glass had reported that the ionomer glass network must be the link of tetrahedral  $[\text{SiO}_4]$  and  $[\text{AlO}_4]$ , which the  $\text{Al}^{3+}$  ions substituted in a site of  $\text{Si}^{4+}$  [12–14]. This substitution resulted in an excessive negative charge in the glass network. Additional positive charge ions (e.g.,  $\text{Ca}^{2+}$ ) were required for neutralizing this charge deficient, leading to the formation of non-bridging oxygen (NBO), which was susceptible to acid attack [11]. In order to maintain the  $[\text{AlO}_4]$  tetrahedron formation, the ratio of  $\text{Al}/(\text{Si}+\text{P})$  is less than or equal to 1, according to the Lowenstein's rule [13, 15]. Interestingly, it has been reported that the ionomer glass with  $\text{Al}/(\text{Si}+\text{P})$  ratio higher than 1 synthesized by the sol-gel method provided the higher compressive strength than that of synthesized by the melt-quenching method [16]. However, there was no report of the relationship

between glass composition and the properties of GIC synthesized by the sol-gel method.

Therefore, this study aimed to investigate the influence of  $\text{Al}_2\text{O}_3$  and  $\text{P}_2\text{O}_5$  content,  $\text{Al}/(\text{Si}+\text{P})$  ratio in glass composition on the glass structure synthesized by the sol-gel method. According to the previous literature of the melt-quenching glass, the glass ionomer in  $4.5\text{SiO}_2\text{-}3.0\text{Al}_2\text{O}_3\text{-}1.5\text{P}_2\text{O}_5\text{-}3\text{CaO}\text{-}2\text{CaF}_2$  glass system, which  $\text{Al}/(\text{Si}+\text{P})$  ratio was 0.8, was commonly prepared [17]. However, there were a few studies on the effect of  $\text{Al}/(\text{Si}+\text{P})$  ratio for the sol-gel glass. Tu and his colleague successfully prepared the sol-gel glass formula of  $4.5\text{SiO}_2\text{-}4.3\text{Al}_2\text{O}_3\text{-}0.15\text{P}_2\text{O}_5\text{-}2\text{Ca}\text{-}\text{F}_2$  which  $\text{Al}/(\text{Si}+\text{P})$  ratio was 1.79 [16]. In this study, the glass formula was designed to determine the effect of  $\text{Al}_2\text{O}_3$  and  $\text{P}_2\text{O}_5$  contents obtaining  $\text{Al}/(\text{Si}+\text{P})$  ratio in a range of 0.74–1.79, which covered the glass composition for both the melt-quenching and the sol-gel process. In addition, the relationship between the sol-gel glass structure and the physical properties of the sol-gel GIC were also determined. This study was designed by  $2^k$  factorial design (Minitab 16 statically software) to evaluate the interaction between  $\text{Al}_2\text{O}_3$  and  $\text{P}_2\text{O}_5$  contents on the properties of the sol-gel GIC. Moreover, the cell viability of NIH/3T3 fibroblast cells was observed for the cytotoxicity test.

## 2 Materials and method

### 2.1 Synthesis of the ionomer glass by the sol-gel method

The composition of the sol-gel ionomer glass of this study was designed and analyzed using  $2^k$  full factorial experimental design by Minitab 16 statistical software. The glass composition based on  $4.5\text{SiO}_2\text{-}X\text{Al}_2\text{O}_3\text{-}Y\text{P}_2\text{O}_5\text{-}2\text{CaO}\text{-}2\text{F}_2$  in the molar ratio was selected, where X was varied of 2, 2.5, 4, and 4.3 moles while Y was varied of 0.15, 0.3, 0.45, and 1.5 moles designed by  $2^k$  factorial design as summarized in Table 1.

Analytical grade of tetraethyl orthosilicate (TEOS, 98%, Acros), aluminum nitrate ( $\text{Al}(\text{NO}_3)_3$ , 98%, Ajax), triethyl phosphate (TEP, 99%, Acros), calcium nitrate tetrahydrate ( $\text{Ca}(\text{NO}_3)_2\cdot 4\text{H}_2\text{O}$ , Ajax), hexafluorosilicic acid ( $\text{H}_2\text{SiF}_6$ , Acros), and absolute ethanol (EtOH, Carlo Erba) were used as the chemical precursors for the sol-gel synthesis of ionomer glass in this study.

**Table 1** The variation of the sol-gel ionomer glass compositions for  $4.5\text{SiO}_2\text{-XAl}_2\text{O}_3\text{-YP}_2\text{O}_5\text{-2CaO}\cdot 2\text{F}_2$  using  $2^3$  factorial design

Sample annotation	Mol ratios		Al/(Si+P) ratio
	$\text{Al}_2\text{O}_3$ (X)	$\text{P}_2\text{O}_5$ (Y)	
2Al-0.15 P	2	0.15	0.83
2.5Al-0.15 P	2.5		1.04
4Al-0.15 P	4		1.67
4.3Al-0.15 P	4.3		1.79
2Al-0.3 P	2	0.3	0.78
2.5Al-0.3 P	2.5		0.98
4Al-0.3 P	4		1.57
4.3Al-0.3 P	4.3		1.69
2Al-0.45 P	2	0.45	0.74
2.5Al-0.45	2.5		0.92
4Al-0.45 P	4		1.48
4.3Al-0.45 P	4.3		1.59

**Fig. 1** Photograph of as-received semi-dry gel with white color obtained by the sol-gel synthesis before calcination.

First, the mixed solution of the TEOS,  $\text{H}_2\text{O}$ ,  $\text{EtOH}$  with a molar ratio of 1:50:10 was prepared using a magnetic stirrer at room temperature [10]. No catalyst was added in this experiment. Next,  $\text{Al}(\text{NO}_3)_3$ , TEP, and  $\text{Ca}(\text{NO}_3)_2\cdot 4\text{H}_2\text{O}$  were sequentially added and mixed by a magnetic stirrer for 30 min. Then, the solution was aged at  $80\text{--}85^\circ\text{C}$  for 15 h. After ageing in the oven for 15 h, the gel was a semi-dry condition and white color as shown in Fig. 1. The dry gel was calcined at  $700^\circ\text{C}$  for 2 h for removing of any organic substances and solvent and rearranging the glass network by heat-treatment. Finally, the obtained glass was ground into the fine powder by the planetary mill using alumina vessele with 10 mm alumina balls at 440 rpm rotation speed for 2 h.

## 2.2 Characterization of the sol-gel ionomer glass

The phase identification of the ionomer glass was analyzed using a German Bruker D2 X-ray diffractometer with a step time of  $0.02^\circ/\text{min}$  and a scan range of  $10\text{--}60^\circ$ . The chemical structure of the sol-gel glass was analyzed

by X-ray photoelectron spectroscopy (XPS, PHI5000 Versa Probe II, ULVAC-PHI, Japan) at the SUT-NANOTEC-SLRI joint research facility, Synchrotron Light Research Institute (SLRI), Thailand. The monochromatic Al K-alpha radiation ( $1486.6\text{ eV}$ ) was used as an excitation source. All binding energies of the samples were calibrated with the C 1s peak at  $284.8\text{ eV}$ . The fitting curved of XPS spectra were processed by PHI MultiPak XPS software using a combination of Gaussian-Lorentzian lines with a fixed value of FWHM.

To determine the ion releasing from the sol-gel ionomer glasses, the sol-gel glass was immersed in 5% acetic acid for the period of times (2, 6, 10, 60, and 1440 min), and filtrated to collect the solution. The concentrations of released ions ( $\text{Si}^{4+}$ ,  $\text{P}^{5+}$ ,  $\text{Al}^{3+}$ , and  $\text{Ca}^{2+}$ ) in the immersed solution were measured by the inductively coupled plasma—optical emission spectrometry (ICP-OES optima 8000, Perkin) for evaluating the susceptibility of the glass to the acid.

## 2.3 Preparation of the sol-gel glass ionomer cement (GIC)

The mixture of the polyacrylic acid (35 wt.% in  $\text{H}_2\text{O}$  PAA; M.W.  $\sim 100,000$ ) and tartaric acid (PAA-TA) in the ratio of 9:1 w/w supplied by Sigma-Aldrich were used as the liquid solution in this study. The mixing ratio for this GIC was set at 1:1 (w/w) for the powder to liquid ratio. The mixture was blended on the clean bench for 40 s before place into the mold for testing.

## 2.4 Setting time and compressive strength testing

The net setting time of the GIC was measured with Gillmore Apparatus (Humboldt, H-3 150F) in accordance with ISO 9917-1 for dental glass polyalkenoate cement. After the mixing of the cement paste, the paste was filled into the cylindrical Teflon mold with 10 mm in diameter and 2 mm in height. The net setting time was started recorded after molding till a heavy and thin needle (453.6 g,  $\varnothing 1.06\text{ mm}$ ) was placed on their surface, and no mark occurred. The setting time was measured in room temperature. The mean value of at least three samples was recorded.

Compressive strength was measured according to ISO 9917-1:2007 using the universal testing machine (UTM, Instron 5565, Instron GmbH, Germany) with 5 kN load cell at a cross speed of  $0.75\text{ mm}/\text{min}$ . The specimens were prepared in the cylindrical shape ( $\varnothing = 4\text{ mm}$ ,  $h = 6\text{ mm}$ ). All the specimens were kept in DI water at  $37^\circ\text{C}$  for 24 h before testing. At least eight specimens were prepared for each experimental condition. The compressive strength was calculated by using the equation,  $\text{CS} = 4P/\pi d^2$ . Where CS was compressive strength (MPa), P was the maximum load applied (N), and d was specimens radius (mm).

## 2.5 Cell viability

The NIH/3T3 fibroblast cell was used as a cell model for cell viability testing. The cells were maintained in culture flask with a complete medium consisting of 44% Dulbecco's Modified Eagle Medium (DMEM (1X) from Invitrogen, USA), 44% F-12 Nutrient mixture (HAM form Invitrogen, USA), 10% Fetal Bovine Serum (FBS from Invitrogen, USA), 1% L-glutamine, and 1% Penicillin streptomycin (Invitrogen, USA). The cells were maintained in an incubator with an atmosphere of 5% CO<sub>2</sub> in air at 37 °C. The medium was exchanged every 48 h.

The sol-gel glass composition of 4Al-0.3P was chosen for cytotoxicity testing. The cement paste was molded in disc shape ( $\phi = 12$  mm,  $h = 2$  mm) at room temperature. After set in the air for 1 h, the cement was sterilized by UV light for 30 min in each side. Consequently, the cement disks were immersed in 1 ml the complete medium and incubated at 37 °C for 5 days. The mediums were collected and changed with fresh medium every 24 h. The blank medium was also incubated with the same condition for using as the negative control. The extracts medium was filtrated using a 0.2  $\mu$ m pore membrane in order to sterilization.

NIH/3T3 fibroblast cells were seeded at  $5 \times 10^3$  cells per well into a 96-well plate and cultured for 24 h. Consequently, the medium was exchanged with 100  $\mu$ l of the GIC extract. Each extract was tested in triplicate. Cells were further incubated at 37 °C in a 5% CO<sub>2</sub> incubator for 24 h. The cell viability was determined by MTS assay (CellTiter 96<sup>®</sup> AQueous). The MTS assay protocol was performed by adding 20  $\mu$ l of the MTS reagent directly into the cell culture then incubated in the darkroom at 37 °C in a 5% CO<sub>2</sub> for 2 h. The optical density of each well was determined on a microplate reader at 490 nm (O.D.490). The percentage of viable cells was calculated from O.D. values using the following equation [18]:

$$\% \text{Cell viability} = \left( \frac{\text{Sample absorbance value}}{\text{Control group absorbance value}} \right) \times 100$$

## 3 Results and discussions

### 3.1 Structural analysis and ions releasing from the sol-gel ionomer glasses

In the sol-gel synthesis of glass, the calcination temperature was important to the glass structure. In our preliminary study, the as-received gel was calcined at various temperatures. The results showed that the lower temperature could not convert gel to an appropriated glass structure which could not use as GIC. When the gel was calcined at high temperature (>700 °C), it found the phase separation and

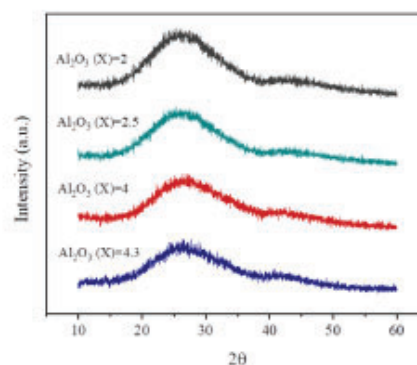


Fig. 2 XRD patterns of the sol-gel ionomer glasses belonging to  $4.5\text{SiO}_2\text{-XAl}_2\text{O}_3\text{-}0.3\text{P}_2\text{O}_5\text{-}2\text{CaO}\text{-}2\text{F}_2$  glass system, where X = 2, 2.5, 4, and 4.3.

crystal formation which affected to setting reaction of GIC. According to Taira's report and our preliminary study, the gel calcined at 700 °C for 2 h was fully converted to ionomer glass [10]. Therefore, the calcination temperature was selected at 700 °C for 2 h for the best condition in this study.

### 3.2 Effect of Al<sub>2</sub>O<sub>3</sub> contents in the sol-gel ionomer glass composition

The effect of Al<sub>2</sub>O<sub>3</sub> contents in the ionomer glasses,  $4.5\text{SiO}_2\text{-XAl}_2\text{O}_3\text{-}0.3\text{P}_2\text{O}_5\text{-}2\text{CaO}\text{-}2\text{F}_2$  composition, where X = 2, 2.5, 4, and 4.3 moles, were investigated in this study. XRD patterns of the sol-gel glasses with the different of Al<sub>2</sub>O<sub>3</sub> contents are illustrated in Fig. 2. All sol-gel glasses presented a broad diffraction peak at  $2\theta$  of 20–40° indicating that the main phase of the sol-gel glass was amorphous. This XRD pattern showed the amorphous of aluminosilicate glass characteristic, which presented broad band at  $2\theta$  of 20–40° and 40–50° [5, 19]. In addition, the second broad band at  $2\theta$  of 40–50° could be indicated that the sol-gel glass was high structural-disorder material, consistent to radial distribution function (RDF) [20].

The chemical structure of the sol-gel glasses was investigated using XPS technique. Figure 3a shows the high-resolution spectra in the Al2p region for the sol-gel glasses. The Al2p peaks can be deconvoluted into two main peaks at the binding energies of 74 eV and 75.5 eV indicating to the occupied site of Al<sup>3+</sup> ions, which are the [AlO<sub>4</sub>] tetrahedral and [AlO<sub>6</sub>] octahedral site, respectively [21]. The percentages of [AlO<sub>4</sub>] tetrahedral and [AlO<sub>6</sub>] octahedral site was calculated from the area of the deconvoluted peaks [22]. The result showed that the sol-gel glass with 2 moles of Al<sub>2</sub>O<sub>3</sub> revealed a high fraction of tetrahedral site whereas

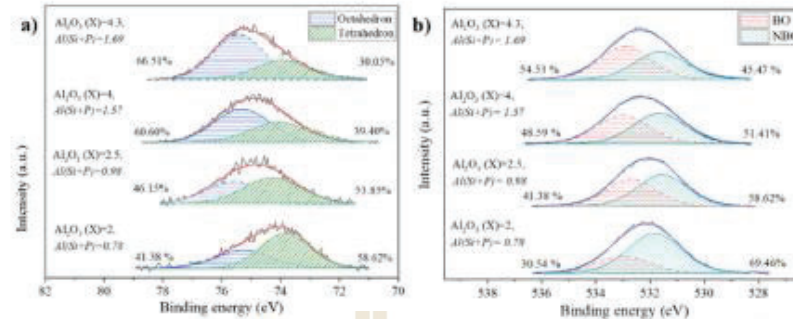


**Fig. 3** High resolution XPS spectra in the (a) Al2p and (b) O1s regions of the sol-gel ionomer glasses belonging to  $4.5\text{SiO}_2\text{-XAl}_2\text{O}_3\text{-}0.3\text{P}_2\text{O}_5\text{-}2\text{CaO-}2\text{F}_2$  glass system, where  $X = 2, 2.5, 4, \text{ and } 4.3$ .

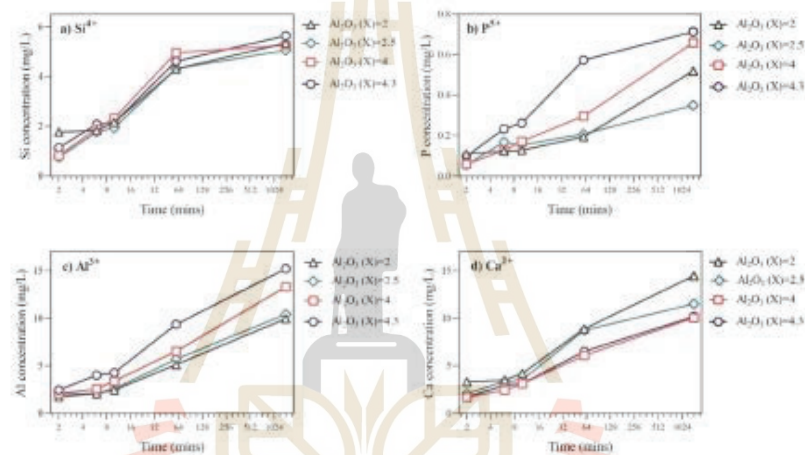


**Fig. 4** The concentration of (a)  $\text{Si}^{4+}$ , (b)  $\text{P}^{5+}$ , (c)  $\text{Al}^{3+}$ , and (d)  $\text{Ca}^{2+}$  ions releasing from the sol-gel ionomer glasses belonging to  $4.5\text{SiO}_2\text{-XAl}_2\text{O}_3\text{-}0.3\text{P}_2\text{O}_5\text{-}2\text{CaO-}2\text{F}_2$  system, where  $X = 2, 2.5, 4, \text{ and } 4.3$ , as function of the immersion times

the sol-gel glasses with  $\text{Al}_2\text{O}_3$  mole of 4 and 4.3 presented a higher fraction of the octahedral site.

Figure 3b illustrates the high-resolution XPS spectra in the O1s region of the sol-gel glasses. The spectra showed the characteristics of bridging oxygen (BO) and non-bridging oxygen (NBO) in the sol-gel structure. The deconvoluted O1s peak at the binding energy of around 532.5 eV was assigned to the BO in Si-O-Si unit, while the peak at the binding energy of around 531.6 eV was associated with the NBO [22]. The result showed that the fraction of NBO structure was reduced when the  $\text{Al}_2\text{O}_3$  content increased.

The ions releasing behavior in acetic acid for the sol-gel glass with various  $\text{Al}_2\text{O}_3$  contents were determined as the period of times as shown in Fig. 4a revealed that the concentration of  $\text{Si}^{4+}$  ions from all glasses increased with time. At 2 min of soaking time, the glass with  $\text{Al}_2\text{O}_3$  of 2 moles presented the highest level of the  $\text{Si}^{4+}$  ion, which related to the highest NBO structure in the glass network. However, no significant difference of the  $\text{Si}^{4+}$  ions releasing was observed after 6 min of soaking time.

The releasing level of the  $\text{P}^{5+}$  ion increased with the content of  $\text{Al}_2\text{O}_3$  in the glass composition and the immersion time as shown in Fig. 4b. The similar trend also found

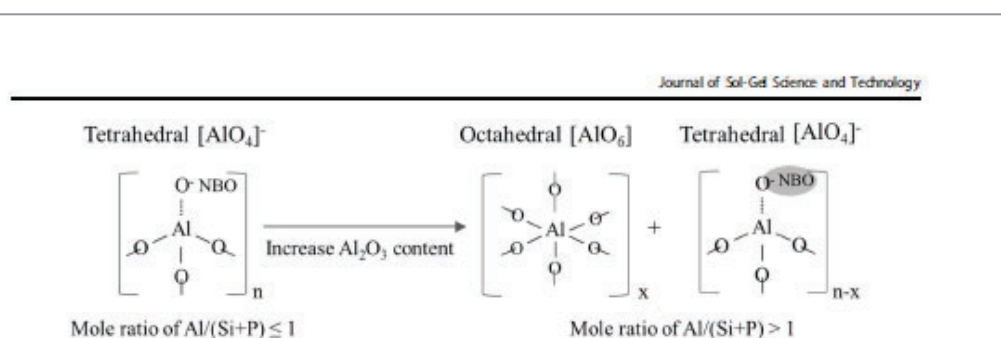


Fig. 5 A proposed glass network structure for sol-gel ionomer glass with a variation of  $Al_2O_3$  contents in the glass composition.

in Fig. 4c that illustrated the concentrations of  $Al^{3+}$  ions released from the sol-gel glasses.

Interestingly, the highest concentration of  $Ca^{2+}$  ions was found for the sol-gel glass with low  $Al_2O_3$  ( $X = 2$  moles). Meanwhile, the sol-gel glasses with  $Al_2O_3$  moles of 4 and 4.3 released significantly low  $Ca^{2+}$  ions as shown in Fig. 4d.

The structural unit of the general silicate glass structure is formed in  $SiO_4$  tetrahedral units, which are connected by sharing one corner bridging oxygen (BO). The addition of  $Al_2O_3$  into pure  $SiO_2$  glass network led to the substitution of the  $Al^{3+}$  ions in a tetrahedral site of  $Si^{4+}$  ions. This substitution of  $Al^{3+}$  ions in the tetrahedral site of the glass network would happen where the  $Al/(Si+P)$  ratio was less than or equal to 1, according to the Lowenstein's rule [13]. Whereas at  $Al/(Si+P)$  ratio  $> 1$ , the excessive  $Al^{3+}$  ions would be formed in  $[AlO_6]$  octahedral site [23]. Many previous works reported that  $[AlO_4]$  tetrahedral unit in the glass structure led to susceptibility to acid attack [12]. The high acid susceptible glass can release the high metal ions ( $Al^{3+}$  and  $Ca^{2+}$  ions) concentration for cross-linking with  $-COOH$  group of the polyacid following by extension of the polysalt network of GIC [24].

According to the background of the melt-derived glass at  $Al/(Si+P)$  less than or equal to 1, the increasing of  $Al_2O_3$  content in the glass composition should be accompanied by increasing NBO structure [12–14, 25]. However, our sol-gel glass at  $Al/(Si+P)$  ratio in a range of 0.74–1.79 showed the different structure which increasing of  $Al_2O_3$  content reduced the fraction of NBO structure, as shown in Fig. 3. It was noted that the thermal history of the synthesis process strongly affected the glass network structure [3]. In the sol-gel process, the network formation was proceeded gradually by polymerization reaction at a low temperature then achieved by calcination. This allowed the glass network to rearrange, then the excessive  $Al^{3+}$  ions (high  $Al/(Si+P)$  ratio) which formed in  $[AlO_6]$  octahedral site could connect to the glass network as a network former through BO structure [26]. Therefore, the fraction of BO structure was increased then the fraction of NBO structure was reduced in the glass network structure in this study.

According to our finding, the increasing of  $Al_2O_3$  content in the glass composition to  $Al/(Si+P) > 1$  resulted in the formation of  $[AlO_6]$  octahedron and the BO structure. The change of expected glass network structure for a variation of  $Al_2O_3$  contents in the sol-gel GIC was illustrated in Fig. 5.

It can be indicated that the increase of Al content resulted to the structural changing from  $[AlO_4]$  tetrahedron (CN = 4) to  $[AlO_6]$  octahedron (CN = 6) and decreased the fraction of NBO. The decreasing of NBO structure in the glass network could lead to poor acid susceptibility of the glass which was determined in term of the ions releasing level in acid solution in the previous report [27]. Our finding presented that the glass with  $Al/(Si+P) > 1$  released a high amount of  $Al^{3+}$  ions even though there were lower tetrahedral species than the octahedral species. This could be assumed that the  $Al^{3+}$  ion could be released from the octahedral site, which might be a benefit for the setting reaction.

$Ca^{2+}$  ions were a glass network modifier to charge balancing with  $[AlO_4]$  tetrahedron in the glass structure and created NBO in glass network trending to acid susceptibility. The high releasing level of  $Ca^{2+}$  ions from the glass with  $X = 2$  moles possibly resulted from the presence of NBO in the glass structure. In addition, the glass with higher  $Al_2O_3$  ( $X = 4$  and 4.3) exhibited a lower fraction of NBO structure,  $Ca^{2+}$  ions released from the glass was lower.

### 3.3 Effect of $P_2O_5$ content in the sol-gel ionomer glass composition

Figure 6 shows XRD patterns of the sol-gel ionomer glasses based on  $4.5SiO_2-4Al_2O_3-YP_2O_5-2CaO-2F_2$  compositions, where  $Y = 0.15, 0.3, \text{ and } 0.45$  moles. The XRD patterns of the sol-gel glasses with different amount of  $P_2O_5$  indicated amorphous characteristics.

The high-resolution XPS spectra in the  $Al2p$  and  $O1s$  regions were presented in Fig. 7a, b, respectively. It was found that the tetrahedral  $[AlO_4]$  structure increased with the increasing of  $P_2O_5$  contents in the glass composition.

This indicated that the  $[\text{AlO}_6]$  octahedron structure was dominated for the sol-gel glass with  $\text{P}_2\text{O}_5$  from 0.15 moles.

The O1s peak in Fig. 7b reveals the fraction of BO and NBO in the ionomer glass structure. The result demonstrated that the NBO fraction reduced when the  $\text{P}_2\text{O}_5$  content in the glass composition increased.

The concentrations of ions releasing for  $\text{Si}^{4+}$ ,  $\text{Al}^{3+}$ , and  $\text{Ca}^{2+}$  ion concentrations from the sol-gel glasses were increased with the period of immersion times while all ions releasing significantly decreased with increasing of  $\text{P}_2\text{O}_5$  in the glass composition as shown in Fig. 8a, c and d, respectively. This result could be indicated that the acid susceptibility of the glass was reduced with increasing of  $\text{P}_2\text{O}_5$  content in the glass composition relating to the low amount of NBO.

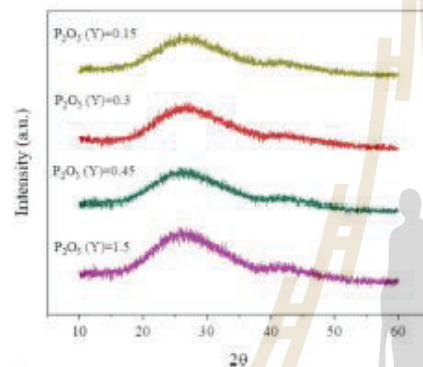


Fig. 6 XRD pattern of the sol-gel ionomer glasses belonging to  $4.5\text{SiO}_2\cdot 4\text{Al}_2\text{O}_3\cdot \text{Y}\text{P}_2\text{O}_5\cdot 2\text{CaO}\cdot 2\text{F}_2$  glass compositions, where  $Y = 0.15, 0.3, 0.45, \text{ and } 1.5$ .

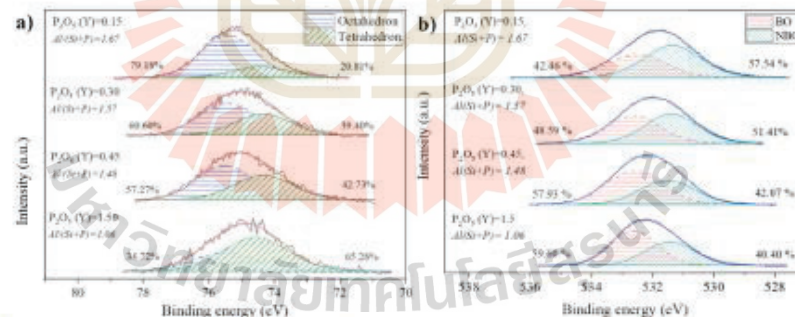


Fig. 7 High resolution XPS spectra in the (a)  $\text{Al}2p$  and (b)  $\text{O}1s$  regions of the sol-gel ionomer glasses based on  $4.5\text{SiO}_2\cdot 4\text{Al}_2\text{O}_3\cdot \text{Y}\text{P}_2\text{O}_5\cdot 2\text{CaO}\cdot 2\text{F}_2$  glass compositions, where  $Y = 0.15, 0.3, 0.45, \text{ and } 1.5$ .

Figure 8b presents that there was no significant difference in the  $\text{P}^{3+}$  ions releasing in the acid solution for the sol-gel glasses with  $\text{P}_2\text{O}_5$  in the range of 0.15–0.45 moles. However, the  $\text{P}^{3+}$  ions releasing tended to significantly increasing for the sol-gel glass with  $\text{P}_2\text{O}_5$  up to 1.5 moles.

$\text{P}^{3+}$  ions acted as a network former in glass network and formed  $[\text{PO}_4]$  tetrahedron with one double bond [23, 28]. When the  $\text{P}^{3+}$  ions were added to the aluminosilicate based glass, it preferred to share the valence electron with  $\text{Al}^{3+}$  ions. Consequently, the linking formation between  $[\text{AlO}_4]$  and  $[\text{PO}_4]$  tetrahedra connected by sharing one corner bridging oxygen (BO). It can be indicated that the increase of  $\text{P}_2\text{O}_5$  content resulted to the structural changing form  $[\text{AlO}_6]$  octahedron (CN = 6) to  $[\text{AlO}_4]$  tetrahedron (CN = 4) resulting in the reduction of NBO fraction in the glass structure, as illustrated in Fig. 9.

### 3.4 Setting time and compressive strength of the sol-gel GICs

The interaction between  $\text{Al}_2\text{O}_3$  and  $\text{P}_2\text{O}_5$  in the sol-gel glass composition on the setting time and compressive strength was studied using DOE technique [29]. This study was designed and analyzed using  $2^k$  full factorial experimental design by the Minitab Release 16 program as presented in Table 1.

Figure 10a shows ANOVA test for the net setting times of the sol-gel GIC with the variance of  $\text{Al}_2\text{O}_3$  and  $\text{P}_2\text{O}_5$  contents in the glass compositions, respectively. The significant effects on the net setting times of the sol-gel GIC were determined at 95% confidence level ( $P \leq 0.05$ ). The results revealed that the net setting time was not significantly affected by the variation of the  $\text{Al}_2\text{O}_3$  contents ( $P = 0.058$ ). Meanwhile, the variation of  $\text{P}_2\text{O}_5$  contents and the interaction between  $\text{Al}_2\text{O}_3$  and  $\text{P}_2\text{O}_5$  showed significant

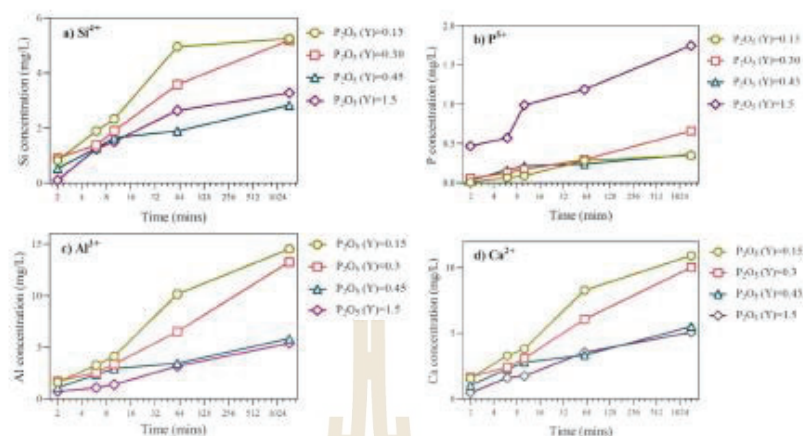


**Fig. 8** The concentration of (a) Si<sup>4+</sup>, (b) P<sup>5+</sup>, (c) Al<sup>3+</sup>, and (d) Ca<sup>2+</sup> ions releasing from the sol-gel ionomer glasses based on 4.5SiO<sub>2</sub>-4Al<sub>2</sub>O<sub>3</sub>-YP<sub>2</sub>O<sub>5</sub>-2CaO-2F<sub>2</sub> compositions, where Y = 0.15, 0.3, 0.45, and 1.5, as function of the immersion times.

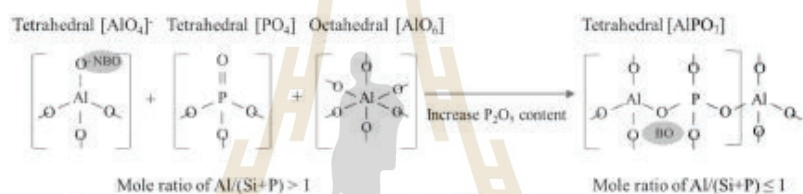


**Fig. 9** A proposed glass network structure for sol-gel ionomer glass with a variation of P<sub>2</sub>O<sub>5</sub> contents in the glass composition.

influence on the net setting time ( $P = 0.000$ ). The main effect plot in Fig. 10b showed that the net setting time was drastically depended on the P<sub>2</sub>O<sub>5</sub> content whereas that did not depend on the Al<sub>2</sub>O<sub>3</sub> content in the sol-gel glass composition. The graphs of the interaction plot in Fig. 10c confirmed the interaction of the two parameters (Al<sub>2</sub>O<sub>3</sub> and P<sub>2</sub>O<sub>5</sub> variation) in the glass structure. The net setting time of the sol-gel glasses with Al<sub>2</sub>O<sub>3</sub> moles varied from 3, 4.0, and 4.3 moles showed significantly increased with the interaction of P<sub>2</sub>O<sub>5</sub> moles varied from 0.15, 0.30, and 0.45 as shown in Fig. 10e. Interestingly, there was no significant effect on the net setting time for the sol-gel glass with the interaction between 2 moles of Al<sub>2</sub>O<sub>3</sub> and 0.15–0.30 moles of P<sub>2</sub>O<sub>5</sub>. In contrast, the net setting time of the interaction between 2 moles of Al<sub>2</sub>O<sub>3</sub> and 0.45 moles of P<sub>2</sub>O<sub>5</sub> was rapidly increased. The setting time of the sol-gel with increasing of P<sub>2</sub>O<sub>5</sub> content showed longer due to the low susceptibility to the acid attack of the glass. This result was similar to Griffin and Hill work that the melt-quenched glass

with increasing of P<sub>2</sub>O<sub>5</sub> moles in glass composition led to longer setting time while that glass composition without P<sub>2</sub>O<sub>5</sub> mole was rapidly setting [17].

Figure 11a reveals the ANOVA test for the compressive strength of the sol-gel GIC with the different Al<sub>2</sub>O<sub>3</sub> and P<sub>2</sub>O<sub>5</sub> moles. The result demonstrated that both of Al<sub>2</sub>O<sub>3</sub> and P<sub>2</sub>O<sub>5</sub> contents and the interaction among them had significant affected on the compressive strength of the sol-gel GIC at 95% confidence level ( $P \leq 0.05$ ).

Figure 11b illustrates the main effect plot for the compressive strength on the effect of Al<sub>2</sub>O<sub>3</sub> and P<sub>2</sub>O<sub>5</sub> moles variation in the sol-gel glass composition. The result showed that the compressive strength reached a maximum at 4 moles of Al<sub>2</sub>O<sub>3</sub> and 0.3 moles of P<sub>2</sub>O<sub>5</sub>, then the further increase in Al<sub>2</sub>O<sub>3</sub> and P<sub>2</sub>O<sub>5</sub> could be caused in a reduction of the compressive strength. The reduction of compressive strength at 0.45 mole of P<sub>2</sub>O<sub>5</sub> was due to the decrease of Ca<sup>2+</sup> and Al<sup>3+</sup> released ions during setting reaction as discussed above, while the reduction of compressive strength at 4.3 moles of

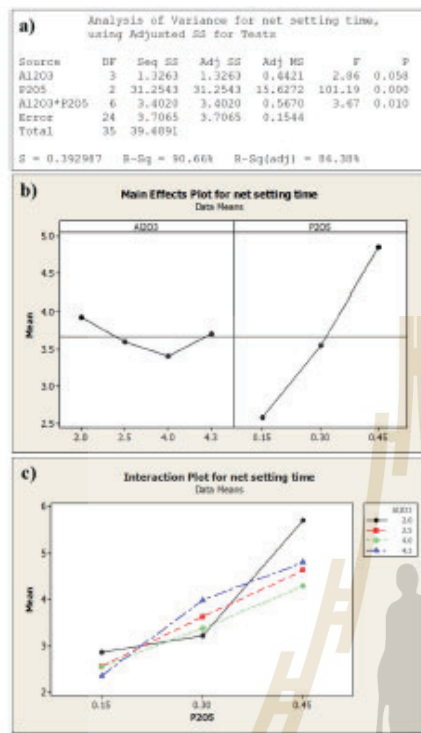


**Fig. 10** The DOE analysis for the net setting times of the sol-gel GIC with Al<sub>2</sub>O<sub>3</sub> and P<sub>2</sub>O<sub>5</sub> variation. (a) ANOVA analysis of variance, (b) the main effects plot and (c) the interaction plot of Al<sub>2</sub>O<sub>3</sub> and P<sub>2</sub>O<sub>5</sub> contents in glass compositions for the net setting times of the sol-gel derived GICs.

Al<sub>2</sub>O<sub>3</sub> was consistent to an error of data due to rapidly set of GIC obtaining a non-homogeneous sample.

Figure 11c shows the interaction plot for the compressive strength on the effect of Al<sub>2</sub>O<sub>3</sub> and P<sub>2</sub>O<sub>5</sub> contents variation in the sol-gel glass composition. All non-parallelism of the lines indicated strong interaction between the variation of Al<sub>2</sub>O<sub>3</sub> and P<sub>2</sub>O<sub>5</sub> contents. The result confirmed that the highest compressive strength of the sol-gel GIC was found for 4 moles of Al<sub>2</sub>O<sub>3</sub> and 0.3 moles of P<sub>2</sub>O<sub>5</sub>. Therefore, the compressive strength was significantly affected by both factors of Al<sub>2</sub>O<sub>3</sub> and P<sub>2</sub>O<sub>5</sub> moles in the sol-gel glass composition.

This study found that Al<sub>2</sub>O<sub>3</sub> content in glass composition was significantly affected by the compressive strength of GIC as not related to the previous report [30]. This study revealed that the compressive strength was improved with

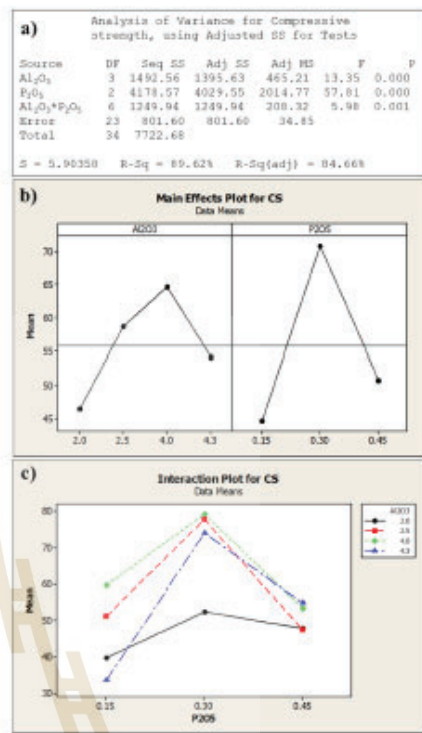


**Fig. 11** The DOE analysis for the compressive strength of the sol-gel GIC with Al<sub>2</sub>O<sub>3</sub> and P<sub>2</sub>O<sub>5</sub> variation. (a) ANOVA analysis, (b) the main effects plot, and (c) the interaction plot of Al<sub>2</sub>O<sub>3</sub> and P<sub>2</sub>O<sub>5</sub> contents in glass compositions for the compressive strength of the sol-gel derived GICs.

Al/(Si+P) ratio in glass composition >1. This could occur by the three-dimensional crosslinking networks of Al<sup>3+</sup> ions after reacting with the polymeric liquid [31].

Since the GIC prepared from the sol-gel glass with P<sub>2</sub>O<sub>5</sub> (Y) = 0.15 was difficult to mold for uniform test specimens due to rapid set, the compressive strength provided low as compared to others. The improving of the compressive strength of GIC depended on the Al<sup>3+</sup> and Ca<sup>2+</sup> ions releasing during the setting reaction. When increasing of P<sub>2</sub>O<sub>5</sub> content in the glass composition, Al<sup>3+</sup> and Ca<sup>2+</sup> ions releasing trended to decrease as the result in Fig. 8a, b, respectively. Moreover, excessive releasing of those ions could affect to rapid setting and difficult to handle. Thus, the optimum of ions releasing should be considered for suitable properties of GIC. In this study, the sol-gel glass

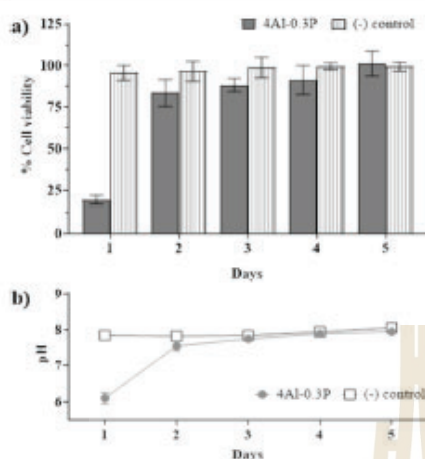


**Fig. 12** (a) Cell viability of NIH/3T3 fibroblast cells treated with extract solution of 4Al-0.3P sol-gel GIC and (b) pH values of the extracted solution at various immersion times (1, 2, 3, 4 and 5 days). The control was the blank medium. Values are expressed as the mean  $\pm$  standard error of the mean of three independent experiments.

with 0.3 moles of  $P_2O_5$  and 0.4 moles of  $Al_2O_3$  was the compromised glass composition for setting and sufficient compressive strength. It was indicated that the interaction between  $Al_2O_3$  and  $P_2O_5$  contents influenced the properties of GIC and Al(Si+P) ratio might not be equal to 1 for the glass synthesized by the sol-gel method.

In this study, the best formula of the sol-gel ionomer glass was prepared with Al(Si+P) = 1.57. Therefore, it indicated that the Al(Si+P) ratio nearby 1 should not be fixed for the sol-gel glass synthesis.

### 3.5 Cell viability

The cytotoxicity of dental materials should be fully understood because of the possibility of indirect contact between their components and pulp cells. Residual components released from these materials may diffuse through the dentinal tubules and reach the subjacent odontoblast layer. According to the compressive strength result in this study, the most remarkable GIC was prepared with the sol-gel glass with 4 moles of  $Al_2O_3$  and 0.3 moles of  $P_2O_5$  (4Al-0.3P). Figure 12 showed cell viability of NIH/3T3 fibroblast cells after incubating for 24 h with the extract of the sol-gel GIC of 4Al-0.3P. The MTS assay demonstrated that the cell viability of NIH/3T3 fibroblast cells was increased with a period of times. The cell viability for the 4Al-0.3P sol-gel GIC exhibited low on the first day, but it was increased after 2 days of incubation.

In addition, the pH of the extracted mediums at the periods of 1, 2, 3, 4, and 5 days was evaluated to understand the cytotoxicity effect of the GIC samples, as shown in Fig. 12b. At 1 day, the pH of the extract medium (pH 6.2) was much lower than that of the blank (pH 7.8). After 2 days of immersion, the extracted pH was continuously increased to the normal as similar to the blank control. This result could be explained that the low cell viability on the first days depended on the low pH of the extracted medium, which might result from the organic compounds released from the GIC, as reported in the previous literature [32]. During the setting reaction, it was possible that the crosslinking between PAA and the metal ion was not complete at the first stage. Thus, the residual PAA could be released into the extracted medium resulting in low pH value of the extracted medium.

## 4 Conclusions

This study presented an effect of the optimization of  $Al_2O_3$  and  $P_2O_5$  contents in the glass composition synthesized by the sol-gel method for GIC. The result showed that the compressive strength of the sol-gel GIC could be improved by the increase of  $Al_2O_3$  in the glass formula, even though the structure composed of the high fraction of  $[AlO_6]$  octahedron and BO. On the other hand, the setting reactivity could be controlled by the  $P_2O_5$  content in the glass. The increase of  $P_2O_5$  led to increasing of  $[AlO_4]$  tetrahedron and BO resulting in the extension of setting time and lowering compressive strength. The GIC with maximum compressive strength was prepared with the composition of 4.0 moles  $Al_2O_3$  and 0.3 moles  $P_2O_5$  (Al(Si+P) = 1.57). The interaction between the  $Al_2O_3$  and  $P_2O_5$  contents in glass composition on the setting time and compressive strength was confirmed by the DOE analysis. In addition, the cytotoxicity test of the sol-gel GIC showed good cell viability on the NIH/3T3 fibroblast cell line. These finding suggested a promising result, which was an advantage for the development of sol-gel glass synthesis for the GIC application.

**Acknowledgements** This work was financial supported by the Royal Golden Jubilee (RGJ) PhD Program PHD0058/2558 from Thailand Research Fund and Suranaree University of Technology. The author would like to thank the local contract at the beamline 5.3 SUT-NANOTEC-SLRI joint research facility, Synchrotron Light Research Institute (SLRI), Thailand for their help in the data analysis.

**Funding** This work was financial supported by the Royal Golden Jubilee (RGJ) PhD Program from Thailand Research Fund (PHD/0058/2558) and Suranaree University of Technology.

### Compliance with ethical standards

**Conflict of Interest** The authors declare no competing interests.

**Publisher's note** Springer Nature remains neutral with regard to jurisdictional claims in published maps and institutional affiliations.

## References

- Ju J, Ji G, Tang C, Yang K, Zhu Z (2020) Investigation of fluoride evaporation from  $\text{CaF}_2\text{-CaO-Al}_2\text{O}_3\text{-MgO-TiO}_2\text{-(Li}_2\text{O)}$  slag for electroslag remelting. *Sci Rep* 10(1):12284. <https://doi.org/10.1038/s41598-020-69283-6>
- Kajihara K (2013) Recent advances in sol-gel synthesis of monolithic silica and silica-based glasses. *J Asian Ceram Soc* 1(2):121–133. <https://doi.org/10.1016/j.jascer.2013.04.002>
- Mukhejee SP (1980) Sol-gel processes in glass science and technology. *J Non Cryst Solids* 42(1):477–488. [https://doi.org/10.1016/0022-3093\(80\)90046-0](https://doi.org/10.1016/0022-3093(80)90046-0)
- Eickert H (2018) Structural characterization of bioactive glasses by solid state NMR. *J Sol-Gel Sci Technol* 88(2):263–295. <https://doi.org/10.1007/s10971-018-4795-7>
- Bertolini MJ, Zaghe MA, Gimenes R, Padovani GC, Cruz CAS (2009) Preparation and evaluation of an experimental luting glass ionomer cement to be used in dentistry. *J Mater Sci: Mater Med* 20(9):1781–1785. <https://doi.org/10.1007/s10856-009-3748-7>
- Cestari A (2016) Sol-gel methods for synthesis of aluminosilicates for dental applications. *J Dent* 55:105–113. <https://doi.org/10.1016/j.jdent.2016.10.012>
- Fujihara S (2018) Sol-Gel processing of fluoride and oxyfluoride materials. In: Klein L, Aparicio M, Jitani A (eds) *Handbook of Sol-Gel science and technology: processing, characterization and applications*. Springer International Publishing, Cham, pp 333–359. [https://doi.org/10.1007/978-3-319-32101-1\\_10](https://doi.org/10.1007/978-3-319-32101-1_10)
- Pipronti T, Clare CK, Berndt G, de Campos EA, Fernandes MHV, de Campos SD (2019) Glass ionomer cements based in  $\text{TaO}_2$  by Sol-gel method. *Orbital: Electron J Chem* 11(1):1–9. <https://doi.org/10.17807/orbital.v11i1.1176>
- Pierre AC (2019) From random glass networks to random silica gel networks and their use as host for biocatalytic applications. *J Sol-Gel Sci Technol* 90(1):172–186. <https://doi.org/10.1007/s10971-018-4798-4>
- Taira M, Yamaki M (1995) Preparation of  $\text{SiO}_2\text{-Al}_2\text{O}_3$  glass powders by the sol-gel process for dental applications. *J Mater Sci: Mater Med* 6(4):197–200. <https://doi.org/10.1007/bf00146855>
- Winn A, Clarin O, Laffr F, Ohtsuki C, Kim IY, Towler M (2009) The effect of glass synthesis route on mechanical and physical properties of resultant glass ionomer cements. *J Mater Sci: Mater Med* 20:1991–1999. <https://doi.org/10.1007/s10856-009-3781-6>
- Bertolini MJ, Zaghe MA, Gimenes R (2005) Development of an experimental glass ionomer cement containing niobium and fluoride. *J Non Cryst Solids* 351(52):3884–3887. <https://doi.org/10.1016/j.jnoncrysol.2005.10.008>
- Stamboulis A, Hill RG, Law RV (2004) Characterization of the structure of calcium aluminosilicate and calcium fluoro-aluminosilicate glasses by magic angle spinning nuclear magnetic resonance (MAS-NMR). *J Non Cryst Solids* 333(1):101–107. <https://doi.org/10.1016/j.jnoncrysol.2003.09.049>
- Nicholson J, Czarnicka B (2016) 6 - Conventional glass-ionomer cements. In: *Materials for the Direct Restoration of Teeth*. Woodhead Publishing, pp 107–136. <https://doi.org/10.1016/B978-0-08-100491-3.00006-4>
- Loewenstein W (1954) The distribution of aluminum in the tetrahedra of silicates and aluminates. *Am Miner* 39(1-2):92–96
- Tu X-m, Su B-h, Ran J-g (2016) Preparation by sol-gel method and evaluation of lanthanum-containing filling glass ionomer cement powder. *Mater Lett* 183:236–239. <https://doi.org/10.1016/j.matlet.2016.07.108>
- Griffin SG, Hill RG (2000) Influence of glass composition on the properties of glass polyalkenoate cements. Part II: influence of phosphate content. *Biomaterials* 21(4):399–403. [https://doi.org/10.1016/S0142-9612\(99\)00202-1](https://doi.org/10.1016/S0142-9612(99)00202-1)
- Kamalak H, Kamalak A, Taghizadeh ghaleh joughi A, Hasmithoglu A, Naki KA (2018) Cytotoxic and biological effects of bulk fill composites on rat cortical neuron cells. *Odontology* 106(4):377–388. <https://doi.org/10.1007/s10266-018-0354-5>
- Rampe E, Bish DL, Chipera S, Morris R, Achilles C et al. (2013) Detecting nanophase weathering products with ChemMin: reference intensity ratios of allophane aluminosilicate gel, and ferrihydrite. Paper presented at the 44th Lunar and Planetary Science Conference, The Woodlands Waterway Marriott Hotel and Convention Center, The Woodlands, Texas
- Hu ZQ, Wang AM, Zhang HF (2017) Chapter 22 - Amorphous Materials. In: Xu R, Xu Y (eds) *Modern inorganic synthetic chemistry*, 2nd edition. Elsevier, Amsterdam, pp 641–667. <https://doi.org/10.1016/B978-0-444-63591-4.00022-7>
- Duan X, Wang X, Yu F, Yuan D (2012) Effects of annealing temperature and  $\text{SiO}_2$  matrix on the structure and optical properties of Co-Doped  $\text{ZnAl}_2\text{O}_4/\text{SiO}_2$  Nano-glass-Ceramic Composites. *J Phys Chem C* 116(3):2313–2321. <https://doi.org/10.1021/jp209837q>
- Roy B, Jain H, Saha SK, Chakravorty D (1995) Comparison of structure of alkali silicate glasses prepared by sol-gel and melt-quench methods. *J Non Cryst Solids* 183(3):268–276. [https://doi.org/10.1016/0022-3093\(94\)00633-4](https://doi.org/10.1016/0022-3093(94)00633-4)
- scholze H. (1964) *Glass: nature, structure, and properties*. englische Übersetzung der 3. deutschen Auflage, 1991 Springer-Verlag, New York, Berlin, Heidelberg. <https://doi.org/10.1002/bbpc.19910951166>
- Lobhauer U (2010) Dental glass ionomer cements as permanent filling materials? - Properties, limitations and future trends. *Materials* 3(1):76–96. <https://doi.org/10.3390/ma3010076>
- Zeng H, Ye F, Li X, Jiang Q, Chen G, Chen J, Sun L (2017) Elucidating the role of  $\text{AlO}_6$ -octahedra in aluminum silicophosphate glasses through topological constraint theory. *J Am Ceram Soc* 100:1395–1401. <https://doi.org/10.1111/jace.14671>
- Brow RK, Kirkpatrick RJ, Turner GL (1993) Nature of alumina in phosphate glass: II. structure of sodium aluminophosphate glass. *J Am Ceram Soc* 76(4):919–928. <https://doi.org/10.1111/j.1151-2916.1993.tb05316.x>
- Nicholson JW, Czarnicka B (2009) Review paper: role of aluminum in glass-ionomer dental cements and its biological effects. *J Biomat Appl* 24(4):293–308. <https://doi.org/10.1177/0885328209344441>
- Brow RK (2000) Review: the structure of simple phosphate glasses. *J Non Cryst Solids* 263:264–1–28. [https://doi.org/10.1016/S0022-3093\(99\)00620-1](https://doi.org/10.1016/S0022-3093(99)00620-1)
- Tang V, Otto K, Seering W (2014) Using design of experiments (DOE) for decision analysis. Paper presented at the International Conference on Engineering Design, ICED'07 Cite des sciences et de l'industrie, Paris, France, 01/23
- Griffin SG, Hill RG (1999) Influence of glass composition on the properties of glass polyalkenoate cements. Part I: influence of aluminum to silicon ratio. *Biomaterials* 20(17):1579–1586. [https://doi.org/10.1016/S0142-9612\(99\)00588-7](https://doi.org/10.1016/S0142-9612(99)00588-7)
- Kim D-A, Lee J-H, Jun S-K, Kim H-W, Eltohamy M, Lee H-H (2017) Sol-gel-derived bioactive glass nanoparticle-incorporated glass ionomer cement with or without chitosan for enhanced mechanical and biomineralization properties. *Dent Mater* 33(7):805–817. <https://doi.org/10.1016/j.dental.2017.04.017>
- Lan WH, Lan WC, Wang TM, Lee YL, Tseng WY, Lin CP, Jeng JH, Chang MC (2003) Cytotoxicity of conventional and modified glass ionomer cements. *Oper Dent* 28(3):251–259



## Structural evaluation of ZnO substitution for CaO in glass ionomer cement synthesized by sol-gel method and their properties

Oranich Thongsri<sup>1</sup>, Sawitri Srisuwan<sup>1</sup>, Paritai Thaitalay<sup>1</sup>, Pawee Dangwiryakul<sup>1</sup>, Prasert Aengchuan<sup>2</sup>, Narong Chanlek<sup>3</sup>, Pinit Kidkhunthod<sup>3</sup>, Chutima Talabnin<sup>4</sup>, Sanong Suksaweang<sup>5</sup>, and Sirirat Tubsungnoen Rattanachan<sup>1,\*</sup>

<sup>1</sup>School of Ceramic Engineering, Institute of Engineering, Suranaree University of Technology, Nakhon Ratchasima, Thailand

<sup>2</sup>School of Manufacturing Engineering, Institute of Engineering, Suranaree University of Technology, Nakhon Ratchasima, Thailand

<sup>3</sup>Synchrotron Light Research Institute (Public Organization), Nakhon Ratchasima, Thailand

<sup>4</sup>School of Biochemistry, Institute of Science, Suranaree University of Technology, Nakhon Ratchasima, Thailand

<sup>5</sup>School of Pathology and Laboratory Medicine, Institute of Medicine, Suranaree University of Technology, Nakhon Ratchasima, Thailand

**Received:** 13 June 2021

**Accepted:** 7 September 2021

**Published online:**  
3 January 2022

© The Author(s), under exclusive licence to Springer Science+Business Media, LLC, part of Springer Nature 2021

### ABSTRACT

The substitution of ZnO for CaO site and the limitation of ZnO addition in the sol-gel ionomer glass composition at different calcination temperatures were evaluated and characterized in-depth by X-ray powder diffraction and X-ray photoelectron spectroscopy techniques in this study. The relationship between the compressive strength and the final cement structure was demonstrated by the ion-releasing behavior and synchrotron-based X-ray absorption spectroscopy (XAS) technique. The setting time, in vitro cytotoxicity, bioactivity and tooth adhesion ability of the sol-gel GICs were also evaluated. As expected, ZnO containing GICs presented antibacterial properties under the visible light condition as photocatalysis effect. Although the low crosslinking ability of Zn atoms to the polyacrylic liquid reduced the compressive strength, the compressive strength could be improved by compromising the calcination temperature. Moreover, this study also shows that the ZnO containing GICs had promising results on the biological properties which offered potential advantages in clinical use.

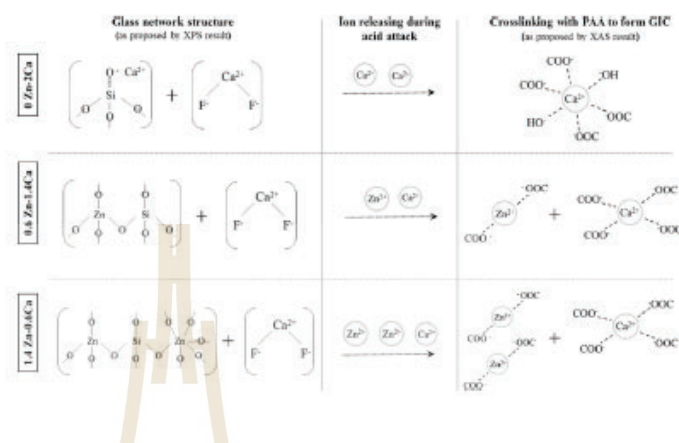
Handling Editor: David Cann.

Address correspondence to E-mail: sirirat.b@g.sut.ac.th

<https://doi.org/10.1007/s10853-021-06517-6>

Springer

## GRAPHICAL ABSTRACT



## Introduction

Dental caries is the leading oral health problem which mainly caused by acid-produced bacteria resulting in subsurface demineralization of the teeth [1]. The main treatment option when caries have progressed is filling with a dental restorative material.

The conventional glass ionomer cement (GIC) is attractive for dental restoration because it can release fluoride ions into the oral cavity leading to tooth decay resistivity [2]. This material is made of acid-base reactions of two compositions which were polyacrylic acid and ion-leachable glass based on aluminosilicate glass composed of fluoride and various metal oxide i.e., CaO, SrO, NaO, P<sub>2</sub>O<sub>5</sub>, etc. [3].

Zn<sup>2+</sup> ions are known as a bactericidal agent inhibiting the formation of caries [4, 5]. The incorporation of zinc in GIC was reported several benefits, including enhancement of flexural strength, surface roughness, good abrasive wear [6, 7]. Additionally, it was known that Ca<sup>2+</sup> ions (or Sr<sup>2+</sup> ion) played important role in the glass network structure as a charge balancing agent and the GIC structure as a crosslinking ion [3, 8]. Since Zn<sup>2+</sup> ions have the same charge as Ca<sup>2+</sup> ions, Zn<sup>2+</sup> ions were supposed to act

as a replacement for Ca<sup>2+</sup> ions. However, there was literature reporting that the incorporation of zinc in the aluminosilicate glass which derived by traditional melt-quenching process increased a glass structural density and induced some crystallization [9]. The traditional melt-quenching preparation of the glass ionomer is carried out at 1,300–1,500 °C [10]. This temperature range could result in fluoride loss during melting and uncontrollable glass composition [11].

The sol-gel process becomes an attractive option for glass synthesis. This process is based on the hydrolysis and condensation reaction; hence, it is possible to prepare homogeneous, high-temperature glasses at low temperature (600–800 °C), with the controllable doping content at a molecular level [12, 13]. Although the sol-gel technique has numerous benefits, it is sensitive to the synthesis conditions especially the thermal history of the process that influence the final product structure which should be investigated [11, 13–15]. Moreover, there was a lack of literature reporting the effect of ZnO contents instead of CaO in GIC synthesized by the sol-gel method on the relationship of the glass network structure, the GIC structure and their properties.

In this study, we aimed to investigate the effect of ZnO doping instead of CaO in the ionomer glass

composition and the calcination temperature on the sol-gel glass structure affecting the compressive strength and antibacterial property under dark condition and visible light. The chemical structure of the ionomer glasses and the GICs were in-depth analyzed by XPS and XAS characterization techniques to evaluate ZnO substitution in CaO of the sol-gel glass structure. To understand the setting reaction and the limit of ZnO content in the ionomer glass composition, the ion-releasing behavior of the sol-gel ionomer was investigated. Additionally, cytotoxicity, bioactivity and adhesion to the tooth surface for this sol-gel GIC were evaluated as well.

## Material and method

### Preparation of ionomer glass

The ionomer glass was synthesized by the sol-gel method using an analytical grade of tetraethyl orthosilicate (TEOS, 98%, Acros), aluminum nitrate ( $\text{Al}(\text{NO}_3)_3$ , 98%, Ajax), triethyl phosphate (TEP, 99%, Acros), calcium nitrate tetrahydrate ( $\text{Ca}(\text{NO}_3)_2 \cdot 4\text{H}_2\text{O}$ , Ajax), hydrofluoric acid ( $\text{H}_2\text{SiF}_6$ , Acros), and absolute ethanol (EtOH, Carlo Erba) as the chemical precursors.

The synthesis process in this experiment was adapted from the previous work [8]. Briefly, the synthesis process started by adding TEOS into the mixed solution of DI water and EtOH. Next,  $\text{Al}(\text{NO}_3)_3$ , TEP and  $\text{Ca}(\text{NO}_3)_2$  were sequentially added and stirred by a magnetic stirrer. Then, the solution was aged under an acid condition at a temperature in a range of 80–85 °C, and the gel was dried at 100 °C. The dried gel was calcined at 600–750 °C, then ground in a planetary mill to obtain the fine glass powder.

### Design of experiment (DOE)

DOE technique was used for the preliminary study in order to survey the significant factor and design the further experiment [16]. The 2 k full factorial was designed by Minitab 16 statistical software to determine the effect of ZnO substitution for CaO in the ionomer glass on the compressive strength of the sol-gel GICs. The ionomer glass compositions in this experiment were designed as presented in Table 1. Moreover, the calcination temperatures for gel-

**Table 1** Design composition for the sol-gel ionomer glass

Sample code	Mol ratio					
	Si	Al	P	F	Ca	Zn
0Zn	4.5	4	0.16	4	2	0
0.6Zn					1.4	0.6
1.0Zn					1	1
1.4Zn					0.6	1.4

derived glass at 650 °C and 750 °C were also studied in this work.

### Characterization of the sol-gel glass for glass ionomer cement

The chemical structure of the sol-gel glass was analyzed by a German Bruker D2 X-ray diffractometer (XRD) with a step time of 0.02°/min and a scan range of 10–60°. X-ray photoelectron spectroscopy (XPS) technique was used to characterize the glass network structure of the sol-gel ionomer glass. The measurement was performed using PHI5000 Versa Probe II, ULVAC-PHI, Japan, at the SUT-NANOTEC-SLRI joint research facility, Synchrotron Light Research Institute (SLRI), Thailand. The monochromatic Al K-alpha radiation (1486.6 eV) was used as an excitation source. The C1s peak of carbon at 284.8 eV binding energy was used to calibrate the binding energies. The fitting curves of XPS spectra were processed by PHI MultiPak XPS software using a combination of Gaussian-Lorentzian lines.

In this study, ion-releasing concentrations of the sol-gel glass powders were evaluated to determine the ions that affected the setting reaction in GIC. Thus, the ion-releasing behavior of the ionomer glass was conducted in acetic acid. The sol-gel ionomer glass was soaked in 5% acetic acid for 2, 6, 10, and 60 min, respectively. The concentrations of ions (Si, Al, P, Ca and Zn) released from the ionomer glass were measured by the Inductively Coupled Plasma (ICP-OES optima 8000, Perkin).

After the setting reaction, the GIC specimens were evaluated by the synchrotron-based X-ray absorption spectroscopy (XAS) technique including in-situ X-ray absorption near edge structure (in-situ XANES) and in-situ extended X-ray absorption fine structure (in-situ EXAFS) in order to analyze local structural information around Ca and Zn atoms. The

measurement was conducted at the SUT-NANOTEC-SLRI XAS Beamline (BL5.2) at the Synchrotron Light Research Institute (Public Organization), Thailand [17]. The data were analyzed and fitted by Athena and Artemis program as implemented in the IFEFFIT packages [18]. The reference standard curves were from the material project (file number; mp-2605\_CaO and mp-1986\_ZnO) [19].

### GIC sample preparation and testing

The liquid solution for GIC preparation was the mixture of the polyacrylic acid (35 wt.% in H<sub>2</sub>O PAA; MW ~ 100,000) and tartaric acid in the ratio of 9:1 w/w supplied by Sigma-Aldrich. The GIC samples were prepared by mixing the sol-gel glass powders with the liquid solution at a powder to liquid ratio (P/L) of 1/1 (w/v).

The net setting time of the GICs was determined by Gillmore Apparatus (Humboldt, H-3150F) following ISO 9917-1 for dental glass polyalkenoate cement. After mixing the cement paste, the paste was filled into the cylindrical Teflon mold with 10 mm in diameter and 2 mm in height. The net setting time was measured when a heavy and thin needle (453.6 g, Ø 1.06 mm) was placed on the paste surface every 5 s until no mark occurred. The testing was carried out at room temperature three times.

Compressive strength was measured according to ISO 9917-1:2007 using the universal testing machine (UTM, Instron 5565, Instron GmbH, Germany) with 5 kN load cells. The cross-head speed was 0.75 mm/min according to the previous literature [20]. The GIC specimens were prepared in the cylindrical shape Teflon mold with 4 mm in diameter and 6 mm in height. After being molded for 1 h, all the specimens were kept in DI water at 37 °C for 23 h before testing. At least eight specimens were prepared for each experimental condition. The compressive strength was calculated using the equation,  $CS = 4P/\pi d^2$ , where CS was compressive strength (MPa), P was the maximum load applied (N), and d was specimens radius (mm).

### Antibacterial testing

The antibacterial activity of the sol-gel-derived GICs was tested against *Streptococcus mutans* (ATCC 27,145) using the agar disk diffusion method in comparison with the commercial GIC (Fuji IX extra,

GC corporation, Tokyo, Japan). The *Streptococcus mutans* was cultured at 37 °C, 5%CO<sub>2</sub> for 24 h. The bacteria were swabbed uniformly on the newly made Mueller-Hinton agar plate. The disk-shaped GIC samples were then placed onto the agar and incubated at 37 °C for 48 h. The antibacterial testing was subjected to both dark and visible light conditions. For a dark condition, the plates were immediately placed in the black box before putting into the incubator. For the visible light condition, the plates were processed and incubated without placing them in the black box. The inhibition zone of bacterial activities was evaluated by measuring the diameter of inhibition zones around the GIC disks. The calculation of inhibition zone size was provided as follows: size of inhibition zone (mm) = (diameter of inhibition zone – diameter of disk)/2.

### Cell viability

Cytotoxicity of GICs was demonstrated by the cell viability of NIH/3T3 fibroblast after GIC extracts treatment that was evaluated by MTS assay. The GICs were molded in disk shape (Ø = 12 mm, h = 2 mm) and set in the air for 1 h. Consequently, the GIC disks were sterilized by UV light for 30 min on each side and rinsed by 1 × PBS. The GIC extracts were prepared by immersing the cement disks in 1 ml of the cell culture medium and incubated at 37 °C for 24 h. The culture medium consisted of 44% Dulbecco's Modified Eagle Medium (DMEM (1X) from Invitrogen, USA), 44% F-12 Nutrient mixture (HAM from Invitrogen, USA), 10% Fetal Bovine Serum (FBS from Invitrogen, USA) 1% L-glutamine and 1% Penicillin streptomycin (Invitrogen, USA). The NIH/3T3 fibroblast cells were seeded at a density of 5,000 cells/well in 96 well plates. After 24 h of seeding, the cells were treated with various concentrations of the GIC extract (0, 0.6 and 1.4 ZnO) for 24 h. The cells with culture media were used as a negative control. The cell viability was tested by dropping 20 µl of MTS reagent (CellTiter 96® AQueous) into each well plate. After incubation for 2 h, the optical density was measured at 490 nm (OD490) using an automated plate reader. The percentage of viable cells was calculated from OD values using the following equation [21]: %Cell viability = (Sample absorbance value/Control group absorbance value) × 100.

Additionally, the extracted medium was also collected and diluted into 20-fold DI water to evaluate the concentration of released  $Zn^{2+}$  ions by using the ICP-OES technique (ICP-OES optima 8000, Perkin).

#### Ability of apatite-like formation and tooth-GIC interface

To investigate the ability of apatite-like formation on the GIC surface, the GIC doping with 0, 0.6 and 1.4 ZnO were prepared in a cylindrical shape, with 2 mm in height and 10 mm in diameter. Then, the specimens were soaked in artificial saliva for 5 days. The composition of the artificial saliva employed in this study was 0.4 g Sodium chloride (NaCl, 98%, Carlo Erba), 0.4 g Potassium chloride (KCl, 99.5%, Merck), 0.795 g Calcium chloride ( $CaCl_2 \cdot H_2O$ , Merck), 0.69 g Sodium phosphate monobasic monohydrate ( $NaH_2PO_4 \cdot H_2O$ , 98%, Merck), 0.005 g Sodium sulfide nonahydrate ( $Na_2S \cdot 9H_2O$ , 98%, Carlo Erba) and 1000 mL DI water [22].

In order to observe the tooth-GIC interface, the premolar teeth were drilled and filled with the GIC doping with 0, 0.6 and 1.4 ZnO. After leaving in the air for 1 h, all specimens were transferred to the artificial saliva and incubated at 37 °C for 7 days. Consequently, the specimens were mounted in the resin following by cutting a cross-section to observe the interfacial area between the tooth and the GIC. The surface morphology of both bioactivity and tooth adhesive specimens were observed by scanning electron microscope (SEM, JEOL-6010LV) at an acceleration voltage of 15 kV. All specimens were coated with gold before the examination.

## Result and discussion

### Characterization of the sol-gel-derived ionomer glass

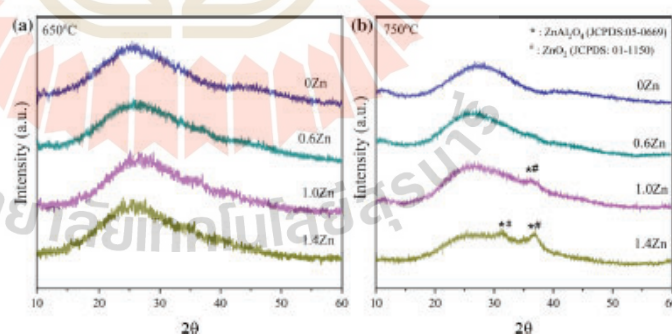
Figure 1 presents XRD patterns of  $4.5SiO_2 \cdot 4Al_2O_3 \cdot 0.16P_2O_5 \cdot (2-x)Ca \cdot xZnO \cdot 2F_2$ , where  $x = 0, 0.6, 1.0$  and 1.4, synthesized by the sol-gel method at the different calcination temperatures. All XRD patterns show the amorphous phase. However, 1.4 mol doped ZnO sol-gel glass calcined at 750 °C revealed a peak around 2θ of 38, attributing to the formation of the crystal  $ZnAl_2O_4$  (JCPDS:05-0669) and  $ZnO$  (JCPDS:01-1150) phase. The crystallinity of the glass increased with increasing the calcination temperature, as shown in Fig. 1b.

In general, the sol-gel process, colloidal suspension or sol is formed by hydrolysis of the starting composition. The liquid sol then transforms to be a wet gel during polymerization. Finally, the wet gel converts into dense ceramic by drying and heat treatment [23]. The heating step and slow cooling rate of the sol-gel process easily induced phase separation and crystal growth [14, 24]. This can be seen in Fig. 1 that the crystal structure was found when the calcination temperature was increased.

The chemical states of oxygen, aluminum and zinc for the sol-gel glasses were evaluated using the XPS technique as shown in Fig. 2. Deconvolution curves were processed by PHI MultiPak XPS software using a combination of Gaussian-Lorentzian lines with a constant value of full width at half maximum (FWHM).

As can be seen in Fig. 2a, all O1s spectra of the glass showed two deconvoluted peaks locating

**Figure 1** XRD pattern of the sol-gel ionomer glass belonging to the system of  $4.5SiO_2 \cdot 4.0Al_2O_3 \cdot 0.16P_2O_5 \cdot (2-x)Ca \cdot xZnO \cdot 2F_2$ , where  $x = 0, 0.6, 1.0$  and 1.4 calcined at a 650 °C and b 750 °C.



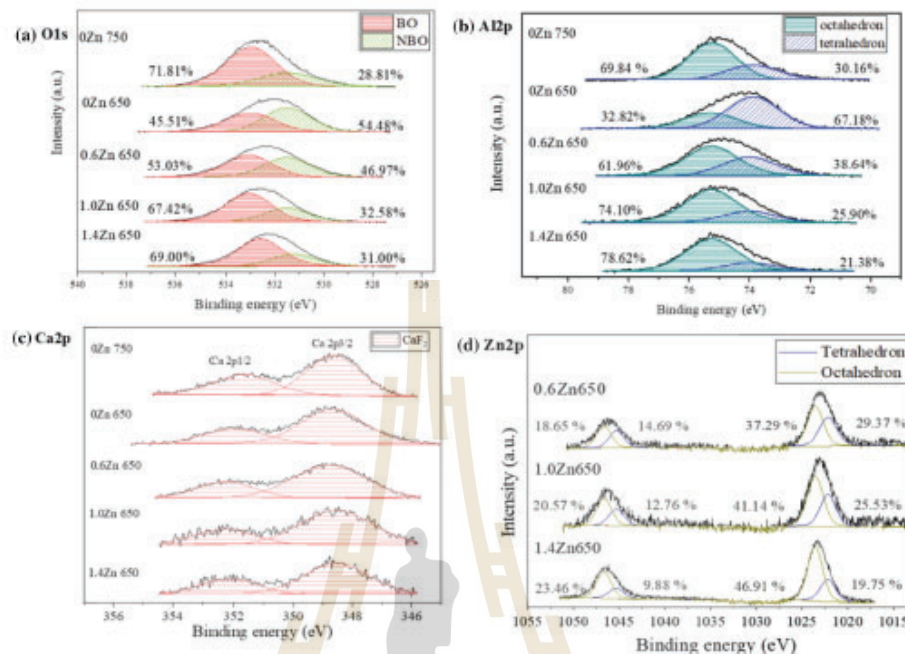


**Figure 2** The high-resolution XPS spectra of a Oxygen (O1s) b Aluminum (Al2p) and c) Zinc (Zn2p) for the sol-gel ionomer glass belonging to the system of  $4.5\text{SiO}_2\text{-}4.0\text{Al}_2\text{O}_3\text{-}0.16\text{P}_2\text{O}_5\text{-}(2-x)\text{Ca-xZnO-}2\text{F}_2$ , where  $x = 0, 0.6, 1.0$  and  $1.4$  calcined at  $650^\circ\text{C}$  as compared to the Zn-free ionomer glass calcined at  $750^\circ\text{C}$ .

around  $532.9\text{ eV}$  and  $531.0\text{ eV}$  which were associated with the bridging oxygen (BO) and non-bridging oxygen (NBO) group, respectively. Without ZnO doping in the sol-gel glass, a fraction of the NBO structure was drastically decreased with the increase of the calcination temperature. Meanwhile, the fraction of NBO also decreased with the increase of ZnO doping in the glass composition.

Figure 2b presents the high-resolution XPS spectra in the Al2p region of the sol-gel glass. The deconvoluted Al2p peaks at the binding energies around  $75.3\text{ eV}$  and  $74\text{ eV}$  attributed to  $[\text{AlO}_6]$  octahedral and  $[\text{AlO}_4]$  tetrahedral structure, respectively [25]. For the Zn-free sol-gel glasses, the proportion of  $[\text{AlO}_4]$  tetrahedral structure reduced with increased calcination temperature from  $650^\circ\text{C}$  to  $750^\circ\text{C}$ . As increasing Zn content in the glass composition, the  $[\text{AlO}_4]$  tetrahedron was also decreased.

Figure 2c revealed the spin-orbit doublet of Ca2p with the binding energies around  $348.37\text{ eV}$  and  $352.02\text{ eV}$ . These peaks exhibited a characteristic of  $\text{CaF}_2$  [26]. In the case of Zn-free sol-gel glass calcined at  $650^\circ\text{C}$ , the peak was slightly broadened and shifted to the higher binding energy. This is attributed to the presence of Ca–O and Ca–OH bonds [27].

The Zn2p double spectra of the ZnO-doped glass is shown in Fig. 2d. The binding energies around  $1045$  and  $1021.5\text{ eV}$  corresponded to tetrahedral  $\text{Zn}^{2+}$  ions, and the peaks at  $1047.5$  and  $1024.0\text{ eV}$  were assigned to octahedral  $\text{Zn}^{2+}$  ions [28]. Additionally, the octahedral  $\text{Zn}^{2+}$  ions fraction increased with ZnO content in the glass composition.

XPS spectra showed the existence of  $\text{Al}^{3+}$  ions in the form of tetrahedron and octahedron. When ZnO was added to the glass composition, the  $[\text{AlO}_6]$  octahedral fraction was increased. According to the

report of Kusumoto, the reason for an increase in  $[\text{AlO}_6]$  octahedral species might be due to the charge balancing of  $\text{Zn}^{2+}$  ions in  $\text{Al-O-PO}_3^{3-}$  species resulting in insufficient charge balancing ion for maintaining  $[\text{AlO}_4]$  tetrahedron [10]. Our finding showed the probability of  $\text{ZnAl}_2\text{O}_4$  existence where  $\text{Al}^{3+}$  ions were in the octahedral site, and  $\text{Zn}^{2+}$  ions were in the tetrahedral site. Additionally,  $\text{Zn}^{2+}$  ions in the octahedral site were increased with ZnO content in the glass composition. It was possible that the excessive  $\text{Zn}^{2+}$  ions formed with  $\text{O}^{2-}$  ions at sixfold coordination and played a role as a charge compensation for the glass network [29].

The deconvoluted XPS spectra also presented that the increase of calcination temperature and ZnO content increased the BO fraction in the sol-gel glass structure. This structure was reported that decreased the acid susceptibility of the glass [15].

#### Ion-releasing behavior

The ion-releasing behavior in the acidic condition of the ionomer glasses was evaluated in order to determine the setting reaction. Figure 3 shows the ion-releasing level of the glass in the 5% acetic solutions evaluated by the ICP-OES technique. The data revealed the release of Al, Ca, Zn, Si, and P. The level of Al was exhibited in Fig. 3a. Without Zn-doped, the level of Al ions of the sample calcined at 650 °C was higher than that calcined at 750 °C. For the group of ZnO-doped glass, Al ions releasing level had no significant difference.

Figure 3b, c present that the ZnO addition in the glass composition caused the reduction of the releasing level of Ca ions and increased the releasing level of Zn ions along with the increase of ZnO content, respectively. In addition, the increase of calcination temperature reduced the level of calcium ions released from the glass as well.

The addition of ZnO in the glass reduced the amount of Si ions release. However, there was no significant difference in level Si ions release among the ZnO-doped series, as shown in Fig. 3d. Meanwhile, the glass calcined at 650 °C released a higher level of Si ions than that of the 750 °C. The ion species of Si that released to the acid solution was considered to be  $\text{Si}(\text{OH})_4^{2-}$  or  $(\text{SiO}_3)^{2-}$  [30].

Finally, Fig. 3e presents that all the sol-gel glasses released very small amounts of P ions and there was no significant difference among the samples. In the

case of P ions, the species that was released to the acid solution was reported to be  $\text{PO}_4^{3-}$  [31].

The initial setting reaction of the GIC was an acid-base reaction between the polymeric acid solution and the glass powder. This reaction immediately produced calcium (or strontium and zinc) polyacrylate, followed by aluminum polyacrylate slightly later. This setting took place in a period of 2–6 min. After the initial setting, it was following the secondary setting. It seemed to be that the phosphate network also played a role during the maturation reaction [32]. However, this study found no significant difference as an effect of the phosphate species. The ion species that influenced the setting reaction in this study seem to be aluminum, calcium, and zinc.

#### DOE analysis of the compressive strength

In order to determine the significant factor for the compressive strength of the sol-gel GICs, ZnO content in sol-gel ionomer glass and the calcination temperature were designed by the DOE technique for the primary study. This study synthesized the glass with a composition of  $4.5\text{SiO}_2\text{-}4.3\text{Al}_2\text{O}_3\text{-}0.16\text{P}_2\text{O}_5\text{-}(2-x)\text{Ca-xZnO-}2\text{F}_2$ , where  $x = 0, 0.6, 1.0$  and  $1.4$  by the sol-gel method and calcined at 650 °C and 750 °C.

ANOVA analysis in Table 2 presents the influence of ZnO content and calcination temperature on the compressive strength of the sol-gel GICs. The statistical difference between the groups was judged to be significant when  $p \leq 0.05$ . This result showed that  $P$ -values of ZnO content and calcination temperature were lower than 0.05; thus, these two factors were significantly affected by the compressive strength of the sol-gel GICs. However, there was no interaction between ZnO content and the calcination temperature ( $P > 0.05$ ) which affected the compressive strength of the cement.

Figure 4 illustrates the interaction and main effect plot for compressive strength of GIC with different ZnO contents and the calcination temperatures. Compressive strength decreased significantly where ZnO content of the glass was at  $x = 0.6\text{--}1.0$ , but ZnO content had not been significantly affected at  $x = 1.0\text{--}1.4$ . Moreover, it was found that the increasing of calcination temperature had an adverse effect on compressive strength. It should be noted that the compressive strength tended to increase when ZnO content was below 0.6 and the calcination temperature at 650 °C. From these results, therefore, the effect

**Figure 3** Concentration of a Al, b Ca/Sr, c Zn, d Si and e P ions releasing from the sol-gel ionomer glass belonging to the system of  $4.5\text{SiO}_2\text{-}4.0\text{Al}_2\text{O}_3\text{-}0.16\text{P}_2\text{O}_5\text{-}(2-x)\text{Ca-xZnO-}2\text{F}_2$ , where  $X = 0, 0.6, 1.0$  and  $1.4$  calcination temperature of  $650^\circ\text{C}$  in comparison to Zn-free ionomer glass calcined at  $750^\circ\text{C}$  as a function of the immersion time.

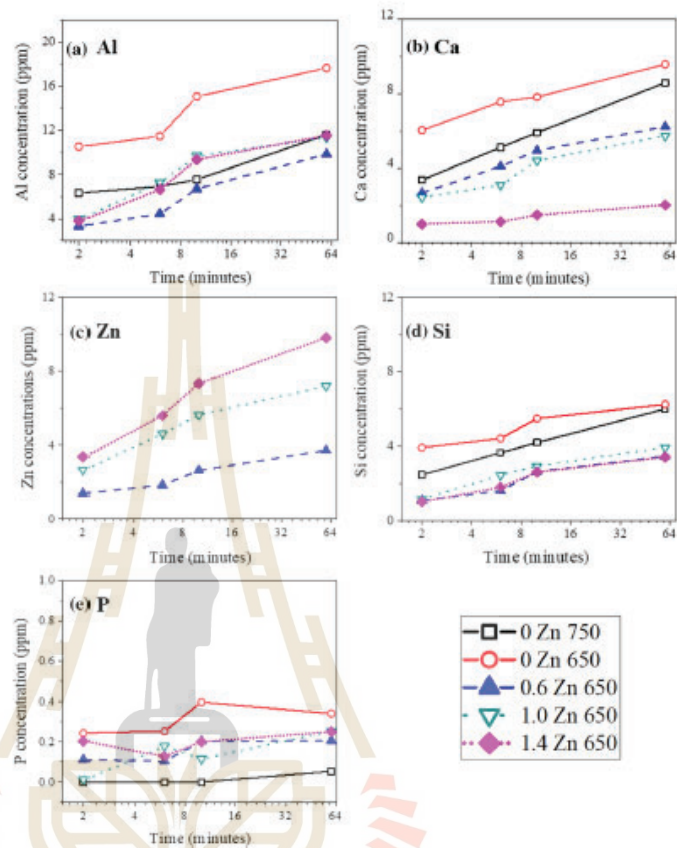


**Table 2** ANOVA analysis for the compressive strength for the sol-gel-derived GICs containing different ZnO doping and the calcination temperatures

Source	DF	Seq SS	Adj SS	Adj MS	F	P
Zn	2	1686.88	1686.88	843.44	14.95	0.001
Temperature	1	1195.28	1195.28	1195.28	21.19	0.001
Zn*temperature	2	380.94	380.94	190.47	3.38	0.069
Error	12	676.84	676.84	56.40		
Total	17	3939.94				

of ZnO content (x) of 0.2, 0.6 and 1.0 and calcination temperature at  $600^\circ\text{C}$ ,  $650^\circ\text{C}$ ,  $700^\circ\text{C}$  and  $750^\circ\text{C}$  on the setting time and compressive strength of the sol-gel GICs were studied in the next experiment.

**Setting time and compressive strength**

The net setting time of the cement paste in Fig. 5 demonstrates that increasing the calcination temperature of the sol-gel glass extended the setting time of

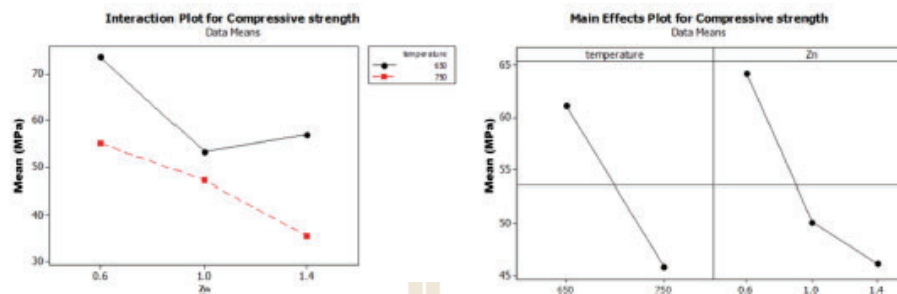


**Figure 4** Main effect plot and the interaction plot for compressive strength of the sol-gel-derived GIC containing different ZnO doping and the calcination temperatures.

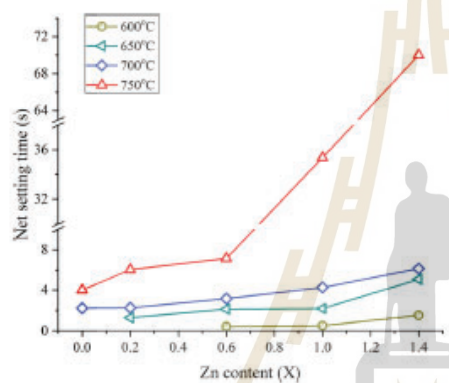


**Figure 5** Net setting time of the GIC prepared from the sol-gel ionomer glass belonging to the system of  $4.5\text{SiO}_2\text{-}4.0\text{Al}_2\text{O}_3\text{-}0.16\text{P}_2\text{O}_5\text{-}(2-x)\text{Ca-xZnO-}2\text{F}_2$ , where  $x = 0, 0.2, 0.6, 1.0$  and  $1.4$  and calcined at  $600^\circ\text{C}$ ,  $650^\circ\text{C}$ ,  $700^\circ\text{C}$  and  $750^\circ\text{C}$ .

GICs. The increasing of ZnO content slightly increased the setting time as well. The cement with low ZnO content and calcined at below  $650^\circ\text{C}$  was unable to form because of rapid setting time. Meanwhile, the cement with 1 mol of ZnO calcined at  $750^\circ\text{C}$  presented a drastic increase of setting time due to the existence of crystal structure.

The extension of the setting time for the sol-gel GIC can be explained from the glass structural change of the sol-gel glass. According to the structural analysis, the increase of calcination temperature and ZnO content led to an increase in BO structure. This structure was reported that decreased the acid

susceptibility of the glass [15]. Moreover, increasing ZnO content and the calcination temperature reduced the release level of  $\text{Ca}^{2+}$  ions. Thus, there might have been a lack of ions to crosslink with the polymeric liquid in the setting reaction resulting in the extension of the setting time.

Figure 6 revealed the compressive strength of the sol-gel GIC doped with different ZnO contents and calcination temperatures. At a calcination temperature of  $750^\circ\text{C}$ , the compressive strength of the cement decreased as adding of ZnO content in the glass composition. Whereas the calcination

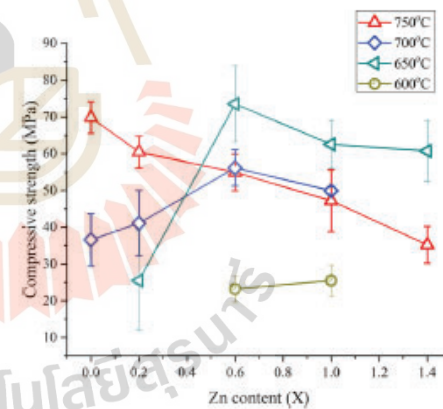


**Figure 6** Compressive strength of the sol-gel GIC belonging to the system of  $4.5\text{SiO}_2\text{-}4.0\text{Al}_2\text{O}_3\text{-}0.16\text{P}_2\text{O}_5\text{-}(2-x)\text{Ca-xZnO-}2\text{F}_2$ , where  $x = 0.2, 0.6,$  and  $1.0$  and calcination temperature of  $600^\circ\text{C}$ ,  $650^\circ\text{C}$ ,  $700^\circ\text{C}$  and  $750^\circ\text{C}$ .

temperature at 700 °C and 650 °C, the cement with 0.6 mol of ZnO exhibited the highest compressive strength as compared in the group of ZnO-doped sol-gel cement. However, below 0.6 mol of ZnO content, the compressive strength was poor because it was difficult to handle and could not be molded for homogeneous samples.

Our results showed that the calcination temperature should be considered when optimizing the setting time and compressive strength of the sol-gel GIC. Since the increase of ZnO content in the sol-gel glass composition can extend the setting time and reduce the strength, the calcination temperature should be compromised to obtain the suitable setting time and the compressive strength.

The mechanical properties of glass ionomer cement could be influenced by various factors, such as glass composition, powder to liquid ratio (P/L), type of the liquid phase, reinforcement, etc. [33–35]. The glass powder in this study was synthesized by the sol-gel method with different glass compositions as compared to the commercial product resulting in significantly different glass structure and ion-releasing behavior. In addition, the type of liquid solution and the powder to liquid ratio were different from the commercial product. The sol-gel ionomer glass was limited with a liquid solution at a P/L ratio of 1 while most commercial GIC was mixing with a liquid solution at a P/L ratio of more than 1. The compressive strength in this study can be further improved by increasing the P/L ratio and modifying the glass structure.

According to the good results of the compressive strength and setting time of the sol-gel GIC sample prepared with 0.6 ZnO calcined at 650 °C, it was evaluated in comparison with 0 and 1.4 ZnO GICs as the substitution of ZnO instead of CaO in the glass structure by using the XAS technique. In addition, the effect of the biological properties for the sol-gel 0, 0.6 and 1.4 ZnO GICs was also investigated.

#### The local structure of ZnO containing GICs

Figure 7a, b show the absorption spectra of the sol-gel GICs from Ca-XANES and Zn-XANES results, respectively. The position of the main energetic transition edge was the same in all samples. This characteristic indicated a similar structure among both sample groups, but the intensity of the spectra was different. The intensity referred to the number of

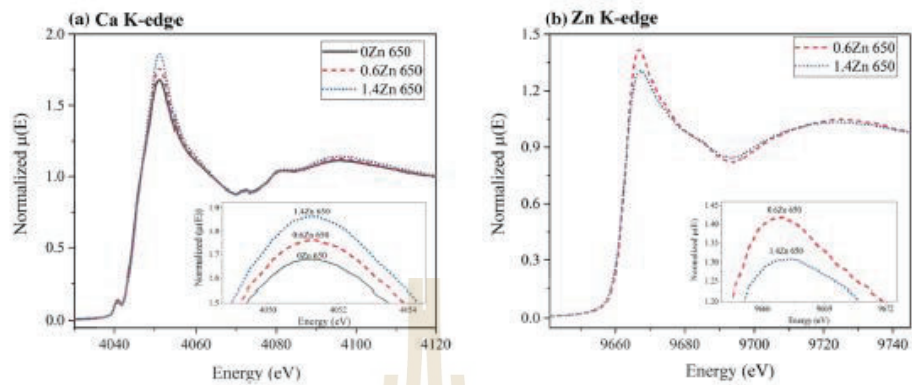
O atoms around the core atoms which the high intensity indicated the high amount of O atoms. Figure 7a shows that the increase of ZnO content in GIC increases O atoms around Ca atoms. Figure 7b shows that the increase of ZnO content in GIC reduces O atoms around Zn atoms. The number of O atoms around the core atom was further analyzed by the EXAFS technique as shown in Fig. 8.

After the setting reaction of the sol-gel GICs, the local environment of Ca and Zn atoms in the Zn-doped GIC were determined by EXAFS spectra. Figure 8 shows the spectra in R-space at Ca and Zn K-edge. This study observed the coordination number (CN) of O atoms in the first shell of Ca and Zn atoms. The fitting parameter in Table 3 confirmed the XANES result that the increasing of ZnO content increased the average CN of O atoms around Ca atoms but decreased the CN of O atoms around Zn atoms.

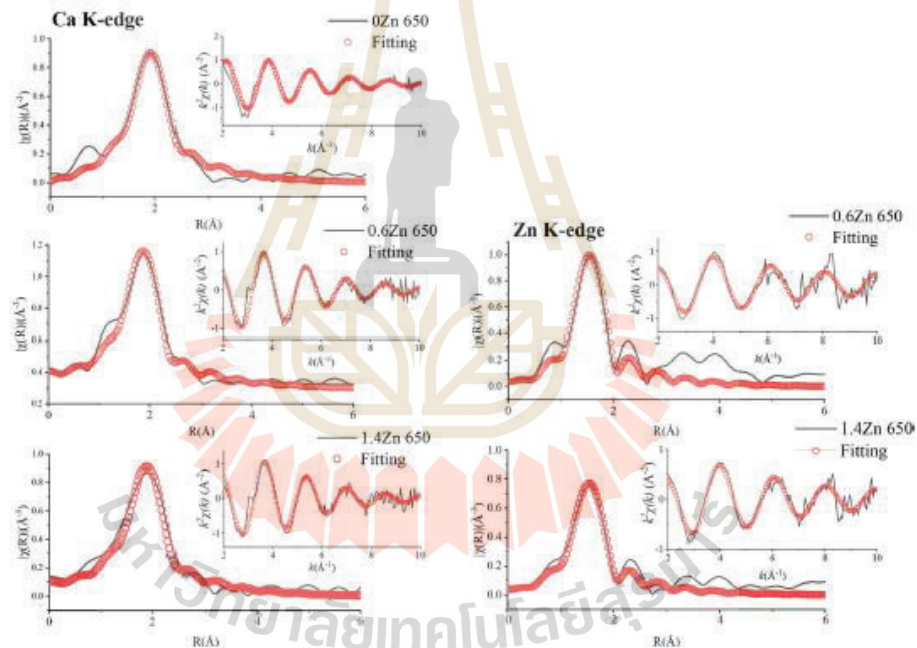
According to the fitting parameter of EXAFS results, the O atoms preferred to bond with the Ca atoms than Zn atoms after the setting reaction. This could be assumed that the O atom from the carboxyl group of PAA preferred to crosslink with Ca atoms than Zn atoms. Therefore, the substitution of ZnO instead of CaO depleted the crosslinking ions for the setting reaction of GIC resulting in reducing compressive strength.

Figure 9 illustrates the proposed glass network structure related to  $\text{Ca}^{2+}$  ions and  $\text{Zn}^{2+}$  ions location in the sol-gel glass network structure before and after setting to glass ionomer cement which were analyzed by the XPS and XAS techniques in this study. According to the XPS result,  $\text{Ca}^{2+}$  ions in the Zn-free ionomer glass existed as a network modifier and formed as  $\text{CaF}_2$ . When CaO in the glass composition was substituted by ZnO,  $\text{Ca}^{2+}$  ions were only found in the form of  $\text{CaF}_2$ , and  $\text{Zn}^{2+}$  ions formed in the tetrahedral site and connected to the glass network as a network former through BO structure. The increase of ZnO in the glass composition to 1.4 mol resulted in an increasing fraction of octahedral structure which also connected to the glass network through BO structure.

After these ionomer glasses were attacked by the acid liquid, the glasses released both  $\text{Ca}^{2+}$  and  $\text{Zn}^{2+}$  ions with relative amounts of respective CaO and ZnO content in the glass composition. Consequently, the XAS results showed that these two metal ions could crosslink with the  $\text{-COO}^-$  a group of PAA with



**Figure 7** XANES spectra of GIC samples prepared with 0, 0.6 and 1.4 Zn-doped sol-gel glasses calcined at 650 °C at **a** Ca K-edge and **b** Zn K-edge.



**Figure 8** Ca and Zn K-edge EXAFS (weighted by  $k^2$ ) from the experiment (black line) and fitting (red circle) of GIC samples prepared with 0, 0.6 and 1.4 Zn-doped sol-gel glasses calcined at 650 °C.

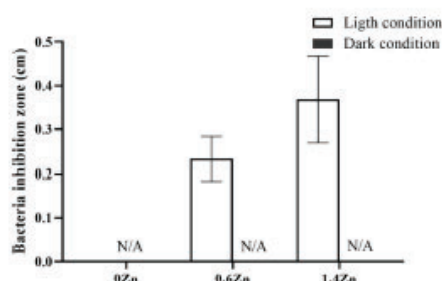


**Figure 10** The diameter of inhibition zone against *S.mutan* of the GIC samples prepared with 0, 0.6 and 1.4 Zn-doped sol-gel glasses calcined at 650 °C.

presented the inhibition zone around the sample under the light condition, and the inhibition zone was extended with the addition of the amount of ZnO in the glass composition.

The inhibition zone of all Zn-doped incubating under light conditions was greater than 0.1 cm and increased with increasing ZnO content as compared to Zn-free GIC. This was considered to have an antibacterial effect according to the standard SNV 195.920-199 [44]. The antibacterial activity of ZnO was regulated through three mechanisms: photochemical reaction, direct contraction of ZnO particles to the bacteria cell wall, and the release of bactericidal  $Zn^{2+}$  ions [45, 46]. Our data showed that the antibacterial activity of ZnO-doped GIC was only activated under light condition; thus, this effect was attributed to the photochemical reaction. The photochemical reaction was described as a photo-induced oxidation process in that ZnO could absorb UV light and generate ROS species such as hydrogen peroxide ( $H_2O_2$ ) and superoxide ions ( $O_2^{\cdot-}$ ). These ROS species were able to penetrate the cells, then inhibit or kill microorganisms [46].

### Cell viability

Figure 11a shows the cell viability of NIH/3T3 fibroblast cells after treatment with extracts of the sol-gel GIC with the variation of ZnO contents in glass for 24 h. The MTS assay showed that cell viability of NIH/3T3 fibroblast cells was decreased after treatment with the ZnO-doped sol-gel GICs at 0.6ZnO and 1.4ZnO whereas less cytotoxicity was found for the sol-gel GIC without ZnO doping. With diluting of

the extract concentration to 1:2 and 1:4, cell viability for all samples trended to continuously increase.

$Zn^{2+}$  ions seemed to have disadvantages in terms of biocompatibility. Brauer et al. demonstrated that the possible reason for cytotoxicity was a large amount of  $Zn^{2+}$  ions release [47]. Several studies reported that the cytotoxicity of  $Zn^{2+}$  ions associated with the production of ROS species which was the same mechanism with the antibacterial effect [48, 49]. However, the dilution of  $Zn^{2+}$  ions concentration seemed to reduce the toxicity and have a benefit to cell growth [47].

The previous study reported that the optimum concentration of  $Zn^{2+}$  ions on cell toxicity was 350  $\mu$ M [47]. According to our result, 523  $\mu$ M of  $Zn^{2+}$  ions was released from the sol-gel GIC prepared with 0.6ZnO calcined at 650 °C, as shown in Fig. 11b. This concentration was higher than 350  $\mu$ M which could be the reason for an adverse effect on the cell viability. After dilution (1:2) of the extracted, the concentration of  $Zn^{2+}$  ions might reduce to around 260  $\mu$ M which drastically increased the cell viability. This improvement of the cell viability was possible to be a benefit in clinical use. It was because the concentration of  $Zn^{2+}$  released from the GIC was diluted by the fluid circulation in the oral environment.

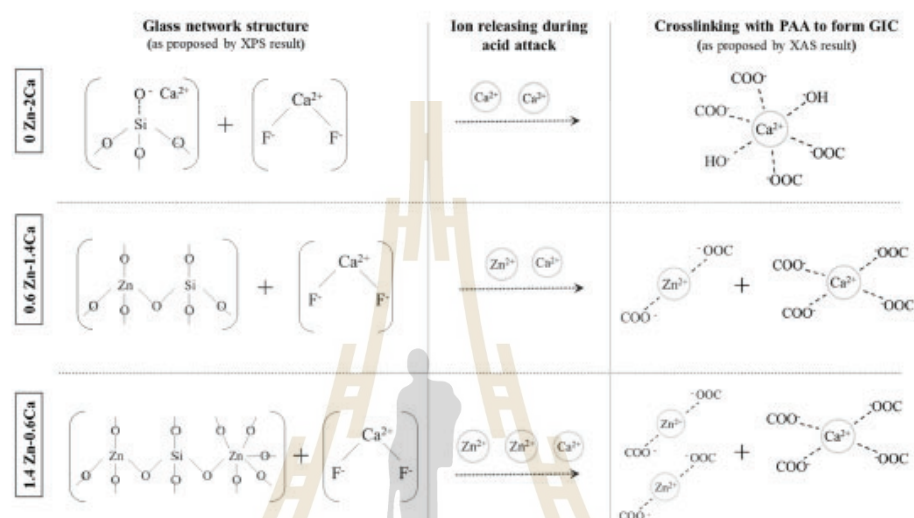
### Apatite-like formation and tooth-GIC interface

Figure 12 shows the SEM images and EDS results of the sol-gel GIC surfaces after soaking in the DI water and artificial saliva for 5 days. The apatite-like layer occurred on all GIC surfaces after soaking in artificial saliva, and the thickness of the apatite-like layer was greater when ZnO content increased. Meanwhile, there was no apatite-like layer on all GIC surfaces soaking in DI water. The apatite-like layer could be confirmed by EDS results that the ratio of Ca/P should be in the range of 1.30–1.67 [50]. Our result presented that the Ca/P ratio was around 1.40 where ZnO was substituted for CaO in the ionomer glass composition. This could be indicated that there was an apatite-like layer on the GIC surfaces for artificial saliva immersion.

The formation of the apatite layer was associated with the deposition of calcium and phosphate on the cement surface, then precipitated into an apatite-like crystal lattice [51]. This apatite layer was reported to enhance a chemical bond between GIC and tooth

**Table 3** EXAFIT fitting parameters including average coordination number of oxygens around the atom (CN), Debye-Waller factor ( $\sigma^2$ ), interatomic distance ( $R$ ), and ( $R$ -factor)

Sample	Ca K-edge				Zn K-edge			
	CN	$\sigma^2$	$R(\text{\AA})$	$R$ -factor	CN	$\sigma^2$	$R(\text{\AA})$	$R$ -factor
0Zn	4.326	0.00909	2.380	0.0101	—	—	—	—
0.6Zn	4.746	0.00901	2.382	0.0242	2.092	0.00084	1.993	0.0329
1.4Zn	6.000	0.01068	2.392	0.0257	1.88	0.00265	1.998	0.0198



**Figure 9** A proposed glass network structure for ZnO instead of CaO in the sol-gel ionomer glass network and form crosslinking with polyacrylic acid in glass ionomer cement after setting.

different coordination complexes. The CN seemed to be determined by many factors i.e., the metal's size, the ligand charge, the charge-donating ability of the ligand and the reaction acidity [36, 37]. The previous study presented that Ca atoms were possibly surrounded by O atoms of carboxylate group with CN in a range of 2–8 [38–40]. The CN of O atoms around Zn atoms was also found in various values in a range of 2–6, where it was compounded with water and bulky organic molecules [41–43]. According to our result, Ca atoms were found to be surrounded by O atoms with CN = 6 for the Zn-free GIC. In the case of CN = 6, Bonapasta reported that 4 of O atoms of the PAA chains placed at the square bases of the octahedron and O atoms of the OH<sup>-</sup> ions occupy the two vertices of the octahedron [38]. The substitution of ZnO for CaO resulted in the changing of CN around

Ca atoms from 6 to 4, and Zn atoms were surrounded by O atoms with the CN = 2. Therefore, increasing ZnO content in the ionomer glass reduced the crosslinking for setting reaction of GIC resulting in the reduction of compressive strength.

#### Antibacterial property

Figure 10 demonstrates the antibacterial activity of the GIC samples with various concentrations of ZnO (0, 0.6 and 1.4 Zn) doped ionomer glass against *S. mutans* under light and dark conditions. In a dark condition, external light exposure was prevented by keeping it in the black box during the incubation period. The result presented that there was no inhibition zone occurring in the sol-gel GIC samples for the dark condition. Interestingly, the ZnO-doped GIC

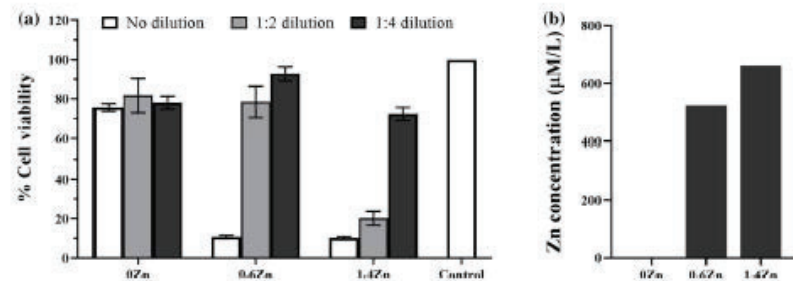


**Figure 11** Effect of Zn content in the sol-gel GIC on the NIH/3T3 cell viability (indirect contact). **a** %cell viability treated with different concentrations of the extracted solutions. The cells with fresh culture medium was used as a negative control. Values were expressed as the mean  $\pm$  standard error of the mean of three independent experiments and **b** the Zn<sup>2+</sup> ion-releasing concentration in the as-received extracted solutions analyzed by the ICP-OES technique.

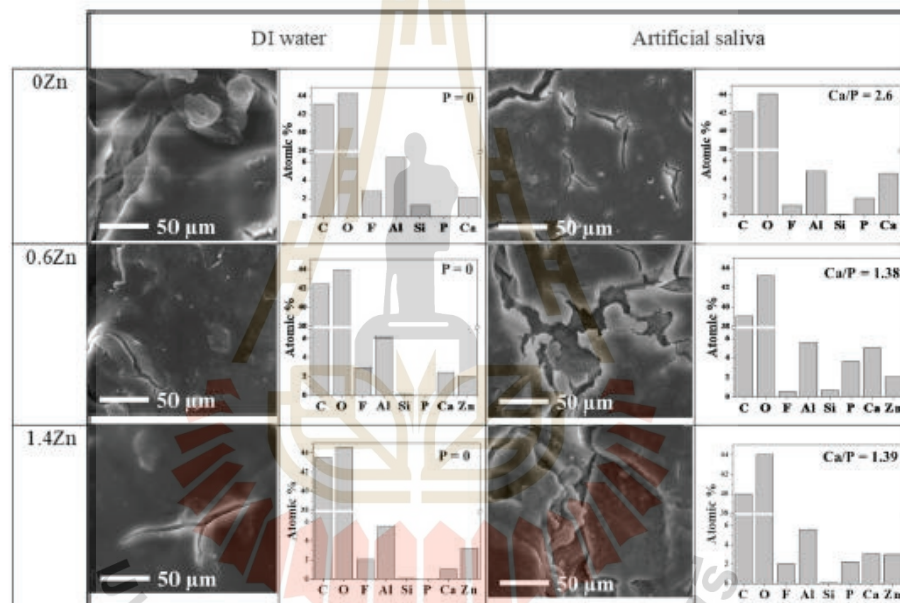


**Figure 12** SEM micrographs of GIC surface for the sol-gel GIC prepared with the sol-gel glasses doped different ZnO contents and calcined at 650 °C after soaking in DI water and artificial saliva for 5 days, respectively (magnification  $\times$  5000).

structure [52]. Therefore, the ability of apatite-like formation on the GIC surface after soaking in saliva solution could indicate the potential for having a high level of bioactivity.

Figure 13 illustrates the interfacial area between the tooth and the sol-gel GIC with and without ZnO contents, observed by the SEM technique, to determine the probability of the success and failure of the

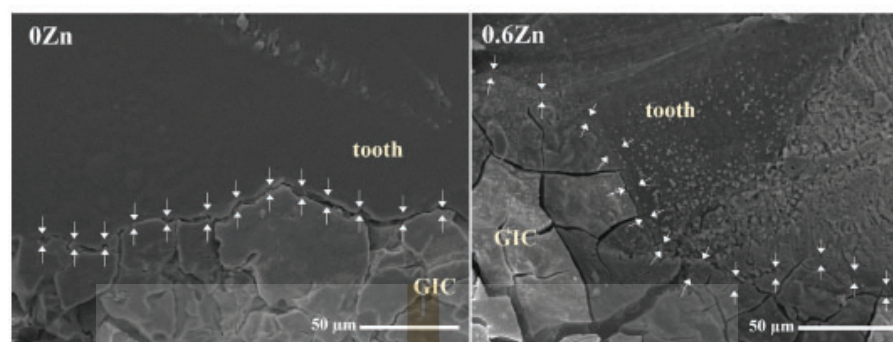


**Figure 13** SEM images of the interfacial area between the tooth and the sol-gel GIC samples prepared with 0.6 ZnO-doped glass and calcined at 650 °C as compared to ZnO free GIC.

restoration. The result showed a detachment between Zn-free GIC and the tooth, while ZnO-doped GIC showed complete adaptation to the tooth. This detachment between GIC and tooth structure could happen because of drying the specimens for SEM evaluation. The main mechanism of GIC bonding with tooth structure is based on the ionic reaction of the carboxyl group with calcium and phosphate on the tooth surface. However, this result demonstrated that the presence of zinc in the glass structure could promote the sealing of the tooth surface. Moreover, the previous work reported that zinc potentially stimulates hard-tissue mineralization by interaction with the phosphate in the tooth structure [51]. This interaction might enhance the bonding response between the tooth and the GIC.

The manufacturers recently introduced zinc containing GIC, i.e., CAREDYNE RESTORE from GC Japan and ChemFil™ Rock from Dentsply USA. CAREDYNE RESTORE is a new GIC product composing of “BioUnion Filler”, which releases fluoride, zinc and calcium ions. The releasing level of zinc from this product was reported to reach the level to inhibit biofilm formation [53]. This product also shows a high remineralization performance, appropriate for the prevention and restoration of root caries [54, 55]. For the ChemFil™ Rock, it is a new type of GIC with an enhanced setting reaction by the presence of zinc in glass composition. The presence of zinc increased durability and able to use in stress-bearing situations along with posterior tooth restoration [6]. These commercial products showed

the benefit of zinc containing GIC for dental restorative materials. This study also demonstrated the substitute of zinc for calcium site in glass composition synthesized by the sol-gel method at low temperature, which improved both of biological and antibacterial characteristics of the glass ionomer cement.

### Conclusions

ZnO doping instead of CaO in the glass composition and the calcination temperature for the glass synthesized by the sol-gel method was studied in this work. The result showed that ZnO was unable to replace the CaO in the sol-gel ionomer glass. The increasing of ZnO content and calcination temperature induced the crystal structure of  $ZnAl_2O_4$  and  $ZnO_2$ . After the setting reaction, the EXAFS data revealed that O atoms from the  $-COO^-$  functional group of PAA liquid preferred to bond with  $Ca^{2+}$  ions than  $Zn^{2+}$  ions. Thus, the compressive strength of the ZnO-doped GIC decreased with the increase of ZnO content. However, the compressive strength could be maintained by decreasing the calcination temperature. This study presented that the sol-gel GIC prepared with 0.6Zn glass calcined at 650 °C had the most promising result in terms of setting time and compressive strength.

Interestingly, the antibacterial effect of ZnO content in glass composition was excellent under the light condition as the photocatalysis effect. Additionally,

the GIC prepared with the 0.6ZnO glass presented slightly toxic to cells. This could be improved in further study by reducing the amount of ZnO in the glass composition. Furthermore, the sol-gel GIC with ZnO doping also improved bioactivity and tooth adhesion.

### Acknowledgements

The authors would like to thank the Synchrotron Light Research Institute (Public Organization), Thailand for the XPS (BL5.3) and XAS (BL5.2) facilities. Thanks to Mr Chinawat Ekwongsa for helping in XANES and EXAFT data analysis.

### Funding

This paper was financially supported by the Royal Golden Jubilee (RGJ) PhD Program from Thailand Research Fund (PHD/0058/2558) and Suranaree University of Technology.

### Declarations

**Conflict of interest** The authors have no conflicts of interest to declare that are relevant to the content of this article.

### References

- [1] Wong A, Subar PE, Young DA (2017) Dental caries: an update on dental trends and therapy. *Adv Pediatr* 64:307–330. <https://doi.org/10.1016/j.yapd.2017.03.011>
- [2] California DB (2005) The fact about filling. Department of consumer affairs, California
- [3] Sidhu SK, Nicholson JW (2016) A review of glass-ionomer cements for clinical dentistry. *J Funct Biomater* 7:16. <http://doi.org/10.3390/jfb7030016>
- [4] Li Y, Zhang W, Niu J, Chen Y (2012) Mechanism of photogenerated reactive oxygen species and correlation with the antibacterial properties of engineered metal-oxide nanoparticles. *ACS Nano* 6:5164–5173. <https://doi.org/10.1021/nl300934k>
- [5] Tiama T, Abd N, Tohamy K, Soliman I (2017) In vitro bioactivity and antibacterial activity of zn and sr containing glass ionomer cement prepared by a quick alkali-mediated sol-gel method. *EC Dent Sci* 4:136–146
- [6] Patil K, Patel A, Kunte S, Shah P, Kaur B, Paranna S (2020) Comparative evaluation of the mechanical properties of zinc-reinforced glass ionomer cement and glass ionomer type IX cement: an in vitro study. *Int J Clin Pediatr Dent* 13:381–389. <https://doi.org/10.5005/jp-journals-10005-1798>
- [7] Kumar A, Raj A, Singh D, Donthagini S, Kumar M, Ramesh K (2021) A new zinc reinforced glass ionomer cement: a boon in dentistry. *J Pharm Bioallied Sci* 13:272–275. [http://doi.org/10.4103/jpbs.JPBS\\_730\\_20](http://doi.org/10.4103/jpbs.JPBS_730_20)
- [8] Thongsri O, Srisuwan S, Thaitalay P, Dangwiriyakul R, Aengchuan P, Chanlek N, Talabnin C, Suksaewang S, Rattanachan ST (2021) Influence of Al<sub>2</sub>O<sub>3</sub> and P<sub>2</sub>O<sub>5</sub> contents in sol-gel ionomer glass system on the structure and their cement properties. *J Sol-Gel Sci Technol* 98:441–451. <http://doi.org/10.1007/s10971-021-05519-9>
- [9] Zhang S, Stamboulis A (2016) Effect of zinc substitution for calcium on the crystallisation of calcium fluoro-aluminosilicate glasses. *J Non Cryst Solids* 432:300–306. <https://doi.org/10.1016/j.jnoncrysol.2015.10.025>
- [10] Kusumoto H (2009) Characterisation of Mg, Sr, and Zn containing fluoro-aluminosilicate glasses and their glass polyalkenoate cements. PhD Dissertation, Imperial College, London
- [11] Bertolini MJ, Zaghele MA, Gimenes R (2005) Development of an experimental glass ionomer cement containing niobium and fluoride. *J Non Cryst Solids* 351:3884–3887. <https://doi.org/10.1016/j.jnoncrysol.2005.10.008>
- [12] Kajihara K (2013) Recent advances in sol-gel synthesis of monolithic silica and silica-based glasses. *J Asian Ceram Soc* 1:121–133. <https://doi.org/10.1016/j.jascer.2013.04.002>
- [13] Mukherjee SP (1980) Sol-gel processes in glass science and technology. *J Non Cryst Solids* 42:477–488. [https://doi.org/10.1016/0022-3093\(80\)90046-0](https://doi.org/10.1016/0022-3093(80)90046-0)
- [14] Roy B, Jain H, Saha SK, Chakravorty D (1995) Comparison of structure of alkali silicate glasses prepared by sol-gel and melt-quench methods. *J Non Cryst Solids* 183:268–276. [https://doi.org/10.1016/0022-3093\(94\)00633-4](https://doi.org/10.1016/0022-3093(94)00633-4)
- [15] Wren A, Clarkin O, Laffir F, Ohtsuki C, Kim IY, Towler M (2009) The effect of glass synthesis route on mechanical and physical properties of resultant glass ionomer cements. *J Mater Sci Mater Med* 20:1991–1999. <https://doi.org/10.1007/s10856-009-3781-6>
- [16] Tang V, Otto K, Seering W (2014) Using design of experiments (DOE) for decision analysis. Paper presented at the International Conference on Engineering Design, ICED'07 Cite des sciences et de l'industrie, Paris, France, 01/23
- [17] Kikkhuthod P (2017) Structural studies of advanced functional materials by synchrotron-based x-ray absorption spectroscopy. BL5.2 at SLRI, Thailand. *Adv Nat Sci*

- Nanosci 8:035007. <https://doi.org/10.1088/2043-6254/aa7240>
- [18] Neville M (2001) IFEFFIT: interactive XAFS analysis and FEFF fitting. *J Synchrotron Radiat* 8:322–324. <https://doi.org/10.1107/S0909049500016964>
- [19] Jain A, Ong SP, Hautier G, Chen W, Richards WD, Dacek S, Cholia S, Gunter D, Skinner D, Ceder G, Persson KA (2013) Commentary: the Materials Project: a materials genome approach to accelerating materials innovation. *APL Mater* 1:011002. <https://doi.org/10.1063/1.4812323>
- [20] Paiva L, Fidalgo TKS, da Costa LP, Maia LC, Balan L, Anselme K, Ploux L, Thiré RMSM (2018) Antibacterial properties and compressive strength of new one-step preparation silver nanoparticles in glass ionomer cements (NanoAg-GIC). *J Dent* 69:102–109. <https://doi.org/10.1016/j.jdent.2017.12.003>
- [21] Kamalak H, Kamalak A, Taghizadehghalehjouhi A, Haemüftüoğlu A, Nalci KA (2018) Cytotoxic and biological effects of bulk fill composites on rat cortical neuron cells. *Odontology* 106:377–388. <https://doi.org/10.1007/s10266-018-0354-5>
- [22] El Mallakh BF, Sarkar NK (1990) Fluoride release from glass-ionomer cements in de-ionized water and artificial saliva. *Dent Mater* 6:118–122. [https://doi.org/10.1016/S0109-5641\(05\)80041-7](https://doi.org/10.1016/S0109-5641(05)80041-7)
- [23] Bogomolova LD, Pavlushkina TK, Morezova IV (2006) Formation of glass synthesized by sol-gel technology. *Glass Ceram* 63:254–258. <https://doi.org/10.1007/s10717-006-0092-y>
- [24] Zanotto ED (1992) The formation of unusual glasses by sol-gel processing. *J Non Cryst Solids* 147–148:820–823. [https://doi.org/10.1016/S0022-3093\(05\)80723-9](https://doi.org/10.1016/S0022-3093(05)80723-9)
- [25] Tshabalala KG, Cho SH, Park JK, Pitale SS, Nagpure IM, Kroon RE, Swart HC, Ntwaaborwa OM (2011) Luminescent properties and X-ray photoelectron spectroscopy study of ZnAl<sub>2</sub>O<sub>4</sub>:Ce<sup>3+</sup>, Tb<sup>3+</sup> phosphor. *J Alloys Compd* 509:10115–10120. <https://doi.org/10.1016/j.jallcom.2011.08.054>
- [26] Stranick MA, Root MJ (1991) Influence of strontium on monofluorophosphate uptake by hydroxyapatite XPS characterization of the hydroxyapatite surface. *Colloids Surf* 55:137–147. [https://doi.org/10.1016/0166-6622\(91\)80088-6](https://doi.org/10.1016/0166-6622(91)80088-6)
- [27] Bezerra CdS, Valerio MEG (2016) Structural and optical study of CaF<sub>2</sub> nanoparticles produced by a microwave-assisted hydrothermal method. *Physica B: Condens Mater* 501:106–112. <https://doi.org/10.1016/j.physb.2016.08.025>
- [28] Zhang D, Qingjie G, Ren Y, Wang C, Shi Q, Wang Q, Xiao X, Wang W, Fan Q (2017) Influence of inversion defects and Cr–Cr pairs on the photoluminescent performance of ZnAl<sub>2</sub>O<sub>4</sub> crystals. *J Sol-Gel Sci Technol* 85:121–131. <https://doi.org/10.1007/s10971-017-4527-4>
- [29] Bernasconi A, Dapiaggi M, Pavese A, Agostini G, Bernasconi M, Bowron DT (2016) Modeling the structure of complex aluminosilicate glasses: the effect of zinc addition. *J Phys Chem B* 120:2526–2537. <https://doi.org/10.1021/acs.jpcc.5b10886>
- [30] Nicholson JW, Coleman NJ, Sidhu SK (2021) Kinetics of ion release from a conventional glass-ionomer cement. *J Mater Sci Mater Med* 32:1–10. <https://doi.org/10.1007/s10856-021-06501-1>
- [31] Kunle A, Nicholson John W (2014) A study of phosphate ion release from glass-ionomer dental cements. *Ceram-Silik* 58:210–214
- [32] Nicholson JW (2018) Maturation processes in glass-ionomer dental cements. *Acta Biomater Odontol Scand* 4:63–71. <https://doi.org/10.1080/23337931.2018.1497492>
- [33] Alhalawani AMF, Curran DJ, Boyd D, Towler MR (2016) The role of poly(acrylic acid) in conventional glass polyalkenoate cements. *J Polym Eng* 36:221–237. <https://doi.org/10.1515/polyeng-2015-0079>
- [34] Baig MS, Fleming GJP (2015) Conventional glass-ionomer materials: a review of the developments in glass powder, polyacid liquid and the strategies of reinforcement. *J Dent* 43:897–912. <https://doi.org/10.1016/j.jdent.2015.04.004>
- [35] Fleming G, Farooq A, Barralet J (2003) Influence of powder/liquid mixing ratio on the performance of a restorative glass-ionomer dental cement. *Biomaterials* 24:4173–4179. [https://doi.org/10.1016/S0142-9612\(03\)00301-6](https://doi.org/10.1016/S0142-9612(03)00301-6)
- [36] Dudev M, Wang J, Dudev T, Lim C (2006) Factors governing the metal coordination number in metal complexes from cambridge structural database analyses. *J Phys Chem B* 110:1889–1895. <https://doi.org/10.1021/jp054975n>
- [37] Pan HB, Darvell BW (2007) Solubility of calcium fluoride and fluorapatite by solid titration. *Arch Oral Biol* 52:861–868. <https://doi.org/10.1016/j.archoralbio.2007.03.002>
- [38] Bonapasta AA, Buda F, Colombet P (2001) Interaction between Ca ions and poly(acrylic acid) chains in macro-defect-free cements: a theoretical study. *Chem Mater* 13:64–70. <https://doi.org/10.1021/cm000505o>
- [39] Katz AK, Glusker JP, Beebe SA, Bock CW (1996) Calcium ion coordination: a comparison with that of beryllium, magnesium, and zinc. *J Am Chem Soc* 118:5752–5763. <https://doi.org/10.1021/ja953943i>
- [40] Vao-soongnem V, Merat K, Horpibulsuk S (2015) Interaction of the calcium ion with poly(acrylic acid) as investigated by a combination of molecular dynamics simulation and X-ray absorption spectroscopy. *J Polym Res* 23:7. <https://doi.org/10.1007/s10965-015-0895-z>

- [41] Daley T, Opuni KB, Raj E, Dent AJ, Cibin G, Hyde TL, Sankar G (2021) Monitoring the process of formation of ZnO from ZnO<sub>2</sub> using in situ combined XRD/XAS technique. *J Condens Matter Phys* 33:264002. <https://doi.org/10.1088/1361-648x/abfb91>
- [42] Thomas SA, Mishra B, Myneni SCB (2019) High energy resolution-X-ray absorption near edge structure spectroscopy reveals Zn ligation in whole cell bacteria. *J Phys Chem Lett* 10:2585–2592. <https://doi.org/10.1021/acs.jpclett.9b01186>
- [43] Krężel A, Maret W (2016) The biological inorganic chemistry of zinc ions. *Arch Biochem Biophys* 611:3–19. <https://doi.org/10.1016/j.abb.2016.04.010>
- [44] Schuhlackn K, Stüch L, Schmidt J, Steinkasserer A, Boccacini AR, Zinser E (2020) Cu, Zn doped bonite bioactive glasses: antibacterial efficacy and dose-dependent in vitro modulation of murine dendritic cells. *Biomater Sci* 8:2143–2155. <https://doi.org/10.1039/C9BM01691K>
- [45] Joe A, Park S-H, Shim K-D, Kim D-J, Jhee K-H, Lee H-W, Heo C-H, Kim H-M, Jang E-S (2017) Antibacterial mechanism of ZnO nanoparticles under dark conditions. *J Ind Eng Chem* 45:430–439. <https://doi.org/10.1016/j.jiec.2016.10.013>
- [46] Sirekhatim A, Mahmud S, Seeni A, Kaus NHM, Ann LC, Bakhori SKM, Hasan H, Mohamad D (2015) Review on zinc oxide nanoparticles: antibacterial activity and toxicity mechanism. *Nanomicro Lett* 7:219–242. <https://doi.org/10.1007/s40820-015-0040-x>
- [47] Brauer DS, Gentleman E, Farrar DF, Stevens MM, Hill RG (2011) Benefits and drawbacks of zinc in glass ionomer bone cements. *Biomater* 6:045007. <https://doi.org/10.1088/1748-6041/6/4/045007>
- [48] Patrón-Romero L, Luque PA, Soto-Robles CA, Nava O, Vilchis-Nestor AR, Barajas-Carrillo VW, Martínez-Ramírez CE, Chávez Méndez JR, Alvelais Palacios JA, Leal Avila MÁ, Almanza-Reyes H (2020) Synthesis, characterization and cytotoxicity of zinc oxide nanoparticles by green synthesis method. *J Drug Deliv Sci Technol* 60:101925. <https://doi.org/10.1016/j.jddst.2020.101925>
- [49] Saber M, Hayaei-Tehrani R-S, Mokhtari S, Hoorzad P, Esfandiari F (2021) In vitro cytotoxicity of zinc oxide nanoparticles in mouse ovarian germ cells. *Toxicol Vitro* 70:105032. <https://doi.org/10.1016/j.tiv.2020.105032>
- [50] Drouot C (2013) Apatite formation: why it may not work as planned, and how to conclusively identify apatite compounds. *BioMed Res Int* 2013:490946. <https://doi.org/10.1155/2013/490946>
- [51] Lynch R (2011) Zinc in the mouth, its interactions with dental enamel and possible effects on caries; a review of the literature. *Int Dent J* 61(Suppl 3):46–54. <https://doi.org/10.1111/j.1875-595X.2011.00049.x>
- [52] Chen S, Cai Y, Engqvist H, Xia W (2016) Enhanced bioactivity of glass ionomer cement by incorporating calcium silicates. *Biomater* 6:e1123842. <https://doi.org/10.1080/021592535.2015.1123842>
- [53] Kohno T, Tsuboi R, Kitagawa H, Imazato S (2019) Zinc-Ion release and recharge ability of gic containing bioion filler. In: Paper presented at the 2019 IADR/AADR/CADR general session, Vancouver, BC, Canada
- [54] Kaga N, Nagano-Takebe F, Nezu T, Matsuura T, Endo K, Kaga M (2020) Protective effects of GIC and S-PRG filler restoratives on demineralization of bovine enamel in lactic acid solution. *Materials* 13:2140. <https://doi.org/10.3390/ma13092140>
- [55] Nagano Y, Mori D, Kumagai T (2019) Evaluation of carelyn restore on shear-bond strength and remineralization. In: Paper presented at the the third biennial meeting of the international academy of adhesive dentistry, the Palazzo della Cultura e dei Congressi, Bologna, Italy

**Publisher's Note** Springer Nature remains neutral with regard to jurisdictional claims in published maps and institutional affiliations.

## APPENDIX B

**Table I** material for ionomer glass synthesis by the sol-gel method

Chemical name	Compound formular	Abbrev.	Conc.	Density (g/cm <sup>3</sup> )	Manufacturer	Function
Tetraethyl orthosilicate	Si(OC <sub>2</sub> H <sub>5</sub> ) <sub>4</sub>	TEOS	98%	0.940	Acros	SiO <sub>2</sub> source
Aluminum nitrate	Al(NO <sub>3</sub> ) <sub>3</sub>	AlN	98%	-	Ajax	Al <sub>2</sub> O <sub>3</sub> source
Triethylphosphate	((C <sub>2</sub> H <sub>5</sub> O) <sub>2</sub> P(O)) <sub>2</sub> O	TEP	99%	1.072	Acros	P <sub>2</sub> O <sub>5</sub> source
Calcium nitrate tetrahydrate	Ca(NO <sub>3</sub> ) <sub>2</sub> ·4H <sub>2</sub> O	CN	98%	-	Ajax	CaO source
Calcium fluoride	CaF <sub>2</sub>	CaF <sub>2</sub>	99%	-	Carlo Erba	CaF <sub>2</sub> source
Hexafluorosilicic acid	H <sub>2</sub> SiF <sub>6</sub>	H <sub>2</sub> SiF <sub>6</sub>	25%	1.220	Acros	F <sub>2</sub> source
Absolute ethanol	C <sub>2</sub> H <sub>6</sub> O	EtOH	100%	0.789	Carlo Erba	Solvent
Deionized water	H <sub>2</sub> O	DI	-	1.000	-	Solvent
Nitric acid	HNO <sub>3</sub>	HNO <sub>3</sub>	65%	1.390	Carlo Erba	Catalyst
Ammonium hydroxide solution	NH <sub>4</sub> OH	NH <sub>4</sub> OH	30%	0.802	Carlo Erba	Catalyst
polyacrylic acid Mw ~ 100,000	(C <sub>3</sub> H <sub>4</sub> O <sub>2</sub> ) <sub>n</sub>	PAA	35 wt.%	1.140	Sigma-Aldrich	Liquid phase of GICs
poly(acrylic acid-co-maleic acid) M.W. ~ 3,000	C <sub>7</sub> H <sub>8</sub> O <sub>6</sub>	PAA-Co-MA	50 wt.%	1.230	Sigma-Aldrich,	Liquid phase of GICs
Tartaric acid	C <sub>4</sub> H <sub>6</sub> O <sub>6</sub>	TTA	99%	-	Sigma-Aldrich	Chelating comonomers Liquid phase of GICs

**Table II** Chemical calculation example for the synthesis of 6 g of ionomer glass with a composition of  $4.5\text{SiO}_2-4\text{Al}_2\text{O}_3-0.3\text{P}_2\text{O}_5-2\text{CaO}-2\text{F}_2$

Glass composition	Chemical reagents	Mol ratio	Density (g/ml)	Mw (g/mol)	Mol*Mw (g)	Weight (g)	Volume (ml)
$\text{SiO}_2$	TEOS (ml)	3.83 (4.5-0.67)	0.94	208.33	798.00	6.11 (798.6/130.6 <sup>a</sup> )	6.5 (6.11/0.94)
$\text{F}_2$	$\text{H}_2\text{SiF}_6$ (ml)	0.67	1.22	144.9	96.60	0.74 (96.60/130.6 <sup>a</sup> )	0.60 (0.74/1.22)
$\text{Al}_2\text{O}_3$	$\text{Al}(\text{NO}_3)_3 \cdot 9\text{H}_2\text{O}$ (g)	8	-	375.13	3,001.04	22.97 (3001.0/130.6 <sup>a</sup> )	-
$\text{P}_2\text{O}_5$	$\text{C}_6\text{H}_{13}\text{O}_4\text{P}$ (TEP) (ml)	0.6	1.07	182.15	109.29	0.83 (109.2/130.6 <sup>a</sup> )	0.78 (0.83/1.07)
$\text{CaO}$	$\text{Ca}(\text{NO}_3)_2 \cdot 4\text{H}_2\text{O}$ (g)	2	-	236.75	330.61	2.53 (330.61/130.6 <sup>a</sup> )	-

<sup>a</sup> was calculated from  $798.00/6.11=130.6$  since the volume of TEOS was fixed to 6.5 ml according to Chapter 3, section 3.2.1.1 experiment.

**Chemical calculation method for synthesis of 6 g of ionomer glass in the system of  $4.5\text{SiO}_2-4\text{Al}_2\text{O}_3-0.3\text{P}_2\text{O}_5-2\text{CaO}-2\text{F}_2$**

**TEOS;  $\text{Si}(\text{OC}_2\text{H}_5)_4$  (ml)**

TEOS has density of 0.94 g/ml and molecular weight of 208.33 g/mol

We needed  $\text{SiO}_2$  for 3.83 mol. (From 4.5 mol of TEOS minus 0.67 mol of  $\text{H}_2\text{SiF}_6$ )

According to the result of Chapter 3, TEOS was fixed to 6.5 ml.

Hence, the weight of TEOS in the actual experiment was  $6.5 \text{ ml} \times 0.94 \text{ g/ml} = 6.11 \text{ g}$

\* The calculated weight of TEOS was molecular weight (g)  $\times$  mol =  $208.33 \text{ g/mol} \times 3.83 \text{ mol} = 798.00 \text{ g}$

\* The constant value from the calculated weight divided by the actual weight ( $798.00 \text{ g} / 6.11 \text{ g} = 130.6$ ) was used as divisor to calculate the actual weight of other chemical reagents

**H<sub>2</sub>SiF<sub>6</sub> (ml)**

H<sub>2</sub>SiF<sub>6</sub> has density of 1.22 g/ml and molecular weight of 144.9 g/mol

We needed F<sub>2</sub> for 2 mol, which means we required 0.67 mol of H<sub>2</sub>SiF<sub>6</sub> (obtained by dividing 4 by 6).

The calculated weight of H<sub>2</sub>SiF<sub>6</sub> was 144.9 g/mol x 0.67 mol = 96.60 g

The weight of H<sub>2</sub>SiF<sub>6</sub> in the actual experiment was 96.60 g/130.6 = 0.74 g

Hence, the volume of H<sub>2</sub>SiF<sub>6</sub> in the experiment was 0.74 g/1.22 g/ml = **0.60 ml**

**TEP; ((C<sub>2</sub>H<sub>5</sub>O)<sub>2</sub>P(O))<sub>2</sub>O (ml)**

TEP has density of 1.07 g/ml and molecular weight of 182.15 g/mol.

We needed P<sub>2</sub>O<sub>5</sub> for 0.3 mol, which means we required 0.6 mol of TEP.

The calculated weight of TEP was 182.15 g/mol x 0.6 mol = 109.29 g

The weight of TEP in the actual experiment was 109.29 g/130.6 = 0.83 g

Hence, the volume of TEP in the experiment was 0.83 g/1.07 g/ml = **0.78 ml**

**Al(NO<sub>3</sub>)<sub>3</sub>.9H<sub>2</sub>O (g)**

Al(NO<sub>3</sub>)<sub>3</sub>.9H<sub>2</sub>O has molecular weight of 375.13 g/mol.

We needed Al<sub>2</sub>O<sub>3</sub> for 4 mol, which means we required 8 mol of Al(NO<sub>3</sub>)<sub>3</sub>.9H<sub>2</sub>O.

The calculated weight of Al(NO<sub>3</sub>)<sub>3</sub>.9H<sub>2</sub>O was 375.13 g/mol x 8 mol = 3,001.04 g

Hence, the weight of Al(NO<sub>3</sub>)<sub>3</sub>.9H<sub>2</sub>O in the actual experiment was 3,001.04 g/130.6 = **22.97 g**

**Ca(NO<sub>3</sub>)<sub>2</sub>.4H<sub>2</sub>O (g)**

Ca(NO<sub>3</sub>)<sub>2</sub>.4H<sub>2</sub>O (g) has molecular weight of 236.75 g/mol.

We needed CaO for 2 mol, which means we required 2 mol of Ca(NO<sub>3</sub>)<sub>2</sub>.4H<sub>2</sub>O (g).

The calculated weight of Ca(NO<sub>3</sub>)<sub>2</sub>.4H<sub>2</sub>O (g) was 236.75 g/mol x 2 mol = 330.61 g

Hence, the weight of Ca(NO<sub>3</sub>)<sub>2</sub>.4H<sub>2</sub>O (g) in the actual experiment was 330.61 g/130.6 = **2.53 g**

**Table III** Chemical Content of Chapter 4 experiment synthesizing of 6 g of ionomer glass with varying molar ratios of  $4.5\text{SiO}_2\text{-XAl}_2\text{O}_3\text{-YP}_2\text{O}_5\text{-2CaO-2F}_2$ , where X ranges from 2 to 4.3 moles and Y ranges from 0.15 to 1.5 moles.

Sample annotation	Mol ratios		Chemical content						
	$\text{Al}_2\text{O}_3$ (X)	$\text{P}_2\text{O}_5$ (Y)	EtOH (ml)	DI water (ml)	TEOS (ml)	$\text{Al}(\text{NO}_3)_3 \cdot 9\text{H}_2\text{O}$ (g)	TEP (ml)	$\text{Ca}(\text{NO}_3)_2 \cdot 2\text{H}_2\text{O}$ (g)	$\text{H}_2\text{SiF}_6$ (ml)
2Al-0.15P	2	0.15	17	50	6.50	11.44	0.39	2.52	0.60
2.5Al-0.15P	2.5		17	50	6.50	17.17	0.39	2.52	0.60
4Al-0.15P	4		17	50	6.50	22.89	0.39	2.52	0.60
4.3Al-0.15P	4.3		17	50	6.50	24.60	0.39	2.52	0.60
2Al-0.3P	2	0.3	17	50	6.50	11.44	0.78	2.52	0.60
2.5Al-0.3P	2.5		17	50	6.50	17.17	0.78	2.52	0.60
4Al-0.3P	4		17	50	6.50	22.89	0.78	2.52	0.60
4.3Al-0.3P	4.3		17	50	6.50	24.60	0.78	2.52	0.60
2Al-0.45P	2	0.45	17	50	6.50	11.44	1.17	2.52	0.60
2.5Al-0.45P	2.5		17	50	6.50	17.17	1.17	2.52	0.60
4Al-0.45P	4		17	50	6.50	22.89	1.17	2.52	0.60
4.3-0.45P	4.3		17	50	6.50	24.60	1.17	2.52	0.60

**Table IV** Chemical content for Chapter 5 experiment synthesizing of 6 g of ionomer glass with a composition of  $4.5\text{SiO}_2\text{-4Al}_2\text{O}_3\text{-0.15P}_2\text{O}_5\text{-(2-x)Ca-xZnO-2F}_2$ , where  $x = 0, 0.6, 1.0$  and  $1.4$ .

Sample annotation	Chemical content							
	EtOH (ml)	DI water (ml)	TEOS (ml)	$\text{Al}(\text{NO}_3)_3 \cdot 9\text{H}_2\text{O}$ (g)	TEP (ml)	$\text{Ca}(\text{NO}_3)_2 \cdot 2\text{H}_2\text{O}$ (g)	$\text{Zn}(\text{NO}_3)_2 \cdot 6\text{H}_2\text{O}$ (g)	$\text{H}_2\text{SiF}_6$ (ml)
0Zn	17	50	6.50	11.44	0.78	3.60	0.00	0.60
0.6Zn	17	50	6.50	11.44	0.78	0.72	1.08	0.60
1.0Zn	17	50	6.50	11.44	0.78	1.80	1.80	0.60
1.4Zn	17	50	6.50	11.44	0.78	2.88	2.52	0.60

## BIOGRAPHY

Name: Oranich Thongsri

### Education Background:

- 2011-2015 B.Sc. (Material science and Nanotechnology) Khon Kean University, Khon Kean, Thailand
- 2015-2023 Ph.D. (Material Engineering) Suranaree University of Technology, Nakhorn Ratchasima, Thailand.

### Academic Experience:

- 2022 Research visit at University of Manchester, United Kingdom in topic of "Cytocompatibility of the sol-gel derived glass ionomer cements"
- 2015 Co-operative education, Chiba University, Japan in topic of "Synthetic of complex oxide particles by hydrothermal conversion of hydrous titania"
- 2014 Senior project, Khonkean University, Thailand in topic of "The computational investigation of CO<sub>2</sub> and H<sub>2</sub> adsorptions in Mg-based metal-organic framework-74"
- 2014 Trainee, beamline 5.2, X-ray Absorption Spectroscopy, Synchrotron Light Research Institute, Nakhorn Ratchasima, Thailand.